NUREG/CR-4072

The Estimation of Atmospheric Dispersion at Nuclear Power Plants Utilizing Real Time Anemometer Statistics

Prepared by W. W. Li, R. N. Meroney

Fluid Dynamics and Diffusion Laboratory
Colorado State University

Prepared for
U.S. Nuclear Regulatory
Commission

NOTICE

Availability of Reference Materials Cited in NRC Publications

Most documents cited in NRC publications will be available from one of the following sources:

1. The NRC Public Document Room, 1717 H Street, N.W.
   Washington, DC 20555
2. The NRC/GPO Sales Program, U.S. Nuclear Regulatory Commission,
   Washington, DC 20555
3. The National Technical Information Service, Springfield, VA 22161

Although the listing that follows represents the majority of documents cited in NRC publications, it is not intended to be exhaustive.

Referenced documents available for inspection and copying for a fee from the NRC Public Document Room include NRC correspondence and internal NRC memoranda; NRC Office of Inspection and Enforcement bulletins, circulars, information notices, inspection and investigation notices; Licensee Event Reports; vendor reports and correspondence; Commission papers; and applicant and licensee documents and correspondence.

The following documents in the NUREG series are available for purchase from the NRC/GPO Sales Program: formal NRC staff and contractor reports, NRC-sponsored conference proceedings, and NRC booklets and brochures. Also available are Regulatory Guides, NRC regulations in the *Code of Federal Regulations,* and *Nuclear Regulatory Commission Issuances.*

Documents available from the National Technical Information Service include NUREG series reports and technical reports prepared by other federal agencies and reports prepared by the Atomic Energy Commission, forerunner agency to the Nuclear Regulatory Commission.

Documents available from public and special technical libraries include all open literature items, such as books, journal and periodical articles, and transactions. *Federal Register* notices, federal and state legislation, and congressional reports can usually be obtained from these libraries.

Documents such as theses, dissertations, foreign reports and translations, and non-NRC conference proceedings are available for purchase from the organization sponsoring the publication cited.

Single copies of NRC draft reports are available free, to the extent of supply, upon written request to the Division of Technical Information and Document Control, U.S. Nuclear Regulatory Commission, Washington, DC 20555.

Copies of industry codes and standards used in a substantive manner in the NRC regulatory process are maintained at the NRC Library, 7920 Norfolk Avenue, Bethesda, Maryland, and are available there for reference use by the public. Codes and standards are usually copyrighted and may be purchased from the originating organization or, if they are American National Standards, from the American National Standards Institute, 1430 Broadway, New York, NY 10018.

GPO Printed copy price: $6.50

NUREG/CR-4072
RB

The Estimation of Atmospheric Dispersion at Nuclear Power Plants Utilizing Real Time Anemometer Statistics

Manuscript Completed: October 1984
Date Published: January 1985

Prepared by
W. W. Li, R. N. Meroney

Fluid Dynamics and Diffusion Laboratory
Department of Civil Engineering
Colorado State University
Fort Collins, CO 80523

Prepared for
Division of Radiation Programs and Earth Sciences
Office of Nuclear Regulatory Research
U.S. Nuclear Regulatory Commission
Washington, D.C. 20555
NRC FIN B7585
Under Contract No. NRC-04-81-202

ABSTRACT

THE ESTIMATION OF ATMOSHPERIC DISPERSION AT NUCLEAR POWER PLANTS UTILIZING REAL TIME ANEMOMETER STATISTICS

Dispersion and turbulence measurements were conducted in a simulated atmospheric boundary layer. Field experiments and wind tunnel results for the behavior of lateral plume dispersion are compared to three semi-empirical expressions based on the Taylor's diffusion theory. These relations imply a direct connection between dispersion coefficients and the Lagrangian integral time scale. Agreement between the field data and laboratory measurements support using wind tunnel results to simulate atmoshperic transport phenomena.

Eulerian space-time correlations with streamwise separations were measured for all three velocity components in the simulated boundary layer. Results were compared to previous measurements which were performed under different flow configurations. A universal shape of the Eulerian space-time correlation seems to exist when presented in a normalized time coordinate.

Turbulance measurements of fixed-point Eulerian velocity statistics were employed to estimate the Lagrangian velocity statistics through the Baldwin and Johnson approach. The approach was modified to account for the uniform shear stress effect in a homogeneous turbulent flow field. The estimated Lagrangian integral time scale agrees with estimates inferred from dispersion measurements within only a 20% error. Such agreement supports the methodology of using real time anemometer statistics to predict the atmospheric turbulent dispersion near a nuclear reactor site.

ACKNOWLEDGMENTS

This study was performed under Contract NRC 04-81-202 Mod. 1 with the Site Safety Research Branch, Office of Nuclear Regulatory Research, U.S. Nuclear Regulatory Commission. Financial support is gratefully acknowledged.

The authors are indebted to Drs. L. V. Baldwin and G. R. Johnson for their introduction to the problem and advice during this research. They also wish to express their gratitude to Dr. H. A. Panofsky of Penn State University for discussion about scaling of dispersion data, and to Dr. M. M. Siddiqui for statistical advice concerning data handling techniques.

Special thanks are due to Mr. D. E. Neff for advice concerning instrumentation calibration; his help during data collection using the split-film technique is gratefully appreciated. Cooperation from faculty members and technicians of the Fluid Dynamics and Diffusion Laboratory is also acknowledged.

Gratitude is extended to the technical typing personnel and drawing personnel at the Engineering Research Center for their assistance during the preparation of this report.

TABLE OF CONTENTS

LIST OF TABLES

LIST OF FIGURES

LIST OF SYMBOLS

Symbol	Description	
A	constant	-
a	constant	-
b	constant	-
Br	Bowen ratio, $\frac{C_p}{L}\frac{(\bar{T}_2-\bar{T}_1)}{\bar{q}_2-\bar{q}_1}$	-
C	concentration	$ppmL^{-3}$
$\bar{C}$	mean concentration	$ppmL^{-3}$
C_p	specific heat at constant pressure	$L^2T^{-1}{}_oK^{-1}$
d	width of source	L
E	voltage output from hot wire anemometer	volt
$E_1(n)$	one-dimensional energy spectrum function	L^2T^{-1}
e	fluctuating voltage	volt
$F_1(t_*)$	emperical Eulerian space-time correlation function	-
f_i	Pasquill's f curve	-
$f(x_1)$	longitudinal spatial correlation, $E^{R}{}_{11}(x_1,0,0;0)$	-
$G(\alpha,t_*)$	bracket term in Equation 3.12	-
g	acceleration due to gravity	LT^{-2}
$g(x_1)$	transverse spatial correlation $E^{R}{}_{22}(x_1,0,0;0)$	-
H	height of point source	L
$I(t_*)$	normalized Taylor's diffusion term	-

Symbol	Description	
I_{-v}	modified Bessel function of first kind	-
i	turbulent intensity	-
K_h	eddy conductivity	L^2T^{-1}
K_{ij}	turbulent diffusivity tensor	L^2T^{-1}
K_m	eddy viscosity	L^2T^{-1}
L	Isotropic Eulerian integral length scale, $L_{11} = L_{22} = L_{33}$	L
L_{ij}	Eulerian length scale, $\int_0^\infty \frac{[u_i(x_j)u_i(x_j+dx_j)]}{[u_i^2]^{\frac{1}{2}}\,[u_i^2]^{\frac{1}{2}}}\,dx_j$	L
m	emperical constant	-
N(0,1)	normal distribution with mean 0 and standard deviation 1	-
n,p	exponent in power law representation of velocity profile	-
n	random variable of a probability density function	-
n	exponent in power law representation of diffusivity profile	-
n	frequency	T^{-1}
n	King's law exponential	-
r_k	Lagrangian position of a fluid particle	L
P	probability density function	-
Q	source strength	$ppmT^{-1}$
$\bar{q}_1, \bar{q}_2$	heat flux per unit area	$HL^{-2}T^{-1}$
R	radius of a pipe	L
$E^{Rij}(x_1,x_2,x_3;\tau)$	Eulerian space-time correlation function, $\frac{[u_i(x_1,x_2,x_3;t)u_j(x_1,x_2,x_3;t+\tau)]}{[u_i^2]^{\frac{1}{2}}\,[u_j^2]^{\frac{1}{2}}}$	-

Symbol	Description	
$_{E}R_{ij}(\tau)$	Eulerian autocorrelation function, $\frac{[u_i(t)u_j(t+\tau)]}{[u_i^2]^{\frac{1}{2}}[u_j^2]^{\frac{1}{2}}}$	-
$_{L}R_{ij}(\tau)$	Lagrangian autocorrelation function, $\frac{[v_i(t)v_j(t+\tau)]}{[v_i^2]^{\frac{1}{2}}\ [v_j^2]^{\frac{1}{2}}}$	-
R_e	Reynolds number	-
R_f	flux Richardson number	-
R_i	gradient Richardson number	-
$_{E}T_{ij}$	Eulerian integral time scale	T
$_{L}T_{ij}$	Lagrangian integral time scale	T
$_{S}T_{ij}$	integral time scale of Eulerian space-time correlation function	T
T_a	average temperature in a layer	^oK
T_h	temperature at height h	^oK
T_i	diffusion time required for Pasquill's f_1 curve to become equal to 0.5	T
T_o	temperature at the surface	^oK
$\bar{T}_1, \bar{T}_2$	mean temperature at height 1,2	^oK
t	time	T
U	mean velocity in the streamwise direction	LT^{-1}
U_*	friction velocity	LT^{-1}
U_∞	free-stream velocity	LT^{-1}
u_i	Eulerian velocity fluctuation	LT^{-1}
V	mean velocity in x_2 direction	LT^{-1}
v_i	Lagrangian velocity fluctuations	LT^{-1}
v_i'	random uncorrelated velocity fluctuation	LT^{-1}
X_i^2	mean square particle displacement	L^2

Symbol	Description	
x_i'	Eulerian moving frame coordinate	L
x_k	Eulerian fixed coordinate	L
z_o	surface roughness	L
α	Eulerian parameter when $\alpha_1 = \alpha_2 = \alpha_3$	-
α_i	Eulerian parameter, $\frac{[u_i^2]^{\frac{1}{2}} S T_{11}}{L}$	-
β	scale ratio, ${}_L T_{ii} / {}_E T_{ii}$	-
γ	lapse rate at sunrise	$^\circ K L^{-1}$
γ_d	adiabatic lapse rate	$^\circ K L^{-1}$
τ	time	T
ζ	length scale, $x_1 / B\sqrt{u_1^2}$	L
τ_m	optimum delay time	T
κ_ℓ	three-dimensional wave number	L^{-1}
ξ_i	non-dimensional coordinate, $\frac{x_i'}{L}$	-
ξ,θ,ϕ	spherical coordinates	L,-,-
r,θ	polar coordinates	-
δt	time increment	T
δx_i	spatial separation distance	L
$\delta(x)$	Dirac delta function	-
δ	boundary layer thickness	L
σ	ideal standard deviation of the concentration profile	L
σ_2	observed standard deviation of the concentration profile	L
σ_p	standard deviation of the concentration profile predicted from the Lagrangian estimates	L
σ_y	standard deviation of the concentration profile from a finite-width source	L

Symbol	Description	
Γ	velocity gradient, $\frac{dU}{dx_3}$	T^{-1}
Λ	length scale	L
Λ_f	integral length scale calculated from energy spectrum	L
λ_f	turbulent dissipation scale	L
GAMMA	gamma function	
[]	ensemble average of N fluid particles	-
II	normalized diffusion term in a uniform shear flow	-

Subscript

A,B	probe A and B
E	Eulerian autocorrelation
h	height h
i,j	directional tensor
L	Lagrangian autocorrelation
S	Eulerian space-time correlation
wi	number of hot-wire
θ	temperature
δ	boundary layer thickness
-	time average

Chapter 1

INTRODUCTION

1.1 Statement of Work

The dispersive nature of turbulent flow is an object of consideration in many branches of engineering and applied science. Reliable predictive relations applicable to a broad range of scales are not yet known. Indeed, most atmospheric transport predictive schemes for a nuclear reactor site still depend upon relating mean wind field characteristics measured at particular site to regression formulae developed from data collected at other sites at other times.

Recent research on the turbulent dispersion phenomenon suggest that the concentration field in a wide variety of situations can be generated if the Lagrangian statistics/properties of the flow field are known. Unfortunately, because it is difficult to tag the particles initially in a manner that does not influence their future behavior, to obtain necessary trajectories and the subsequent laborious data analyses, it is not possible to obtain the Lagrangian statistics by tracking individual particles. Attempts have been made to deduce the Lagrangian autocorrelation from the Eulerian turbulent velocity at fixed point in space. Theoretical and empirical approaches to the Lagrangian-Eulerian relationship are quite diverse. Nevertheless, most of the attempts have been based on the assumption that the Lagrangian autocorrelation and the Eulerian autocorrelation, or Eulerian space-time cross correlation, are of similar shape but different scales. Whereas the importance of the shapes of those two autocorrelation functions is still disputable except for short range dispersion, the importance of the integral scales in turbulent diffusion has met with agreement. One of the purposes of this research is to demonstrate how a systematic scheme based on a probability method can estimate those Lagrangian statistics by a few anemometers located in the fixed Eulerian frame of reference. Of course, the major intent of this research is to predict dispersive phenomenon in the atmospheric boundary layer from the estimated Lagrangian statistics. A meteorological wind tunnel was used to simulate an atmospheric boundary layer to provide velocity correlation measurements and diffusion measurements.

An inhomogeneous turbulence field is realistic but complicates the mathematical description of the turbulent mechanism; hence, most statistical theories assume a homogeneous wind field. As a first estimate of the atmospheric dispersion, a homogeneous statistical turbulent diffusion theory is applied for an isotropic analysis and later extended to a non-isotropic analysis in the present study.

1.2 Introduction to the Text

The statistical theory by continuous movements and the relation between Lagrangian and Eulerian autocorrelation functions are reviewed in Chapter 2. In addition, classical and statistical solutions using the Lagrangian estimates to the diffusion equation are presented. Chapter 3 states the probability method of estimating the Lagrangian autocorrelation function in a generalized non-isotropic, uniformly sheared turbulence. Chapter 4 displays experimental facilities, measurement procedures and related measurement errors. Laboratory results of the turbulence field are presented and discussed in Chapter 5. Comparison between the laboratory dispersion measurement and the atmospheric dispersion experiments is included in this chapter. Lagrangian estimates obtained from a numerical iterative scheme based on the present analysis are compared with previous findings reported by various researchers in Chapter 6. Estimation of turbulent dispersion utilizing the Lagrangian estimates are compared with the laboratory dispersion measurements; the discrepancy is discussed. Chapter 7 briefly summarizes the present study and gives recommends for further research.

Chapter 2

LITERATURE REVIEW

2.1 Introduction

The basic theoretical approaches to statistical diffusion are either Lagrangian or Eulerian. Whereas the Lagrangian approach follows the motion of a single fluid particle, and is difficult to measure, the Eulerian approach concentrates on the balance of particle fluxes through a fixed point in the flow field and is normally easier to determine.

The statistical concept of turbulent diffusion is described in Section 2.2 based on theory of continuous movement. Section 2.3 presents several models proposed by different authors to obtain the Lagrangian statistics from Eulerian measurements. The Eulerian space-time correlation plays an important role in the Langrangian-Eulerian relationship and is reviewed in Section 2.4. The diffusion equation based on Eulerian kinematics in connection with the Lagrangian statistics for predictions of turbulent dispersion is considered in Section 2.5.

2.2 Statistical Theory based on Continuous Movement

Diffusion of a fluid particle in a uniform mean velocity, stationary, homogeneous turbulent flow was first described by Taylor (1921). The mean square particle displacement was predicted to depend on the Lagrangian velocity variance and the Lagrangian autocorrelation,

$$[X_i^2(t)] = 2[v_i^2] \int_0^t \int_0^{t_1} {}_L R_{ii}(\tau) d\tau dt_1 \ , \qquad (2.1)$$

where the square bracket indicates an ensemble average of N fluid particles, v_i is the Lagrangian fluctuation in the i^{th} direction, $[v_i^2]$ is an abbreviation for $[v_i^2(t)]$ during stationary turbulence, and ${}_L R_{ij}(\tau)$ is a normalized Lagrangian autocorrelation function,

$${}_L R_{ij}(\tau) = \frac{[v_i(t) v_j(t+\tau)]}{[v_i^2]^{\frac{1}{2}} \ [v_j^2]^{\frac{1}{2}}} \ , \qquad (2.2)$$

where i denotes the directional tensor.

When Equation 2.1 is integrated by parts, Taylor's relationship can also be expressed in the Kampe de Feriet form, i.e.,

$$[X_i^2(t)] = 2[v_i^2] \int_0^t (t-\tau)\, {}_L R_{ii}(\tau)\, d\tau \ . \qquad (2.3)$$

From Equation 2.3 two asymptotic results may be obtained:

(i) Since within a very short dispersive range of the source, ${}_L R_{ii}(\tau)$ approaches unity, then

$$[X_i^2(t)] \cong [v_i^2] t^2 \ . \qquad (2.4)$$

(ii) For a very long dispersion range, the integral of ${}_L R_{ii}(\tau)$ approaches a constant value ${}_L T_{ii}$,

$${}_L T_{ii} = \int_0^\infty {}_L R_{ii}(\tau)\, d\tau \ , \text{ thus}$$

$$[X_i^2(t)] \cong 2[v_i^2]\ {}_L T_{ii}\, t \ , \qquad (2.5)$$

where ${}_L T_{ii}$ is referred to as the Lagrangian integral time scale. The scale is an indication of the size of the largest eddy within the turbulence field.

In a homogeneous turbulent flow with uniform shear Γ and mean velocity U, $U = \Gamma x_3$, Corrsin (1953) derived expressions for the components of the dispersion tensor $[X_i(t)X_j(t)]$:

$$[X_1^2(t)] = \Gamma^2 [v_3^2] \left\{ \frac{2}{3} t^3 \int_0^t {}_L R_{33}(\tau)\, d\tau - 2 \int_0^t \tau\, {}_L R_{33}(\tau)\, d\tau + \frac{1}{3} \int_0^t \tau^3\, {}_L R_{33}(\tau)\, d\tau \right\}$$

(I)

$$+ 2[v_1^2] \int_0^t (t-\tau)\, {}_L R_{11}(\tau)\, d\tau$$

(II)

$$+ \Gamma[v_1v_3] \int_o^t (t-\tau)_L R_{31}(\tau)d\tau + \Gamma[v_1v_3] \int_o^t (t^2-\tau^2)_L R_{13}(\tau)d\tau \ ,$$

(III) (2.6)

$$[X_1(t)X_3(t)] = \Gamma[v_3^2] \int_o^t \tau(t-\tau)_L R_{33}(\tau)d\tau +$$

(I)

$$[v_1^2]^{\frac{1}{2}}[v_3^2]^{\frac{1}{2}} \int_o^t (t-\tau)\{_L R_{13}(\tau) + {}_L R_{31}(\tau)\}d\tau \qquad (2.7)$$

(II)

$$[X_2^2(t)] = 2[v_2^2] \int_o^t (t-\tau)_L R_{22}(\tau)d\tau \qquad \text{and} \qquad (2.8)$$

$$[X_3^2(t)] = 2[v_3^2] \int_o^t (t-\tau)_L R_{33}(\tau)d\tau \ . \qquad (2.9)$$

Notice that the shear-enhanced term (I) in Equation 2.6 and Equation 2.7 dominate the long term dispersion ($t > {}_L T_{11}$). The turbulent shear correlation contribution terms, (III) in Equation 2.6 and (II) in Equation 2.7, are often neglected in the absence of data for ${}_L R_{ij}$, $i \neq j$. Term (II) in Equations 2.6, 2.8 and 2.9 are the Taylor's diffusion terms. Two asymptotic cases can be identified from Equation 2.6 through Equation 2.9 if one neglects the turbulent shear correlation contribution terms.

(i) Within a very short dispersive range, ${}_L R_{ii}(\tau)$ approaches unity for a very short time lag so that

$$[X_1^2(t)] = \frac{2}{3}\Gamma^2[v_3^2]t^3 + [v_1^2]t^2 \ ,$$
$$[X_2^2(t)] = [v_2^2]t^2 \ , \qquad (2.10)$$
$$[X_1(t)X_3(t)] = \Gamma[v_3^2]t^2 \ , \text{ and}$$
$$[X_3^2(t)] = [v_3^2]t^2 \ .$$

(ii) For a long range dispersion, the integral of ${}_{L}R_{ii}(\tau)$ approaches a constant value, ${}_{L}T_{ii}$, and ${}_{L}R_{ii}(\tau)$ approaches zero so that

$$[X_1^2(t)] \cong \frac{2}{3}\Gamma^2[v_3^2]\,T_{33}\,t^3 + [v_1^2]\,T_{11}\,t\ ,$$

$$[X_2^2(t)] \cong 2[v_2^2]_L T_{22} t\ , \qquad (2.11)$$

$$[X_3^2(t)] \cong 2[v_3^2]_L T_{33} t\ ,\ \text{and}$$

$$[X_1(t)X_3(t)] \cong \Gamma[v_3^2]_L T_{33} t^2\ .$$

In particular, for asymptotic forms of the displacement measures, Corrsin (1959) reported that

$$[X_1^2(t)] \cong \frac{2}{3}\Gamma^2[v_3^2]_L T_{33} t^3 \quad \text{and}$$

$$(2.12)$$

$$[X_1(t)X_3(t)] \cong \Gamma[v_3^2]_L T_{33} t^2\ .$$

The mean square particle displacement has been implicitly related to the turbulent diffusivity tensor, K_{ij}, ever since the analogy between molecular diffusion and turbulent diffusion was proposed. Batchelor (1949) generalized the relationship between the time-dependent turbulent diffusivity tensor and Lagrangian autocorrelation functions through Taylor's theory for a homogeneous flow without mean shear.

$$K_{ij}(t) = \frac{1}{2}\frac{d}{dt}[X_i(t)X_j(t)]$$

$$= \frac{1}{2}\int_0^t \{{}_{L}R_{ij}(\tau) + {}_{L}R_{ji}(\tau)\}d\tau \qquad (2.13)$$

For many applications, the asymptotic value of the turbulent diffusivity suffices (Hinze, 1975)

$$K_{ii}(\infty) = \frac{1}{2}\frac{d}{dt}[X_i(t)X_i(t)]_{\tau >> {}_{L}T_{ii}} = [v_i^2]_L T_{ii}\ . \qquad (2.14)$$

Based on the equations of mass conservation and Equations 2.6, 2.7, 2.8 and 2.9, Riley and Corrsin (1974) were able to relate the turbulent diffusivity tensor to the Lagrangian velocity statistics for a simple shear flow. They revealed that in a homogeneous turbulent flow with uniform shear, the turbulent diffusivity tensor differs formally from

those for an unsheared homogeneous flow. The turbulent diffusivity tensors in a sheared homogeneous flow are

$$K_{11}(t) = [v_1^2] \int_o^t {}_L R_{11}(\tau)d\tau + \Gamma[v_1 v_3] \int_o^t \tau_L R_{13}(\tau)d\tau \qquad (2.15)$$

$$K_{13}(t) + K_{31}(t) = [v_1 v_3] \int_o^t \{{}_L R_{13}(\tau) + {}_L R_{31}(\tau)\}d\tau$$

$$+ \Gamma[v_3^2] \int_o^t \tau_L R_{13}(\tau)d\tau \qquad (2.16)$$

$$K_{22}(t) = [v_2^2] \int_o^t {}_L R_{22}(\tau)d\tau \ , \qquad \text{and} \qquad (2.17)$$

$$K_{33}(t) = [v_3^2] \int_o^t {}_L R_{33}(\tau)d\tau \ . \qquad (2.18)$$

Since it is normally not possible to measure the Lagrangian velocity v_i directly, an Eulerian RMS velocity fluctuation, $[u_i^2]$, is usually substituted for $[v_i^2]$.

2.3 Relation between Lagrangian and Eulerian Autocorrelation

The statistical treatment of turbulent diffusion requires an explicit formation for the Lagrangian autocorrelation function. Some direct measurements of Lagrangian velocity fluctuations have been made through simulation of air particle measurement by soap bubbles or by balloons (see Pasquill, 1974). Yet the evidence for correlation shape is still not convincing, quantitatively or qualitatively, because the negligible mass and zero buoyancy of an air parcel cannot be adequately simulated by a finite sized substitute particle. Since it is not feasible to measure the turbulent velocity of each fluid particle, researchers tend to estimate the Lagrangian statistics through conjectures based on physical assertions from Eulerian statistics or through diffusion experiments and Taylor's theory.

The literature on the relationship between the Lagrangian and Eulerian correlation function is quite vast. Nevertheless, the available approaches for the estimation of the Lagrangian autocorrelation can be categorized into four groups based on their salient traits.

2.3.1 Linear correlation method to calculate $_{L}R_{ij}(\tau)$

In a homogeneous turbulence the shape of the Lagrangian autocorrelation function is expected by some researchers to be similar to either an axial Eulerian cross-correlation or a single Eulerian autocorrelation function. Mickelsen (1955) conducted a mass diffusion experiment and made fixed point Eulerian velocity fluctuation measurements in the core of a pipe. He demonstrated that the Lagrangian autocorrelation function may be related to the Eulerian longitudinal cross correlation such that $_{E}R_{11}(x_1) = \frac{1}{B^2}\,{}_{L}R_{11}(\zeta)$, where $\zeta = x_1/B\sqrt{\overline{u_1^2}}$ and B varies from 0.55 to 0.725. It is clear that the relation cannot be correct near $\zeta=0$, and the expression implies that the Lagrangian autocorrelation function decays more slowly than the corresponding Eulerian value.

Gifford (1955) reported simultaneous measurements of both Lagrangian and Eulerian turbulent fluctuations in the atmosphere at a height of 300 ft. With limited data, he suspected that the Eulerian turbulent energy spectra are similar to the Lagrangian spectra but with a displacement toward higher frequency. Based on his finding, Gifford further suggested that the Lagrangian autocorrelation is well represented by an Eulerian measurement observed from a frame moving with the same velocity as the mean flow. He also remarked upon the possible importance of the turbulence intensity in the Lagrangian-Eulerian relationship.

The Lagrangian autocorrelation function is sometimes construed to be a contracted or stretched form of the Eulerian correlation function by means of an empirical factor. Hay and Pasquill (1959) hypothesized that

$$_{L}R_{ii}(\eta) = {}_{E}R_{ii}(t) \ , \qquad (2.19)$$

where $\eta = \beta t$, based on atmospheric observations. They concluded that the Lagrangian autocorrelation function decays more slowly with time than the Eulerian autocorrelation function. Furthermore, the Lagrangian autocorrelation coefficient for a particle decays with time in a similar manner to the Eulerian autocorrelation coefficient but with a different time scale β. The value proposed for β has considerable scatter, but a magnitude of 4.0, independent of wind speed and stability, is recommended. A natural consequence of Equation 2.19 is that $_{L}T_{ii} = \beta\,{}_{E}T_{ii}$. Hence β stands for the ratio of the Lagrangian to Eulerian integral time scale. It is known as Pasquill's β in the literature.

Wandel and Kofoed-Hansen (1962) examined the Lagrangian and Eulerian energy spectra for a fully developed isotropic homogeneous turbulence. They established a more complicated relation between the Eulerian and Lagrangian correlation based on the statistical theory of

"shot" noise and the Helmholtz theorem. A rough approximation in the case of smooth energy spectra indicates that $\beta \cong \frac{\sqrt{\pi/4}}{i}$, where i is the turbulence intensity, $\sqrt{\overline{u_1^2}}/U$.

Corrsin (1963a) compared the shape of Lagrangian and Eulerian energy spectra over the inertial subrange. By assuming that the total turbulent energy was identical in the Lagrangian and Eulerian system, he arrived at a theoretical prediction of β.

$$\beta = \frac{c}{i} \tag{2.20}$$

where c is a constant.

After monitoring the trajectories of tetroons and a tethered balloon system at height of 750 m, Angell (1964) observed an average value for β near 3.3 and recommended relation equal to 0.4/i for β. Angell et al. (1971) made further observations in the atmosphere near Las Vegas, Nevada, by releasing tetroons past tall towers. β was again found to have average values near 3 and varied in direct proportion to the turbulence intensity.

Snyder and Lumley (1971) performed direct measurements of Lagrangian velocity in a grid-generated turbulence field in a laboratory. The fluid particle was simulated by releasing single spherical beads with different weights and sizes. Since light particles have only small inertia and cross-trajectory effect, light-particle correlations were utilized to estimate Lagrangian fluid properties. They concluded that the Lagrangian autocorrelation function has similar shape to the Eulerian spatial correlation and that β is roughly equal to 3 when approximated by 1/i.

Turbulence measurements reported by Hanna (1981) were conducted in the daytime mixing layer near Boulder, Colorado. The average Lagrangian time scale detected was about 70 seconds for a sampling time of 15 minutes. The ratio β was found to be 1.7 and inversely proportional to turbulence intensity, $\beta = 0.7/i$.

The various values for β discussed above are summarized and compared with present wind tunnel results in Section 6.4.

2.3.2 Estimation of ${}_L R_{ij}(\tau)$ from Eulerian Space-Time Correlation

An Eulerian fixed-point time periodogram samples many different fluid points as they pass a fixed point. It is considered important in many turbulence dynamic analyses and is relatively easy to obtain. Unfortunately the conventional measurements do not relate directly to the Lagrangian statistics during turbulent diffusion.

Burgers (1951) proposed a more general Eulerian space-time correlation for the behavior of two particles separated in time and space. He suggested it as a first approximation to the true Lagrangian autocorrelation

$$ {}_{E}R_{11}(U\tau,0,0,\tau) = {}_{L}R_{11}(\tau) \quad . \tag{2.21} $$

The space-time correlation may be obtained from the envelope of a set of Eulerian space-time cross correlations of the longitudinal fluctuating velocity given the assumption of homogeneous and isotropic turbulence. This envelope which connects the peaks of the cross-correlation is interpreted as the moving Eulerian autocorrelation which would be measured by a probe traveling steadily at the mean velocity. It may be thought of as the autocorrelation of the time signal measured by a single probe in a "quasi-Lagrangian" frame of reference. Inoue (1952) and Ogura (1953) also viewed such correlation as an appropriate expression of the Lagrangian autocorrelation.

Baldwin and Walsh (1961) presented experimental data and some theoretical interpretation to support this scheme. On the other hand, Baldwin and Mickelsen (1963) found that their pipe flow data showed a systematic tendency for the Eulerian space-time correlation integral scale, ${}_{S}T_{11} = \int_{0}^{\infty} {}_{E}R_{11}(U\tau,0,0,\tau)d\tau$, to be greater than ${}_{L}T_{11}$ by factors ranging from about 2 to 4 as $\overline{u_1^2}$ increased. Furthermore, their results yielded rough values for β varying from 4 to 18 depending on the mean flow rate.

The advantage of the space-time correlation method is that it preserves the asymptotic value of a Lagrangian autocorrelation function such that the Lagrangian coefficient apparently approaches zero monotonically, whereas the Eulerian correlation dips below zero to slightly negative values before approaching a zero value asymptote. The shortcoming in principle of using the moving Eulerian autocorrelation as the true Lagrangian autocorrelation, as pointed out by Corrsin (1963b), is that the Lagrangian velocity is effectively being approximated by sampling along an unknown random trajectory.

An impediment to the use of such a scheme was revealed by Shlien and Corrsin (1974) in their grid-generated turbulence experiment. They estimated the Lagrangian autocorrelation function from diffusion measurements by double differentiating Taylor's relationship. The estimated Lagrangian statistics were compared with results of Eulerian statistics measurements, although the technique for estimating the Lagrangian autocorrelation was questionable. They concluded that the moving Eulerian velocity autocorrelation function was different in shape from the Lagrangian autocorrelation function based on the disparity between the micro- and integral scale ratios. Further results of their work are compared in Section 6.4 of this study.

2.3.3 Probability method to estimate ${}_{L}R_{ij}(\tau)$

A probability method to estimate ${}_{L}R_{ij}(\tau)$ was derived from Corrsin's (1959) conjecture of Lagrangian autocorrelation function and later modified by Baldwin and Johnson (1972). An Eulerian expression for ${}_{L}R_{ij}(\tau)$ was derived by Corrsin by assuming that u_i and r_k are randomly related through a joint probability function $P(u_i(t),\ u_i(t+\tau),r_k)$,

$$L^{R_{ij}}(\tau) = \int_{-\infty}^{\infty}\int\int\int\int\int \left\{ \int_{-\infty}^{\infty}\int\int\int \frac{u_i(t)u_j(t+\tau)}{u_i^2}\,\delta(x_k-r_k)dr_k \right\}$$

$$P(u_i(t),u_j(t+\tau),r_k)du_i(t)du_j(t+\tau)dr_k \qquad (2.22)$$

where x_k is the Eulerian position and r_k is the Lagrangian position of fluid particle, k=1,2,3. In the limit of very large time τ, there is no reason to expect a statistical connection between r_k and $u_i(t)$ so that

$$L^{R_{ij}}(\tau) = \int_{-\infty}^{\infty}\int\int\int {}_E R_{ij}(r_k,\tau)P(r_k,\tau)dr_k \ . \qquad (2.23)$$

$P(r_k,\tau)$ is visualized as the probability of finding a fluid particle injected at the origin in the region between x_k and x_k+dx_k at any time τ. Equation 2.23 is commonly referred to as "Corrsin's conjecture" or as a mathematical expression of the Independence Hypothesis.

Intuitively, the velocities should be more persistent along the path of a fluid particle than a fixed observation point or a moving observation point. Equation 2.23 clearly suggested a contradictory result, i.e.,

$$L^{R_{ij}}(\tau) \leq {}_E R_{ij}(r_k,\tau) \int_{-\infty}^{\infty}\int\int\int P(r_k,\tau)dr_k$$

$$\leq {}_E R_{ij}(r_k,\tau) = {}_E R_{ij}(r_k,\tau) \qquad (2.24)$$

However, Kraichnan (1963) supported the opposite expectation. He argued that the rate of change of the Lagrangian velocity with time is determined by the rate of spatial variation and magnitude of the Eulerian velocity. Slower variation of the Lagrangian velocity implies slower changes of the Eulerian velocity because the fluid particle must travel a nearly straight line with low acceleration. On the other hand, a slower change of the Eulerian velocity does not consequently imply reduction in the variation of the Lagrangian velocity; because the Eulerian velocity may exhibit an intermittent period of slow local variation, which is not necessarily true for the whole flow field experienced by the particle. Nevertheless, at a high Reynolds number Corrsin (1963a) found that the difference is not significant. Equation 2.23 is also supported by Kraichnan (1970) from his direct interaction approximation.

If Equation 2.23 is transformed into the frequency domain, one finds that

$$R_{ij}(\tau) = \frac{1}{8\pi^3} \iiint \left(\iiint {}_{E}R_{ij}(r_k,\tau)\exp\{-i\kappa_\ell r_k\}dr_k \right)$$

$$\exp\{-\frac{\kappa_\ell^2}{2}[X_i(\tau)X_j(\tau)]\}d\kappa_\ell \qquad (2.25)$$

where κ is the three-dimensional wave number.

Saffman (1963) assumed a spectrum functional form of an Eulerian space-time correlation and an exponential decaying function for r_k. He obtained an ordinary non-linear differential equation which relates the Lagrangian autocorrelation and the mean square particle displacement in an isotropic homogeneous turbulence. Some interesting conclusions may be found in Saffman's work.

1. The scale ratio β was found to be $\frac{0.8}{i}$ in low turbulent flow. Since the Eulerian integral scale was defined by him as $\int_0^\infty {}_{E}R_{ii}(0,Ut,0,t)dt$, it implied that a lateral space-time integral scale was employed. The adoption of mean velocity U in the lateral direction seems somehow unrealistic.

2. The Lagrangian autocorrelation was found to decay algebraically but not exponentially and the asymptotic value approached the Eulerian space-time correlation.

3. The Independence Hypothesis would be exact if those realizations of the turbulence which displace the particle by a given amount in a given time were an unbiased sample of the ensemble of all realization. In a grid-generated turbulence the sample of realizations is not asymptotically unbiased; therefore, the Independence Hypothesis is not expected to be valid in such flow.

By physical reasoning, Philip (1967) proposed a Lagrangian-Eulerian relationship parallel to Equation 2.23. He employed a modified Gaussian function for the general Eulerian space-time correlation because it simplified the rather difficult computation which the independence hypothesis involved, i.e.,

$${}_{E}R_{11}(x_1,\rho;\tau) = \exp\{-\frac{\pi}{4}\left(\frac{x_1^2+3.138\rho^2}{L^2} + \frac{t^2}{{}_{S}T_{11}^2}\right)\} \qquad (2.26)$$

where $\rho = (x_2^2+x_3^2)^{\frac{1}{2}}$. L and ${}_{S}T_{11}$ are integral scales of Eulerian space-time correlation in space and time, respectively. The scale

ratio β was found to be $(1 + \alpha^2/i^2)^{\frac{1}{2}} F(\alpha)$, where $\alpha = \frac{[u_1^2]^{\frac{1}{2}} {}_S T_{11}}{L}$ and $F(\alpha) = {}_L T_{11}/{}_S T_{11}$. Functions like Equation 2.26 represent an Eulerian space-time correlation normalized by the integral scale of itself. Such approximation concerns only the integral time scale instead of the functional form of the Lagrangian autocorrelation. Consequently, Philips' analysis shows that the predicted time scale ${}_L T_{11}$ is insensitive to the imprecision of Equation 2.26.

Baldwin and Johnson (1972) examined the Independence Hypothesis in further detail. Since their work is closely related to the present analysis, their ideas will be discussed separately in Section 3.2.

The Independence Hypothesis was tested by Peskin (1974) in two-and three-dimensional numerical simulated flow fields. The Lagrangian field was determined by tracking 800 particles for 800 time steps twice. The mean square particle displacement from a directly measured Lagrangian autocorrelation was compared with Equation 2.1 to ensure a correct simulation. The Eulerian field was generated by solving the basic equations of velocity and stream function with periodic boundary conditions. The independence hypothesis incorporating a Gaussian probability density function was found to reproduce the Lagrangian autocorrelation function in detail but to have a tendency for overestimation in two-dimensional flow. The overestimation may be reduced by utilizing the computed probability density function from simulation. The calculated Lagrangian autocorrelation agreed with predictions from Independence Hypothesis methods for a three-dimensional turbulence field. Figure 2.1 displays the result reported by Peskin.

Weinstock (1976) was able to derive the independent hypothesis by expanding the Lagrangian trajectory of a fluid particle in terms of its Eulerian ensemble average. Furthermore, he introduced a correction term to the Lagrangian autocorrelation by dividing the probability of finding a fluid particle into an average part and a fluctuating part. He then concluded that the Independence Hypothesis is valid when the turbulent velocity fluctuation is low and satisfies

$$[u_i^2]^{\frac{3}{2}} \gg [u_i(x_i,0)u_i(x_i,0)u_i(x_{i_o},0)] \quad ,$$

where x_{i_o} is the initial particle position.

2.3.4 Other methods

A method to estimate the Lagrangian autocorrelation from Eulerian velocity products was proposed by Koper et al. (1978). The method is based on averaging the Eulerian velocities along the Lagrangian trajectory. The Lagrangian autocorrelation is approximated in a turbulence flow field as a summation of Eulerian cross-correlations between velocities and velocity derivatives, after averaging over trajectory,

particle-space and a reference plane. If the correlations among velocity derivatives and velocity can be ignored, the Lagrangian-Eulerian autocorrelation may be expressed as

$$ {}_{L}R_{ij}(S;\tau) \cong \frac{1}{V} \iiint {}_{E}R_{ij}(x_k,\tau)dx_k \ , $$

where S is the reference plane in the flow field and V is the volume of the integration domain.

The variation of the resulting reference-point Lagrangian autocorrelation coefficient with increasing time delay is depicted in Figure 4 of Koper et al. (1979).

Notice that in a simplified case, their method coincides with the probability method stipulating a uniform weighting function. In an isotropic homogeneous turbulent flow the Eulerian autocorrelation is independent of its position and direction within the domain of the average flow field. The method implies ${}_{L}R_{11}(\tau) = {}_{E}R_{11}(\tau)$ with $\beta=1.0$. In addition, since the derivative of turbulent velocity is not convenient or normally measured precisely, such a scheme remains more academic than practical.

Lee and Stone (1983) assumed that the Eulerian space-time correlation may be approximated by the product of an Eulerian convective correlation and an autocorrelation function for a small time step, δt, so that $\delta x_1 = U\delta t$ and

$$ {}_{E}R_{11}(\delta x_1,0,0;\delta t) = \exp\{-\delta x_1 - U\delta t/L\}\exp\{-\delta t/{}_{S}T_{11}\} \qquad (2.27) $$

They also assumed that the Lagrangian autocorrelation may be approximated by the Eulerian space-time correlation for a small time step during a Monte Carlo simulation of particle velocity,

$$ v_1(t+\delta t) = v_1(t)\,{}_{E}R_{11}(\delta x_1,0,0;\delta t) + v_1' \ . \qquad (2.28) $$

From Equations 2.27 and 2.28, an expression for β was obtained,

$$ \beta = \left(1 + \frac{[u^2]_S T_{11}}{L}\right)\Big/\left(1 + \left(\frac{8}{\pi}\right)^{\frac{1}{2}} [u_1{}^2]_S T_{11}/L\right) \ . $$

A rough estimation of β in low turbulence flow yields $\beta \simeq \frac{0.4}{i}$. One notices that the major concern of their analysis is the integral scale rather than the shape of the Lagrangian autocorrelation. However, they provide an approximation for the Lagrangian-Eulerian relation.

2.4 The Eulerian Space-Time Correlation

Turbulent flow has been described as an irregular fluid motion which is three-dimensional, continuous, diffusive and dissipative in nature. It forms such a complicated mathematical problem that its solution depends heavily on experimental data. A statistical approach to describe the mean motion of turbulent phenomenon seems to be most appropriate. The double velocity correlation function, namely the Eulerian space-time correlation, may be the most appropriate function to examine the structure of turbulence and its evolution in time (Townsend, 1976). The previous section confirms that the Lagrangian auto-correlation is strongly related to the Eulerian space-time correlation.

Pioneer correlation measurements of the space-time correlations in a turbulent flow were produced by Favre and his co-workers (1957, 1958, 1965, 1967). They performed measurements downstream of a grid, in a turbulent boundary layer and in a turbulent jet; both had wall pressure fluctuations. A brief summary of their experimental results reveals that:

1. The longitudinal Eulerian space-time correlation, $E^{R}_{11}(dx_1,0,0;\tau)$, reaches a maximum with an optimum delay time, $\tau_m = \frac{dx_1}{U}$, where dx_1 is the separation distance between two fixed points and U is the convective velocity.

2. The transverse Eulerian space-time correlation, $E^{R}_{11}(0,0,dx_3;\tau)$, for two points on a line perpendicular to the mean flow direction, τ_m is not zero but proportional to the separation from the boundary. However, τ_m is small when compared with the time required for movement with the mean flow over the same range dx_3.

3. In a filtered turbulence field, limitation to higher frequency data results in substantially lower correlation which implies the smaller scale eddies contribute less to the total turbulent energy. Larger separation between two points reduces the contribution of the higher frequency oscillations dramatically.

4. The space-time correlation due to the diffusion effect, i.e., the Lagrangian probability density function of particle displacement, was proposed by Favre as

$$E^{R}_{11}(x_1,0,0;t) = \int_{-\infty}^{\infty}\iiint E^{R}_{11}(X_1,X_2,X_3)\cdot\exp\{-\frac{(x_1-X_1-ut)^2}{2[u_1^2]t^2} - \frac{X_2^2+X_3^2}{2[u_1^2]t^2}\}$$

$$\cdot \frac{dX_1dX_2dX_3}{(2\pi[u_1^2]t^2)^{3/2}} , \qquad (2.29)$$

where the general Eulerian space correlation is

$$R(X_1,X_2,X_3) = \frac{f(X)-g(X)}{X^2} X_1^2 + g(X) \text{ , and}$$

$$X = (X_1^2 + X_2^2 + X_3^2)^{\frac{1}{2}} ,$$

$$f(X) = R_{11}(X,0,0;0) \text{ , and} \qquad (2.30)$$

$$g(X) = R_{11}(0,X,0;0) .$$

The computed correlation from Equations 2.29 and 2.30 was compared with the experimental results. The comparison is considered good though the measured data appears to be slightly lower for shorter time delay and higher than the computed value for longer time delay.

Champagne et al. (1970) and later Harris et al. (1977) conducted measurements in a nearly homogeneous turbulent shear flow. Some observations may be made from their experiments:

1. The optimum delay time may be approximated by the mean convective time in a uniform shear flow.

2. In a situation such that the turbulent energy appears to reach a steady asymptotic state, the stationarity but not homogeneity may hold in the Eulerian frame convected with the mean flow.

3. The longitudinal and vertical two-point space-time correlations with separations in streamline direction, $_{E}R_{11}(U\tau,0,0;\tau)$ and $_{E}R_{22}(U\tau,0,0;\tau)$, were found to be similar in shape.

Comte-Bellot and Corrsin (1971) reported space-time correlation measurements in a roughly isotropic grid-generated uniform flow. Correlations with the two velocity signals pre-conditioned by either a narrow- or a full-band frequency filter were calculated. The matched narrow-band filters were designed to examine the frequency dependence of velocity correlations. The correlation coefficients increased as the wave number decreased which confirms that larger eddies contribute more to the total turbulent energy. A rescaling formula which depends on

wave number and time was suggested to collapse narrow-band velocity correlations upon full-band velocity correlation.

Measurements of the space-time correlation in the atmosphere are rather rare. Attempts to measure such information have been made by Wacongne and Baliano (1982). They performed two-point simultaneous measurements of the velocity fluctuation at a given height in the atmospheric boundary layer. However, the separation distances were too short, less than 0.5 m, to obtain any meaningful results. The results fall between 1.0 and 0.95 as might be expected.

2.5 Diffusion Equation

Considering the mass conservation of a scalar species over fluid control volume but neglecting molecular diffusion, one obtains

$$\frac{\partial C}{\partial t} = - \frac{\partial}{\partial x_i} UC \ . \tag{2.31}$$

By Reynolds averaging and introducing the eddy diffusivity,

$$K_{ij} = - \frac{\overline{U\ C}}{\frac{\partial \bar{C}}{\partial x_j}} \ , \tag{2.32}$$

the conventional diffusion equation is obtained as

$$\frac{\partial \bar{C}}{\partial t} + \frac{\partial (\bar{U}\ \bar{C})}{\partial x_i} = \frac{\partial}{\partial x_j} \left(K_{ij} \frac{\partial \bar{C}}{\partial x_j} \right) \ , \tag{2.33}$$

where K_{ij} is generally a function of spatial variation and time evolution. Knowledge concerning K_{ij} is rather limited. Simplification of Equation 2.33 is generally necessary to obtain any solution. The most plausible simplification assumes that the principal axes of the diffusivity tensor are identical with the Eulerian coordinate axes. Furthermore, if K_{ij}, like all other turbulence characteristics in a planewise homogeneous flow, depends only on the vertical coordinate x_3, then Equation 2.33 would be

$$\frac{\partial \bar{C}}{\partial t} + U(x_3) \frac{\partial \bar{C}}{\partial x_1} = K_{11}(x_3) \frac{\partial^2 \bar{C}}{\partial x_1^2} + K_{22}(x_3) \frac{\partial^3 \bar{C}}{\partial x_2^2} + \frac{\partial}{\partial x_3} \left(K_{33}(x_3) \frac{\partial \bar{C}}{\partial x_3} \right)$$

$$+ K_{13}(x_3) \frac{\partial^2 \bar{C}}{\partial x_1 \partial x_3} + \frac{\partial}{\partial x_3} \left(K_{31}(x_3) \frac{\partial \bar{C}}{\partial x_1} \right) \ , \tag{2.34}$$

where the mean velocity exists only along the x_1-direction and is a function of x_3.

Equation 2.34 is generally presented in a more simplified form by neglecting the K_{13} and K_{31} terms such that

$$\frac{\partial \bar{C}}{\partial t} + U(x_3)\frac{\partial \bar{C}}{\partial x_1} = K_{11}(x_3)\frac{\partial \bar{C}}{\partial x_1^2} + K_{22}(x_3)\frac{\partial^2 \bar{C}}{\partial x_2^2} + \frac{\partial}{\partial x_3}\left(K_{33}(x_3)\frac{\partial \bar{C}}{\partial x_3}\right) . \tag{2.35}$$

However, as noted by Monin and Yaglom (1971), there is some evidence from the atmosphere that K_{13} cannot be treated as a zero term. Indeed, most likely K_{13} is about three times as great as K_{33}. Fortunately, this does not necessary imply that the last two terms in Equation 2.34 are always significant. Nevertheless, Equation 2.34 would be more appropriate than Equation 2.35 for calculations of the diffusion from an instantaneous source (Gee and Davis, 1964).

A number of solutions to Equation 2.35 are available for special cases. If all K_{ii}'s and U's are constants, independent of spatial coordinates and time, Equation 2.35 resembles the Fickian equation for molecular diffusion. This yields the well-known Gaussian solution,

$$\bar{C}(x_1,x_2,x_3,t) = \frac{Q}{(4\pi t)^{\frac{3}{2}}(K_{11}K_{22}K_{33})^{\frac{1}{2}}} \cdot \exp\{-\frac{1}{4t}\left(\frac{(x_1-U\,t)^2}{K_{11}} + \frac{x_2^2}{K_{22}} + \frac{x_3^2}{K_{33}}\right)\} \tag{2.36}$$

where Q is the source strength, $Q = \iiint_{-\infty}^{\infty} \bar{C}(x_1,x_2,x_3,t)dx_1dx_2dx_3$.

In a uniform shear flow where $U = \Gamma x_3$, Equation 2.35 was solved by Novikov (1958), as presented by Monin and Yaglom (1971), for an absorbing boundary condition. In terms of a uniform shear flow, $U = \bar{U}(1 + \Gamma/\bar{U}x_3)$, i.e.,

$$\bar{C}(x_1,x_2,x_3,t) = \frac{1}{(4\pi t)^{\frac{3}{2}}\{(K_{11}+\Gamma^2K_{33}t^2/12)K_{22}K_{33}\}^{\frac{1}{2}}}$$

$$\cdot \exp\{-\frac{(x_1-\bar{U}\,t-\Gamma x_3 t/2)^2}{4K_{11}t+\Gamma^2K_{33}t^3/3} - \frac{x_2^2}{4K_{22}t} - \frac{x_3^2}{4K_{33}t}\} . \tag{2.37}$$

For a continuous point source release, in a stationary flow field, the differential equation becomes

$$U(x_3)\frac{\partial \bar{C}}{\partial x_1} = \frac{\partial}{\partial x_1}\left(K_{11}\frac{\partial \bar{C}}{\partial x_1}\right) + \frac{\partial}{\partial x_2}\left(K_{22}\frac{\partial \bar{C}}{\partial x_2}\right) + \frac{\partial}{\partial x_3}\left(K_{33}\frac{\partial \bar{C}}{\partial x_3}\right) . \tag{2.38}$$

The second term for longitudinal diffusion was shown to be negligible by Walters (1964).

The diffusion equation for a continuous line source in a uniform shear flow is

$$\bar{U}\left(1 + \frac{\Gamma x_3}{\bar{U}}\right)\frac{\partial \bar{C}}{\partial x_1} = \frac{\partial}{\partial x_3}\left(K_{33}\frac{\partial \bar{C}}{\partial x_3}\right) . \tag{2.39}$$

By a simple transformation to a new inertial system of coordinates the solution presented by Robert (unpublished, see Sutton (1953)) can be adopted for a ground release case,

$$\bar{C}(x_1,x_3) = \frac{3Q}{\Gamma\ \mathrm{Gamma}(2/3)}\left\{\frac{\Gamma}{9K_{33}x_1}\right\}^{2/3} \exp\left\{-\frac{\Gamma(x_3+\frac{\bar{U}}{\Gamma})^3}{9\ K_{33}x_1}\right\} . \tag{2.40}$$

The solution stated above is subject to the following boundary conditions,

$$\begin{aligned}
&K_{33} = \text{constant} ,\\
&\bar{C} \to 0 \text{ as } x_1,\ x_2 \to \infty ,\\
&\bar{C} \to \infty \text{ at } x_1 = x_3 = 0 ,\\
&K_{33}\frac{\partial C}{\partial x_3} \to 0 \text{ as } x_3 \to 0,\ x_1 > 0, \text{ and}
\end{aligned} \tag{2.41}$$

$$\int_0^\infty U\,\bar{C}(x_1,x_3)dx_3 = Q ,\ x_1 > 0 .$$

Smith (1957) derived an exact solution to the dispersion of a continuous line source in the constant shear stress region. The vertical eddy diffusivity obeys a simple power law with the power exponent conjugate to a power law velocity profile due to the constant shear stress assumption. For an elevated line source, Smith's solution for a uniform shear flow is:

$$\bar{C}(x_1,x_3) = \frac{Q\,\bar{U}}{3K_{33}x_1\Gamma}\left(1+\frac{x_3\Gamma}{\bar{U}}\right)^{\frac{1}{2}} \exp\left\{-\frac{\bar{U}^3\left(1+\Gamma\frac{x_3}{U}+1\right)^3}{9\,\Gamma^2K_{33}x_1}\right\}$$

$$\cdot\, I_{-\frac{1}{3}}\left\{\frac{2\,\bar{U}^3\left(1+\frac{\Gamma x_3}{U}\right)^{3/2}}{9\,K_{33}x_2\Gamma^2}\right\} \qquad (2.42)$$

where I represents the modified Bessel function and the origin of the coordinates is located at source height.

Equation 2.42 has a similar form to the solution proposed by Lauwerier (1953), and used by Baldwin and Johnson (1972), but it differs from Lauwerier's solution by a K_{33} term in the denominator and the modified Bessel function. The index of Bessel function changes sign from negative to positive when the boundary conditions are changed from Neuman to Dirichlet problem. A dimensional inconsistency is included in Lauwerier's analysis; hence, this equation is incorrect.

It is reasonable to assume a Gaussian distribution of the mean concentration field in the transverse cross-section since the diffusion equation contains only the single derivative with respect to x_2, $K_{22}\frac{\partial^2\bar{C}}{\partial x_2^2}$, and K_{22} is independent of x_2. Hence,

$$\bar{C}(x_1,x_2,x_3) \cong \frac{1}{\sqrt{2\pi\sigma_2}}\exp\left\{-\frac{x_2^2}{2\sigma_2^2}\right\}\cdot\bar{C}(x_1,x_3)\ ;$$

i.e.,

$$\bar{C}(x_1,x_2,x_3) \cong \frac{Q\bar{U}\left(1+\frac{x_3\Gamma}{\bar{U}}\right)^{1/2}}{3K_{33}x_1\Gamma(4\pi)^{\frac{1}{2}}\left(\frac{K_{22}x_1}{\bar{U}}\right)^{\frac{1}{2}}}\cdot I_{-\frac{1}{3}}\left\{\frac{2\bar{U}^3\left(1+\frac{\Gamma x_3}{\bar{U}}\right)}{9K_{33}x_1\Gamma^2}\right\}$$

$$\cdot\exp\left\{-\frac{x_2^2\,\bar{U}}{4K_{22}x_1}-\frac{\bar{U}\left(1+\left(\frac{\Gamma x_3}{\bar{U}}+1\right)^3\right)}{9\,\Gamma^2K_{33}x_1}\right\}. \qquad (2.43)$$

Equation 2.43 implies that $\bar{C}(x_1,x_2,x_3) \sim x_1^{-3/2} K_{22}^{-1/2} K_{33}^{-1} x_3^{-1/2}$ agrees with Walters' (1965) asymptotical solution employing a conjugate power law assumption.

A more generalized solution of the diffusion problem was presented by Yeh (1975) with the same boundary conditions as Equation 2.41. The solution was presented in terms of Green's functions for the Dirichlet boundary condition, $C(x_1,x_2,x_3) = b_1(x_1,x_2,x_3)$ at the boundary, and Neumann boundary condition, $\frac{\partial C(x_1,x_2,x_3)}{\partial x_3} = b_2(x_1,x_2,x_3)$ at the boundary. It is applicable under a power law approximation for the mean velocity and diffusivities such that

$$U(x_3) = ax_3^p ,$$

$$K_{33} = bx_3^n , \text{ and} \qquad (2.44)$$

$$K_{22} = B(x_3)x_3^n .$$

where x_3 is measured from the surface.

The method was extended to a non-Gaussian diffusion model for a turbulent shear flow by modification of K_{22} in view of the statistical theory where $K_{22} = \frac{1}{2}\frac{d\sigma_2^2}{dt} \cong \frac{1}{2} U \frac{d\sigma_2^2}{dx_1}$. An analytic solution was also obtained by Huang (1979). For an elevated point source,

$$\bar{C}(x_1,x_2,x_3) = \frac{Q}{\sqrt{2\pi}\,\sigma_2} \cdot \frac{(x_3 x_{3s})^{(1-n)/2}}{b(\alpha)x_1} \cdot \exp\{-\frac{(x_2-x_{2s})^2}{2\sigma_2^2}\}$$

$$\cdot \exp\{-\frac{a(x_3^\omega + x_{3s}^\omega)}{b\,\omega^2\,x_1}\} \cdot I_{-\nu}\{\frac{2a(x_3 x_{3s})^{\frac{\omega}{2}}}{b\,\omega^2\,x_1}\} , \qquad (2.45)$$

where x_{is} is the coordinate of the point source,

$$\omega = 2.0 + p - n, \text{ and}$$

$$\nu = (1-n)/\omega.$$

In a uniform shear flow with constant diffusivity, n=0 and $\sigma_2 = (2x_1K_{22}/U)^{\frac{1}{2}}$, Equation 2.45 is thus identical to Equation 2.43 as shown by a simple transformation of coordinates where $x_{2s} = 0$ and $x_{3s} = \bar{U}/\Gamma$.

For a point source on the ground, Equation 2.45 reduces to

$$\bar{C}(x_1,x_2,x_3) = \frac{QA_1(\omega,\bar{\beta})}{\sqrt{2\pi\sigma}_2 x_1^{\bar{\beta}}} \exp\{-\frac{x_3^{\omega}+x_5^{\omega}}{A_2}\} \exp\{-\frac{(x_2-x_{2s})^2}{2\sigma 2}\} , \quad (2.46)$$

where

$$A_1(\omega,\bar{\beta}) = \frac{\omega}{a^{v}(b\omega^2)^{\bar{\beta}}Gamma(\bar{\beta})} ,$$

$$\bar{\beta} = \frac{1+P}{\omega} , \text{ and}$$

$$A_2 = \frac{b}{a}\omega^2 x_1 .$$

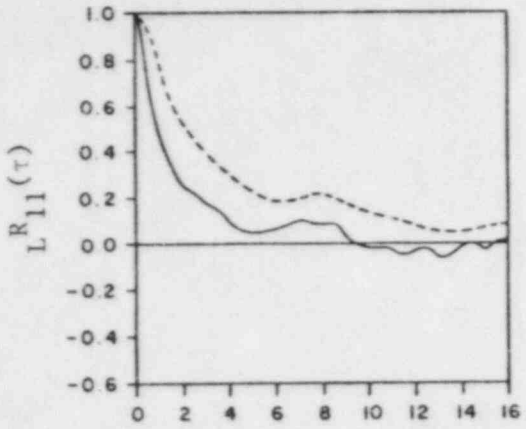

(a) $L^R_{11}(\tau)$ and Independence Hypothesis estimate (dotted curve) using Gaussian probability distribution.

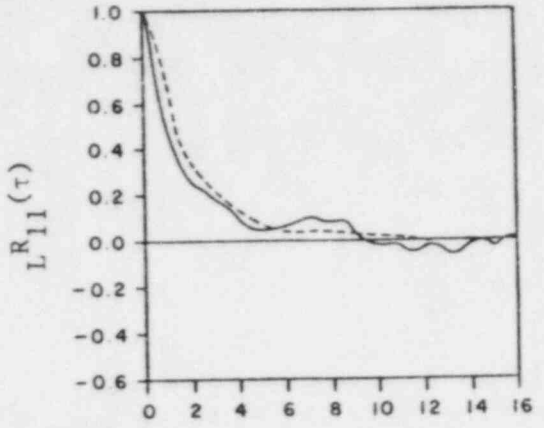

(b) $L^R_{11}(\tau)$ and Independence Hypothesis estimate (dotted curve) using truncated Gaussian probability distribution.

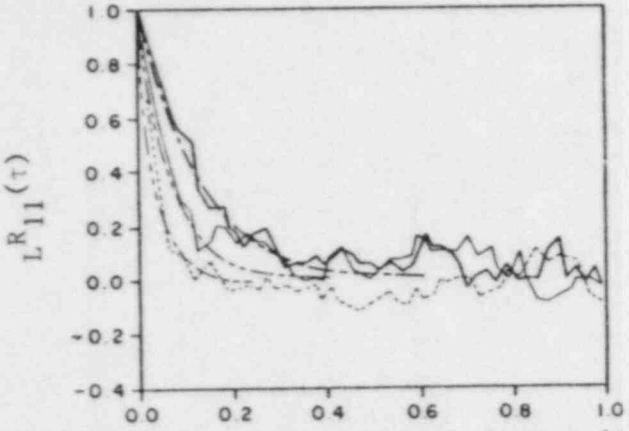

(c) Simulated Lagrangian autocorrelation (dash-dot lines are best fit exponential curve).

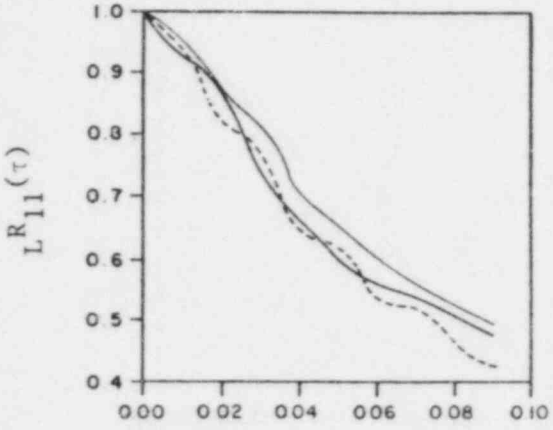

(d) Comparison of calculated $L^R_{11}(\tau)$ (heavy line) with Independence Hypothesis (light line) and Independence Hypothesis using Gaussian probability (dotted line).

Figure 2.1. Lagrangian autocorrelation function and Independence Hypothesis estimate calculated from numerical simulation.

Chapter 3

ESTIMATION OF THE LAGRANGIAN AUTOCORRELATION FUNCTION

3.1 Introduction

A statistical approach to turbulent dispersion requires knowledge of the Lagrangian velocity statistics. A method of obtaining the Lagrangian velocity statistics from Eulerian measurements is proposed in this chapter. Lagrangian autocorrelation functions are formulated in a broad sense in Section 3.2 following the independence hypothesis arguments. These arguments have been previously demonstrated to be appropriate for a homogeneous isotropic uniform flow. Derivations of earlier relations are reviewed in Section 3.3. The arguments are extended to a homogeneous non-isotropic uniform sheared turbulence field in Section 3.4. A numerical iterative procedure to compute the Lagrangian autocorrelation function by the Independence Hypothesis approach is described in Section 3.5. The application of such estimates of the Lagrangian velocity statistics for turbulent dispersion is examined in Section 3.6.

Predictions from the approach will be discussed and compared with laboratory results in Chapter 6.

3.2 General Formulation of the Lagrangian Autocorrelation

The relationship between the Lagrangian autocorrelation and the general Eulerian space-time correlation has been outlined as Equation 2.23 in Section 2.3.3. In this section, the Lagrangian autocorrelation function is formulated from the aspect of Lagrangian kinematics of a fluid particle.

In a stationary turbulent flow field, the general Eulerian space-time correlation is defined as

$$ {}_{E}R_{ij}(x_i,x_j,x_k;\tau) = \frac{[u_i(x_{io},x_{jo},x_{ko};0) \cdot u_j(x_i,x_j,x_k;\tau)]}{[u_i^2(x_{io},x_{jo},x_{ko};0)]^{\frac{1}{2}}\,[u_j^2(x_i,x_j,x_k;\tau)]^{\frac{1}{2}}} , \quad (3.1) $$

and the Lagrangian autocorrelation is defined as:

$$ {}_{L}R_{ij}(x_{io},x_{jo},x_{ko};\tau) = \frac{[v_i(x_{io},x_{jo},x_{ko};t)\; v_j(x_{io},x_{jo},x_{ko};t+\tau)]}{[v_i^2(x_{io},x_{jo},x_{ko};t)]^{\frac{1}{2}}[v_j^2(x_{io},x_{jo},x_{ko};t+\tau)]^{\frac{1}{2}}} , \quad (3.2) $$

where $v_i(x_{io},x_{jo},x_{ko};t)$ is the Lagrangian velocity component in the i^{th} direction of a particle which passes though position (x_{io},x_{jo},x_{ko}).

The Lagrangian autocorrelation may be expressed in terms of the Eulerian correlation, i.e.,

$$L^{R}_{ij}(x_{io},x_{jo},x_{ko};\tau) = \frac{[u_i(x_{io},x_{jo},x_{ko};0)u_j(X(x_{io},x_{jo},x_{ko};\tau);\tau)]}{[u_i^{\,2}(x_{io},x_{jo},x_{ko},0)]^{\frac{1}{2}}[u_j^{\,2}(X(x_{io},x_{jo},x_{ko};\tau);\tau)]^{\frac{1}{2}}}$$

or

$$L^{R}_{ij}(x_{io},x_{jo},x_{ko};\tau) = \iiint \frac{[u_i(x_i,x_j,x_k;0)u_j(x_i,x_j,x_k;\tau)]}{[u_i^{\,2}(x_{io},x_{jo},x_{ko};0)]^{\frac{1}{2}}[u_j^{\,2}(x_i,x_j,x_k,\tau)]^{\frac{1}{2}}} \cdot$$

$$\delta(X(x_{io},x_{jo},x_{ko};\tau)-(x_i,x_j,x_k;\tau))dx_i dx_j dx_k \,, \qquad (3.3)$$

where X is the position of a particle at time τ which was located at (x_{io},x_{jo},x_{ko}) earlier, and δ denotes the Dirac delta function of its argument. In the limit of large τ, we expect there is no relation between the fluctuating velocity u_i and the particle position X. Hence $\delta(X(x_{io},x_{jo},x_{ko};\tau)-(x_i,x_j,x_k))$ may be expressed as a joint normal distribution $P_X(X,\tau)$, i.e.,

$$L^{R}_{ij}(\tau) = \iiint {}_{E}R_{ij}(x_i,x_j,x_k;\tau)P_X(X,\tau)dx_i dx_j dx_k \,. \qquad (3.4)$$

(This is the Independence Hypotnesis.)

One notices that the above expression is valid only when the system is infinitely large so that the particle displacements X_i are all less than the size of the system (Weinstock, 1976).

Consider the joint normal distribution where

$$P_X(X,\tau) = (2\pi)^{-\frac{3}{2}} \Sigma^{-\frac{1}{2}} \exp\{-\tfrac{1}{2} X \Sigma^{-1} X^T\} \,,$$

and $X = (X_1,X_2,X_3)$ and (3.5)

$$\Sigma = \begin{bmatrix} X_1^{\,2}(\tau) & X_1(\tau)X_2(\tau) & X_1(\tau)X_3(\tau) \\ X_2(\tau)X_1(\tau) & X_2^{\,2}(\tau) & X_2(\tau)X_3(\tau) \\ X_3(\tau)X_1(\tau) & X_3(\tau)X_2(\tau) & X_3^{\,2}(\tau) \end{bmatrix} .$$

Equation 3.5 for $P_X(X,\tau)$ introduces a great deal of mathematical complexity to the formulation of the Lagrangian autocorrelation. Further simplifications of the problem are necessary!

Frenkiel (1953) suggested that the probability density function of finding a fluid particle in a spherical cloud should preserve a Gaussian form. It seems that asymptotically the probability density function is not only joint-normally distributed, but it should be independent in each direction such that

$$P_X(X,\tau) = \frac{1}{\sqrt{2\pi}^3 [X_1^2(\tau)]^{\frac{1}{2}} [X_2^2(\tau)]^{\frac{1}{2}} [X_3^2(\tau)]^{\frac{1}{2}}} \cdot$$

$$\exp-\{ \frac{x_1^2}{2[X_1^2(\tau)]} + \frac{x_2^2}{2[X_2^2(\tau)]} + \frac{x_3^2}{2[X_3^2(\tau)]} \} . \qquad (3.6)$$

In accordance with the recent development of the dispersion tensor $[X_i(\tau)X_j(\tau)]$ by Riley and Corrsin (1974), the turbulent flow field is further constrained in a homogeneous uniform shear flow. The homogeneity requires invariance conditions with respect to the x_1x_3 plane such that ${}_LR_{12}(\tau) = {}_LR_{21}(\tau) = [X_1(\tau)X_2(\tau)] = [X_2(\tau)X_3(\tau)] = 0$ in a uniform shear flow.

However, $[X_1(\tau)X_3(\tau)]$ cannot be ignored in a uniformly sheared flow because it increases with time significantly more rapidly than the variance of transverse displacements. This implies that the elliptic cloud evolves with two mutually correlated displacements along the x_1 and x_3 axes.

Based on Equation 3.5 and Riley and Corrsin's finding, the Lagrangian autocorrelation function may be estmated from four integral equations iterated simultaneously with Taylor's Equation. The system of equations is

$${}_LR_{11}(\tau) = \iiint \frac{E^{R_{ij}}(x_1,x_2,x_3;\tau)}{\sqrt{2\pi}\ \ \Sigma} \exp-\{x\Sigma x^T\} dx_1 dx_2 dx_3 , \qquad (3.7)$$

where

$$\Sigma = \begin{bmatrix} [X_1^2(\tau)] & 0 & [X_1(\tau)X_3(\tau)] \\ 0 & [X_2^2(\tau)] & 0 \\ [X_1(\tau)X_3(\tau)] & 0 & [X_3^2(\tau)] \end{bmatrix},$$

$$x = (x_1' - \Gamma t x_3', x_2', x_3') \ ,$$

$${}_L R_{ij}(\tau) = 0 \quad \text{for} \quad i \neq j \quad \text{except} \quad i=1,\ j=3 \ ; \ \text{and}$$

$[X_1^2(\tau)]$, $[X_1(\tau)X_3(\tau)]$, $[X_2^2(\tau)]$ and $[X_3^2(\tau)]$ retain their earlier definition in Equations 2.6, 2.7, 2.8 and 2.9, respectively.

3.3 Estimation of the Lagrangian Autocorrelation in Homogeneous Isotropic Turbulence with Constant Mean Velocity

For a stationary isotropic turbulence in which the turbulent kinetic energy is constant and independent of the resident time, Baldwin and Johnson (1972) proposed a method to estimate the Lagrangian autocorrelation function from statistical measurements of the turbulent velocity in the fixed Eulerian reference frame.

If a frame moves with mean velocity as sketched in Figure 3.1, the desired general Eulerian space-time correlation may be expressed in terms of the mean convective coordinates as

$${}_E R_{ii}(x_1, x_2, x_3; \tau) = {}_E R_{ii}(x_1' + U\tau, x_2', x_3'; \tau) \ ,$$

where x_i is the Eulerian fixed point coordinate and x_i' is the Eulerian moving frame coordinate. Baldwin and Johnson assumed that the general Eulerian space-time correlation may be expressed as the product of time correlation and space correlation in the convective moving frame,

$${}_E R_{ii}(x_1, x_2, x_3; \tau) = {}_E R_{ii}(U\tau, 0, 0, \tau)\ {}_E R_{ii}(x_1', x_2', x_3') \ . \qquad (3.8)$$

Predictions of the general Eulerian space-time correlation are rare and empirical, yet the convective Eulerian space-time correlations are well documented (see Section 2.4). Equation 3.8 represents an appropriate approximation which physically takes into account both the eddy lifetime and the eddy size effect. Baldwin and Johnson adopted an empirical function for the convective space-time correlation, $F(\frac{t}{{}_S T_{11}}) = {}_E R_{11}(U\tau, 0, 0; \tau)$, which was extracted from measurements reported by several researchers (Baldwin and Mickelsen, 1963; Favre, 1965, 1967; Frenkiel and Klebnoff, 1966; Comte Bellot and Corrsin, 1971). ${}_S T_{11}$ is the integral scale of ${}_E R_{11}(U\tau, 0, 0; \tau)$.

By virtue of the Karman-Howarth equation, $f(r) + \frac{r}{2} \frac{\partial f(r)}{\partial r} = g(r)$, where $f(r) = {}_E R_{11}(x_1', 0, 0)$ and $g(r) = {}_E R_{22}(x_1', 0, 0)$. The space correlation was obtained by assuming that homogeneity and isotropy exist in the convective moving frame such that

$${}_E R_{11}(r, \theta) = e^{-\frac{r}{L}} \left\{1 - \frac{1}{2} \frac{r}{L} (1 - \cos^2\theta)\right\} \ , \qquad (3.9)$$

where $r = (x_1'^2 + x_2'^2 + x_3'^2)^{\frac{1}{2}}$ and $\theta = \cos^{-1}\left(\frac{x_1'}{r}\right)$.

The exponential fit of $f(r)$ was simplified to $f(r) = e^{-\frac{r}{L}}$. Such an approximation does not satisfy the requirement of evenness as $r \to 0$, but over the entire range of positive correlation, the exponential function rather closely follows the best fit of the measurements. It also satisfies the inertial subrange theory as noted by Tennekes (1979). Hence, it is adopted in the present analysis.

If Lagrangian isotropy exists in a stationary isotropic turbulence, the mean square displacement tensors will be identical for all diagonal terms and vanish for all off-diagonal terms, i.e.

$$[X_1^2(\tau)] = [X_2^2(\tau)] = [X_3^2(\tau)] ,$$

$$[X_i(\tau)X_j(\tau)] = 0 , \text{ if } i \neq j ,$$

and (3.10)

$$L^{R_{11}}(\tau) = L^{R_{22}}(\tau) = L^{R_{33}}(\tau) ,$$

$$L^{R_{ij}}(\tau) = 0 , \text{ if } i \neq j .$$

A consequence of Lagrangian isotropy is a spherical symmetric probability density function of finding a fluid particle in the turbulence field such as

$$P(r,\tau) = (2\pi[X_1^2(\tau)])^{-\frac{3}{2}} \exp-\left\{\frac{r^2}{2[X_1^2(\tau)]}\right\} . \qquad (3.11)$$

Baldwin and Johnson solved Equation 3.7 in combination with Equations 3.8, 3.9 and 3.11. An analytic solution was found to be

$$L^{R_{11}}(t_*) = F_1(t_*)\left\{e^{\alpha^2 I(t_*)}[1-\mathrm{erf}\sqrt{\alpha^2 I(t_*)}][1+4\alpha^2 I(t_*) + \frac{4}{3}\alpha^4 I^2(t_*)]\right.$$

$$\left. - \frac{2}{3}\left(\frac{\alpha^2 I(t_*)}{\pi}\right)^{\frac{1}{2}}[5 + 2\alpha^2 I(t_*)]\right\} , \qquad (3.12)$$

$$I(t_*) = \int_0^{t_*}\int_0^{t_{1*}} L^{R_{11}}(t_{2*})dt_{2*}dt_{1*} ,$$

where $t_* = \frac{\tau}{S^T_{11}}$, $\alpha = \frac{[u_1^2]^{\frac{1}{2}}}{L} \frac{S^T_{11}}{}$ and

erf represents an error function of its own argument.

Similarly, ${}_L R_{22}(\tau)$ can be evaluated since the lateral space correlation is implied by Equation 3.9 as

$$ {}_E R_{22}(r,\theta) = e^{-\frac{r}{L}} \{1 - \frac{1}{2} \frac{r}{L} (1-\sin^2\theta)\} . $$

To satisfy the requirement of Lagrangian isotropy, the convective space-time correlation in the lateral direction must be

$$ F_2(t_*) = \frac{\iiint {}_E R_{11}(r,\theta) P(r,\tau) dr_1 d\theta_2 d\phi_3}{\iiint {}_E R_{22}(r,\theta) P(r,\tau) dr d\theta d\phi} F_1(t_*) . $$

After some manipulation, it is found that

$$ F_2(t_*) = \frac{H(\alpha,t_*) - \frac{1}{3} K(\alpha,t_*)}{H(\alpha,t_*) - \frac{1}{3} K(\alpha,t_*)} F_1(t_*) , \qquad (3.13) $$

where

$$ H(\alpha,t_*) = \alpha^2 I(t_*)\{-4\alpha^2 I(t_*) + \sqrt{4\pi\alpha^2 I(t_*)}(2\alpha^2 I(t_*)+1) \cdot $$

$$ (1-\mathrm{erf}\sqrt{\alpha^2 I(t_*)}) \cdot \exp(\alpha^2 I(t_*))\} $$

and

$$ K(\alpha,t_*) = \alpha^2 I(t_*)\{8\alpha^2 I(t_*)(1+\alpha^2 I(t_*)) - \sqrt{4\pi\alpha^2 I(t_*)}(4\alpha^4 I^2(t_*)+6\alpha^2 I(t_*)) \cdot $$

$$ (1-\mathrm{erf}\sqrt{\alpha^2 I(t_*)}) \cdot \exp(\alpha^2 I(t_*))\} . $$

Baldwin and Johnson have also shown that $F_2(t/S^T_{11}) \leq F_1(t/S^T_{11})$ numerically. Hence, $S^T_{22} \leq S^T_{11}$.

3.4 Estimation of the Lagrangian Autocorrelation in a Homogeneous Uniform Shear Flow

If one considers an instantaneous plume released from (x_{10}, x_{20}, x_{30}) in a uniform shear flow as shown in Figure 3.2, the plume evolves

as an ellipsoid whose size, eccentricity, and direction are time dependent due to continuity. Such behavior is well understood as a result of the shear and has been demonstrated by Elrick (1962). In lack of information about ${}_L R_{13}(\tau)$ and ${}_E R_{13}(x_1,x_2,x_3;\tau)$, the probability density function of finding a fluid particle in a moving frame travelling with a mean velocity Γx_3 may be approximated with a three-dimensional Gaussian distribution such as

$$P(x_1',x_2',x_3';\tau) = (2\pi)^{-3/2}\,([X^2(\tau)][X_2{}^2(\tau)][X_3{}^2(\tau)])^{-1/2}$$

$$\cdot\quad \exp-\{\ \frac{(x_1'-\Gamma\tau x_3)^2}{2[X_1{}^2(\tau)]} + \frac{x_2'^2}{2[X_2{}^2(\tau)]} + \frac{x_3'^2}{2[X_3{}^2(\tau)]}\ \} \qquad (3.14)$$

where $[X_i{}^2(\tau)]$ is defined as previously in Equations 2.6, 2.8 and 2.9 for i=1,2,3, respectively.

The definition of the Eulerian parameter is generalized to account for the anisotropy, i.e., $\alpha_i = \frac{[u_i^2]_S T_{11}}{L}$. Since the general space correlation in a non-isotropic flow is still unknown, the Karman-Howarth relationship is retained and the Lagrangian autocorrelation functions are assumed to be the same in all three directions. Such assumptions require that,

$$[X_1{}^2(t_*)] = L^2[\Gamma^2{}_S T_{11}{}^2\alpha_3{}^2 II(t_*)+2\alpha_1{}^2 I(t_*)]\ ,$$

$$[X_2{}^2(t_*)] = 2\alpha_2{}^2 L^2 I(t_*)\ ,$$

$$[X_3{}^2(t_*)] = 2\alpha_3{}^2 L^2 I(t_*)\ ,\ \text{and}$$

$${}_L R_{11}(t_*) = \int_{\xi=0}^{\infty}\int_{\theta=0}^{\pi}\int_{\phi=0}^{2\pi} \frac{F_1(t_*)}{\sqrt{2\pi}^3 2\alpha_2\alpha_3 I(t_*)\sqrt{\Gamma^2{}_S T_{11}{}^2\alpha_3{}^2 II(t_*)+2\alpha_1{}^2 I(t_*)}}$$

$$\exp-\{\ \frac{(\xi_1-\Gamma_S T_{11} t_*\xi_3)^2}{2(\Gamma^2{}_S T_{11}{}^2\alpha_3{}^2 II(t_*)+2\alpha_1{}^2 I(t_*))} + \frac{\xi_2{}^2}{4\alpha_2{}^2 I(t_*)} + \frac{\xi_3{}^2}{4\alpha_3{}^2 I(t_*)}\ \}\ .$$

$$\exp\{-\xi\}\cdot(1 - \frac{\xi}{2}\sin^2\theta)\cdot\xi^2\sin\theta d\phi d\theta d\xi\ , \qquad (3.15)$$

where

$$II(t_*) = \frac{2}{3}\,t_*{}^2\int_0^{t_*} {}_L R_{33}(\tau_*)d\tau - t_*{}^2\int_0^{t_*}\tau_*\,{}_L R_{33}(\tau_*)d\tau + \frac{1}{3}\int_0^{t_*}\tau_*{}^3\,{}_L R_{33}(\tau_*)d\tau_*,$$

$$\xi = \sqrt{x_1'^2+x_2'^2+x_3'^2}/L,$$

$$\xi_1 = \xi \cos\theta,$$

$$\xi_2 = \xi \sin\theta \sin\phi, \quad \text{and}$$

$$\xi_3 = \xi \sin\theta \cos\phi.$$

One should refer to Appendix A, which shows how the Lagrangian autocorrelation function in a homogeneous shear flow is obtained after a considerable mathematical manipulation:

$$L^R{}_{11}(t_*) = \frac{F_1(t_*)}{2^{\frac{5}{2}}\pi^{\frac{3}{2}}\alpha_2\alpha_3 I(t_*)A^{\frac{1}{2}}(t_*)} \int_{\theta=0}^{\pi}\int_{\phi=0}^{2\pi} [\{(\frac{\sqrt{\pi}}{4B^{\frac{3}{2}}(t_*)} + \frac{\sqrt{\pi}}{8B^{\frac{5}{2}}(t_*)})e^{\frac{1}{4B(t_*)}}$$

$$(1-\mathrm{erf}(\frac{1}{2B^{\frac{1}{2}}(t_*)})) - \frac{1}{4B^2(t_*)}\} + \frac{\sin^2\theta}{2}\{(\frac{\sqrt{\pi}}{16B^{\frac{7}{2}}(t_*)} + \frac{3\sqrt{\pi}}{8B^{\frac{5}{2}}(t_*)})e^{\frac{1}{4B(t_*)}}$$

$$(1-\mathrm{erf}(\frac{1}{2B^{\frac{1}{2}}(t_*)})) - (\frac{1}{8B^3(t_*)} + \frac{1}{2B^2(t_*)})\}] \sin\theta d\phi d\theta \ , \quad (3.16)$$

where

$$A(t_*) = \Gamma^2 {}_S T_{11}{}^2 \alpha_3{}^2 II(t_*) + 2\alpha_1{}^2 I(t_*) \quad \text{and}$$

$$B(t_*) = \frac{(\cos\theta - \Gamma_S T_{11} t_* \sin\theta\cos\phi)^2}{2A(t_*)} + \frac{\sin^2\theta\sin^2\phi}{4\alpha_2{}^2 I(t_*)} + \frac{\sin^2\theta\cos^2\phi}{4\alpha_3{}^2 I(t_*)} \ .$$

Equation 3.12 may be shown to be a special case of Equation 3.16 if one carries out the integration and assumes that $\alpha_1=\alpha_2=\alpha_3$ and $\Gamma=0$. Appendix B discusses the limitation of Equation 3.16.

3.5 Numerical Estimation of the Lagrangian Autocorrelation Function

A numerical iterative procedure was developed to calculate the Lagrangian autocorrelation function as stated in Section 3.3 and Section 3.4 provided that the convective Eulerian space-time correlation is specified. The computer program is modified to account for experimental values $F_1(t_*)$ and for the presence of uniform shear. The temporary Lagrangian autocorrelation function is assumed during the computation at each time step, to have an exponential form:

$$ {}_{L}R_{11}(t_{*}) = \exp-\{A\alpha_{1}t_{*}\} \qquad (3.17) $$

where A is a function of the Eulerian parameter and time.

After initialization at $t_{*}=0$, A is perturbed by a small magnitude to compute the mean square particle displacement according to the Taylor's integral relation. The Lagrangian autocorrelation function at each successive time step is evaluated from Equation 3.16 and compared for convergence to Equation 3.17. The new value of A is determined by using Newton-Raphson's technique for a quick convergence. The relative convergence criterion for A is set to 10^{-5} which provides a relative error less than 10^{-7} for the estimates of the Lagrangian autocorrelation.

The procedure may be run for various values of α_{i} and the turbulent shear parameter $\Gamma_{S}T_{11}$. With the simple assumptions discussed in Section 3.4, the procedure is able to estimate ${}_{L}R_{11}(t_{*})$ for a non-isotropic uniform shear flow. The double integral of Equation 3.16 is computed by a Gauss-Legendre quadrature integration scheme. Such a scheme is maintained self-convergent during the iteration by using up to 1024 weighting points. Detailed description of the Gauss-Legendre quadrature method may be found in Carnahan et al. (1969).

A brief block diagram is presented in Table 3.1 to show the numerical iterative scheme sequence.

3.6 Estimation of Turbulent Dispersion

The statistical turbulent dispersion method proposed in the present study is to use estimates of the Lagrangian statistics in the Eulerian diffusion equation. Eulerian space-time correlations and concentration distributions from a point source were measured in a simulated planetary boundary layer in a wind tunnel. The Eulerian space-time correlation was employed to estimate the Lagrangian autocorrelation function via the methodology introduced in Section 3.4.

Given the Lagrangian statistics, the asymptotic eddy diffusivities were calculated from Equations 2.15 to 2.18. The calculated eddy diffusivities were used in the diffusion equations, Equations 2.42 and 2.43, to predict the turbulent dispersion. The experimental results from the dispersion measurements were then compared with the predicted results from the estimated Lagrangian statistics. Such comparisons are provided in Chapter 6.

Table 3.1. A computational numerical scheme of calculating the Lagrangian autocorrelation function (Program MEULLAG)

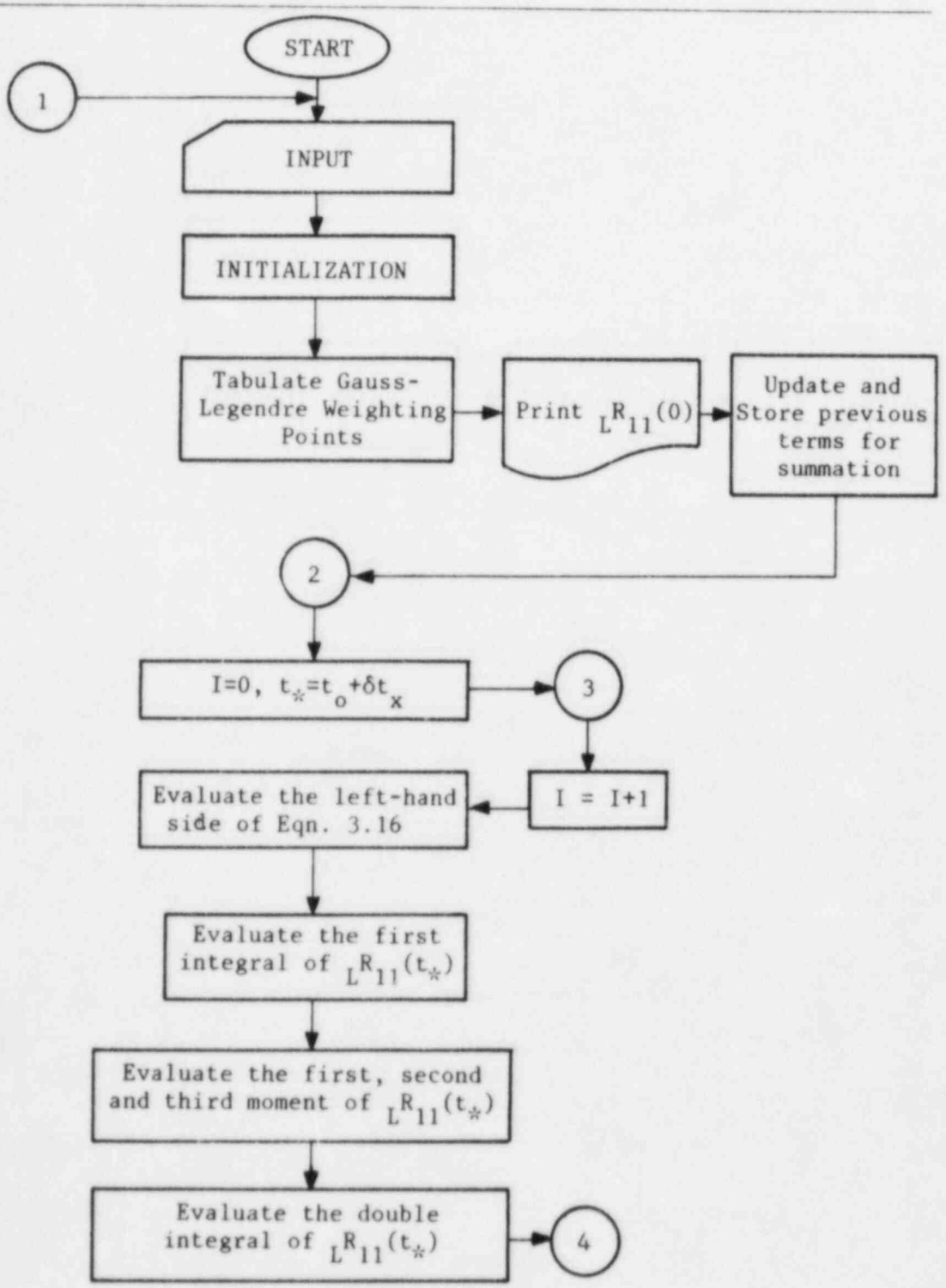

Table 3.1. continued.

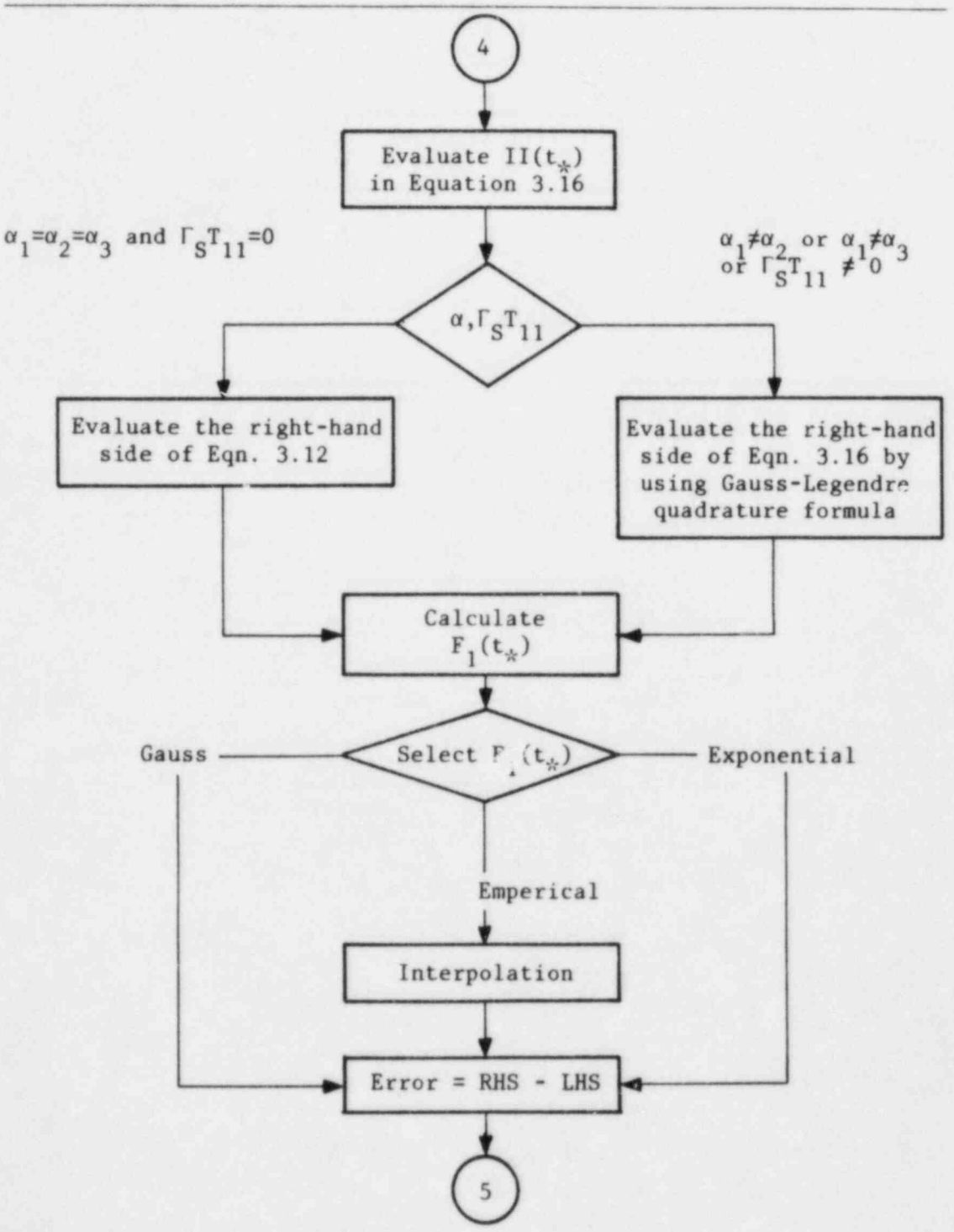

Table 3.1. continued.

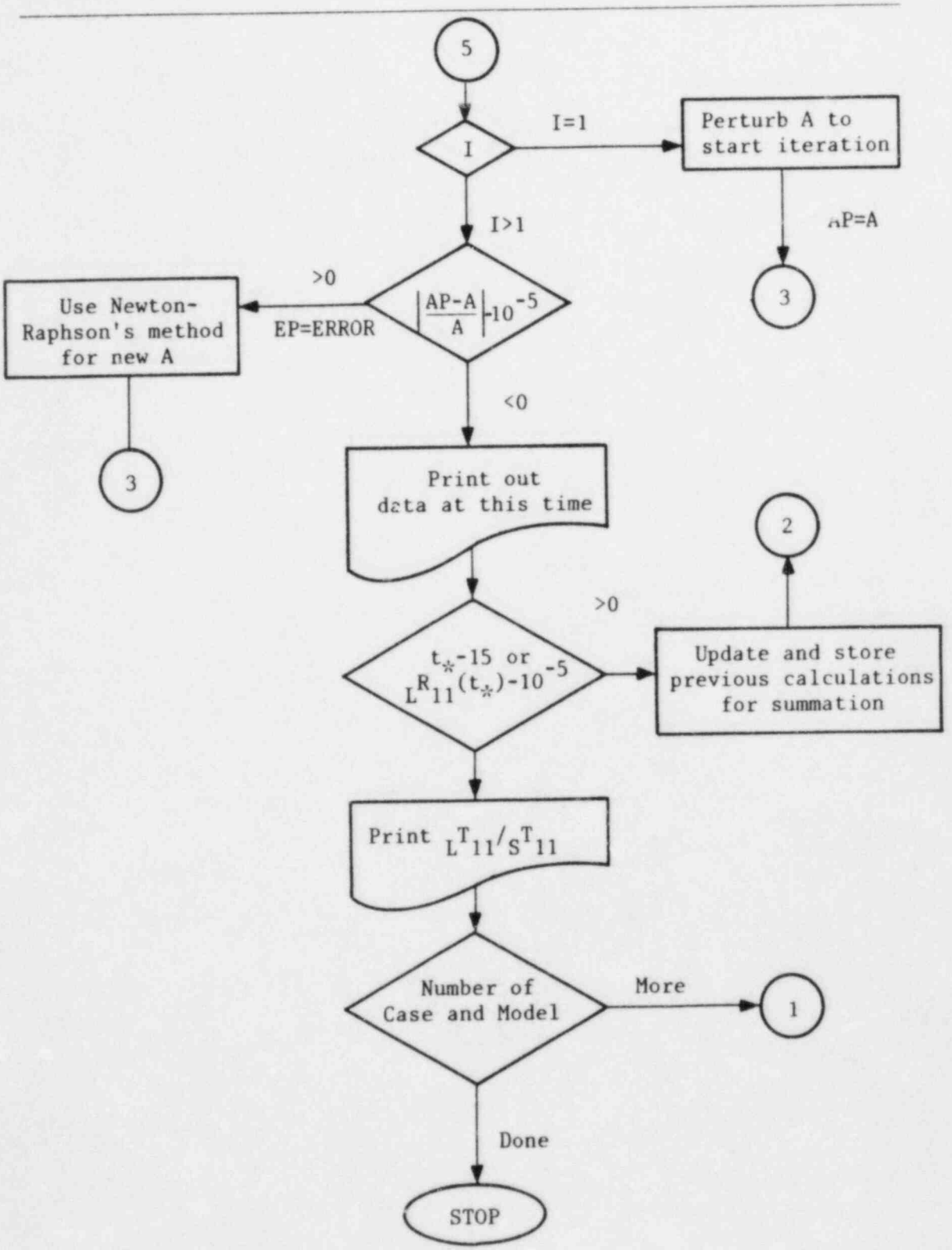

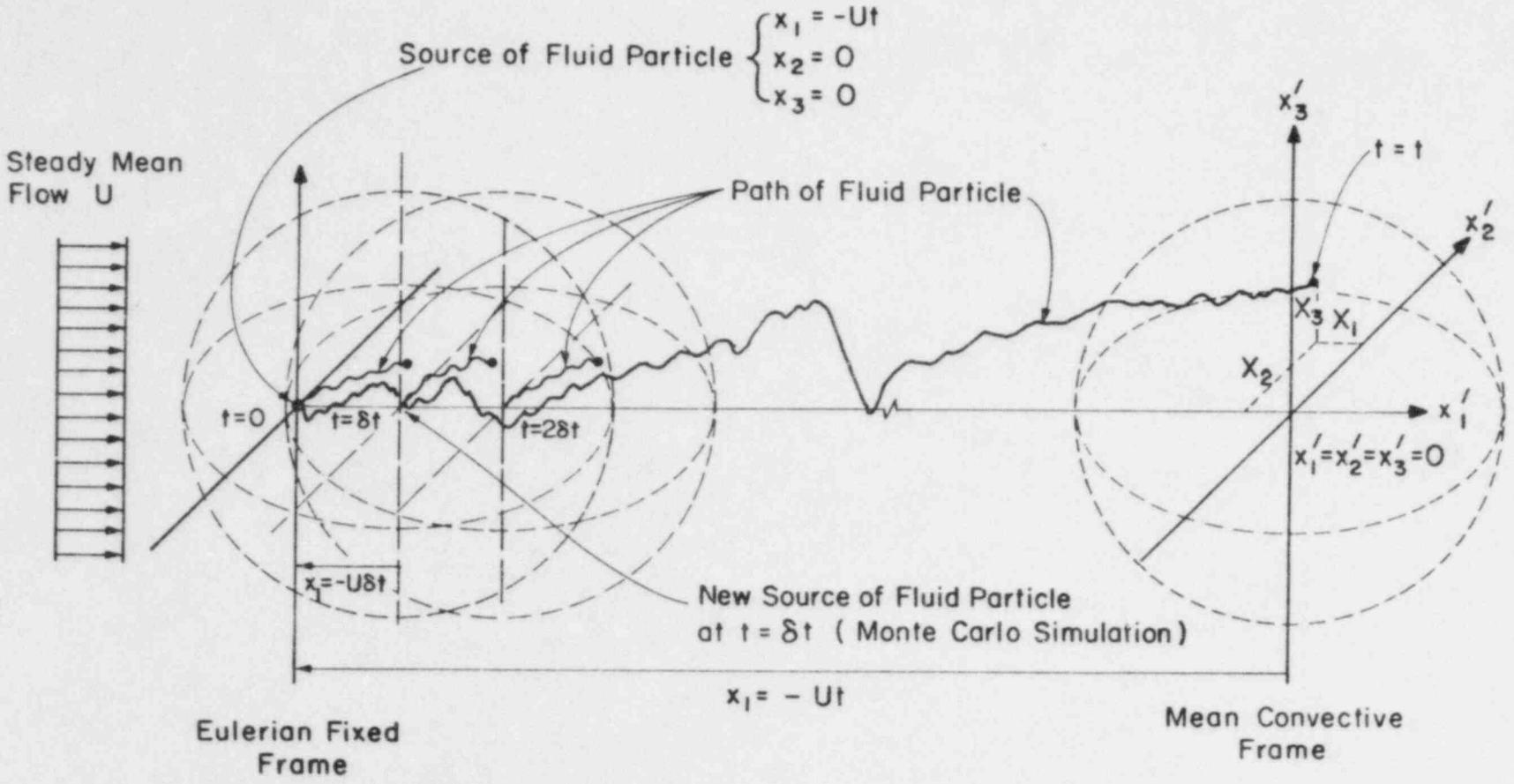

Figure 3.1. General description of coordinates system.

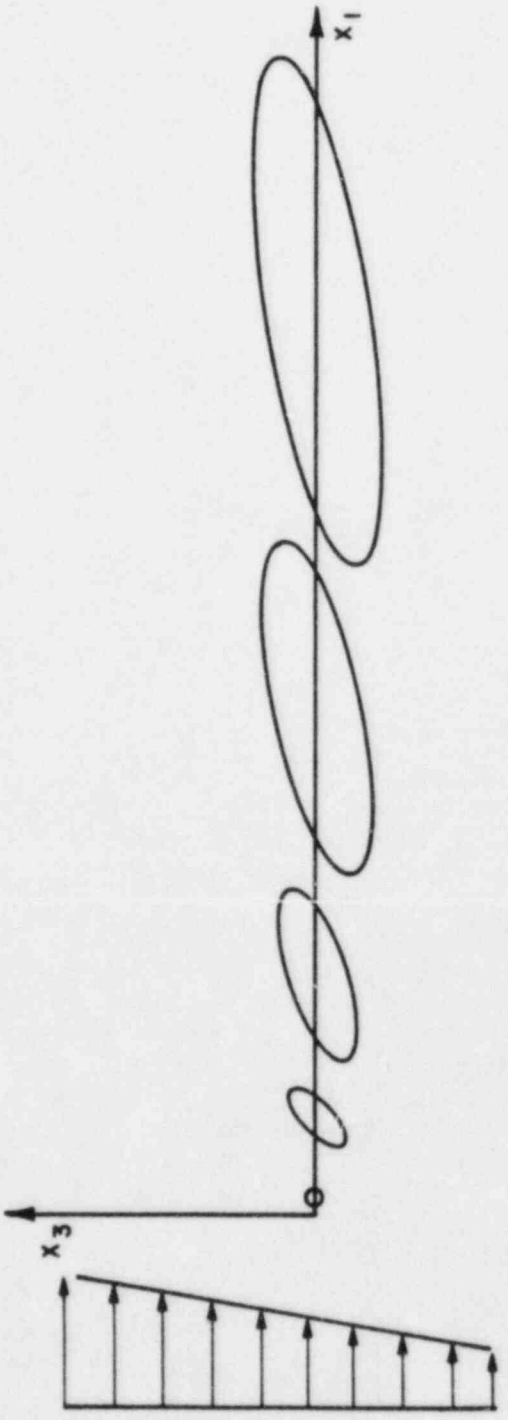

Figure 3.2. Dispersion in uniform shear flow.

Chapter 4

EXPERIMENTAL FACILITIES AND MEASUREMENT PROCEDURES

4.1 Introduction

A brief description of the equipment utilized and the measuring techniques employed is presented in this chapter. Emphasis is also given to the experimental errors that developed from every step during the experiment.

Section 4.2 describes the wind tunnel facility in which all measurements were conducted. Measurement details of the mean flow characteristics are discussed in Section 4.3. Section 4.4 presents the turbulence measurements while diffusion measurements under the same flow configuration are examined in Section 4.5. The experimental procedure in the present study is outlined in Section 4.6.

4.2 Wind Tunnel Facility

New measurements reported in this study were obtained in the Micrometeorological Wind Tunnel (MWT) in the Fluid Dynamics and Diffusion Laboratory at Colorado State University. The MWT is normally operated on a closed circuit principle with the option of an open circuit operation mode. The ceiling of the tunnel is adjustable for control of pressure gradient in the mean flow direction. Thermal control of air stream temperature permits a wide range of thermal stratifications in the test section. The MWT is specially designed to model significant turbulent characteristics of the atmospheric boundary layer. Through selection of proper combinations of wind tunnel length, surface roughness, ambient wind speed, temperature stratification and boundary layer augmentation devices, a range of atmospheric situations may be simulated (Cermak, 1982). A more detailed description of the MWT was prepared by Plate and Cermak (1963).

Turbulence and dispersion measurements discussed in this paper were performed over a smooth floor. The ceiling of the tunnel was adjusted to have a zero pressure gradient in the longitudinal direction. Augmentation devices at the tunnel entrance, 1.8 m in length, included 1.27 cm roughness entrance strips attached on four walls and a 3.8 cm x 7.6 cm sawtooth fence. These devices were employed in order to reduce the wall effects, thicken the boundary layer, and stabilize the flow pattern. One set of turbulence intensity measurements was conducted with additional vortex generators at the entrance. A fully developed turbulent boundary layer was obtained 13 m downwind from the tunnel entrance section. This fully developed boundary layer was maintained for the next 10 m where all the measurements discussed herein were

The triple-wire probe incorporated a cross-wire operated at high overheat ratio and a single wire operated at a very low overheat ratio (effectively cold). The cross-wire was sensitive to both velocity and temperature fluctuations, whereas the temperature wire sensed only temperature fluctuations. The temperature wire was operated in a low overheat constant current mode, thus providing a signal sensitive to temperature. It was located in front of the cross-wire to avoid thermal wake effects as suggested by many researchers (e.g., see Chevray and Tutu, 1972). The temperature wire voltage output was calibrated with temperature variation within a fixed velocity range. Temperature variation was found empirically to produce a voltage output fit by a second degree polynomial curve. The cross-wire was used for simultaneous measurements of two velocity components in a plane parallel to both wires. The methodology and accuracy related to the cross-wire technique is discussed in detail by Sandborn (1972). Bienkiewicz (1981) assumed equal sensitivity of both component wires in order to utilize with a linearizing system. The methodology was employed with some modification for the thermal effect in the present work. If the cross-wire is calibrated as shown in Figure 4.1 and the velocity component parallel to the wire direction is negligible, one obtains

$$U_1(t) = 0.5\{U_{w1}(t)+U_{w2}(t)\} \text{ , and} \tag{4.3}$$

$$U_2(t) = 0.5\{U_{w1}(t)-U_{w2}(t)\} .$$

An empirical best fit to the calibration data, calibrated according to the configuration shown in Figure 4.1, was observed.

$$U_{wi}(t) = \{E_{wi}(t)-m_{i1}\theta(t)-m_{i2}\}^4 \cdot \{m_{i3}-\theta(t)\}^{-2} \cdot \{m_{i4}+\theta(t)\}^{m_{i5}+m_{i6}}, \tag{4.4}$$

where the temperature θ is

$$\theta(t) = n_1 E_\theta^{\,2}(t) + n_2 E_\theta(t) + n_3 . \tag{4.5}$$

Here m_{ij} and n_j are empirical constants and $E_{wi}(t)$ and $E_\theta(t)$ are voltages across cross-wire i and the temperature wire, respectively.

The velocity and temperature sensitivities of each cross-wire component are conveyed in the m_{ij} and n_j coefficients. Among the m_{ij} coefficients, m_{i1} and m_{i4} vary as the overheat ratio of wire varies, whereas m_{i5} and m_{i6} account for the adjustment when the velocity and temperature ranges change.

Signals were recorded simultaneously and processed by a Hewlett-Packard 1000 mini-computer. The probe was rotated 90 degrees in its axial direction for turbulence measurements of transverse motion.

conducted. A heating system located in the section passage before the entrance was set to yield the air temperature in the free stream. The aluminum floor can be heated or cooled to produce a constant temperature along its length. In the present study, the air temperature in the free stream was held at 114°F, and the floor temperature was cooled to 32°F for the stable condition. No heating or cooling to the thermal facility was supplied for the neutral case.

The MWT was modified to prevent the possible occurrence of a transverse temperature gradient. Insulation panels were attached to the side walls to reduce heat loss from the glass window. Nonetheless a slight lateral temperature gradient was detected near the end of the test section.

4.3 Velocity and Temperature Measurements

4.3.1 Velocity measurements under neutral stratification

The longitudinal mean and turbulent velocity under neutral stratification were detected by a TSI-10 quartz coated cylindrical hot-film probe with a TSI Model 1050 anemometer. The hot-film probe was calibrated with a TSI Model 1125 flow calibrator and an MKS Baratron Pressure Meter. Calibration data were fit to the form of King's law,

$$E^2 = A + BU^n \quad , \tag{4.1}$$

using a least-square curve fitting program. The local turbulence intensity is obtained by a linear approximation, i.e.,

$$\frac{\sqrt{u_1^2}}{U} = \frac{2E\sqrt{e^2}}{nBU^{n-1}} \quad . \tag{4.2}$$

A Datametrics model 800 LV linear flowmeter with probe was used to monitor the reference velocity in the wind tunnel. The probe was placed at fixed point in the MWT throughout all measurements. The tunnel was set at various speeds according to the hot-film calibration results. The reading from the Datametric probe was integrated for 1 minute by a Hewlett-Packard Integrating Digital meter. Hence, a calibration curve was obtained between the wind speed and the Datametrics reading. This curve then served as a reference for the mean wind speed during dispersion measurements under neutral stratification.

4.3.2 Velocity and temperature measurements under stable stratification

A multi-wire probe was employed to measure the mean and fluctuating components of velocity and temperature under stable stratification. The lateral and vertical components of turbulence intensities under neutral stratification were also detected by such a probe.

4.4 Velocity Correlation Measurements

4.4.1 The analog method

Two TSI-10 quartz coated cylindrical hot-film probes with TSI Model 1050 anemometers were utilized in the velocity correlation measurements. The upstream probe was mounted above the tunnel floor and placed with the wire axis perpendicular to the floor. The downstream probe was mounted on a three-dimensional traverse mechanism with the wire axis parallel to the lateral direction. Such arrangement was expected to reduce the dynamic wake effect imposed upon the downstream probe from the upstream probe. The three-dimensional traverse is capable of providing displacement in all three directions with an accuracy of 6.35×10^{-3} mm. Analog signals were recorded continuously by an AMPEX FR-1300 Recorder/Reproducer. The record and reproduce modules were carefully calibrated to provide a flat frequency response under 2000 Hz. Near zero distortion was found when tested by sine waves with frequency below 2000 Hz. The turbulent kinetic energy of the present flow configuration was predominantly at frequencies below 300 Hz. A modified switch board was prepared so that two channels of data could be taken simultaneously. A SAICOR correlation and probability analyzer, model SAI-42, was employed for the data analysis. The SAI-42 correlator provides auto- and cross-correlation functions with incremental lag or time delay value from 1 μ second to 1 second resulting in total time delays from 100 μ second to 100 seconds. Precomputation delay of 200 lag values in 50 lag increments allows the correlation function to be viewed symmetrically about zero or up to 200 lag values removed from zero (optionally to 2000 points). The averaging is accomplished digitally with fixed summation ranging from 2^9 to 2^{17} in binary steps. The correlation function was displayed on an oscilloscope and a X-Y plotter in the form of 100 discrete points. A schematic diagram of the experimental set up is shown in Figure 4.2.

Data were continuously recorded on a APMEX-766 Magnetic Tape for 5 minutes for every separation distance between two probes. A sine wave was used for signal separation and calibration was recorded before each set of measurements. Tape was rewound to the same point for the analysis of auto- and cross-correlations. Each set of data was examined by the probability analyzer so that minimum signal attenuation occurred. The range of correlation was selected so that 95 percent of data points were analyzed without smoothing. (This approach covers all signals within two standard deviations from the mean of the probability density function.)

Anemometer voltage output from the velocity sensor was calibrated with the mean wind speed by King's Law. The following relationship was obtained for a linear approximation between two fluctuating quantities.

$$E^{R}_{11}(x_1,x_2,x_3,\tau) = \frac{\overline{w1u_1(t)\,w2u_1(t+\tau)}}{\sqrt{w1\overline{u_1^2}(t)}\sqrt{w2\overline{u_1^2}(t+\tau)}} = \frac{\overline{e_{w1}(t)e_{w2}(t+\tau)}}{\sqrt{\overline{e^2_{w1}}(t)}\sqrt{\overline{e^2_{w2}}(t+\tau)}} \qquad (4.6)$$

4.4.2 The digital method

It was later found that the amplified AC signals from the TSI signal conditioners were automatically filtered by a built-in high pass filter which cut off signals at 2 Hz. 2 Hz corresponds to a length of 1 m at a convective velocity of 2 m/sec. Signals recorded with such a filter apparently eliminated correlations contributed from eddies larger than 1 m. An examination of the turbulent energy reveals that 1/3 of the turbulent energy was filtered out by these high pass filters. Hence, velocity correlation measurements were redone at 3 heights, 2 cm, 10 cm and 20 cm, by analyzing unfiltered signals which included all signals from DC to 2000 Hz. New measurements were performed under the same flow configuration and experimental procedures by using two TSI-1287 split film probes. Velocity signals were digitized and stored in a HP-1000 computer. In addition to the u_1 space-time correlation, u_2, u_3 space-time correlations with longitudinal separations were also computed. The split film sensor incorporates two electrically independent films on a single cylindrical quartz fiber. By operating each film with a separate anemometer circuit, the variation in heat transfer around the cylinder is utilized for a unique measurement capability. Figure 4.3 displays the geometric configuration of the sensor. The sensor is essentially insensitive to flow in the direction along a sensor axis. The total heat transfer on both films gives a measure of the velocity vector perpendicular to the sensor and the difference of heat transfer for the two films gives a measure of the velocity vector perpendicular to the plane of the splits on the sensor. The sensor was calibrated to have the same temperature on both of the films. Maximum error resulting from the calibration was found to be 9 percent on the low (70 cm/sec) end and 3 percent on the high end (230 cm/sec) of the velocity range.

4.5 Concentration Measurements

4.5.1 Gas chromatograph

A Hewlett-Packard Model 5700A gas chromatograph with flame ionization detector was used to determine the mean concentration of scalar tracers. The flame ionization detector functions on the principle that a DC voltage on a collector electrode is proportional to a charge produced by charged particles when organics burn in a hydrogen/air flame. Air samples tagged with two tracer components, methane and ethane, were carried into a combustion column by an inert carrier gas, nitrogen. Tracers arrived at the flame at separate times due to the diffusive properties of different hydrocarbon mixtures in the column. The DC voltage output from the electrode was amplified by an electrometer and fed to a Hewlett-Packard Model 3380 integrator. Separate peaks on the integrator output can be identified as contents of different tracer gases. Flow rates of auxiliary gases (air, hydrogen and nitrogen) were selected to yield a maximum sensitivity of the instrument. Zero drift of the gas chromatograph due to the impurities in the carrier gas was corrected by subtracting the background flow baseline values.

The gas chromatograph can measure samples with sensitivity down to picogram (10^{-12}) quantities. It was calibrated with a methane-ethane mixture of known concentration every four hours during the experiment. The maximum error expected from the gas chromatograph was found to be less than 0.12 percent.

4.5.2 Concentration measurement technique

A neutrally buoyant continuous point source was simulated by either a methane or an ethane mixture. The source flow rate was set at 50 cc/s with an exit velocity of 51.5 cm/s. The source gas flowmeter was pre-calibrated with the source gas, and volume flow rate error was less than ±3 percent. The point source was injected into the wind tunnel in the same direction as the mean flow to avoid possible plume rise effect. The tracer gas was withdrawn from the test section by a sampling grid and trapped in a sampling system for further analysis. The sampling grid consisted of 43 brass 0.16 cm I.D. tubes mounted upwind over a rectangular matrix. The sample draw rate was set to 1.2 cc/s which results in a draw velocity of 60 cm/s. The sampling system is composed of fifty 30 cc air-tight syringes mounted between two circular aluminum plates. A variable-speed motor raises a third plate which lifts the plungers of all fifty syringes simultaneously. Syringes were completely flushed to prevent residual concentrations accumulated from earlier runs before any sample was taken. The sampler was periodically calibrated to insure proper function of every check valve and tubing assembly. A block diagram of the experimental system is shown in Figure 4.4.

The gases were allowed to flow for three minutes before any data were taken in order to reach a steady state of true mean concentration distribution. Forty-five samples were simultaneously drawn in a period of five minutes for each run. Two samplers were employed to monitor the level of background concentration. Forty-three sampling tubes were located on the cross section of a continuous plume while three samplers were used to check plume symmetry. Each run was repeated if necessary to locate the plume center. The background concentration was subtracted from each concentration sampled.

4.6 Experimental Procedure

Mean speed of the approach flow was monitored by the Datametric linear flowmeter. Homogeneity of the wind tunnel was tested by velocity measurements at different mean wind speeds and different downwind locations in the test section.

Velocity measurements under neutral stratification were performed at U = 200 cm/sec, 300 cm/sec and 500 cm/sec. Data were taken at x_1 = 0 cm, 200 cm, 500 cm and 800 cm. Under stable stratification only U = 200 cm/sec was employed and measurements were conducted at x_1 = 0 cm, 200 cm, 500 cm and 700 cm. Velocity spectra were obtained at x_1 = 0 cm for different heights.

Velocity correlation measurements were performed with the upstream probe fixed at x_1 = 0 cm. The longitudinal separation between two probes was extended from 0.5 cm to 200 cm. Transverse separations between two probes were investigated in order to correct the heat wake effect, or the dynamic wake effect, imposed on the downstream probe.

Concentration measurements were conducted under neutral and stable stratification. The flow configuration and source release system were maintained the same but the temperature stratification varied. The free stream velocity was set at 200 cm/sec during all dispersion measurements. Measurements were made for eight different source heights, i.e., H = ground, 2 cm, 4 cm, 6 cm, 8 cm, 10 cm, 15 cm and 20 cm. Cross wind samples were taken at ten different downwind distances, x_1 = 25 cm, 50 cm, 100 cm, 150 cm, 200 cm, 300 cm, 400 cm, 500 cm, and 700 cm for each release height; however, x_1 = 25 cm was not used during stable stratification.

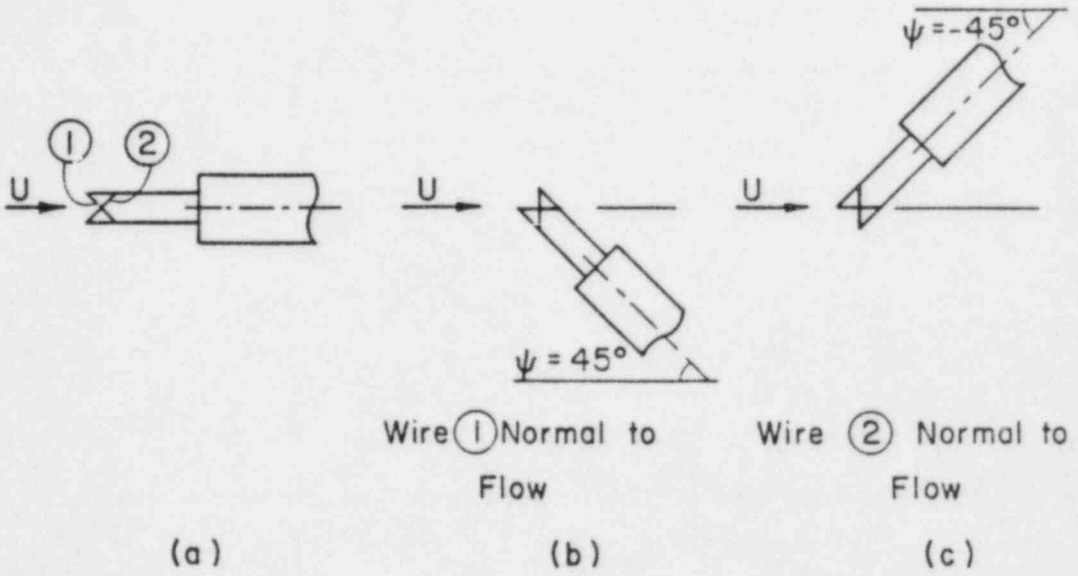

Figure 4.1. Calibration of x-wire probe.

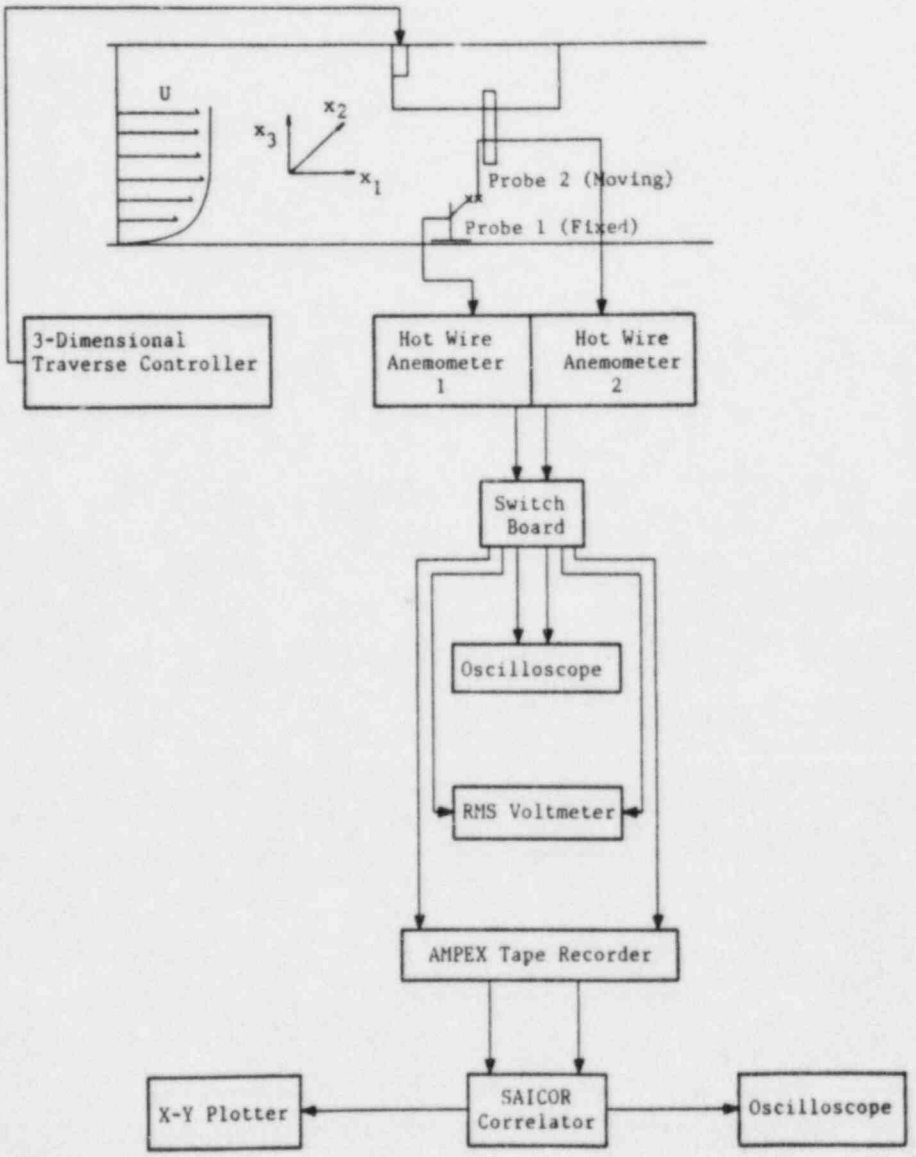

Figure 4.2. Experimental set-up for velocity correlation measurements.

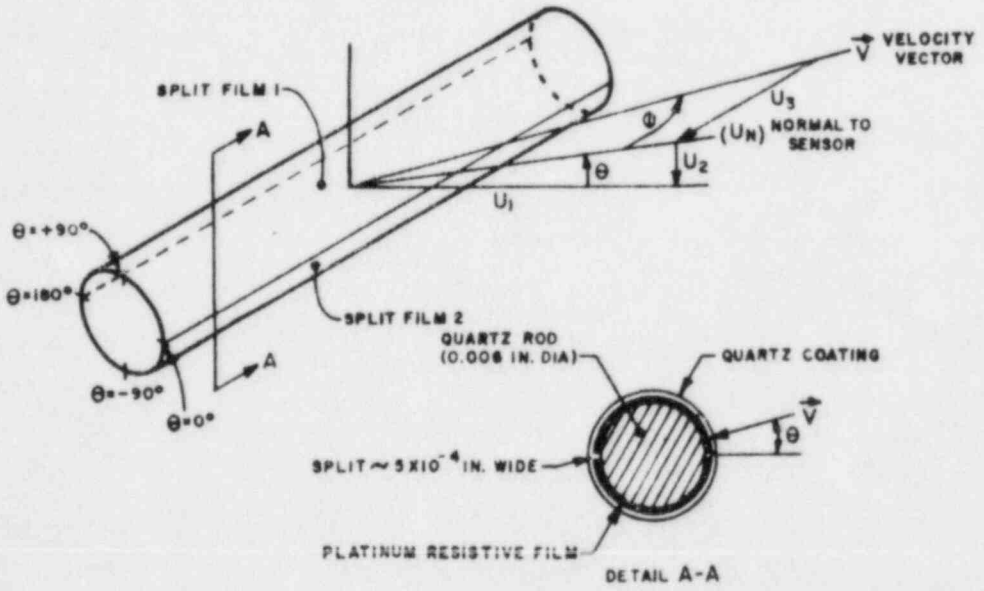

FIGURE 1: CYLINDRICAL SPLIT FILM ANEMOMETER SENSOR

Figure 4.3. Cylindrical split film anemometer sensor.

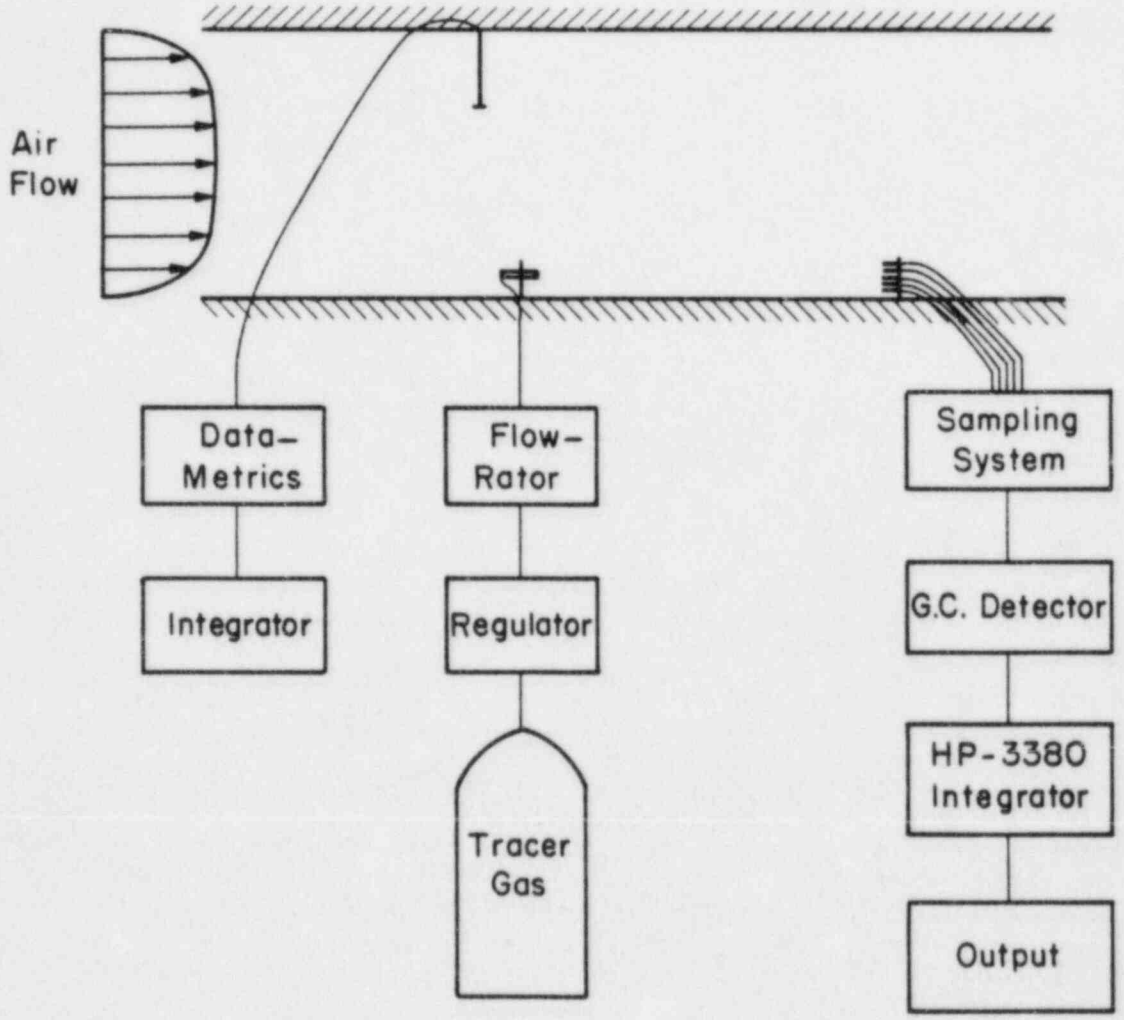

Figure 4.4. Schematic of gas sampling system.

Chapter 5

LABORATORY RESULTS OF TURBULENCE AND DISPERSION MEASUREMENTS

5.1 Introduction

Results of turbulence and dispersion measurements in the wind tunnel are presented in this chapter. The adequacy of laboratory simulation of the atmospheric turbulence and transport phenomenon is investigated. The broad characteristics of a neutral and a stable stratified boundary layer are described in Section 5.2. Turbulence measurements which include energy and temperature spectra are discussed in Section 5.3 for two thermal stratifications. Results of the Eulerian space-time correlation across a neutrally stratified boundary layer are displayed in Section 5.4. Section 5.5 focuses on the laboratory plume simulation of atmospheric dispersion. The point source size effect in source simulation is discussed. Comparison between laboratory simulation and atmospheric dispersion experiments is furnished in terms of standard deviation of plume width.

5.2 Characteristics of the Laboratory Simulated Boundary Layer

The MWT has the advantage of a long test section which permits deep laboratory boundary layers suitable for the simulation of the atmosphere. After a sufficient distance ($\tilde{}$ 10 m) from the tunnel entrance, the boundary has only a slight additional growth. The portion of the test section selected for diffusion experiments was chosen so that velocity, turbulent intensity and temperature profiles do not change noticeably along the streamwise fetch at different stabilities and various wind speeds (i.e., horizontally homogeneous).

5.2.1 Neutral stratified boundary layer

Figures 5.1 to 5.3 show the mean velocity and the local turbulent intensity profiles over the test section for various velocities. Normalized data at different longitudinal stations in the test section are very similar. The variation with distance of the free stream velocity in the test section was found to be less than 1 percent with no trend to either increase or decrease. Figure 5.4 displays the lateral wall effect on the mean velocity and turbulent intensity at a height of 80 cm from the floor. The boundary layer created by the lateral wall is not so significant as the boundary layer along the ground. The velocity correlation measurements and the dispersion measurements were performed within the range where the velocity variation is no greater than 1 percent. Hence, homogeneity in the x_1-x_2 plane is preserved in the simulated boundary layer in the test section. Table 5.1 summarizes the

characteristics of the simulated atmospheric boundary layer. Counihan (1975) reviewed meteorological literature on fully developed adabatic boundary layers, and recommended some empirical formulae for atmospheric turbulence. The present simulated boundary layer is compared in Table 5.1 with his regressive formulae based on a fixed roughness length. Wind tunnel results are within ±30 percent deviation from his results, well within the variation in data he evaluated.

5.2.2 Stable stratified boundary layer

The mean velocity and temperature profiles in the stable stratified boundary layer are shown in Figures 5.5 and 5.6. Neither profile grows appreciably within the test region. The planewise homogeneity requirement for simulating the atmospheric boundary layer was fulfilled in the stable stratified boundary layer in the wind tunnel. Due to the location of thermal conditioning panels, the test section for the thermal stable stratification is 3 m shorter than that for the neutral stratification which is 10 m in length. The boundary layer thickness for the stable case using the same inlet tunnel augmentation device was larger than that for the neutral case (75 cm for stable case and 45 cm for neutral case).

The temperature profile depth is much greater than the velocity profile depth (120 cm when T/T_∞ = 99%). Arya (1969) also found that the temperature gradient abruptly increased before finally leveling off instead of decreasing monotonically to zero near the edge of the thermal layer. He attributed the behavior to incomplete mixing of the air in the core region of the wind tunnel where a residual stratification may exist even after circulation. Arya then suggested that the thermal layer thickness should be determined after correcting for the observed deficit in the temperature profile near the edge of the thermal layer. A similar situation may exist in the current measurements as shown by the fluctuation profiles in Figure 5.7. An abrupt change of the temperature fluctuation at x_3/δ_T = 0.5-0.6 suggests that the turbulent mixing mechanism was suppressed near that region. Hence, the effective thermal layer thickness was probably δ_T' = 75 cm.

Another characteristic of a thermal boundary is the local Richardson number which provides a quantitative measure of the thermal stability. The flux Richardson number, R_f, is derived from the turbulent energy equation as the ratio of the rate of destruction of turbulence by stable stratification to the rate of creation of turbulence by shear. But R_f is not often measured in practice, instead the gradient Richardson number, R_i, is usually stipulated to indicate the relative importance of thermal stratification. R_i is related to R_f through

$$R_i = \frac{K_m}{K_h} R_f \qquad (5.1)$$

where K_m and K_h are eddy viscosity and eddy diffusivity, respectively. In a stable air, K_m/K_h is very close to unity and R_i is commonly defined in the atmosphere as

$$R_i = \frac{\frac{g}{T}(\gamma_d - \gamma)}{(\frac{\partial U}{\partial x_3})^2 + (\frac{\partial V}{\partial x_3})^2} (1 + \frac{.07}{B_r}) \qquad (5.2)$$

where B_r is the Bowen ratio, $B_r = \frac{C_p}{L} \frac{(\bar{T}_2 - \bar{T}_1)}{(\bar{q}_2 - \bar{q}_1)}$,

γ_d is the adiabatic lapse rate,

γ is the lapse rate at sunrise,

C_p is specific heat for dry air at constant pressure, and

q is heat per unit mass.

Further discussions about the Richardson number may be found in Panofsky (1982).

An overall Richardson number which serves as a reference parameter for a thermal layer is defined as (Ellison and Turner, 1960)

$$R_{i_h} = \frac{g}{T_a} \frac{(T_h - T_o)h}{U_h^2} , \quad 0 < x_3 < h , \qquad (5.3)$$

in which T_o is the temperature at the surface and T_a is the average absolute temperature in the layer. $R_{i_h} = 0.25$ was found in the present study. The distribution of R_{i_h} across the thermal boundary is presented in Figure 5.8.

5.3 Turbulent Velocity Fluctuations

5.3.1 Neutral stratified boundary layer

The longitudinal turbulent intensities are also shown in Figures 5.1 through 5.3. The RMS velocity fluctuation is normalized by the local mean velocity and plotted vs. non-dimensional height x_3/δ. Data presented in such a manner collapses on a single curve regardless of the variation of characteristic Reynolds number, $R_e = \frac{U\,\delta}{\nu}$, based on the boundary layer thickness and the freestream velocity. The similarity implies that the absolute velocity fluctation increases as U_∞ increases or x_3/δ decreases.

The one-dimensional energy spectra of longitudinal velocity fluctuations measured at different heights in the boundary layer for U_∞ = 2 m/ are shown in Figure 5.9. The -5/3 slope of the inertial subrange is indicated in the figure. Due to the low velocity employed, the inertial subrange is rather short compared to the velocity spectra reported by Hansen and Cermak (1975) and Chandra (1967) where higher velocities were used. The energy spectra have been normalized with respect to mean square fluctuations so that

$$\frac{1}{[u_1^2]} \int_0^\infty E_1(n)dn = 1 \ . \qquad (5.4)$$

The normalized energy spectra are presented in Figure 5.10 where similarity of the spectrum function is found across the boundary layer.

The longitudinal velocity autocorrelation functions at various heights in the boundary layer are shown in Figure 5.11. Figure 5.11a displays the measured autocorrelation functions from filtered turbulence while Figure 5.11b presents data from unfiltered turbulence.* The autocorrelation function decays much faster in a filtered turbulence due to the absence of large eddy motion. The autocorrelation functions of lateral velocity fluctuations are shown in Figure 5.12. Figure 5.13 gives the measured autocorrelation functions of vertical velocity fluctuations. The area under the autocorrelation curve is seen to increase as the height increases in the boundary layer.

The lateral turbulent intensities were also measured during the general boundary layer survey. However, a related measurement of the lateral turbulent intensity was performed with extra inlet spires. The results are compared with previous measurements conducted in the same wind tunnel by Zoric (1968) and Chaudhry and Meroney (1969) as shown in Figure 5.14. $\frac{\sqrt{\overline{u_2'^2}}}{U_\infty}$ = 0.04 was adopted to represent test section conditions during the verification of dispersion measurements.

5.3.2 Stable stratified boundary layer

The RMS velocity fluctuations for the longitudinal, lateral and vertical directions are plotted in Figures 5.15 through 5.17 against different heights in the layer. The local turbulent intensity (the RMS velocity fluctuation normalized by the free stream velocity) changes slowly except near the edge of the layer for the lateral and vertical directions. Figure 5.18 shows the variation of the lateral turbulent intensity through the boundary layer under stable stratification. The data was compared with Arya's (1969) measurements

---

*Results discussed thereafter are limited to unfiltered turbulence case unless specified.

for different overall Richardson numbers. The RMS velocity fluctuation decreases in a consistent trend as the thermal stratification increases. Figure 5.19 displays the decreasing trend of the lateral turbulent intensity with the Richardson number which also shows consistency with previous measurements. $\frac{\sqrt{\overline{u_2^2}}}{U_\infty} = 0.02$ was selected to represent test section correlations for the analysis of dispersion.

The u_1 energy spectra are shown in Figure 5.20. The area under each spectrum appears to be less than its counterpart at the same height in the neutral boundary layer. It is understood to be the effect of stability which reduces the turbulent energy. The dissipation range is visualized at higher frequency ($\tilde{}$ 200 Hz). The u_2, u_3 energy spectra are presented in Figures 5.21 and 5.22, respectively. These energy spectra start with a lower energy level and decay much faster than the u_1 energy spectra. This is reasonable since when no mean motion exists smaller eddies contribute more to the total energy. The energy containing region is less appreciable because it lacks large eddies and because the dissipation mechanism soon takes over at higher frequency.

All u_1, u_2 and u_3 energy spectra are normalized by the RMS velocity fluctuations and plotted vs. frequency as shown in Figures 5.23, 5.24 and 5.25, respectively. The inertial subrange is broader in the u_1 spectra for various heights in the boundary layer as compared with the -5/3 slope sketched in the figures. The related turbulent scales for all three velocity components are listed in Table 5.2. The integral scale increases as the height increases while the microlength scale remains nearly constant.

Velocity autocorrelation functions presented in Figures 5.26, 5.27 and 5.28 support the calculated length scales in Table 5.2 since the autocorrelation functions persist to longer times for positions farther away from the ground. The autocorrelation functions for the u_2 and u_3 component do not appear to develop large negative magnitudes although they do decay faster than the longitudinal autocorrelation function.

The measured one-dimensional spectra of temperature fluctuations are shown in Figure 5.29. They are normalized with the RMS temperature fluctuations. The temperature spectrum decays with increased frequency in a similar way to that in the velocity spectrum. If the Reynolds number is large enough for an equilibrium range to exist in the kinetic energy spectrum, there is also an equilibrium range (exhibiting local isotropy) in the spectrum of temperature variance, because it is the turbulent motion that is mixing the temperature field (Lumley and Tennekes, 1972). The inertial subrange is insignificant in the figure due to the low velocity employed. The temperature spectrum quickly declines into the dissipation subrange. There is no sign of a viscous-convective subrange as reported in liquids.

5.4 Two-Point Velocity Correlation

5.4.1 Source of error

Errors involved in the measurements of two-point velocity correlations are primarily due to the finite width of the band filter deficiencies, the tape recorder deficiencies, the analog correlator deficiencies and the wake effect of the upstream probe. Cyclic variations of the velocity signal over the mean velocity range employed in the present study were found to be less than 2000 Hz; a low pass filter was selected to eliminate high frequency noise above 2000 Hz.

Instrument deficiencies. Error introduced into the measurement process by the magnetic tape recorder have been described by Comte-Bellot and Corrsin (1971). Mechanical errors such as magnetization, detection, modulation and demodulation were avoided by careful selection of the tape and calibration as described in Section 4.3. The only remaining error resulted when the tape did not rewind to the same point for auto- and cross-correlation calculations. Although the tape may not have been rewound to the exact same data point due to the imperfect motion of the tape, at least 99.9 percent of the same data points were analyzed after rewinding. Furthermore, the stationarity of the time series signal compensates for any differences for finite length signals. Repeated analysis of the same signals by rewinding the tape to new starting points showed that less than 1 percent error was caused by tape position.

The clip mode on the SAICOR correlator can be set to smooth the correlation function. It was carefully selected to preserve the characteristics of the correlation with minimum fluctuations.

Wake effect of upstream probe. When one probe is positioned behind another probe in the streamwise direction, the upstream probe produces not only a thermal wake but also a dynamic wake which caused additional disturbance about the downstream probe. To reduce the consequent error it is common in the laboratory to locate the downstream probe laterally just outside the wake and to assume that such approximation results in negligible change in the correlation measurements. In the present study, the wake effect of the upstream probe was reduced by two methods. First, for single wire measurements, the two probe axes were placed perpendicular to one another so that the upstream probe is only sensitive to u_1 and u_2 components while the downstream probe is sensitive to u_1 and u_3 components. Such an arrangement has the advantage that it enhances the accuracy of the desired correlation $(u_1)_A(u_1)_B$, since $(u_2)_A(u_3)_B$ and $(u_1)_B(u_2)_A$ are less appreciable than $(u_1)_A)(u_3)_B$ and $(u_3)_A(u_3)_B$ which result when the two probe axes are placed parallel to each other. Second, for both single wire and split film measurements, the correlations at $\Delta x_2 = 0$ were extrapolated from a series of correlation measurement with small displacements Δx_2 away from the wake center. Figure 5.30 presents the extrapolation results for cross-correlation with zero time delay. Figure 5.31 shows the same

extrapolations for space-time correlations with optimum delay time. It may be concluded from the slopes of curves in these figures that the wake effect of decays as the downstream probe moves away from the upstream probe, and the wake effect completely disappeared after Δx_1 exceeds 20 cm. The wake effect persists at longer distance for higher velocities.

The extrapolation technique employed in the present study is somehow subjective. In most cases, the curve slopes were kept zero for symmetry.

5.4.2 Eulerian space correlation

Eulerian space correlations presented in this section include two f-type correlations and four g-type correlations according to Hinze's (1975) definition. Their integral scales are represented by L_{ij} where i indicates the velocity component and j indicates the direction of spatial separation.

The longitudinal space correlation functions, ${}_E R_{11}(\Delta x_1,0,x_3;0)$, are given in Figure 5.32. For small Δx_1 the values are improved from extrapolations as discussed in section 5.4.1. Results from filtered turbulence are also plotted for comparison. Figure 5.33 presents the space correlation of lateral velocity fluctuations, ${}_E R_{22}(0,\Delta x_2,x_3;0)$. ${}_E R_{11}(\Delta x_1,0,x_3;0)$ decays much slower than ${}_E R_{22}(0,\Delta x_2,x_3;0)$ which indicates the elongation of turbulent eddies in the streamwise direction. Since both functions are f-type correlations, $L_{11}/L_{22} \tilde{\sim} 4.8$ as compared with 1.0 for isotropic turbulence, which emphasizes the destruction of isotropy in the boundary layer flow. ${}_E R_{11}(0,\Delta x_2,x_3;0)$ and ${}_E R_{33}(0,\Delta x_2,x_3;0)$ are shown in Figures 5.34 and 5.35, respectively. Figure 5.34 displays less deviation between filtered and unfiltered correlation for transverse separation than the streamwise separation data (Figure 5.32). It implies that large eddies are less dominant in the transverse direction. The space correlation function increases as height increases and turbulence decreases in all cases. The other two g-type correlations with streamwise separations are plotted in Figures 5.36 and 5.37. Correlation with longitudinal separations seems to persist for a longer distance than correlation with transverse separations. The corresponding integral length scales for all space correlations are summarized in Table 5.3a. L_{11} is significantly larger than all other scales which is generally observed in the atmospheric boundary layer. Integral scales are normalized with L_{11} and compared to field observations (Teunissen, 1980) in Table 5.3b. Teunissen's measurements were conducted in the neutral-stable planetary boundary layer over typical rural terrain at a height of 11 m. The mean wind velocity in his measurements was about 9 m/sec. The turbulent intensities were 0.16, 0.11 and 0.07 for longitudinal, lateral and vertical direction, respectively. Hence, his measurements are comparable to the present measurements for $x_3/\delta = 0.044$. Considering

the uncertainty involved in the field experiment with its insufficient data and varying wind direction, Teunissen's results qualitatively support our simulated atmospheric boundary layer.

5.4.3 Eulerian space-time correlation

The longitudinal space-time correlation functions, for filtered turbulence ${}_{E}R_{11}(\Delta x_1,0,x_3;\Delta x_1/U)$, are reproduced in Figure 5.38. Each data point represents the peak of the individual cross-correlation observed at optimum delay time, τ_m, although τ_m may be different from the convective time $\Delta x_1/U$. For small Δx_1 the τ_m values are extrapolated from a series of correlation measurements with Δx_2 positioned away from the wake center as illustrated in Figure 5.30. Figure 5.39 displays ${}_{E}R_{11}(\Delta x_1,0,x_3;\Delta x_1/U)$ for unfiltered turbulence. The transverse space-time correlations, ${}_{E}R_{22}(\Delta x,0,x_3;\Delta x_1/U)$ and ${}_{E}R_{33}(\Delta x_1,0,x_3;\Delta x_1/U)$, for unfiltered turbulence are given in Figures 5.40 and 5.41. It is observed in the measurements that the space-time correlation function increases as height increases and ${}_{E}R_{11}(\Delta x_1,0,x_3;\Delta x_1/U) > {}_{E}R_{22}(\Delta x_1,0,x_3;\Delta x_1/U) > {}_{E}R_{33}(\Delta x_1,0,x_3;\Delta x_1/U)$ for a given height.

Notice that the correlation function has a rapid drop at small times in Figure 5.38. Such a drop is more marked as the probe moves closer to the ground. Similar results have been observed in the atmosphere where probe wake effect appears unnoticeable (Lumley and Panofsky, 1964). One explanation for the drop would be that near the ground the turbulence level is stronger and small eddies become more dominant. The small eddies lost their correlation in a shorter period which results in a decrease in the correlation as height decreases. Such effect is somehow diluted when large eddies are dominant in an unfiltered turbulent field.

The inadequacy of Taylor's frozen turbulence hypothesis is clearly seen in a sheared turbulent boundary layer. According to the hypothesis, ${}_{E}R_{11}(\Delta x_1,0,x_3;\tau)$ should reach its maximum value of unity at a time $\tau = \Delta x_1/U$, but as a result of shear, the resultant higher level of turbulence and the small eddy behavior, the peak value of ${}_{E}R_{ii}(\Delta x_1,0,x_3;\tau)$ can never regain its theoretical magnitude as observed in Figures 5.38 through 5.41. Even in the grid-generated turbulence reported by Frenkiel and Klebanoff (1966) as well as Comte-Bellot and Corrsin (1971), where the turbulence is not distorted by mean shear; large departures from a frozen pattern are observed. Most investigators attributed the breakdown of Taylor's hypothesis to the loss of coherence of small eddies when downwind separations slowly exceed the larger eddy sizes. Data reported on the frequency filtered space-time correlation measurements by Favre et al. (1957, 1958) gave equivalent support to the observation in a boundary layer. The turbulence gradually loses some coherence at the edge of the boundary layer where mean shear and turbulence level are low, but near the ground the correlation function losses its identity quickly due to higher mean shear and turbulence level.

Convective velocity. The convective velocity U_c is defined as the ratio of Δx_1 to the optimum delay time where $\frac{\partial}{\partial \tau} {}_E R_{11}(\Delta x_1, 0, x_3; \tau) = 0$. It is closely related to the eddy motion and serves as a characteristic velocity of the large scale disturbances in the turbulence. The convective velocity was found to be identical to the local mean velocity U in both uniform and uniform shear flows by several researchers. Fisher and Davies (1964) examined the convective velocity for various frequency components in a subsonic jet. They reported that U_c increases as frequency increases and deviated from the mean value by as much as 25 percent. Blackwelder and Kovasznay (1972) observed that $U_c/U = 0.958$ at $x_3/\delta = 0.83$ and $U_c/U = 0.975$ at $x_3/\delta = 0.45$ in a turbulent boundary layer. This indicates that the large eddies are traveling at a slower velocity than the mean velocity in the boundary layer. Figure 5.42 presents a comparison between τ_m and $\Delta x_1/U$ where $\tau_m = \Delta x_1/U$ is plotted as a solid line. For small separations such as $\Delta x_1 = 0.5$ cm to 1.0 cm errors are as high as 50 percent due to the vagueness of the correlation peak. Error quickly reduces to less than 3 percent as the separation increases. $\tau_m/(\frac{\Delta x_1}{U})$ is consistently greater than 1.0 at large separation which indicates the slower motion of large eddies in the boundary layer. The fact that the difference between U_c and U is not significant at various heights implies that the autocorrelation observed from a convective moving frame is well represented by the envelope of fixed point space-time correlation.

Normalization of the space-time correlation function. Since accurate space-time correlation magnitudes for large separations could not be obtained in the present study the integral scale, ${}_S T_{ii}$, has to be estimated by approximating the tail of the correlation function. A function, $\frac{1}{(1+P_1\tau)^2} - \frac{P_2\tau}{(1+P_2\tau)^3}$, was employed for the extrapolation where P_i are regression constants. The ratio $\frac{1}{(1+P_1\tau)^2}$ preserves the expected asymptotic characteristics of the space-time correlation while $\frac{P_2\tau}{(1+P_2\tau)^3}$ accounts for the rapid decay at small times. A similar method was used by Blackwelder and Kovasznay (1972) where the sum of two exponential terms was employed to approximate the space-time correlation function. The correlation data was unevenly weighted to obtain the regression constant, P_i, in the present study. The weighting factor for each data point was determined by its logarithmic value of optimum delay time which means more weight was given to data points at large separations. Figure 5.43 compares the fitted curve to a typical set of data points. ${}_S T_{11}$ was obtained by integrating the regression function (Figure 5.36).

The space-time correlation function was finally plotted versus $\frac{\Delta x_1}{U_S T_{ii}}$. The shear layer values for filtered turbulence are included on Figure 5.44 and compared with several sets of Eulerian space-time correlation data from other laboratory experiments. These experiments include data measured in another turbulent boundary layer (Farve, 1965; Frenkiel and Klebnoff, 1966), in grid turbulence corrected for energy decay (Comte-Bellot and Corrsin, 1971), and in a nearly homogeneous turbulent shear flow (Harris et al., 1977).

Space-time correlation functions for an unfiltered turbulence are replotted against normalized time coordinates in Figure 5.45 through Figure 5.47 for all three components of velocity fluctuations. Data are in good agreement with previous results for filtered turbulence. A universal shape for the Eulerian space-time correlation function seems to exist when presented in the non-dimensional coordinates. Such a curve is given in the figures in Figures 5.45 through 5.47.

5.5 Laboratory Plume Simulation

Lateral plume spread was evaluated from laboratory simulation of atmospheric dispersion. Data examined in this section includes the present diffusion measurements and measurements reported by Chaudhry and Meroney (1973). Plume dispersion was studied by Chaudhry and Meroney for three thermal stratification conditions from neutrally buoyant continuous point sources released in a boundary shear layer. Experimental details concerned with the measurements are summarized in their paper.

The diffuson data from all wind tunnel measurements were expressed in terms of the standard deviations of the horizontal concentration profile. The standard deviation of the concentration, σ_2, is defined as

$$\sigma_2^2 = \frac{\Sigma C_j X_{2j}^2}{\Sigma C_j} \quad , \tag{5.5}$$

where C_j is the mean concentration at a sampler, X_{2j} indicates the lateral distance from the plume centerline at the same height, and j is a particular sampler on the array.

A diffusion time t is approximated by the advection time scale x_1/U_a, where U_a represents the average mean velocity between source height and the sampler height.

5.5.1 Source size effect

The laboratory source employed during the dispersion experiments was large compared to an idealized point source.

Assuming a Gaussian form for the concentration distribution in the horizontal direction during plume dispersion, the probability density function for an ideal point source release may be written as

$$P(x_2) = \frac{1}{\sqrt{2\pi}\,\sigma} \exp\left\{-\frac{x_2^2}{2\sigma^2}\right\} . \tag{5.6}$$

But for a finite length source with width d, the probability density function would be

$$P(x_2) = \frac{1}{8\,d}\left\{\operatorname{erf}\left(\frac{x_2 - \frac{d}{2}}{\sqrt{2}\,\sigma_y}\right) - \operatorname{erf}\left(\frac{x_2 - \frac{d}{2}}{\sqrt{2}\,\sigma_y}\right)\right\} . \tag{5.7}$$

After some manipulation, the standard deviation of horizontal concentration for a finite source, σ_y, can be related to the ideal value, σ, by

$$\sigma^2 = \sigma_y^2 - \frac{d}{12} \tag{5.8}$$

provided that $x_2 >> \frac{d}{2}$.

Csanady (1973) remarked that "in the later stage of diffusion the concentrated source model is adequate, but the initial circumstances could only be elucidated by the slightly more complex distributed source model." Fackrell and Robins (1980) conducted an extensive study on the effect of source size on plume behavior in a simulated boundary layer. They concluded that flux of variance in the plume reaches a maximum close to the source, for the smallest source size, and thereafter the variance monotonically decreases. The results presented by Fackrell and Robins indicate that the mean plume width becomes independent of source size after x_1/d exceeds 10.

If the lateral plume spread is approximated by a Gaussian distribution, σ_y would be roughly the same as σ_2. Since the maximum error, $\sqrt{\sigma_2^2 - \sigma^2}/\sigma_2$ for the present configuration was found to be less than 4 percent, and the nearest sampling location to the source was at /d = 20, the influence of source size is negligible.

5.5.2 Comparison of laboratory simulated plumes to field dispersion experiments

Draxler (1976) examined diffusion data from eleven field experiments including elevated and ground release sources over a range of stratification conditions. Wind tunnel simulation results were compared to these experiments for the behavior of lateral plume dispersion based on the Taylor's diffusion theory, Equation 2.1.

Pasquill (1971) suggested a more explicit relationship for the diffusion parameter derived from Taylor's equation. For lateral dispersion,

$$[X_2^2(t)]^{\frac{1}{2}} = [u_2^2]^{\frac{1}{2}} T\, f_1(t/{}_L T_{22}) \,, \qquad (5.9)$$

where ${}_L T_{22}$ is the Lagrangian integral time scale and

$${}_L T_{22} = \int_0^\infty {}_L R_{22}(\tau)\, d\tau \,.$$

Since it is difficult to determine the true Lagrangian integral time scale from field diffusion experiments, Draxler introduced another time scale T_i, which should be proportional to ${}_L T_{22}$. He first suggested that the lateral plume growth may be related to time, t/T; for all data by

$$f_1 = \frac{1}{1+1.0(t/T_i)^{0.6}} \,,$$

where T_i is defined as the diffusion time required for f_1 to become equal to 0.5. In order to satisfy the theoretical limit for f_1 at large time and to provide a satisfactory fit to the data, he subsequently replaced the above equation by

$$f_1 = \frac{1}{1+0.9(t/T_i)^{0.5}} \,. \qquad (5.10)$$

The corresponding Lagrangian autocorrelation function may be derived from Taylor's equation and Equation 5.13. This yields

$${}_L R_{22}(t) = \frac{1-1.125\sqrt{t/T_i}}{(1+0.9\sqrt{t/T_i})^4} \,, \qquad (5.11)$$

but this expression for the autocorrelation function has an unrealistic infinite negative slope in the limit as $t \to 0$.

Phillips and Panofsky (1982) re-examined Draxler's ideas and concluded that Equation 5.11 is inconsistent with the theory of the inertial subrange according to which $R(\tau)$ varies as $1-C\tau$ near $\tau=0$, where C is a constant. They replaced Equation 5.10 by another form,

$$f_1(t/T_i) = 0.617\left[t/T_i - \frac{(T_i/t)^2}{5.25}\, \ell n(1+5.25t/T_i)\right]^{\frac{1}{2}} \,, \qquad (5.12)$$

which was derived from a simple form for ${}_L R_{22}(t)$

$$ {}_{L}R_{22}(t) = \frac{1}{(1+t/{}_{L}T_{22})^2} \quad . \tag{5.13} $$

An exponential Lagrangian autocorrelation function is also consistent with the assumptions of inertial subrange theory (Tennekes, 1979). In addition, the exponential form is consistent with the concept of a Markov process and is frequently preferred by analysts (Newumann, 1978). Thus if

$$ {}_{L}R_{22}(t) = e^{-t/{}_{L}T_{22}} \quad , \tag{5.14} $$

one obtains

$$ f_1(t/T_i) = 0.541 \left[\frac{T_i}{t} - \frac{(T_i/t)^2}{6.83} \left(1-e^{-6.83t/T_i}\right) \right]^{\frac{1}{2}} \quad . \tag{5.15} $$

Plume dispersion data. The laboratory measurements are compared with field data for horizontal diffusion from a ground source in Figure 5.48. Only the data set for strong stable stratification ($Ri_{\delta} = 0.25$) deviate significantly from the field results. The lateral diffusion from an elevated source are plotted in Figure 5.49. The stable elevated case seems to deviate only slightly from the field experiments.

The stable elevated case has been considered separately so that a cleaner comparison with Draxler's results may be made. Draxler utilized an average T_i for a specified stratification category which applied to all experimental sites under that category in his analysis. Unfortunately, this approach results in points which are consistently greater than 0.5 in Figure 5.50. This suggests that the actual value of T_i may be 3-4 times the value recommended by Draxler for the stable elevated source releases. In this case a replot of the field data would lie between $1+t/T_i = 1$ and 2, which agrees with the laboratory results.

Figure 5.51 displays the lateral diffusion measured at the same height as an elevated source. Plume width variations found for the elevated case in Figure 5.51 should theoretically be described most accurately by Taylor's theory. Yet no significant improvement was found in comparison to Figures 5.48, 5.49 and 5.50.

Comparison with Predictions. The proportion of variation explained by prediction (or regressive curve), which describes the coherence between data and formulae, was examined by an analysis of variance. The experimental data employed in the analysis consisted of field experiments in Figure 5.52 and the laboratory results, but not including the stable stratification case SP. The correlation coefficient R appears to be acceptable for all three equations as shown in Table 5.4. The residual, $f_1(t/T_i)-\bar{f}_1(t/T_i)$, is displayed in Figure 5.53a for field

measurements and in Figure 5.53b for laboratory results, where $\hat{f}_i(t/T_i)$ is the predicted value. The residuals were compared to a normal distribution by the Kolmogorov-Smirnov goodness of fit test (Conover, 1971). The level of significance in the test suggests that a normal distribution hypothesis is rejected by residuals of Equation 5.10. Therefore, the probability distribution of residuals is presented with the correlation coefficients in Table 5.4. Equations 5.12 and 5.15 were found to fit the data slightly better. Yet no significant systematic deviation can be found among the three predictions during comparison with field or laboratory experimental results.

Comparison among predictions. Equations 5.10, 5.12 and 5.15 are plotted on Figures 5.49 through 5.52. Comparison between the predictive formulae and the experimental data reveals that:

(1) Difference among the three functional values are not significant. All of the expressions fit the trend of atmospheric field data as shown in Figure 5.52. However, the equations imply different values for the Lagrangian integral time scale, i.e., $T_i = 1.64\ {}_LT_{22}$ for Equation 5.10, $T_i = 5.25\ {}_LT_{22}$ for Equation 5.12 and $T_i = 6.83\ {}_LT_{22}$ for Equation 5.15.

(2) The Lagrangian autocorrelation function corresponding to Equation 5.12 preserves an exponential form for short diffusion times such that

$$ {}_LR_{22}(t) = e^{-2t/{}_LT_{22}} = \frac{1}{(1 + \frac{t}{{}_LT_{22}} + \ldots)^2} \approx \frac{1}{(1 + \frac{t}{{}_LT_{22}})^2} . \quad (5.19) $$

Neglecting higher order terms in the expressions prevents $f_1(t/T_i)$ from dropping rapidly at longer diffusion times. Since a higher correlation at larger times implies a larger value of the Lagrangian integral time scale, removal of higher order terms in the expansion results in an increase in the Lagrangian integral time scale for the same T_i; thus ${}_LT_{22}$ calculated from Equation 5.12 is 1.3 times the value calculated from Equation 5.18.

(3) For the same set of data, the implied Lagrangian integral time scale is seen to vary from $T_i/6.83$ to $T_i/1.64$. Although it is well known that drastically different forms for ${}_LR_{22}(t)$ give very similar results for the dispersion using Taylor's integral relation (Pasquill, 1974), the importance of selecting a correct integral time scale in any predictive scheme becomes clear.

Importance of the Lagrangian time scale. It is obvious that accurate specification of T_i (or ${}_LT_{22}$) is necessary to use Pasquill's f_1 curve as a predictive scheme for plume dispersion. Unfortunately, a

wide range exists in the magnitude for the Lagrangian integral time scale, primarily due to thermal stratification and complex terrain effects. Neumann (1979) used a simple exponential expression for the Lagrangian velocity correlation function during turbulent diffusion. A set of integral time scales was calculated corresponding to the various Hosker-Briggs-Gifford-Pasquill stability categories. Since the integral time scale is difficult to estimate in the atmosphere, researchers tend to simplify the problem and assume that the f_1 curves are only a function of downwind distance. Briggs (1973) suggested a dimensionally inconsistent function for the standard deviation of plume width. Hanna (1982) recommended a simplified function for the f_1 curve compatible with Briggs' formula. Table 5.5 summarizes the integral time scale used (or implied) by the different authors. The variation is indeed astonishing. $_{L}T_{22}$ varies from several hundred seconds as predicted by Draxler (1976) to an order of 10^4 seconds as suggested by Gifford (1982). All these time scales are based on field measurements in the atmosphere; however, their stability classification and the flow configuration may vary. Hence, additional knowledge about the integral time scale and how it relates to basic physical characteristics of a turbulent shear layer is required.

Table 5.1. Characteristics of the simulated atmospheric boundary layer, neutral

Fixed Z_o Scale Ratio: .45/600	MODEL SCALE (1/1250)			PROTOTYPE			FIELD RESULT COUNIHAN (1975)		
	U_∞ = 2 m/s U_* = 0.0725 m/s	U_∞ = 3 m/s U_* = 0.129 m/s	U_∞ = 5 m/s U_* = 0.217 m/s	U_∞ = 2 m/s U_* = 0.0725 m/s	U_∞ = 3 m/s U_* = 0.0129 m/s	U_∞ = 5 m/s U_* = 0.217 m/s	U_∞ = 2 m/s U_* = 0.0725 m/s	U_∞ = 3 m/s U_* = 0.0129 m/s	U_∞ = 5 m/s U_* = 0.217 m/s
δ (m)	0.45	0.45	0.45	600	600	600	600	600	600
n	0.166	0.163	0.146	0.166	0.163	0.146	0.14	0.13	0.12
Z_o (m)	4.0×10^{-5}	2.0×10^{-5}	1.0×10^{-5}	0.05	0.025	0.0125	0.05	0.025	0.0125
$\left(\frac{U_*}{U_\infty}\right)^2$	1.314×10^{-3}	1.85×10^{-3}	1.88×10^{-3}	1.314×10^{-3}	1.85×10^{-3}	1.88×10^{-3}	1.97×10^{-3}	1.79×10^{-3}	1.61×10^{-3}
$\left(\frac{\sqrt{\overline{u'^2}}}{U}\right)_{z/\delta = 1/20}$	0.125	0.155	0.120	0.125	0.155	0.120	0.155	0.140	0.128
$\left(\frac{\sqrt{\overline{u'^2}}}{U}\right)_{z/\delta = 1/6}$	0.10	0.106	0.085	0.10	0.106	0.085	0.131	0.120	0.111
L_x (m) $\left(z/\delta = 0.444\right)$	0.103	0.17		129.1	212.5		220 (approx.)	250 (approx.)	

Table 5.2. Turbulent length scale of the stable stratified boundary layer.

$\frac{x_3}{\delta}$	u_1-component			u_2-component			u_3-component		
	L (cm)	Λ_f (cm)	λ_f (cm)	L (cm)	Λ_f (cm)	λ_f (cm)	L (cm)	Λ_f (cm)	λ_f (cm)
.028	3.96	3.34	1.62	1.74	1.70	.835	1.91	1.73	.627
.053	6.16	4.40	1.56	2.34	2.14	.889	1.87	1.53	.528
.08	5.18	4.48	1.68	2.10	2.07	.904	2.35	2.24	.554
.107	5.20	4.61	1.62	2.88	2.83	1.02	2.15	2.09	.547
.133	7.39	5.31	1.62	3.69	2.78	.945	2.18	2.18	.557
.20	9.21	6.41	1.58	3.72	3.14	.982	2.22	2.12	.515
.267	9.18	6.97	1.67	4.70	4.16	1.03	2.14	1.99	.541
.40	11.79	8.39	1.79	7.60	5.62	1.21	3.19	3.04	.570
.60	10.76	8.44	1.30	7.54	6.43	1.06	3.76	3.65	.593

Table 5.3. Turbulent length scale of the neutral stratified boundary layer.

(a) Integral length scales

$\frac{x_3}{\delta}$	L_{11}	L_{12}	L_{21}	L_{22}	L_{31}	L_{32}
.044	19.5	2.54	--	--	2.10	.78
.22	26.9	4.69	5.22	5.14	4.00	2.35
.44	26.0	5.50	5.59	6.01	5.18	3.46

(b) Normalized integral length scales.

$\frac{x_3}{\delta}$	$\frac{L_{11}}{L_{11}}$	$\frac{L_{12}}{L_{11}}$	$\frac{L_{21}}{L_{11}}$	$\frac{L_{22}}{L_{11}}$	$\frac{L_{31}}{L_{11}}$	$\frac{L_{32}}{L_{11}}$
.044	1	.13	--	--	.11	.040
.22	1	.17	.19	.19	.15	.087
.44	1	.21	.22	.23	.20	.13
Teunissen* (1980)	1	.18	.40	.22	.14	.027
Teunissen (1980)**	1	.19	.31	.23	.089	.040

* From correlation integral
** From exponential fit

Table 5.4. Summary of Comparisons Between Data and Predictions

Formula	% of variation explained by the formula		Correlation Coefficient R		Level of Significance α**		Probability distribution of residual					
							$p(\|e\| \leq 0.05)$		$p(0.05 < \|e\| \leq 0.1)$		$p(\|e\| \geq 0.1)$	
	Field Exp.	Lab.* Data	Field Exp.	Lab. Data	Field Exp.	Lab. Data	Field Exp.	Lab. Data	Field Exp.	Lab. Data	Field Exp.	Lab. Data
Equation 3	80.8	74.7	.899	.864	<0.01	<0.01	.458	.472	.325	.303	.217	.225
Equation 5	78.9	84.5	.888	.919	0.09	0.03	.496	.618	.292	.225	.212	.157
Equation 8	72.9	86.5	.853	.930	0.10	0.10	.496	.630	.275	.202	.222	.168

* Stable Stratification case SP is not included

** Residuals were tested to a normal distribution function by the Kolmogorov-Smirnov goodness of fit test.

Table 5.5. Summary of Lagrangian Integral Time Scales

Stability Category	$\overline{u'^2}$ $(m/s)^2$	U m/s	L^T_{22} (sec) Neumann (1978)	Briggs (1973) $L^T_{22}=T_i/5.23$	Briggs (1973) $L^T_{22}=T_i/6.83$	Hanna (1982) $L^T_{22}=T_i/5.23$	Hanna (1982) $L^T_{22}=T_i/6.83$	Draxler (1976)	Phillips and Panofsky (1982)	Gifford (1982)
A	.19	2	2400	2900	2200	2900	2200	200~600	190~700	~10^4
B	.24	3.5	1700	2300	1800	1640	1250	200~600	190~700	~10^4
C	.36	5	700	900	690	1050	880	200~600	190~700	~10^4
D	.17	5	750	1070	820	1030	880	200~600	190~700	~10^4
E	.044	3.5	1000	1640	1250	1640	1250	200~600	190~700	~10^4
F	.0064	2	2250	2900	2200	2900	2200	200~600	190~700	~10^4

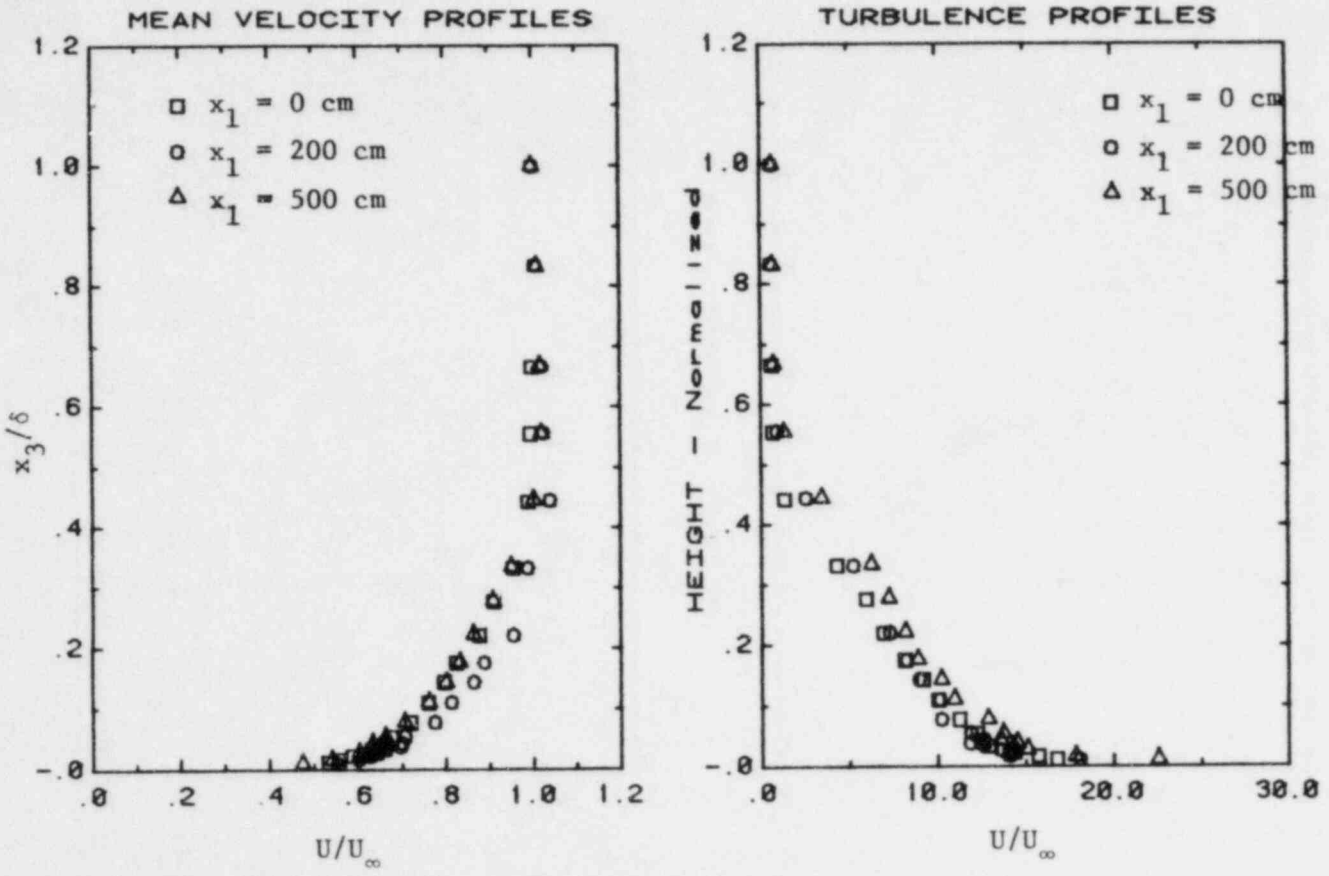

Figure 5.1. Mean velocity and turbulent intensity profiles for neutral stratified boundary layer at U_∞ = 200 cm/sec.

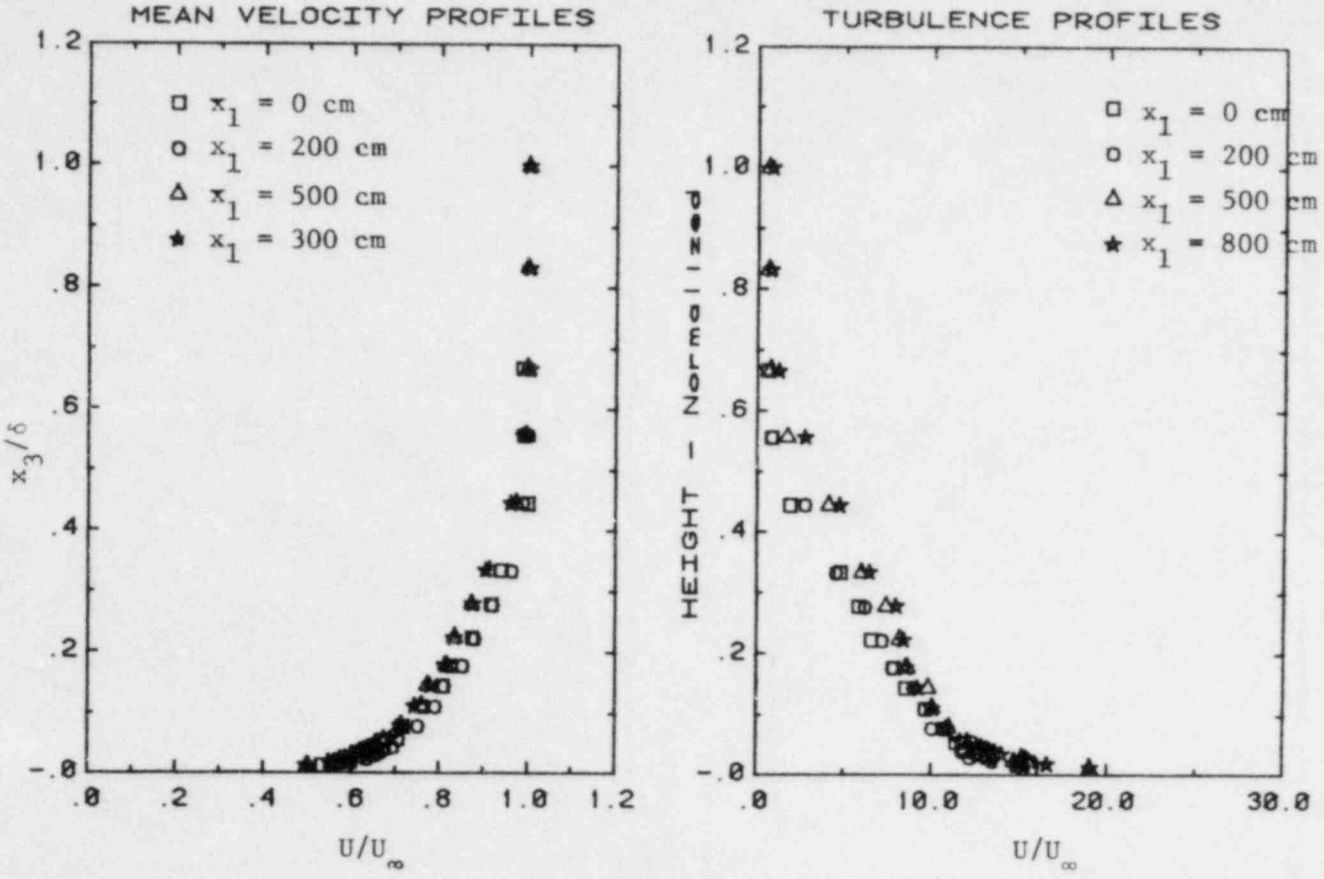

Figure 5.2. Mean velocity and turbulent intensity profiles for neutral stratified boundary layer at U_∞ = 300 cm/sec.

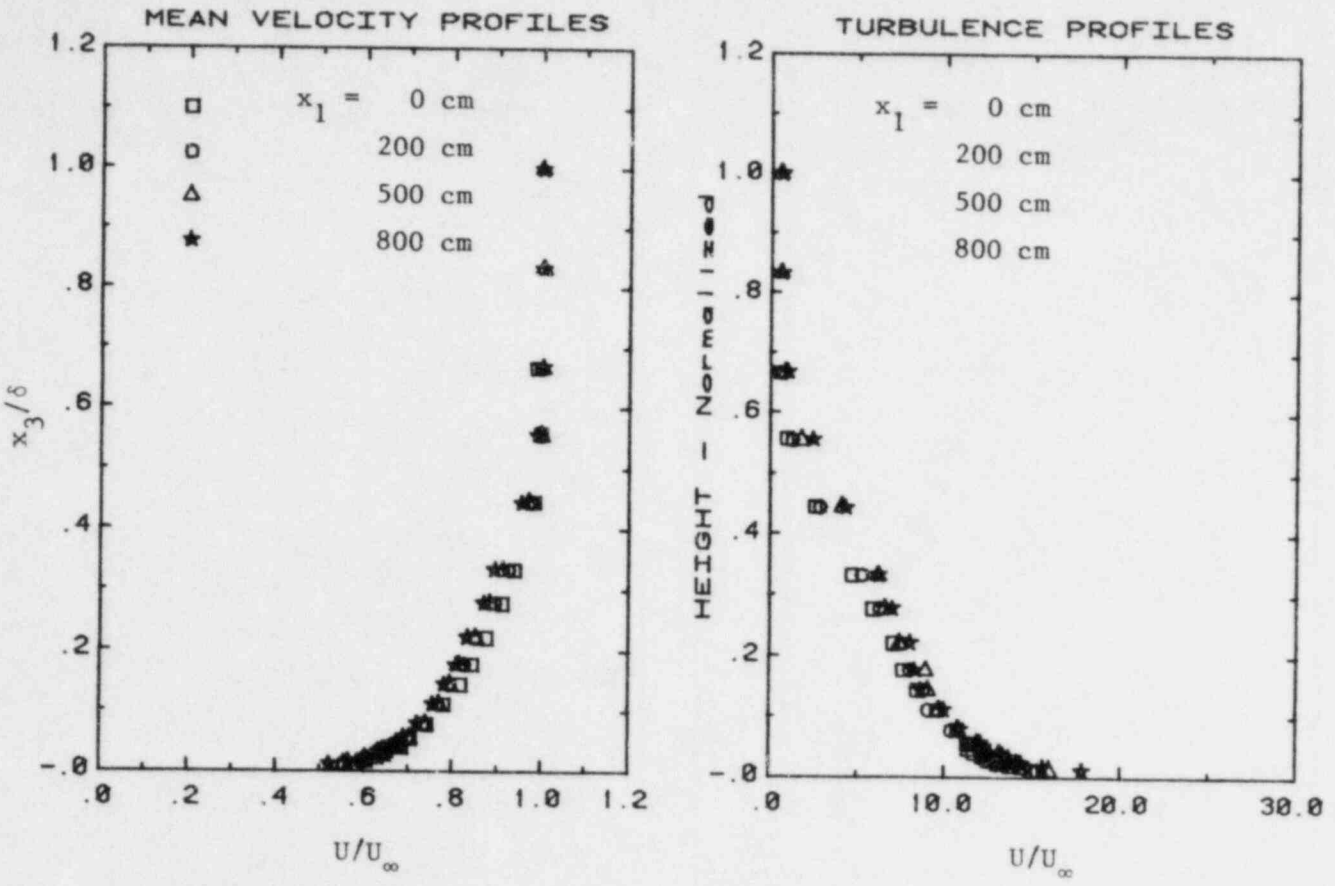

Figure 5.3. Mean velocity and turbulent intensity profles for neutral stratified boundary layer at U_∞ = 500 cm/sec.

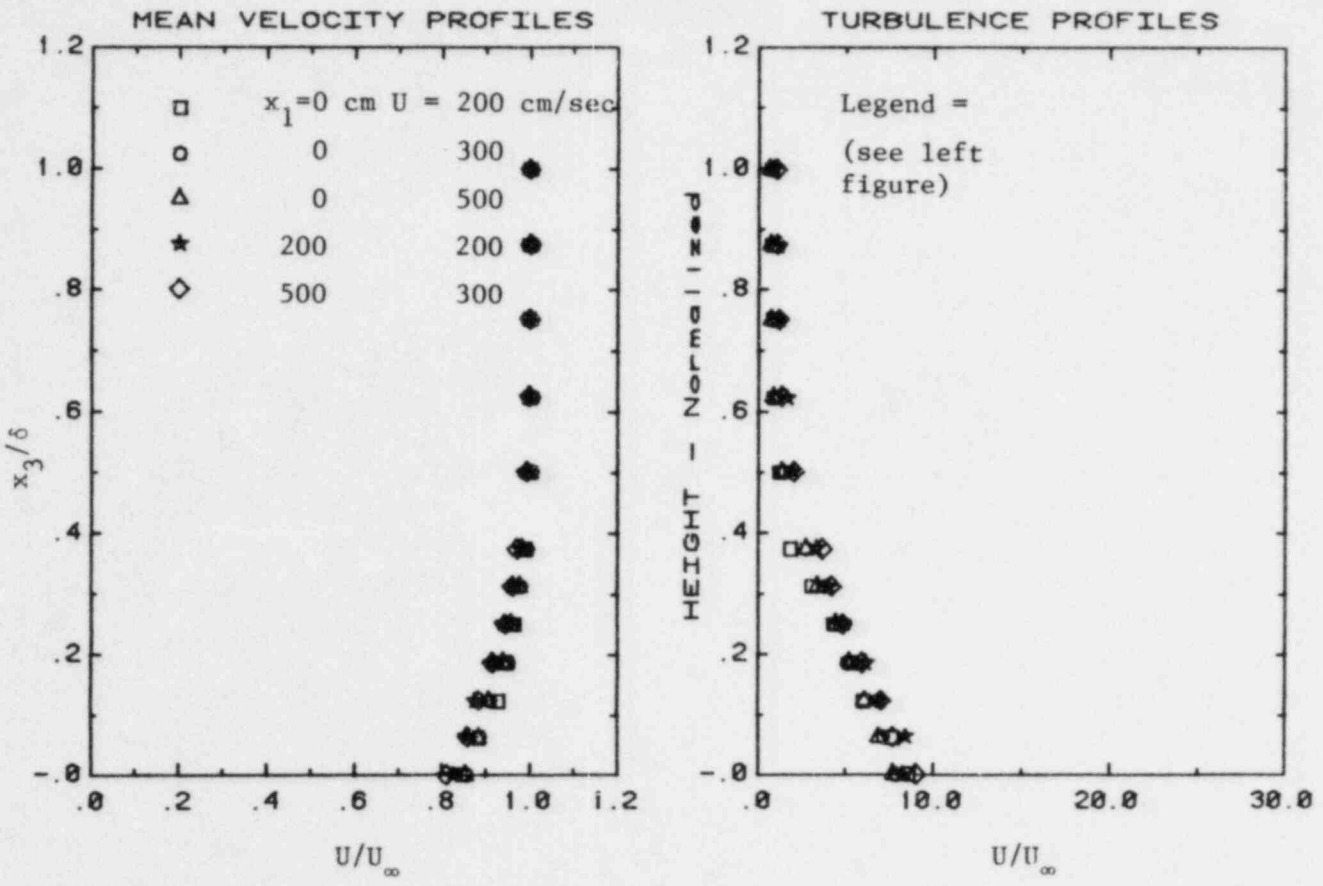

Figure 5.4. Lateral distribution of mean velocity and turbulent intensity profiles for neutral stratified boundary layer at 80 cm height.

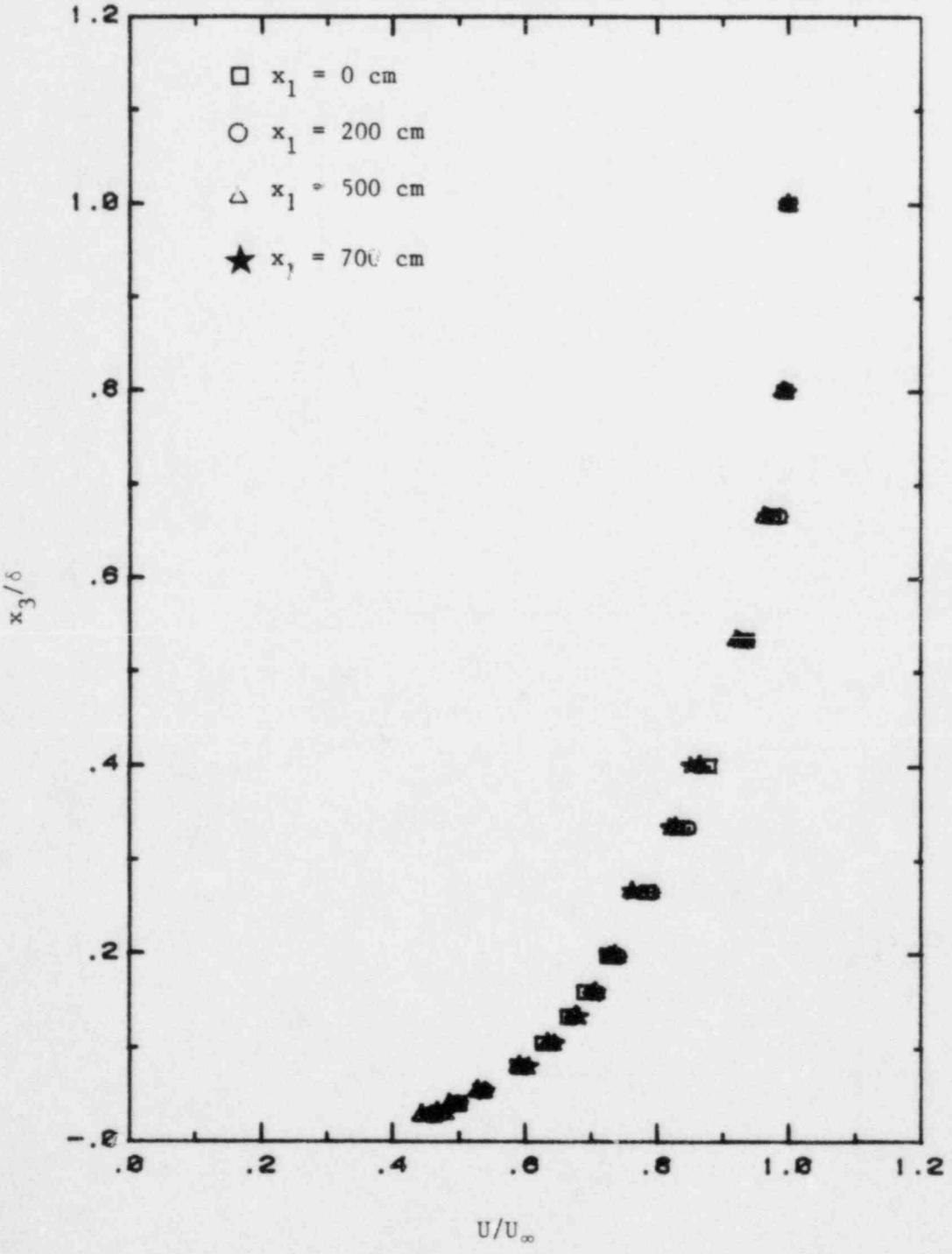

Figure 5.5. Mean velocity profiles for stable stratified boundary layer at U_∞ = 200 cm/sec.

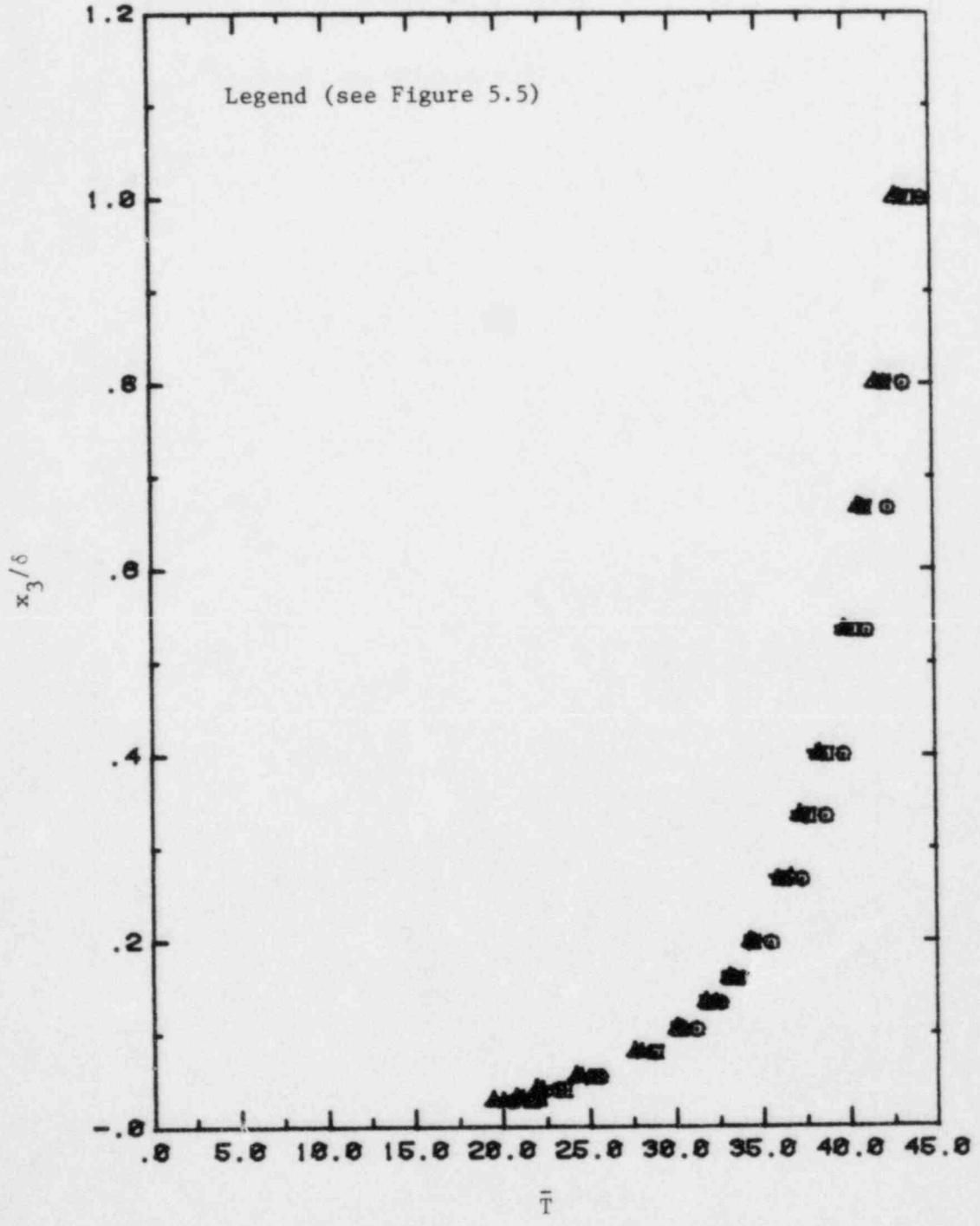

Figure 5.6. Mean velocity profiles for stable stratified boundary layer at U_∞ = 200 cm/sec.

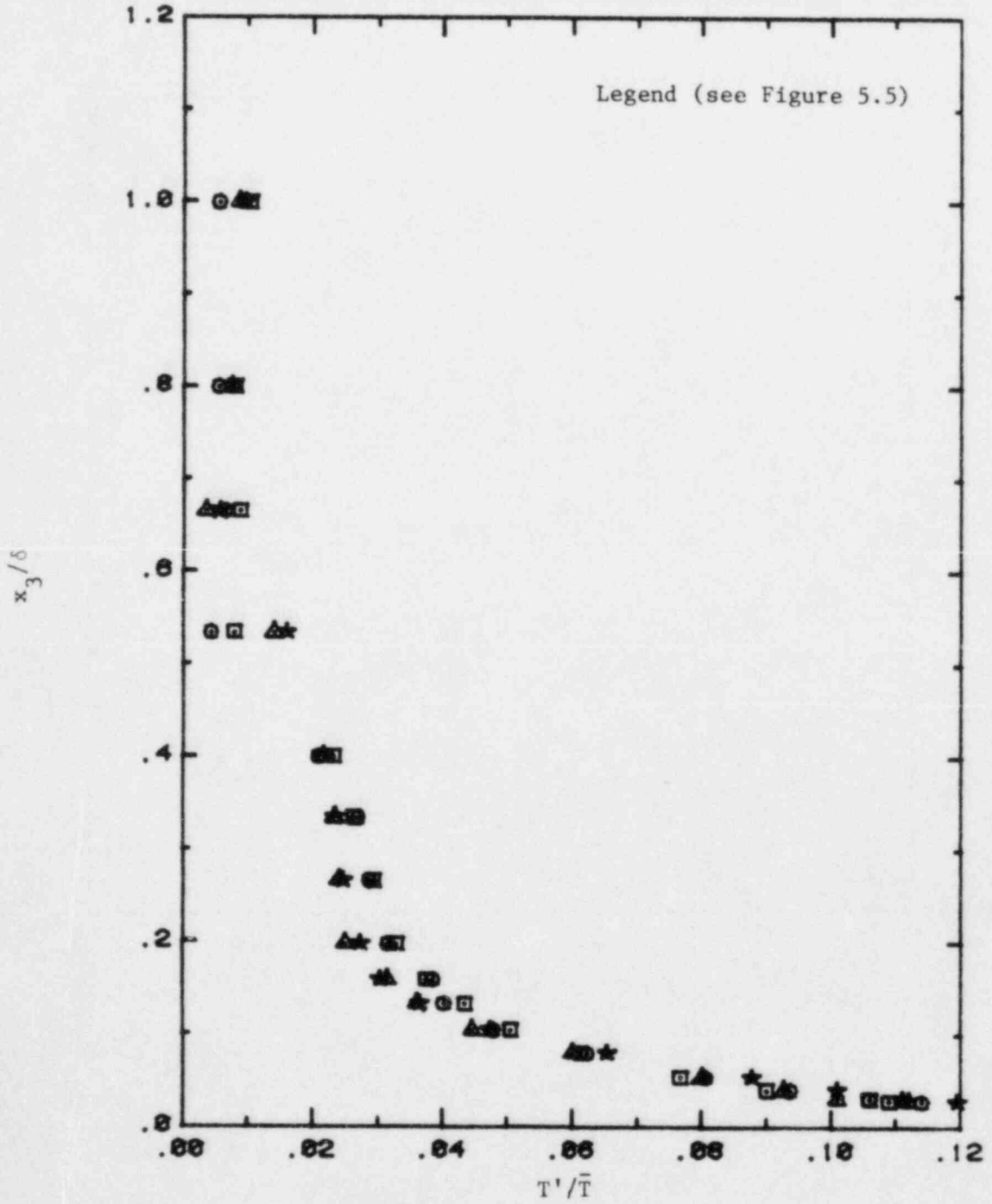

Figure 5.7. Temperature fluctuation profiles for stable stratified boundary layer at U_∞ = 200 cm/sec.

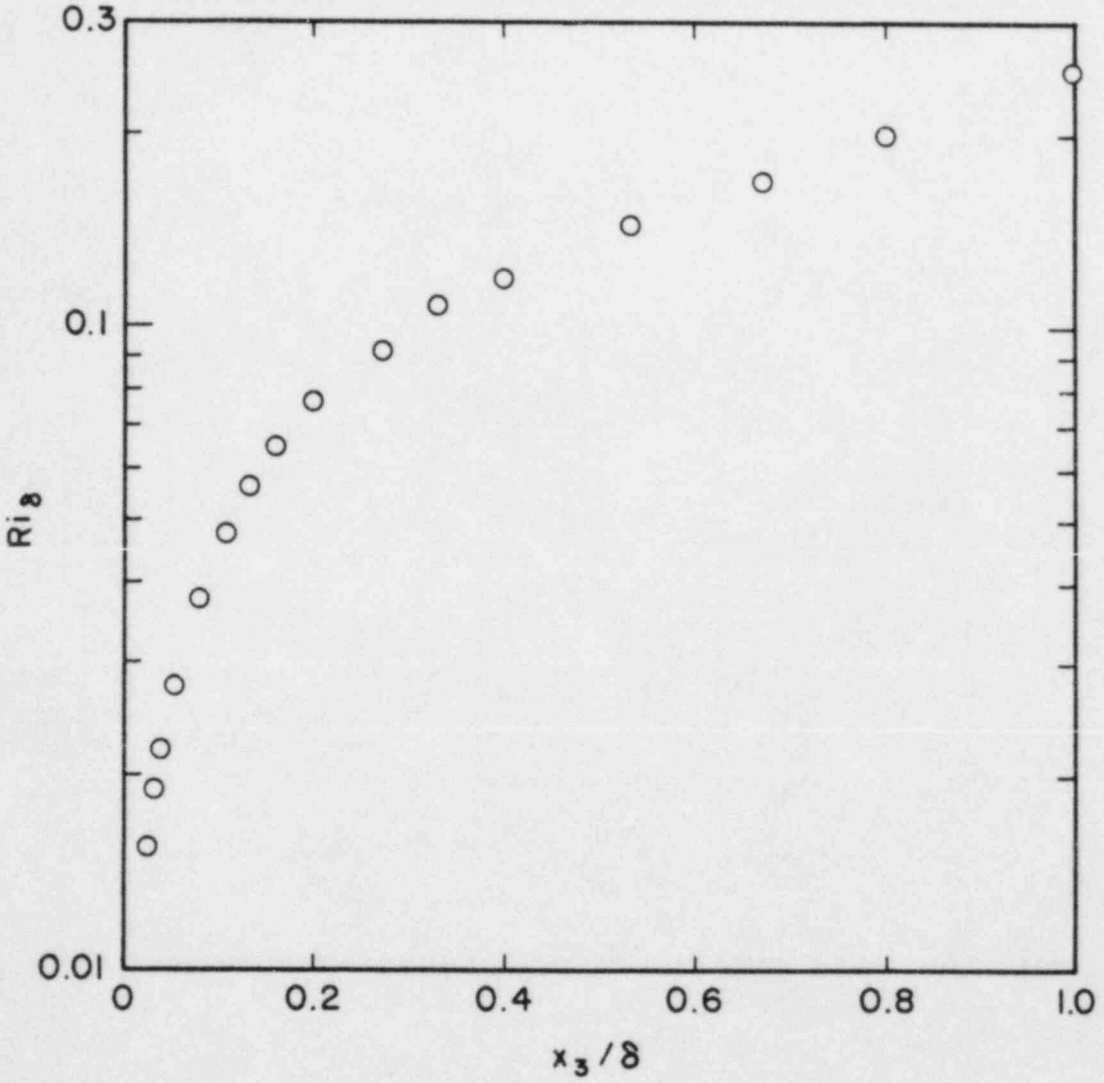

Figure 5.8. Variation of R_i with x_3/δ; U_∞ = 200 cm/sec.

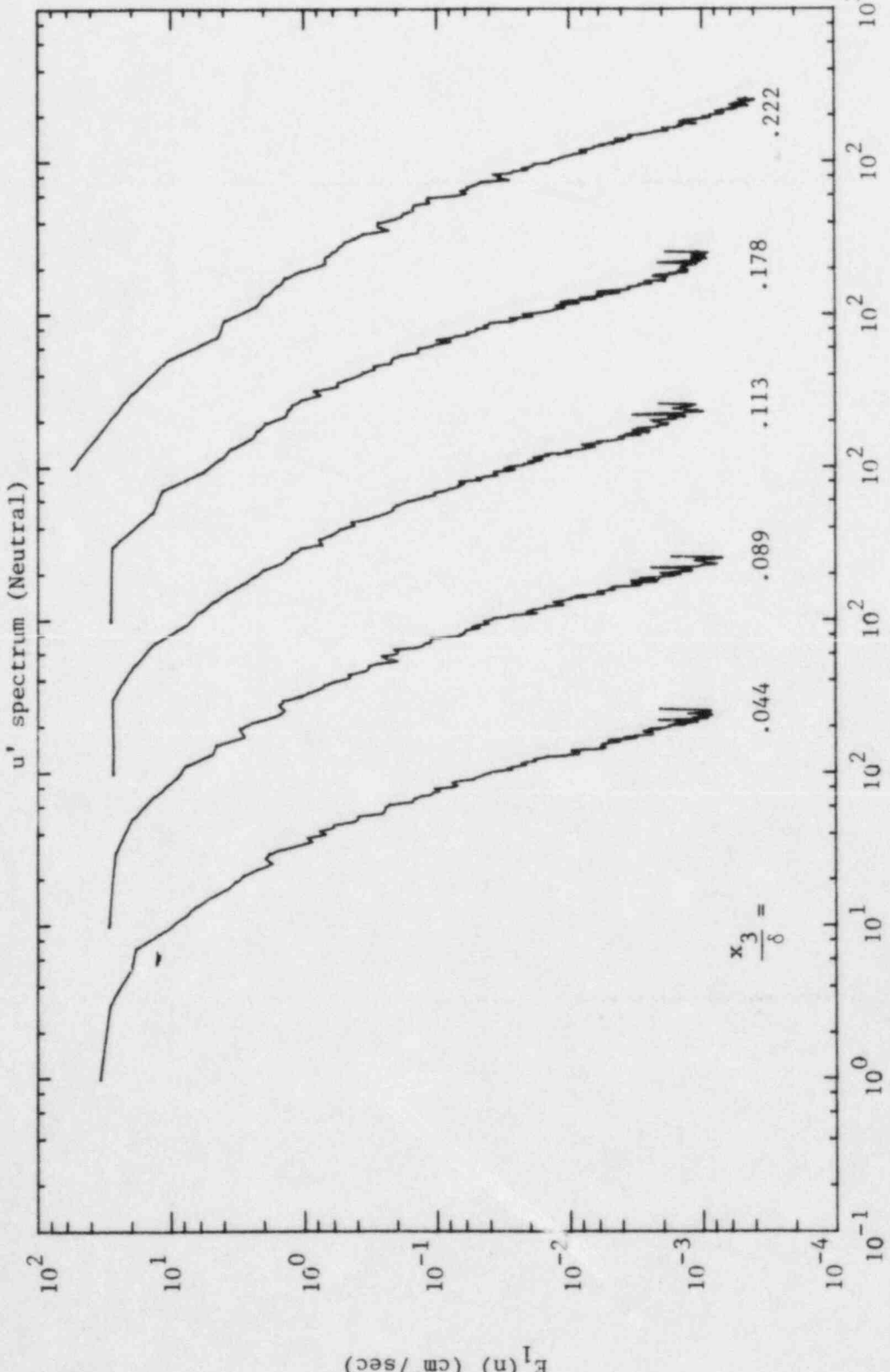

Figure 5.9. Energy spectra of longitudinal velocity fluctuations; U_∞ = 200 cm/sec, neutral, filtered.

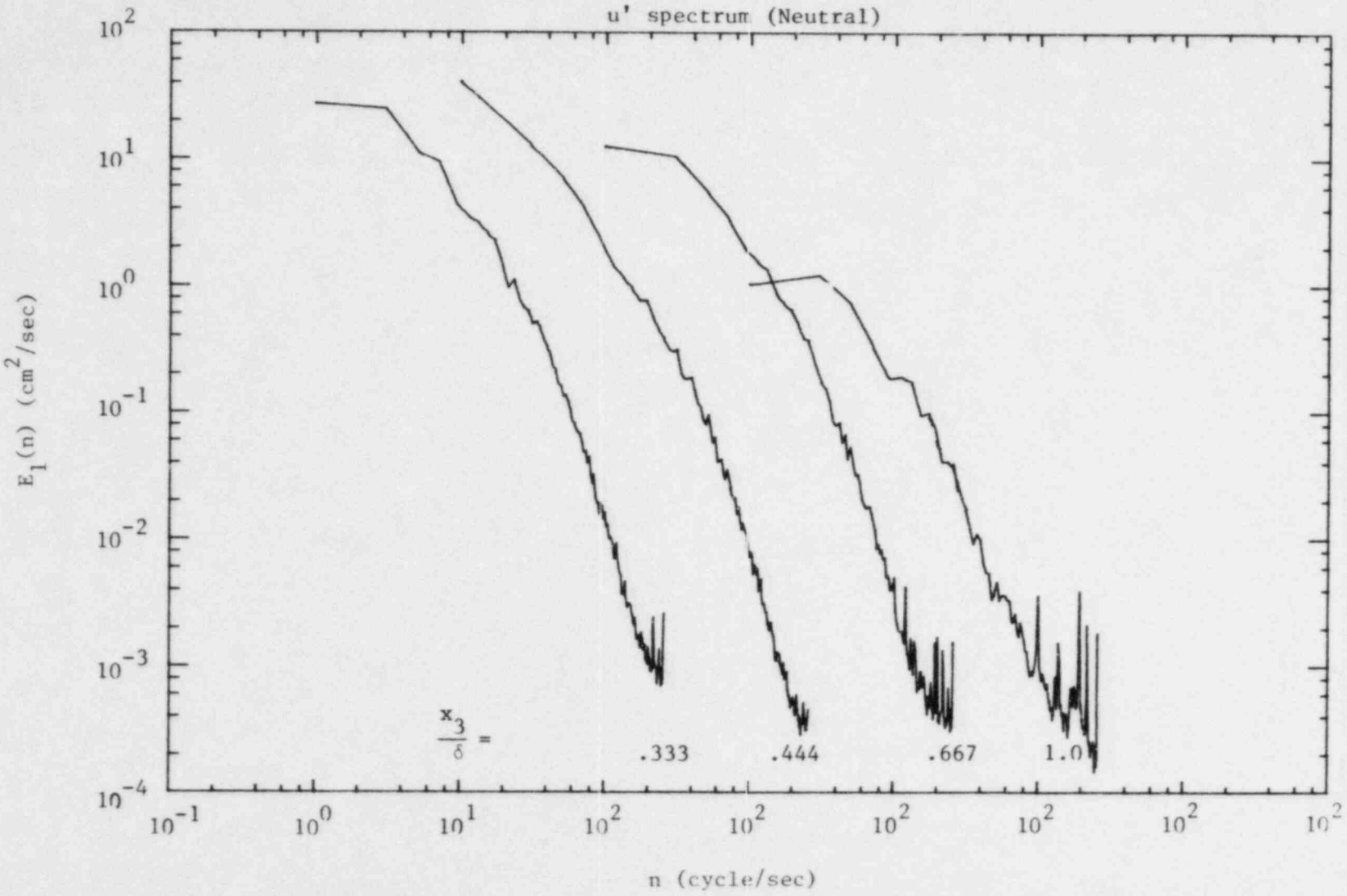

Figure 5.9. Energy spectra of longitudinal velocity fluctuations; U_∞ = 200 cm/sec, neutral, filtered (continued).

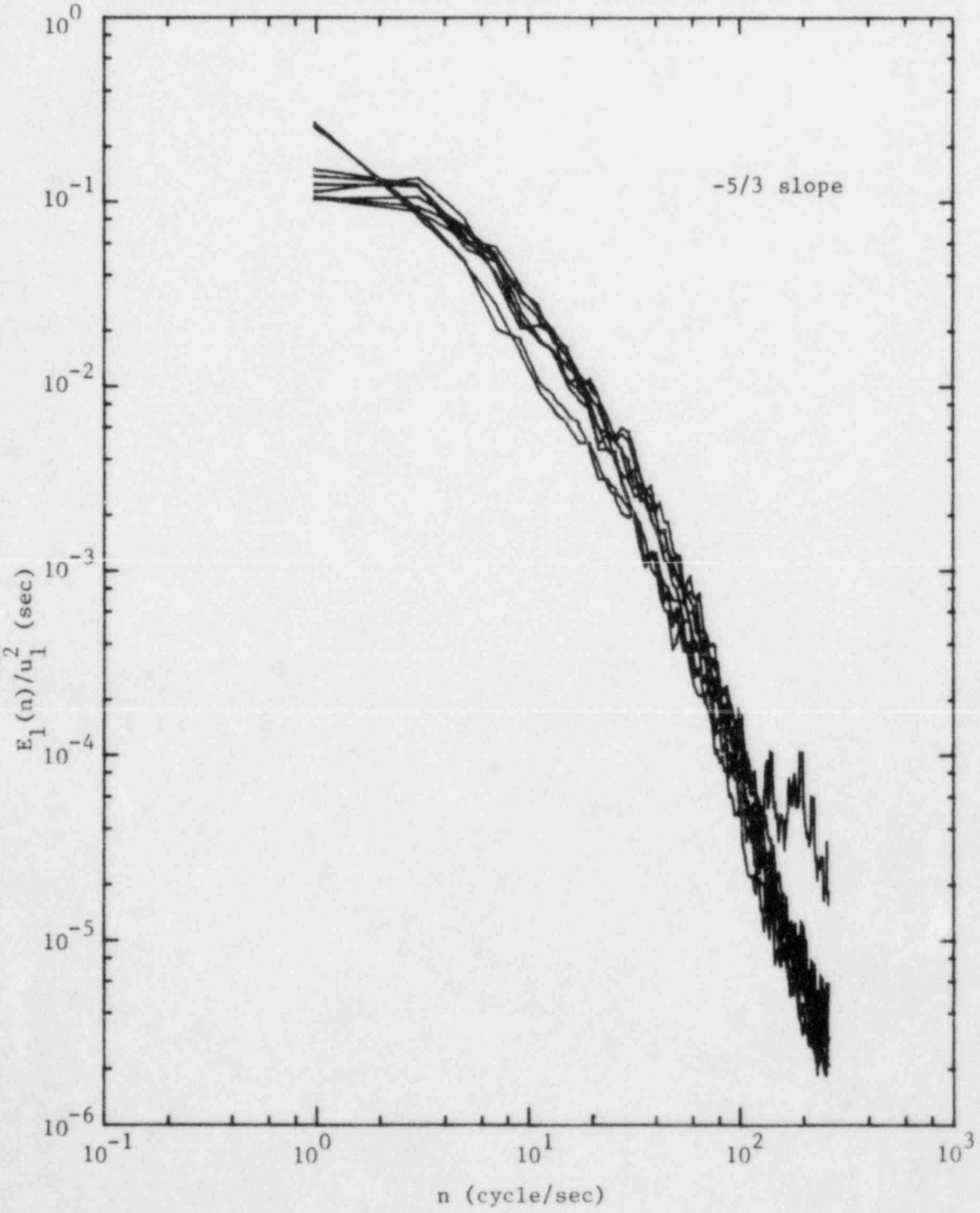

Figure 5.10. Normalized energy spectra of longitudnal velocity fluctuations; U_∞ = 200 cm/sec, neutral, filtered.

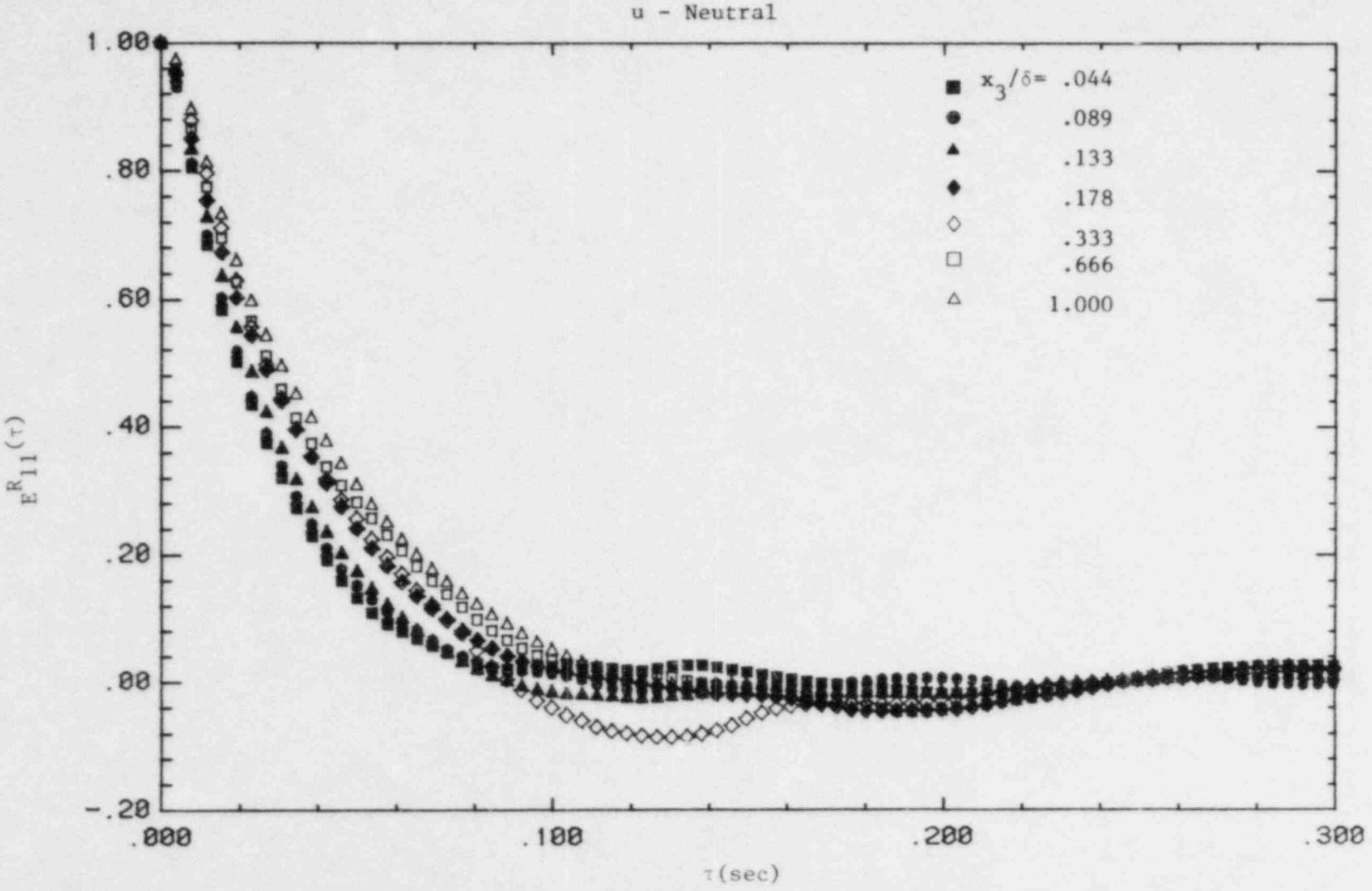

Figure 5.11a. Longitudinal velocity autocorrelation functions; U_∞ = 200 cm/sec, neutral, filtered.

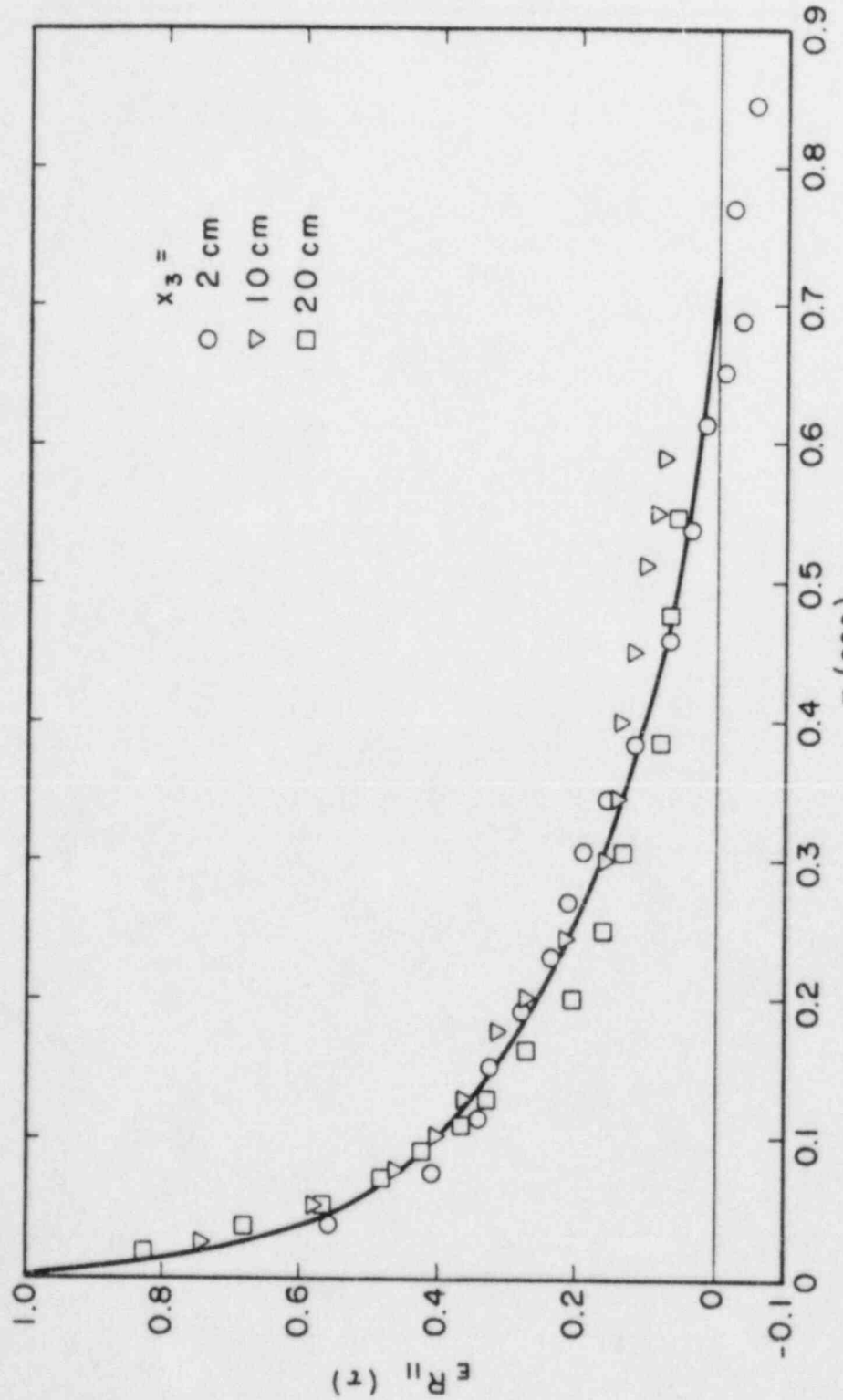

Figure 5.11b. Longitudinal velocity autocorrelation functions; U_∞ = 200 cm/sec, neutral (unfiltered turbulence).

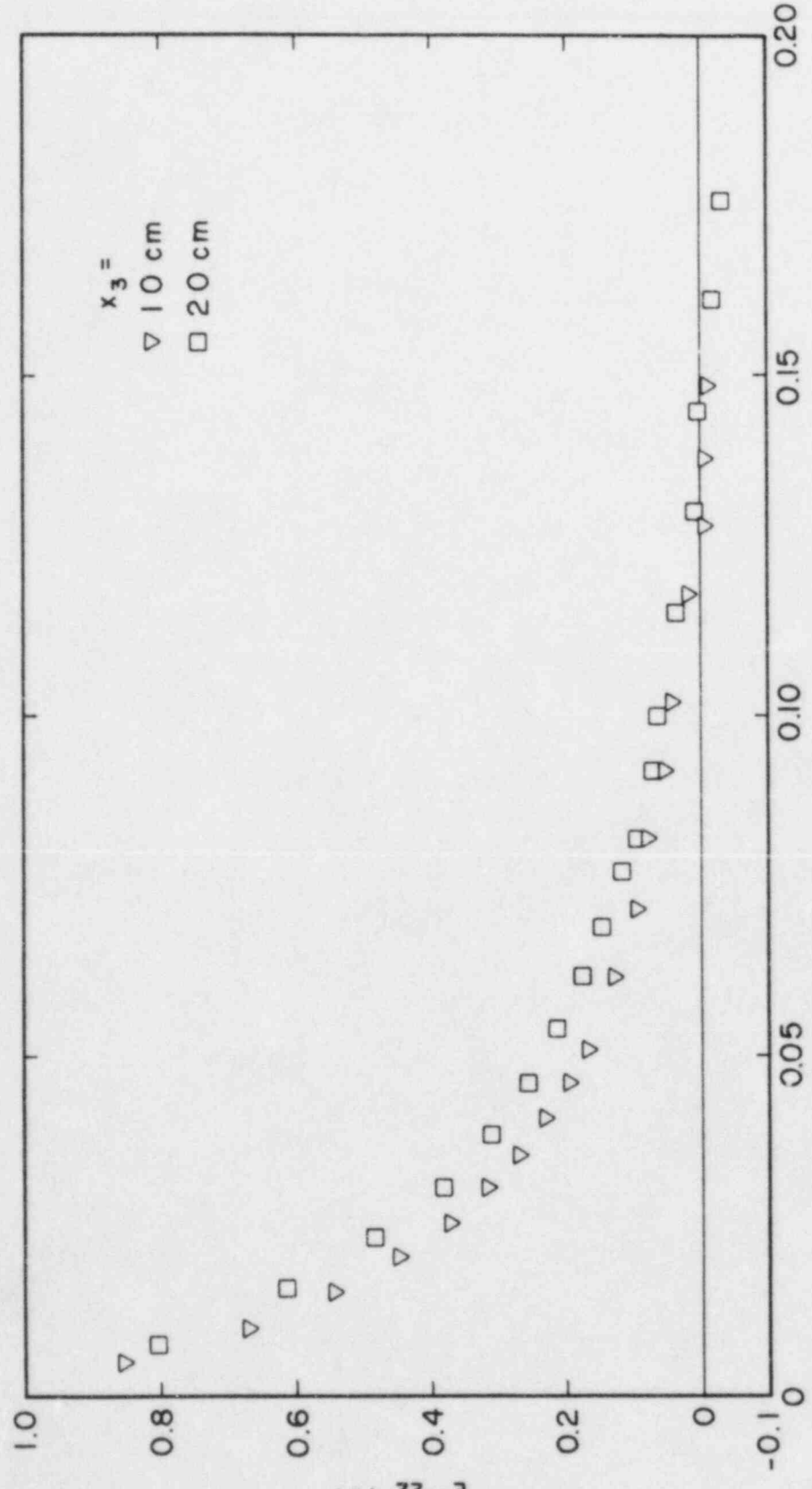

Figure 5.12. Lateral velocity autocorrelation functions; U_∞ = 200 cm/sec, neutral.

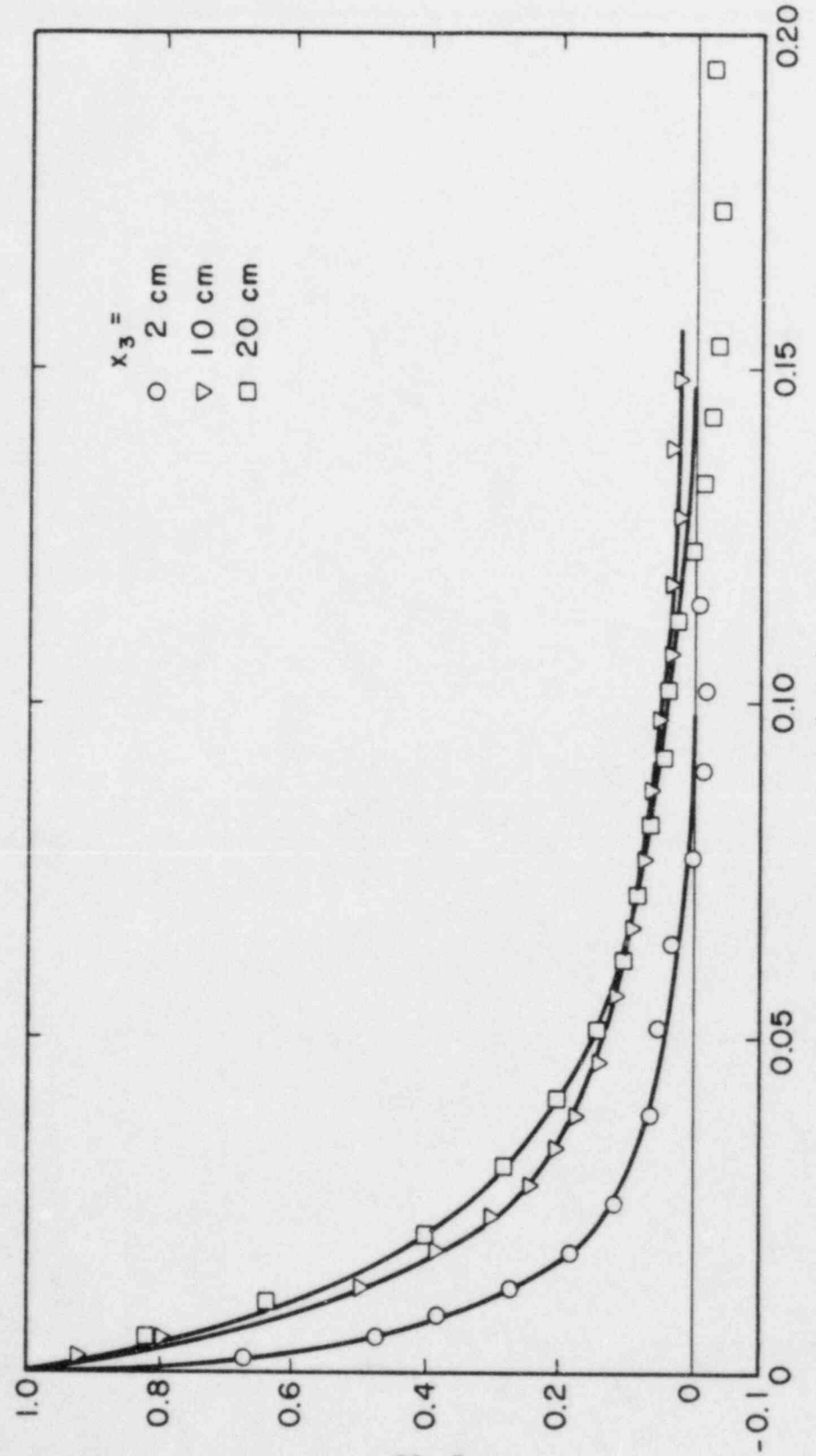

Figure 5.13. Vertical velocity autocorrelation functions; U_∞ = 200 cm/sec, neutral.

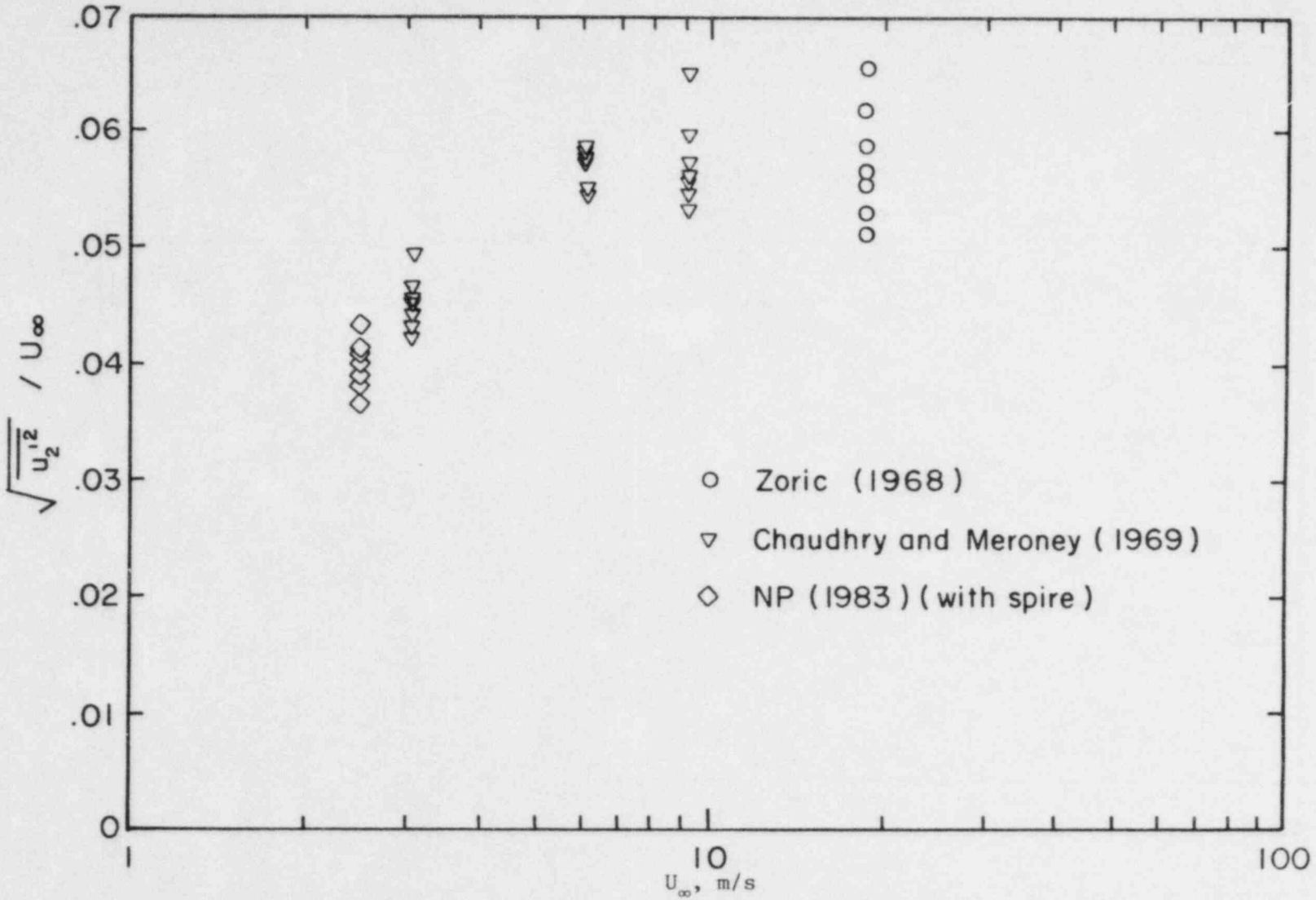

Figure 5.14. Lateral turbulence intensity vs. free stream velocity, neutral.

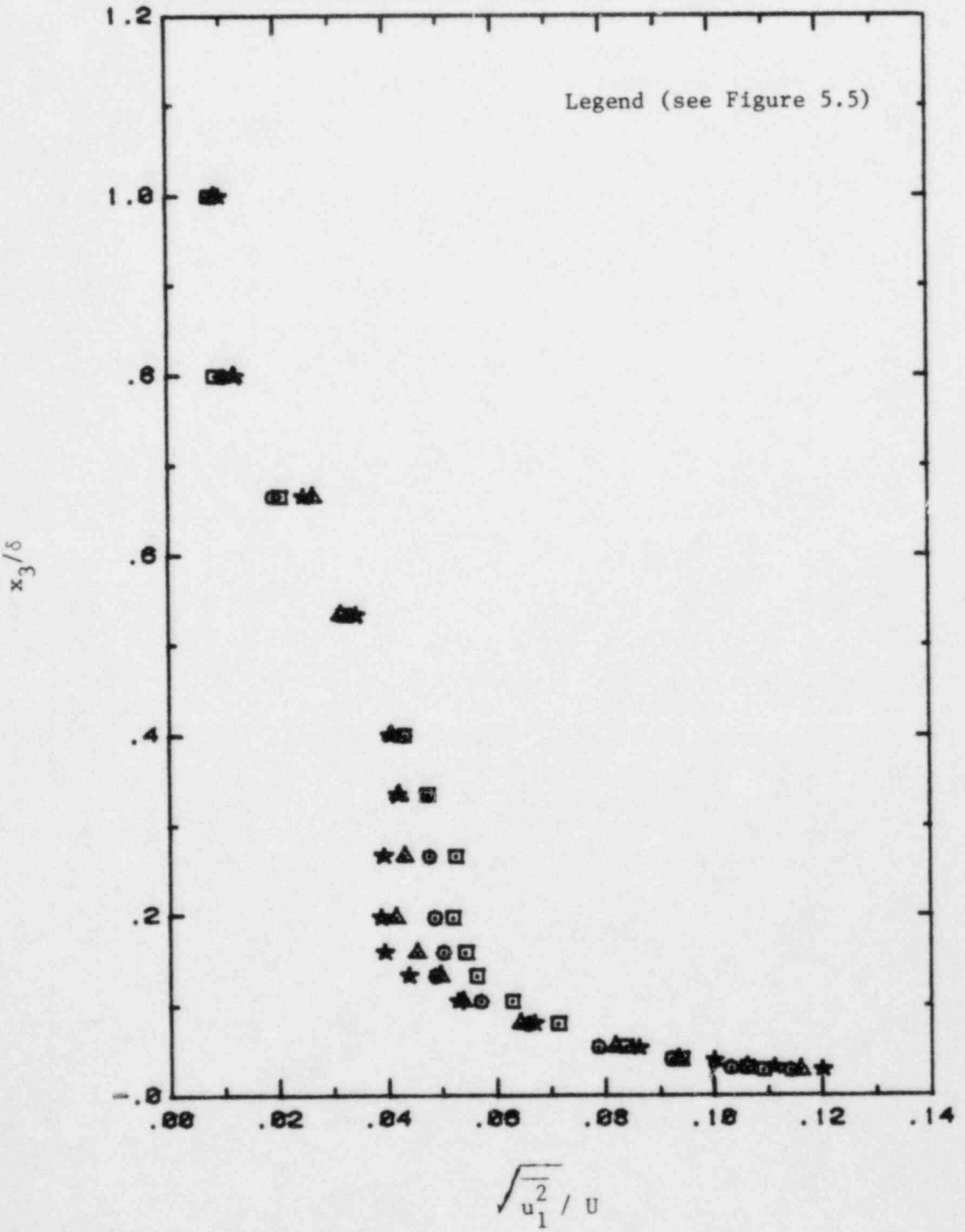

Figure 5.15. Longitudinal turbulent intensity profiles; U_∞ = 200 cm/sec, stable.

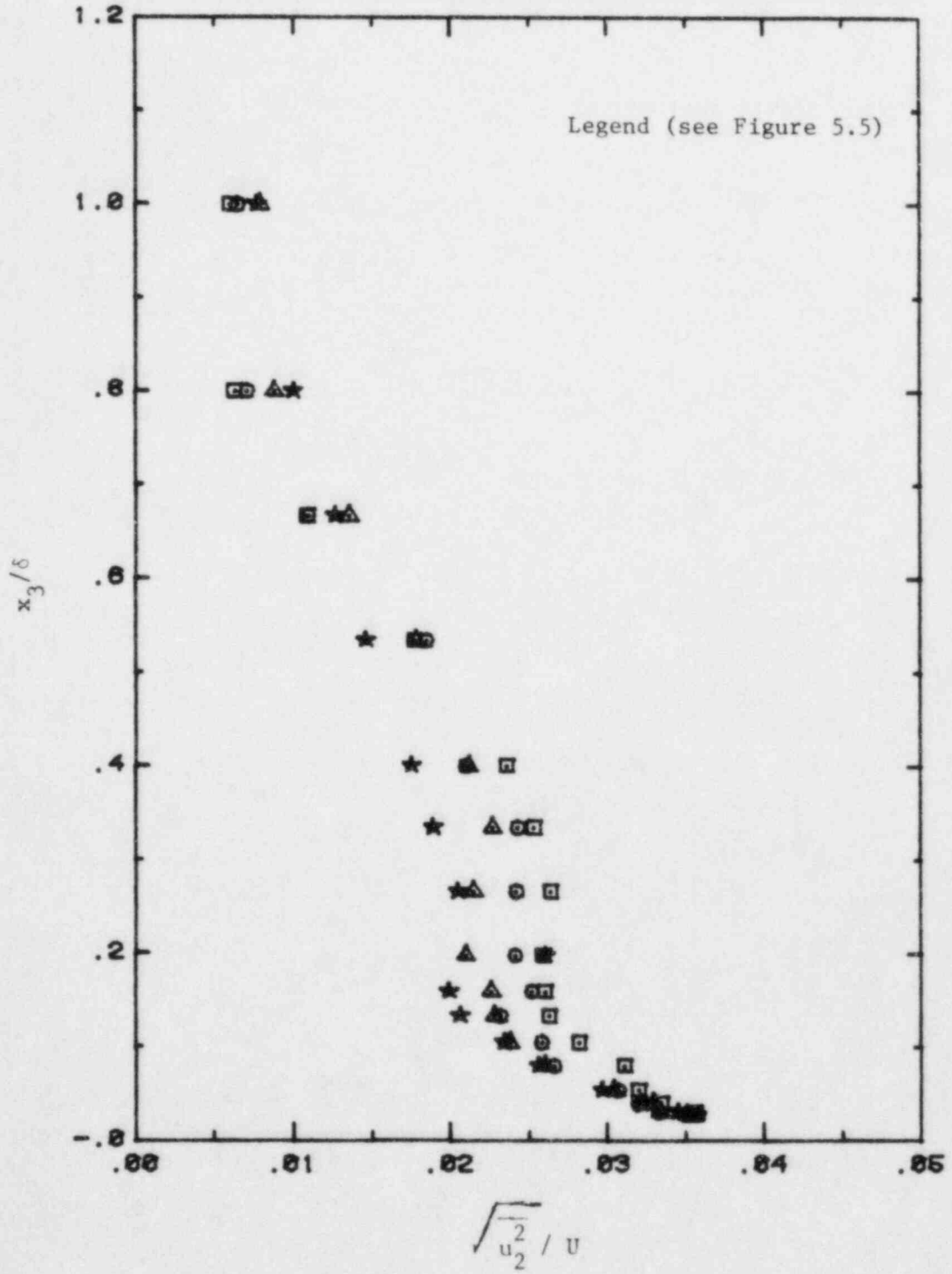

Figure 5.16. Lateral turbulent intensity profiles;
U_∞ = 200 cm/sec, stable.

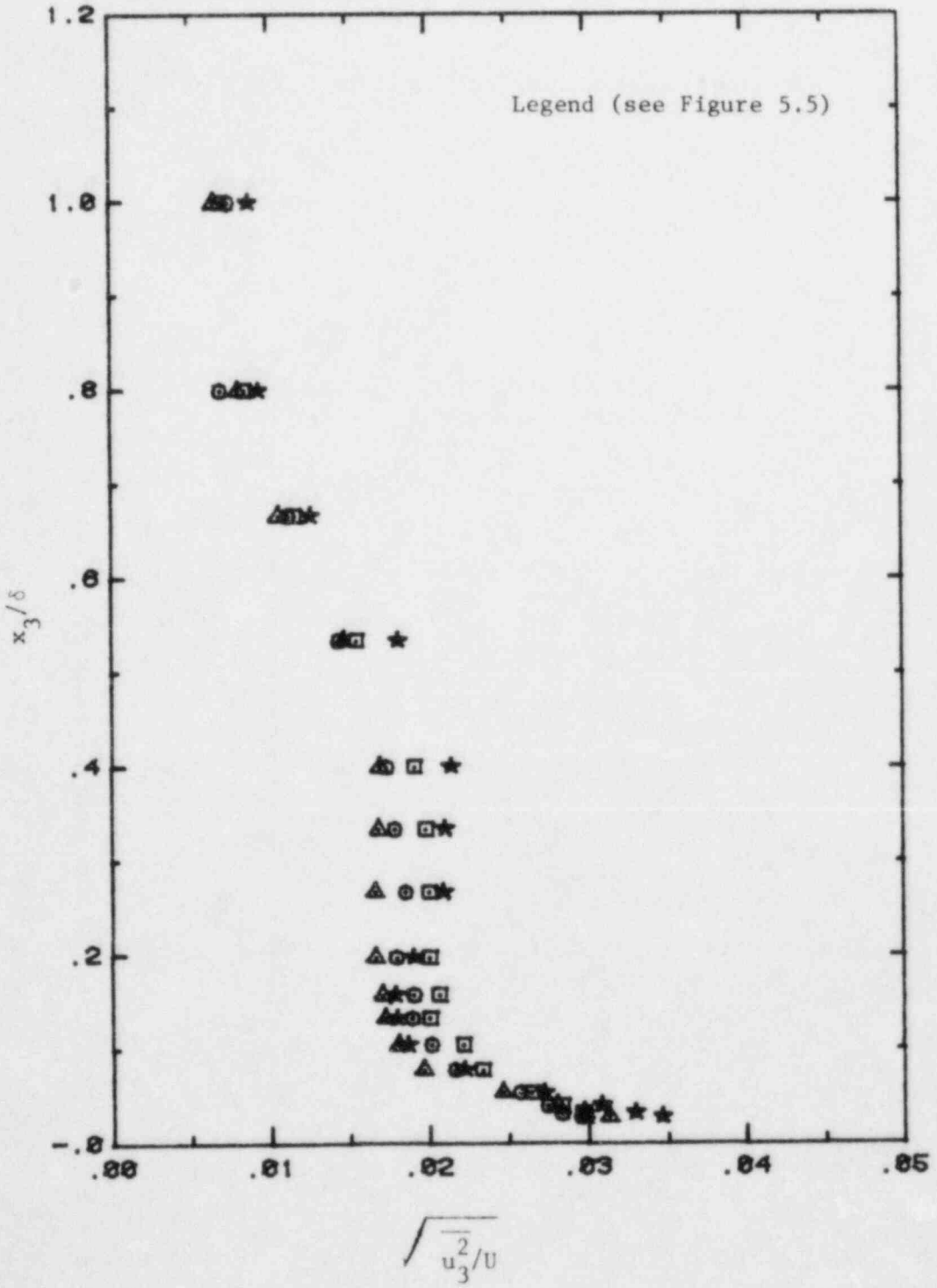

Figure 5.17. Vertical turbulent intensity profiles; U_∞ = 200 cm/sec, stable.

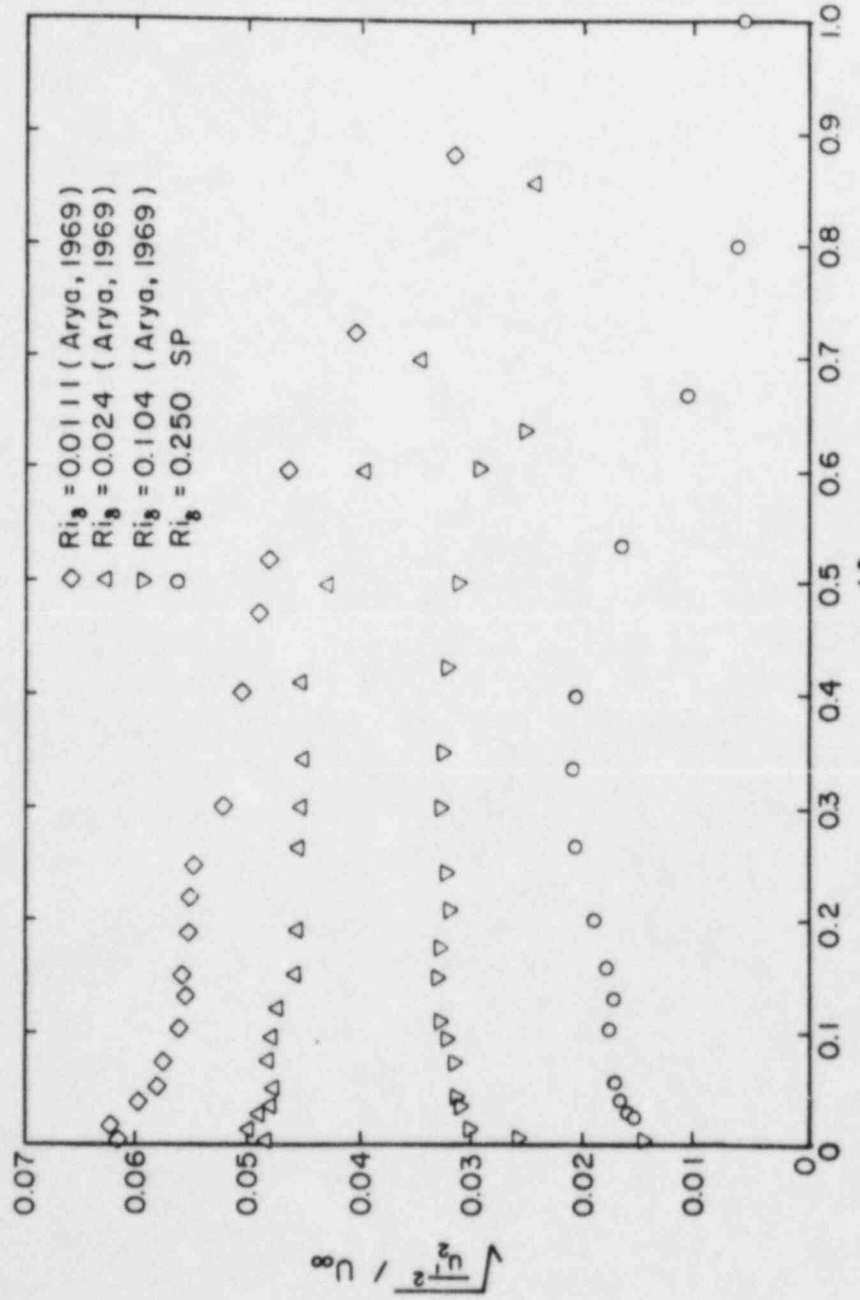

Figure 5.18. Lateral turbulent intensity profiles; stable.

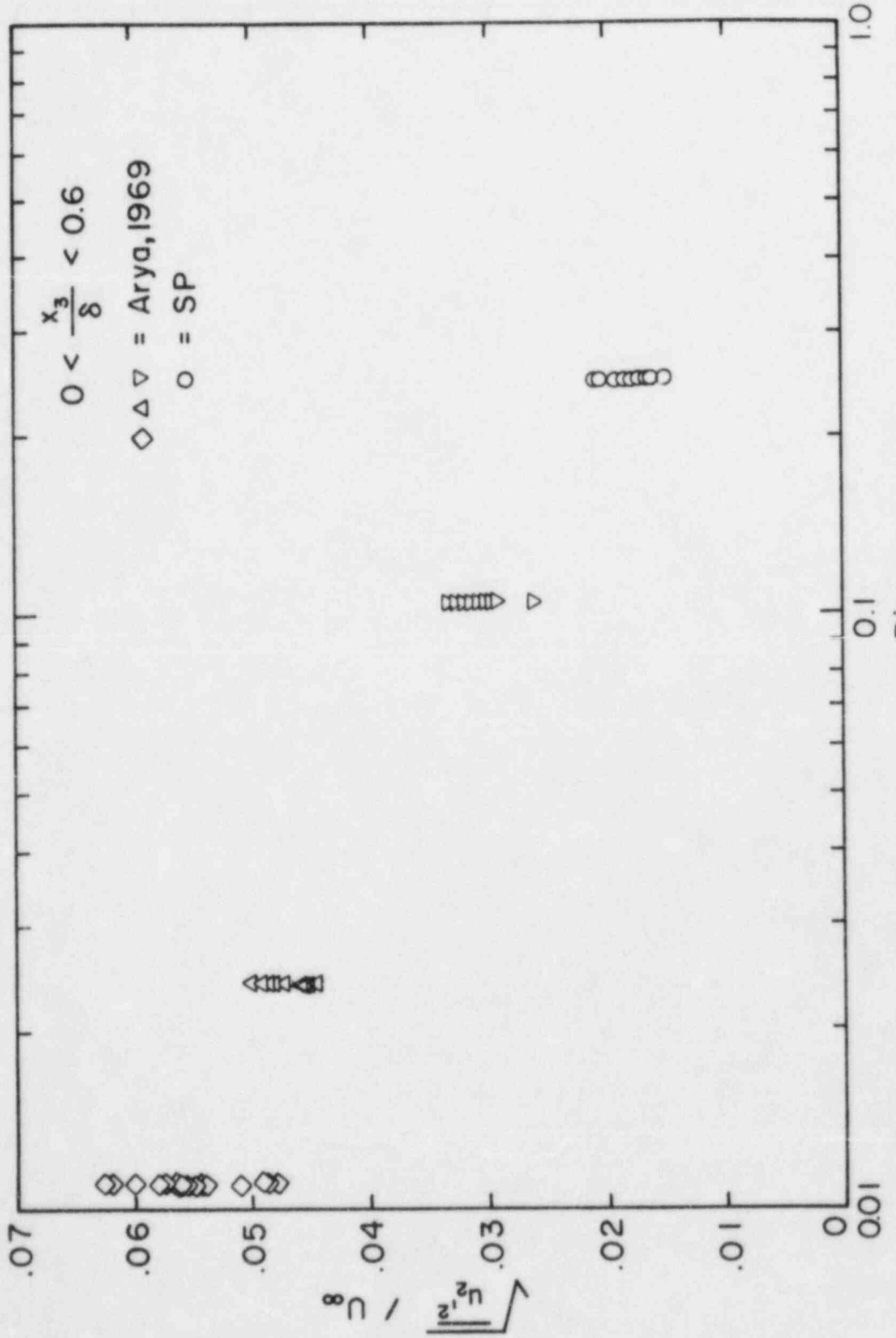

Figure 5.19. Lateral turbulent intensity vs. Richardson number.

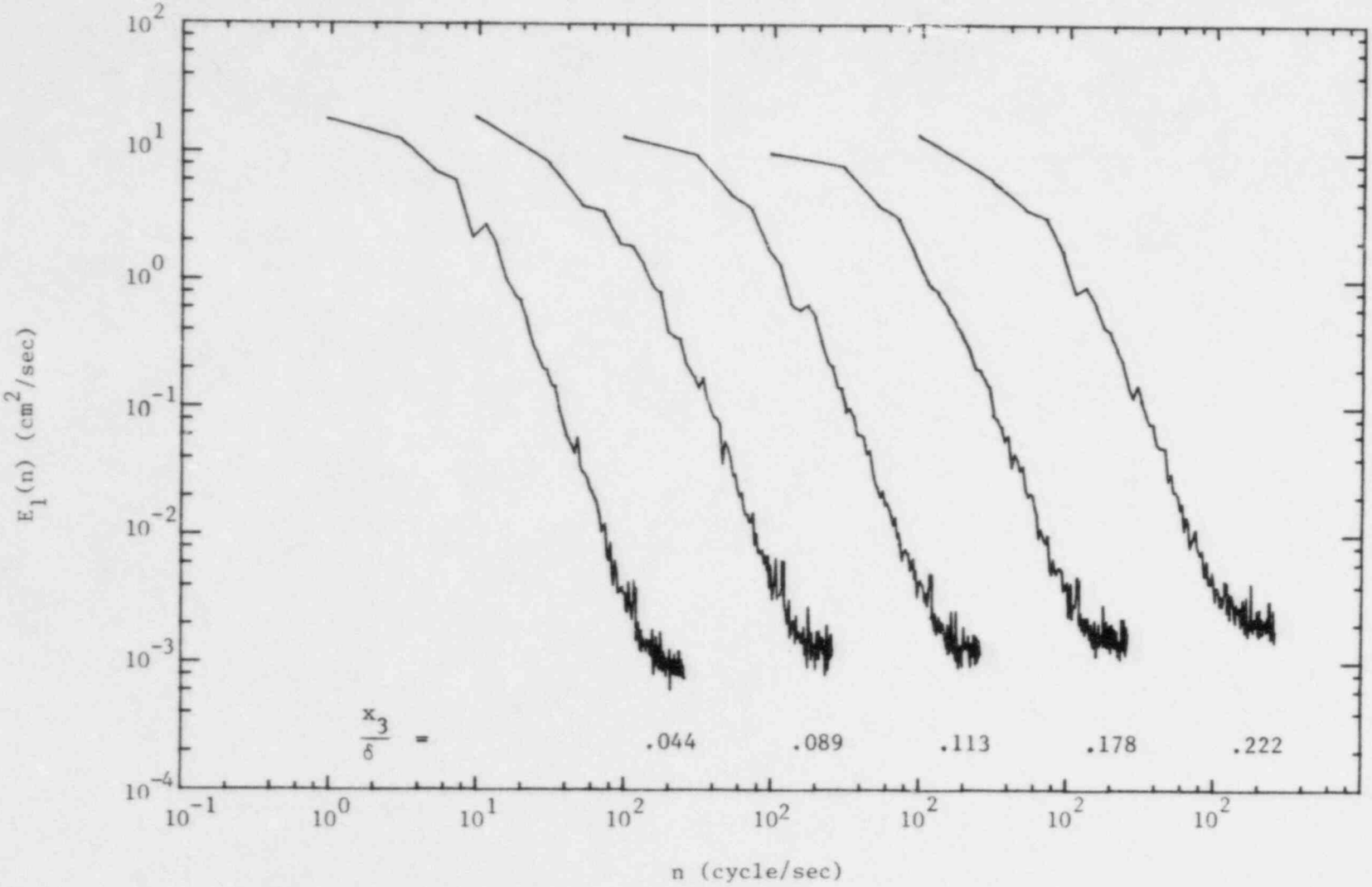

Figure 5.20. Energy spectra of longitudinal velocity fluctuations; U_∞ = 200 cm/sec, stable.

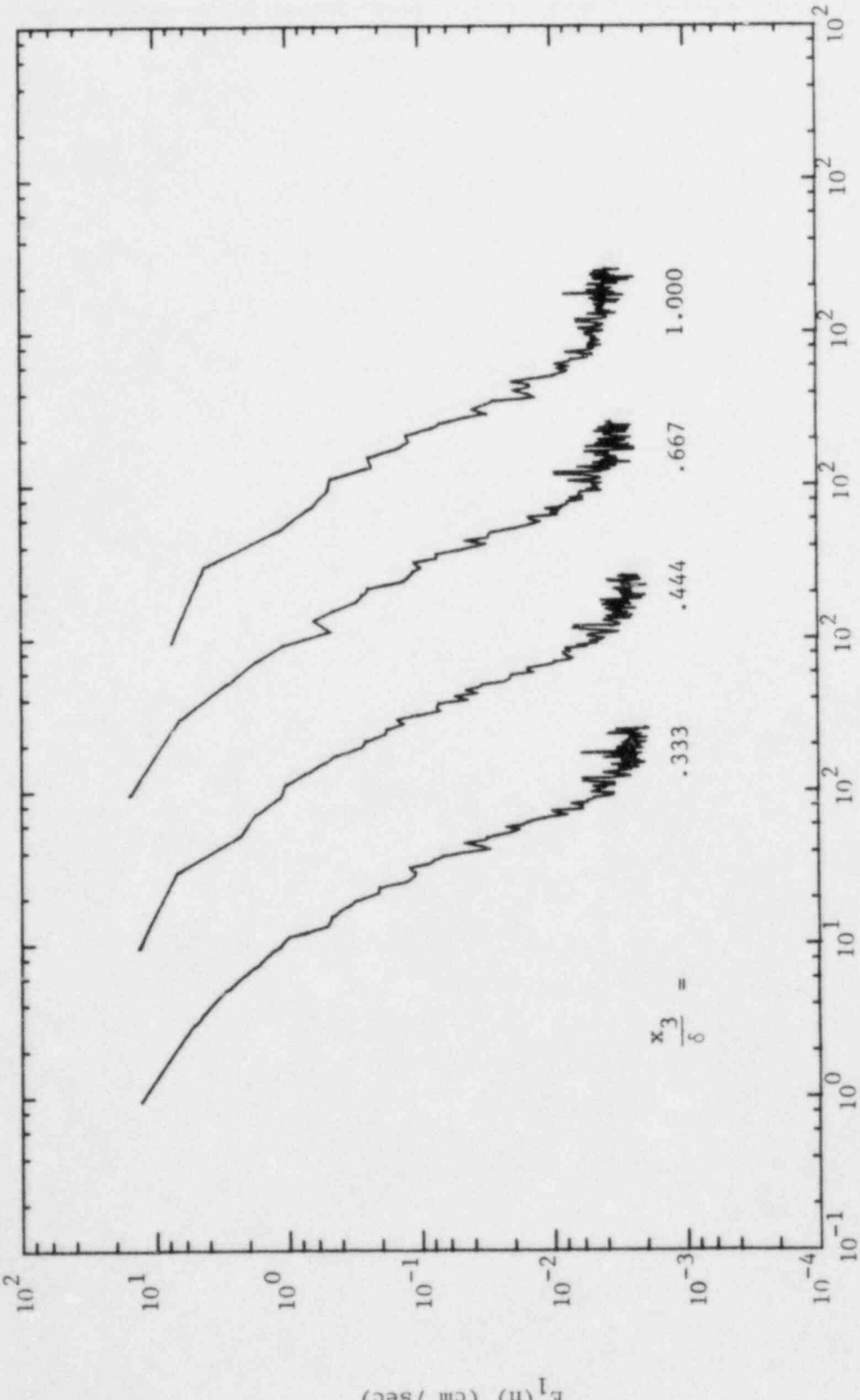

Figure 5.20. Energy spectra of longitudinal velocity fluctuations; U_∞ = 200 cm/sec, stable (continued).

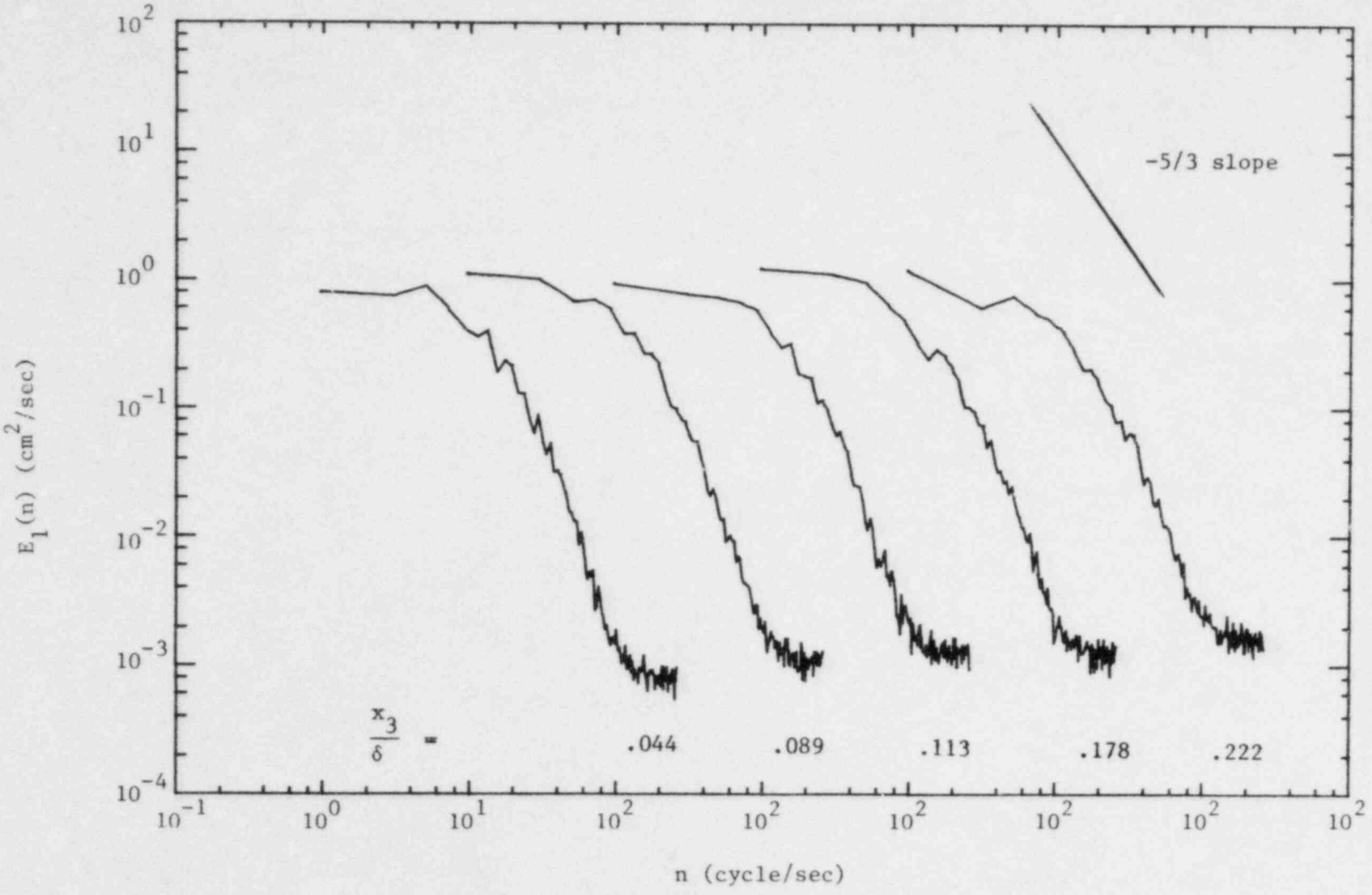

Figure 5.21. Energy spectra of lateral velocity fluctuations; U_∞ = 200 cm/sec, stable.

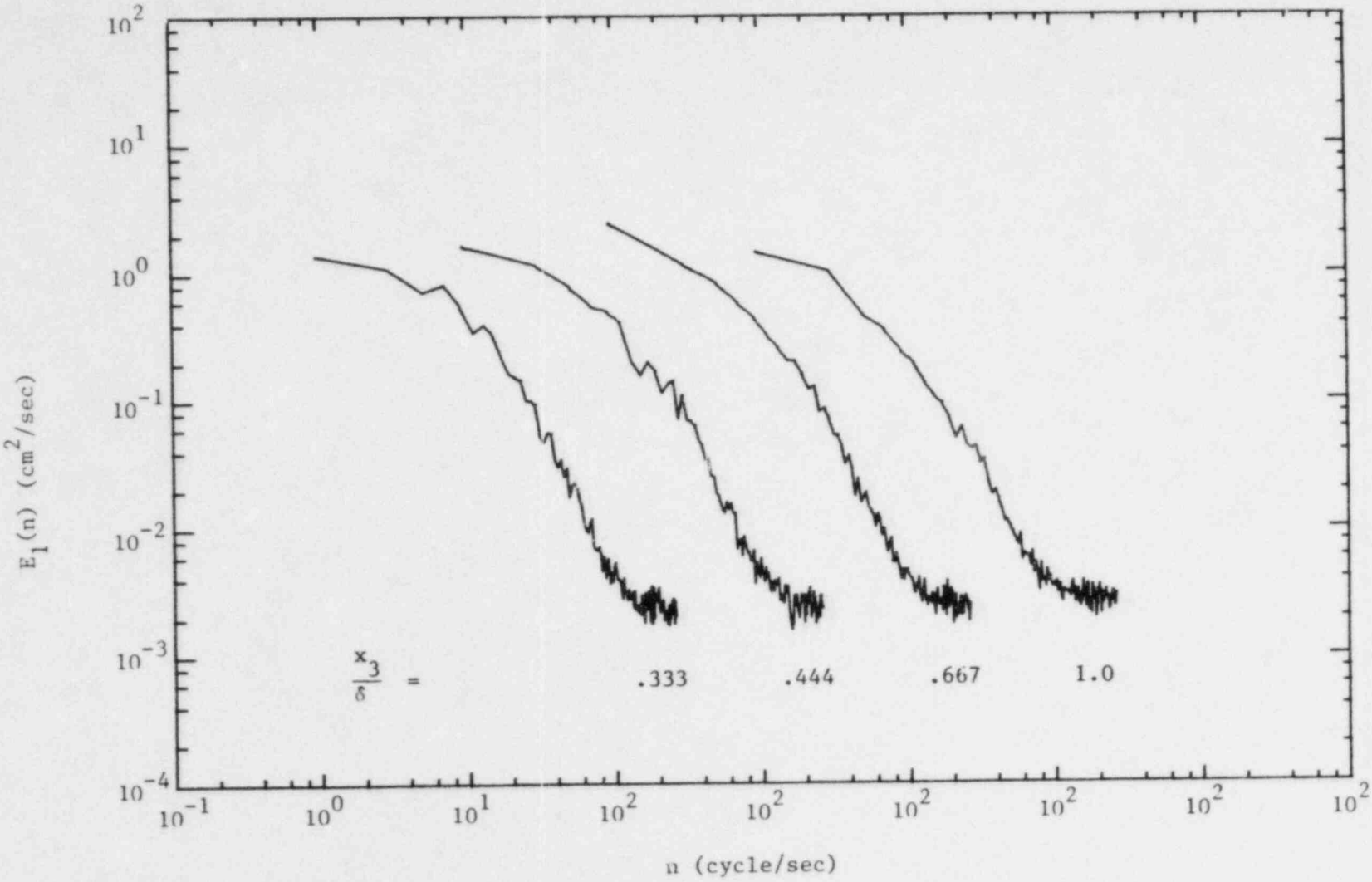

Figure 5.21. Energy spectra of lateral velocity fluctuations; U_∞ = 200 cm/sec, stable (continued).

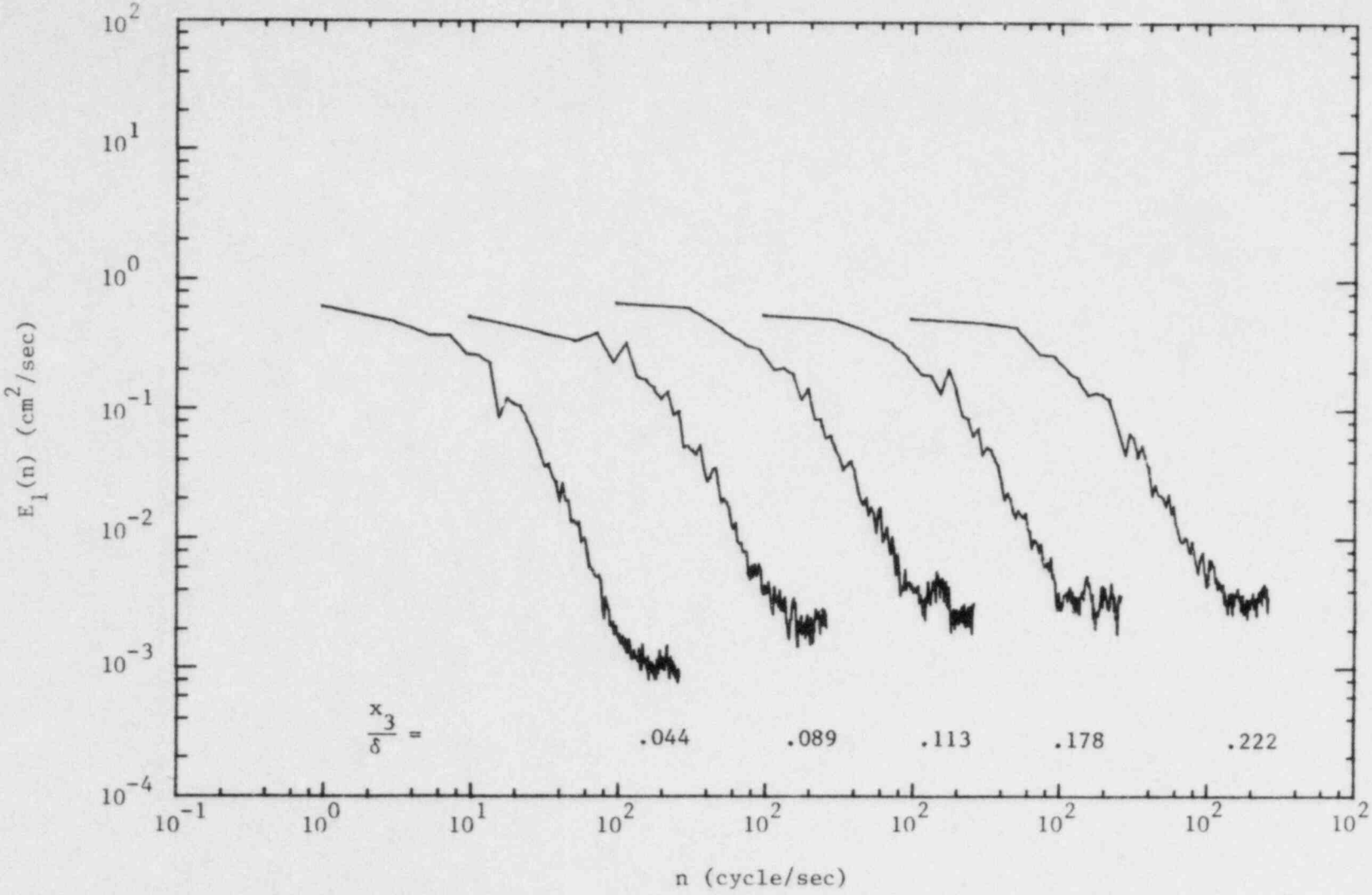

Figure 5.22. Energy spectra of vertical velocity fluctuations; U_∞ = 200 cm/sec, stable.

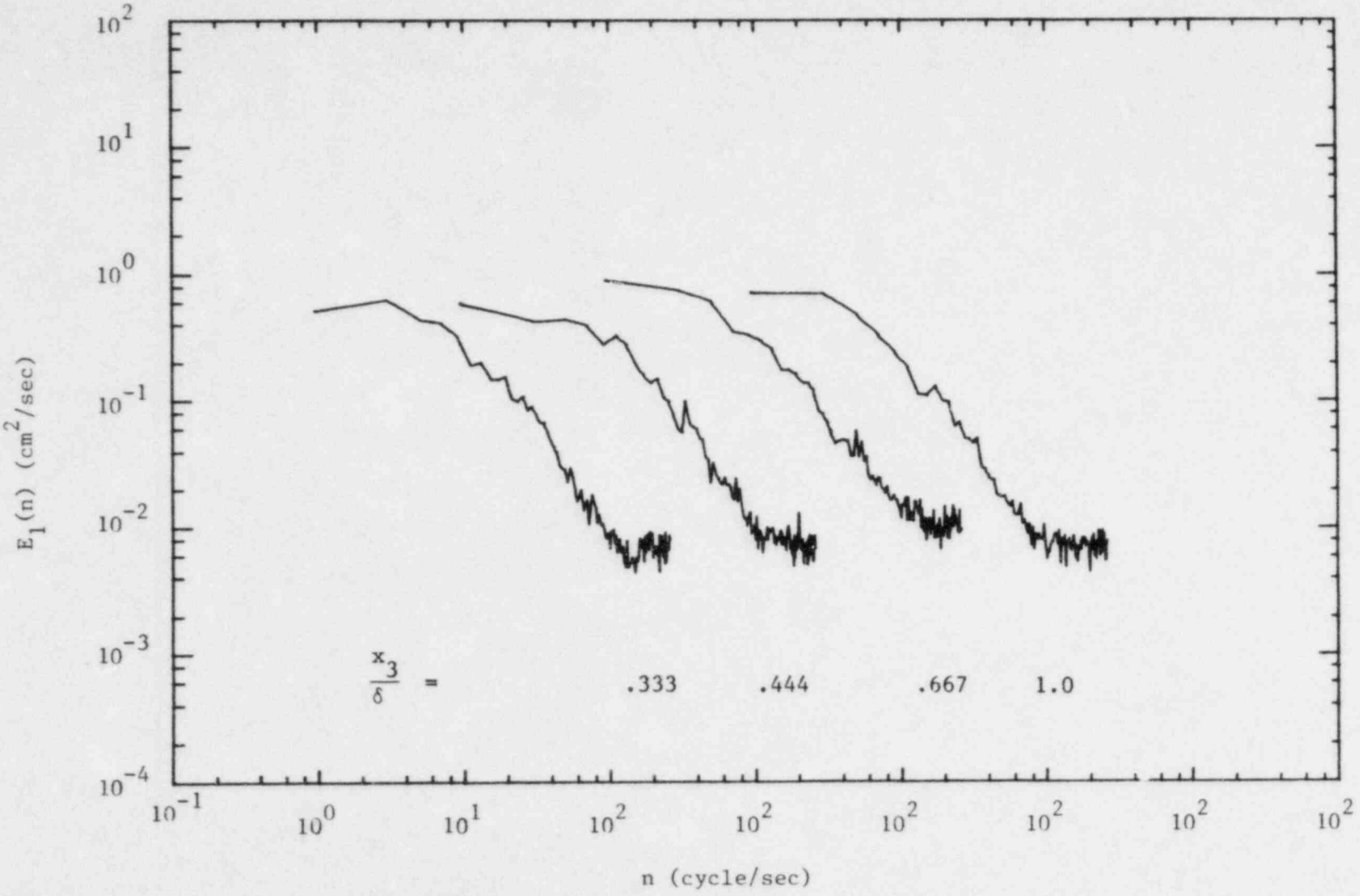

Figure 5.22. Energy spectra of vertical velocity fluctuations; U_∞ = 200 cm/sec, stable (continued).

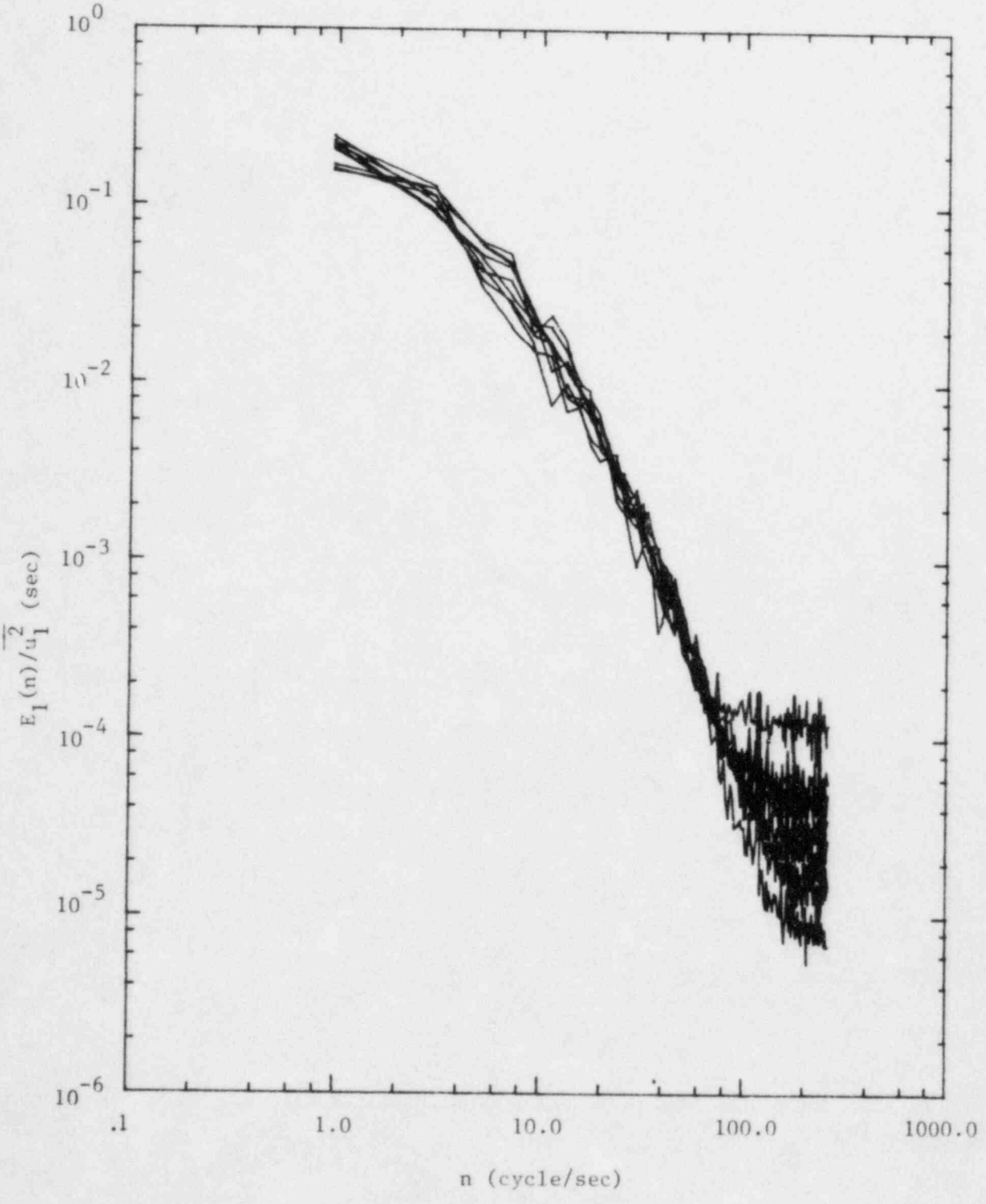

Figure 5.23. Normalized energy spectra of longitudinal velocity fluctuations; U_∞ = 200 cm/sec, stable.

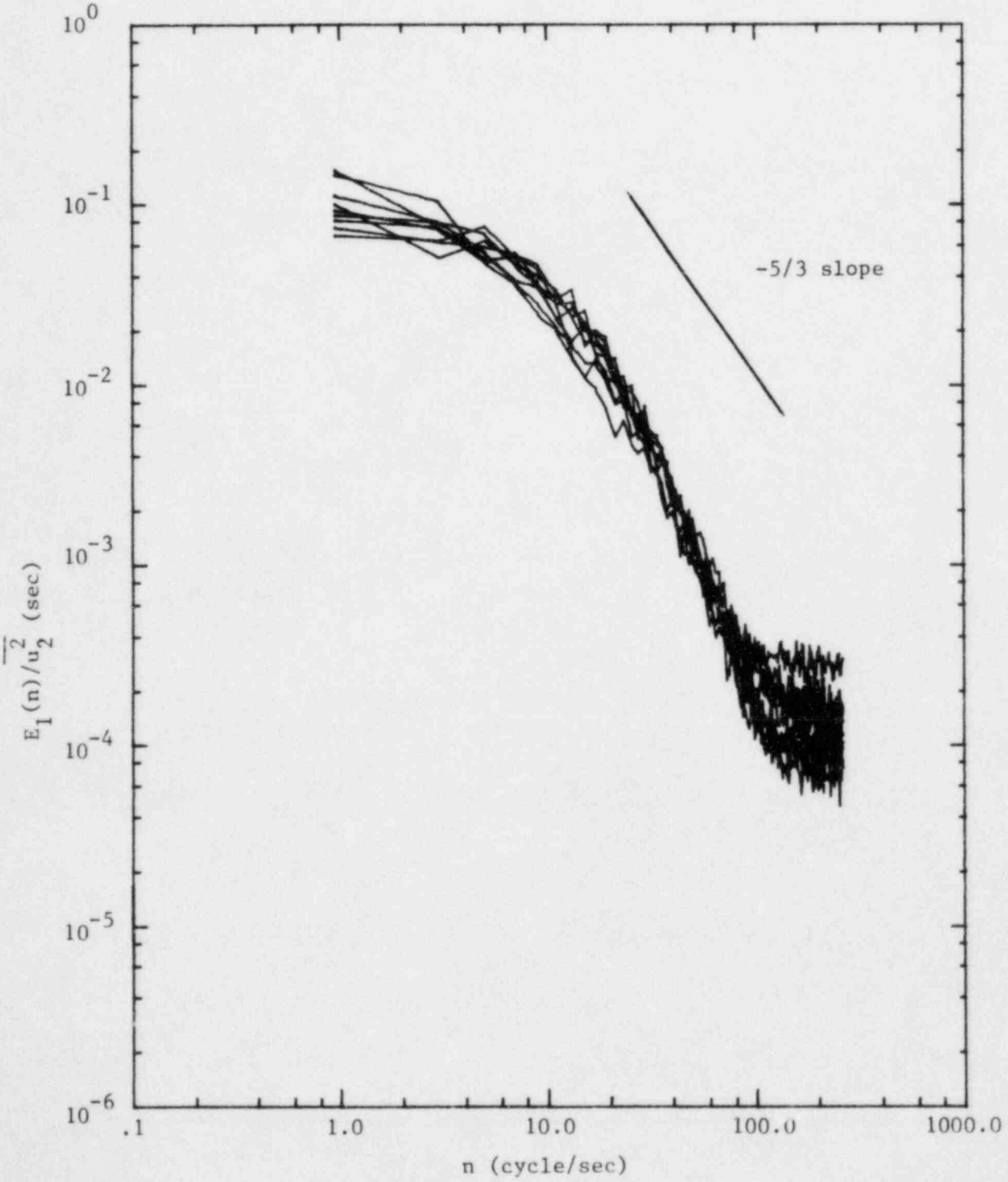

Figure 5.24. Normalized energy spectra of lateral velocity fluctuations; U_∞ = 200 cm/sec, stable.

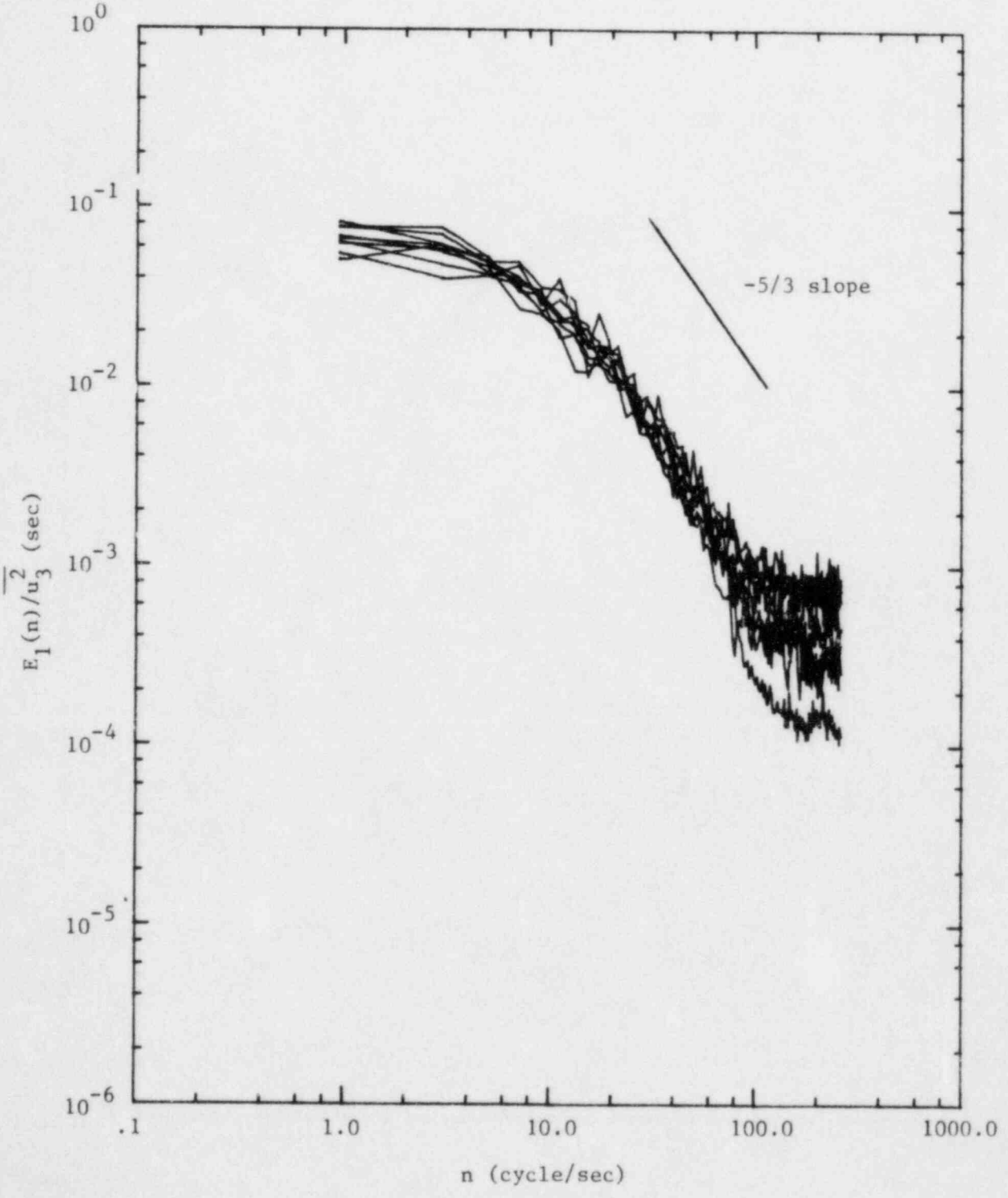

Figure 5.25. Normalized energy spectra of vertical velocity fluctuations; U_∞ = 200 cm/sec, stable.

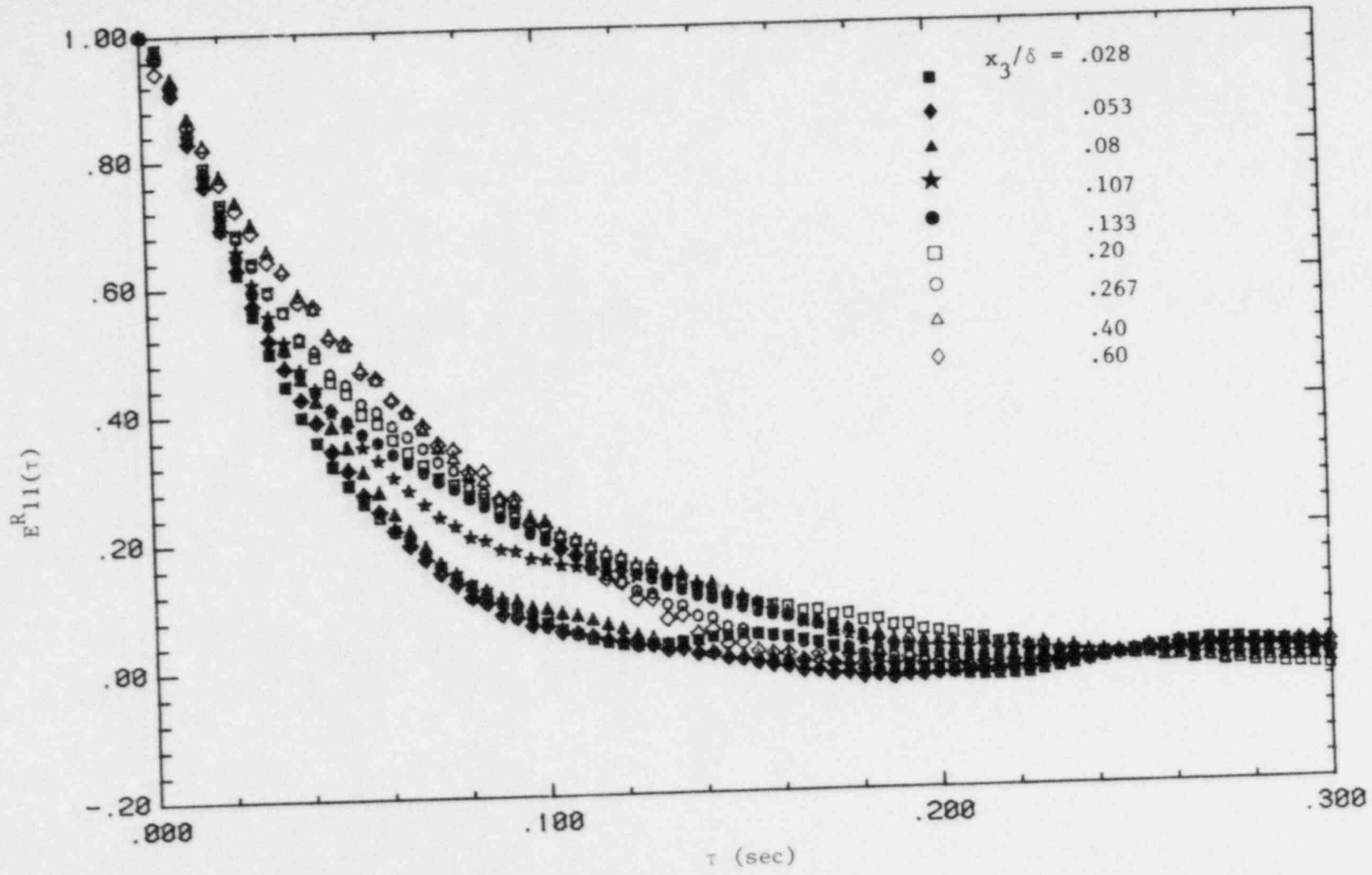

Figure 5.26. Longitudinal velocity autocorrelation functions, U_∞ = 200 cm/sec, stable.

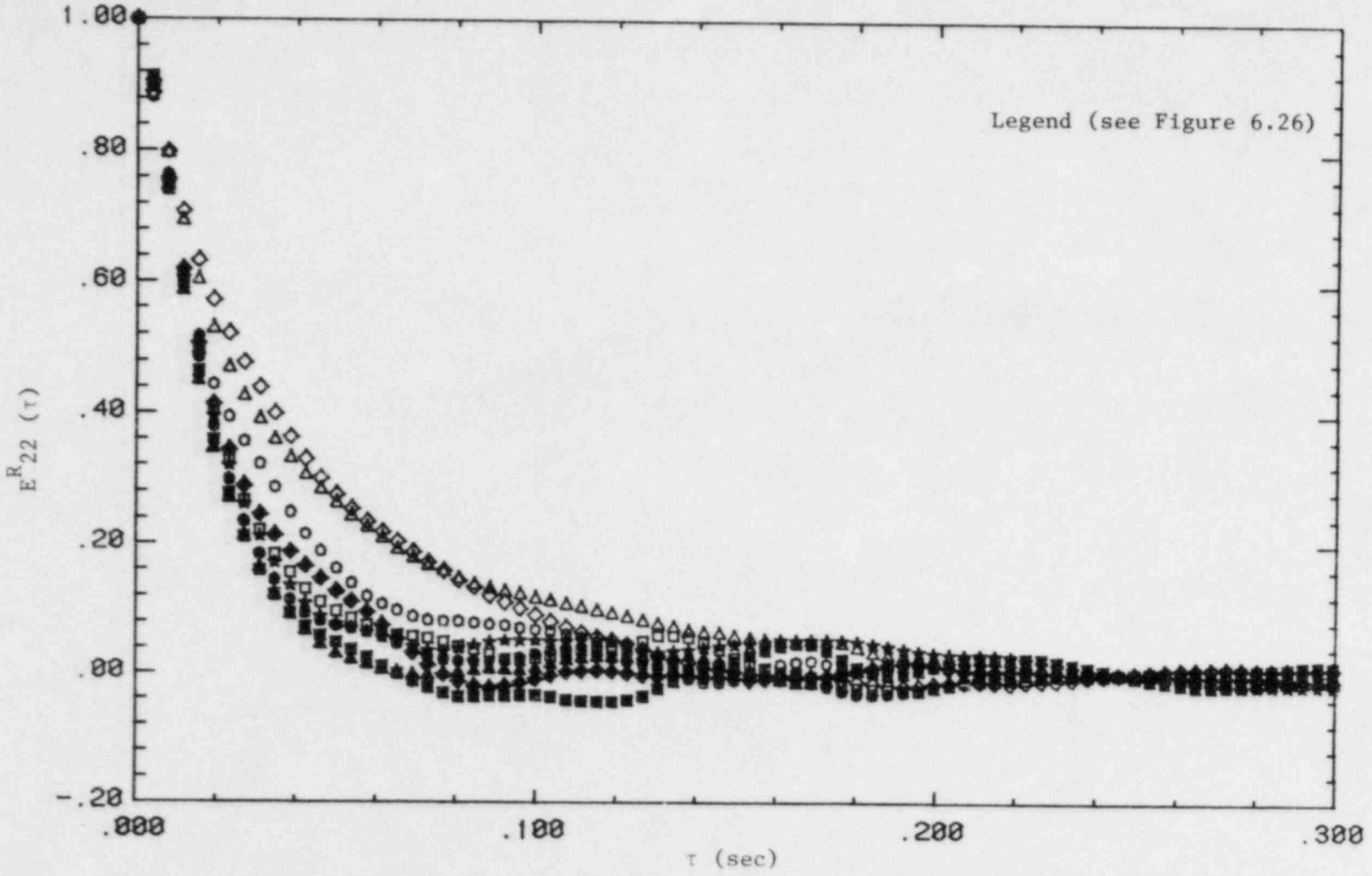

Figure 5.27. Lateral velocity autocorrelation functions, U_∞ = 200 cm/sec, stable.

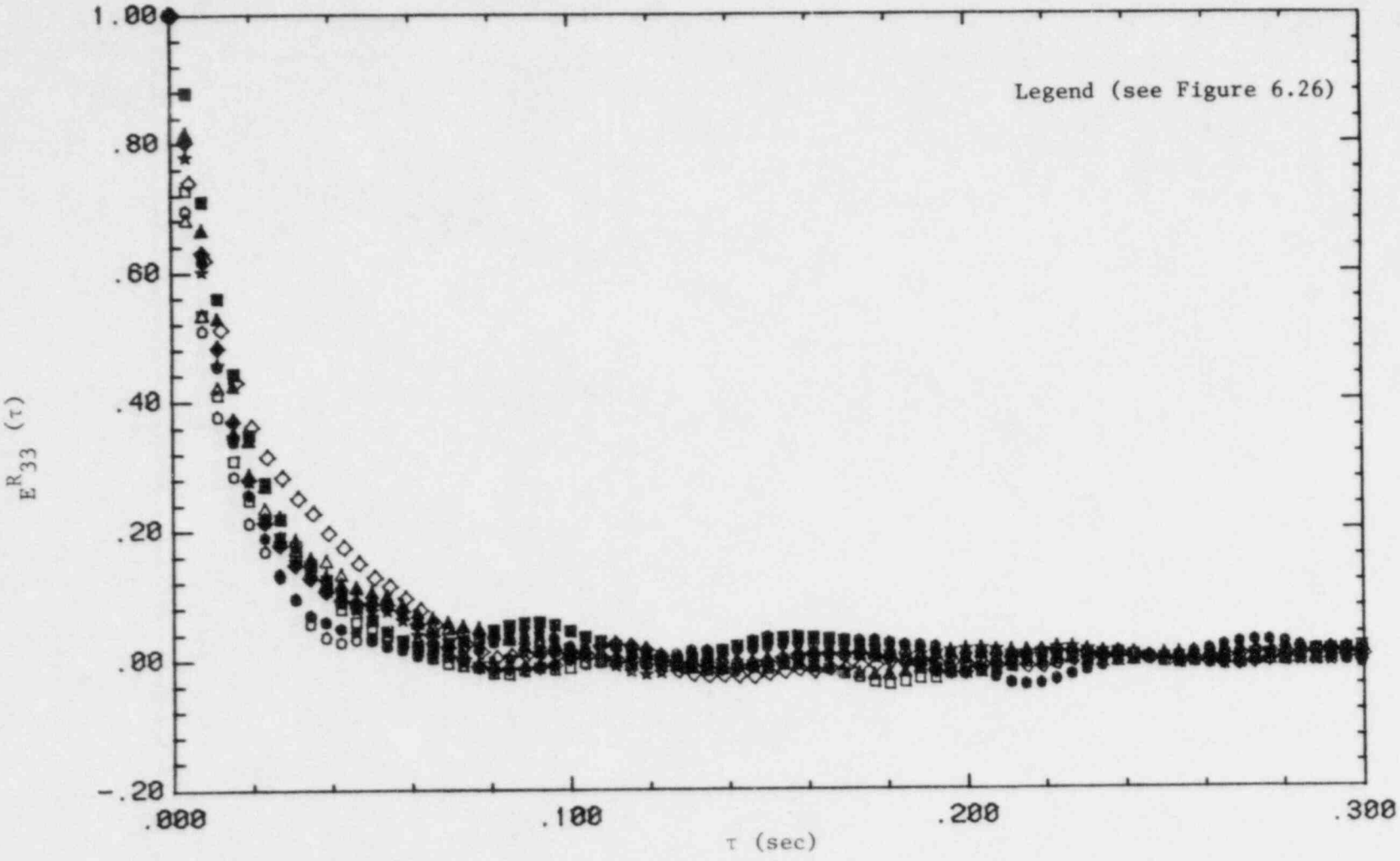

Figure 5.28. Vertical velocity autocorrelation functions, U_∞ = 200 cm/sec, stable.

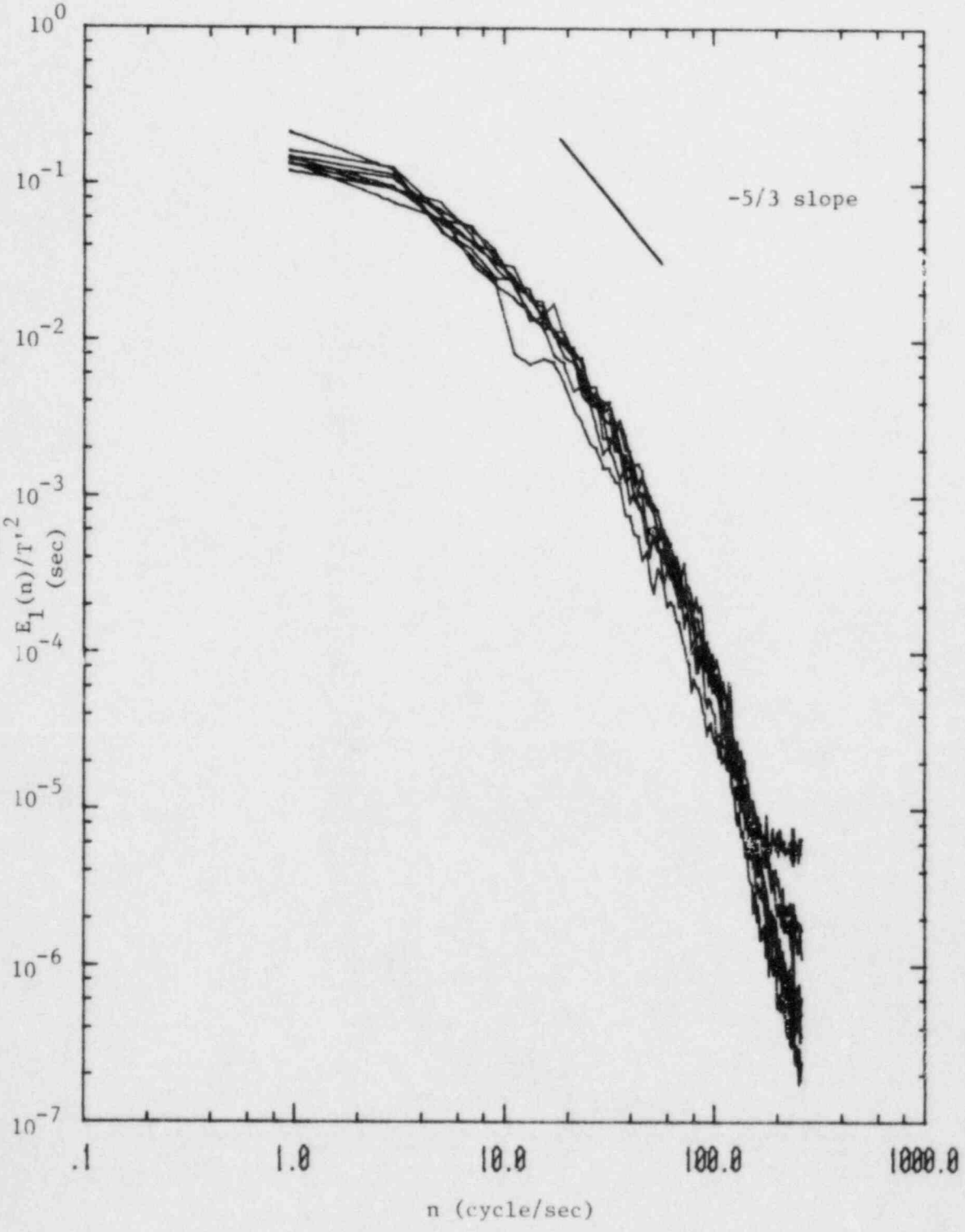

Figure 5.29. Temperature spectra; U_∞ = 200 cm/sec, stable.

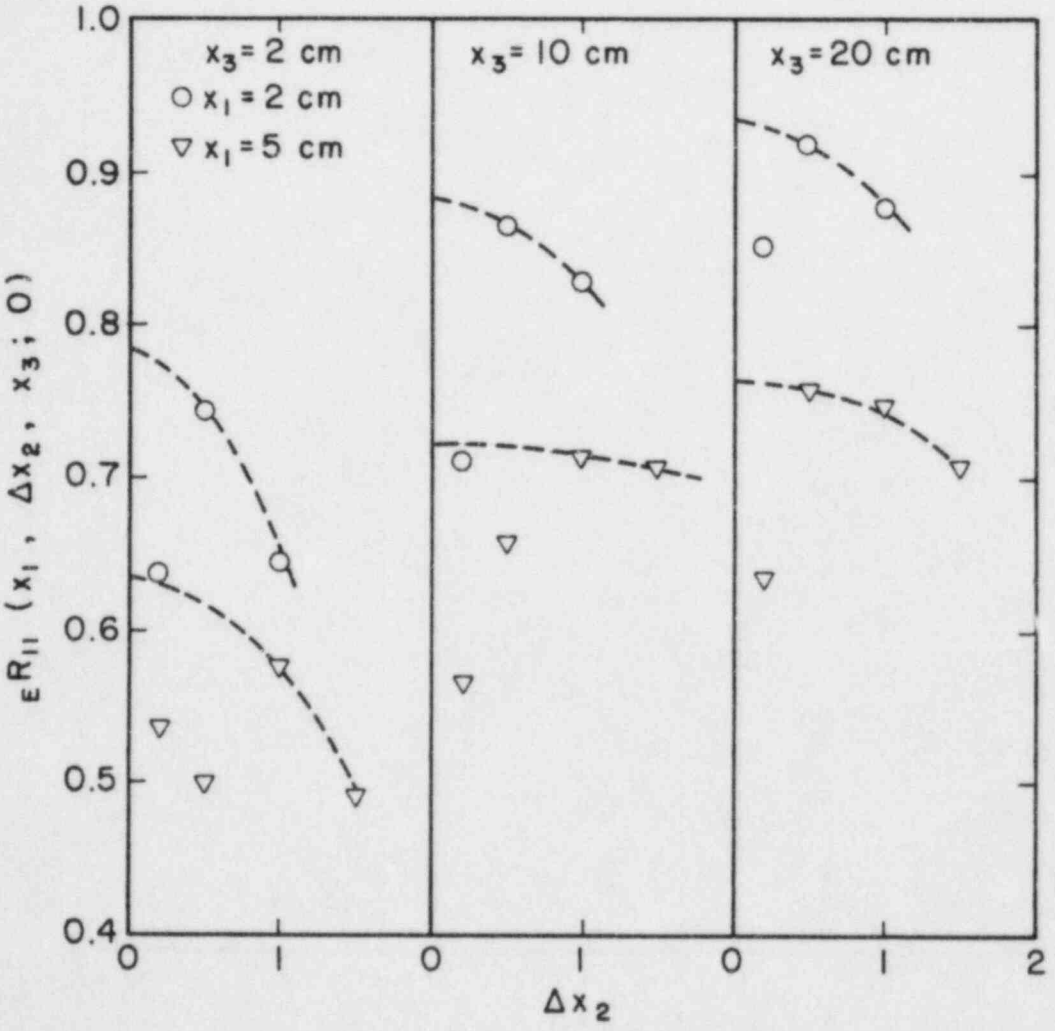

Figure 5.30. Extrapolation of the longitudinal space correlation to zero separation to account for probe wake effect.

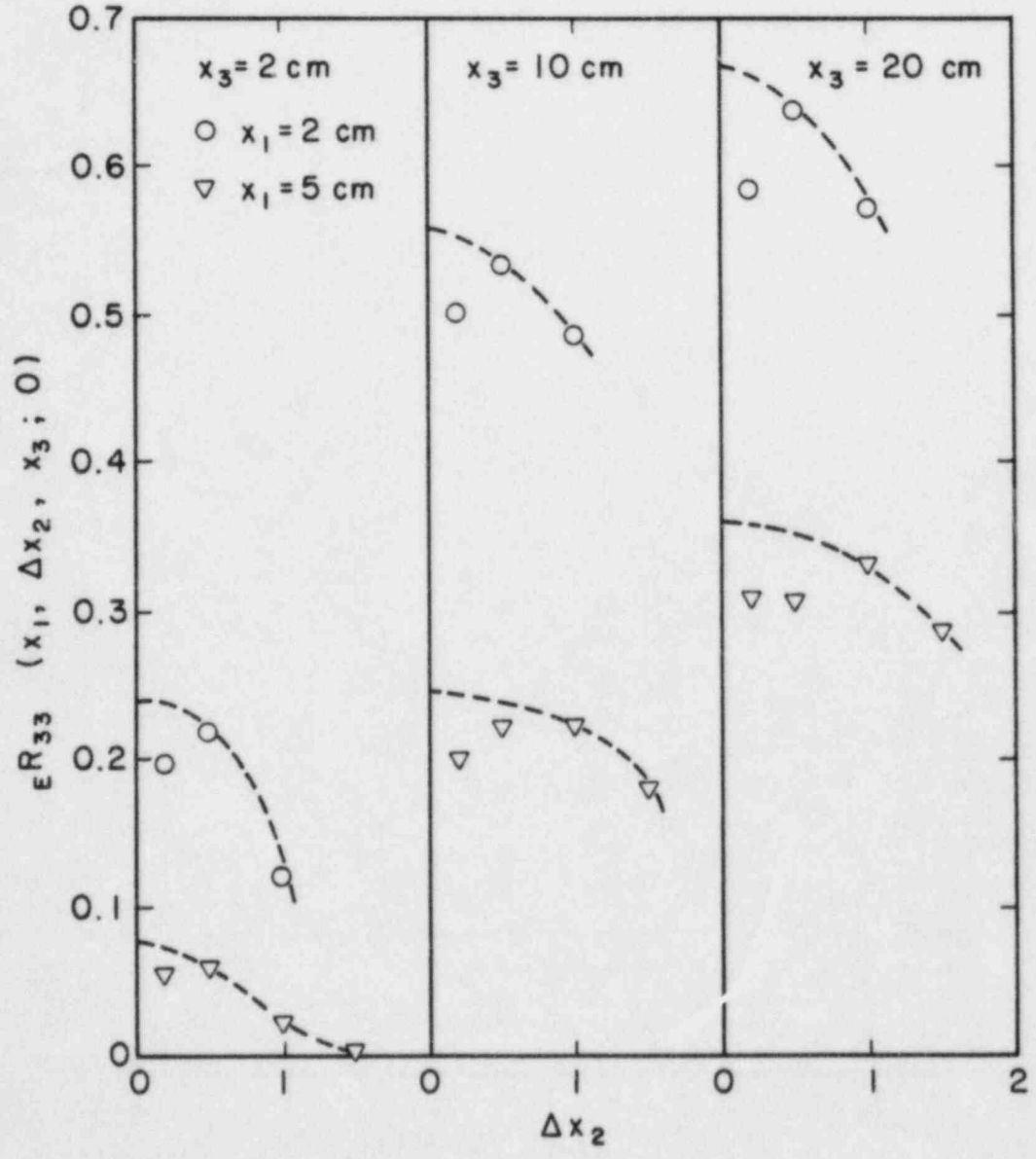

Figure 5.30. Extrapolation of the longitudinal space correlation to zero separation to account for probe wake effect (continued).

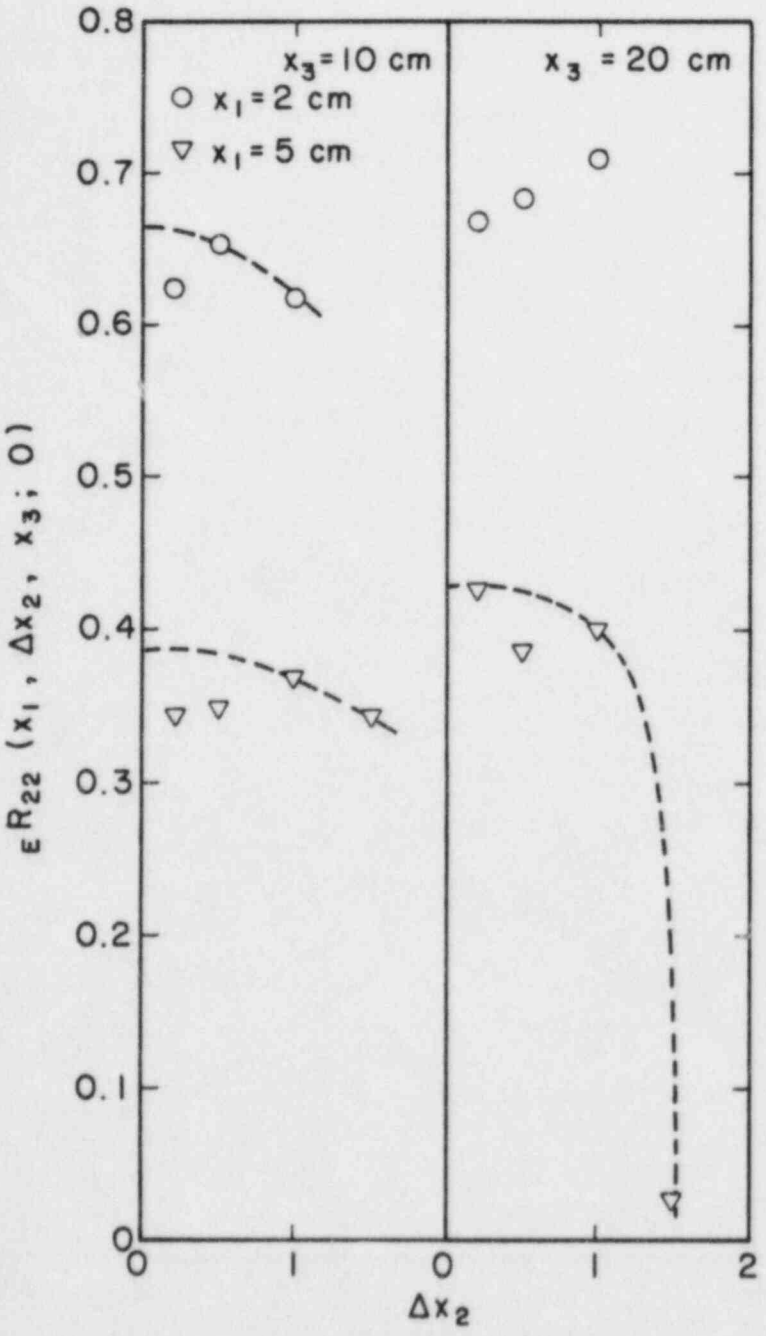

Figure 5.30. Extrapolation of the longitudinal space correlation to zero separation to account for probe wake effect (continued).

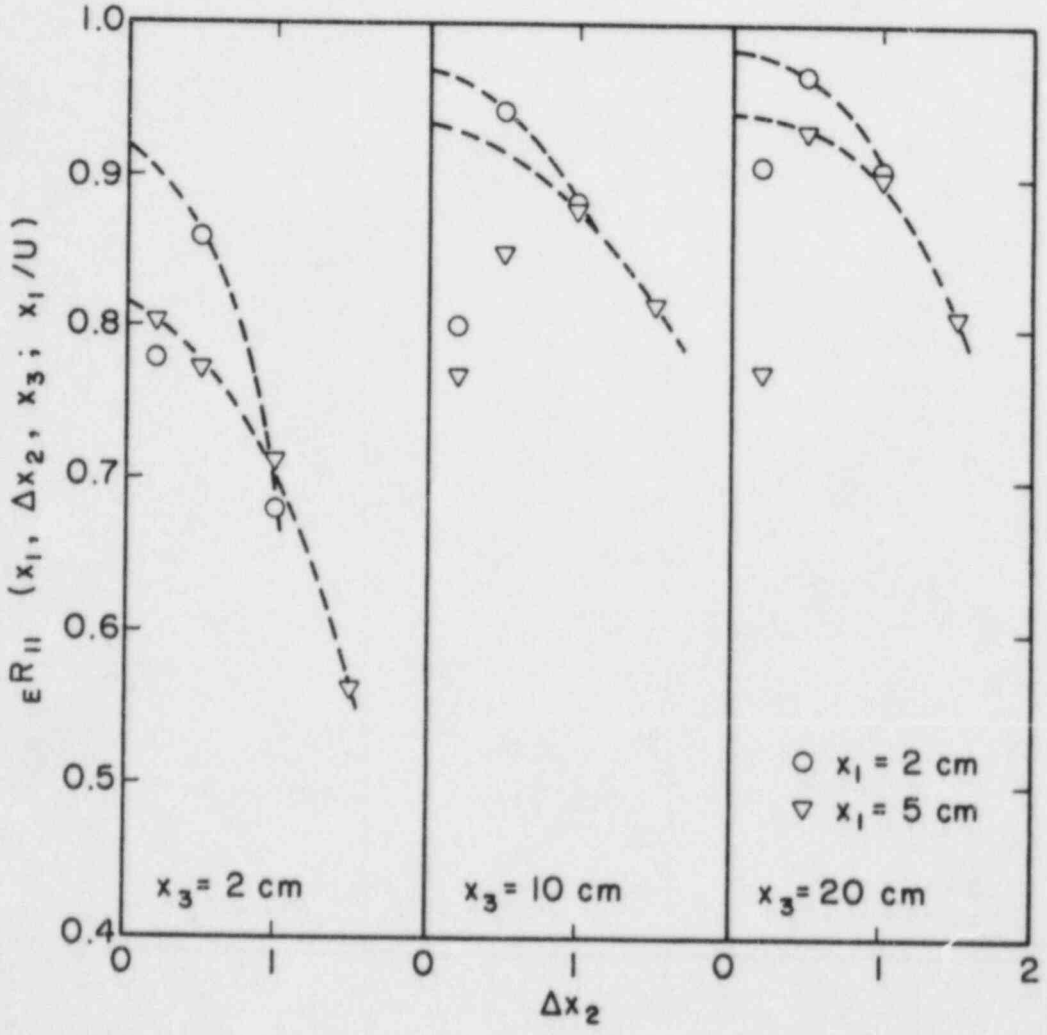

Figure 5.31. Extrapolation to zero separation to correct for probe wake effect of space-time correlation.

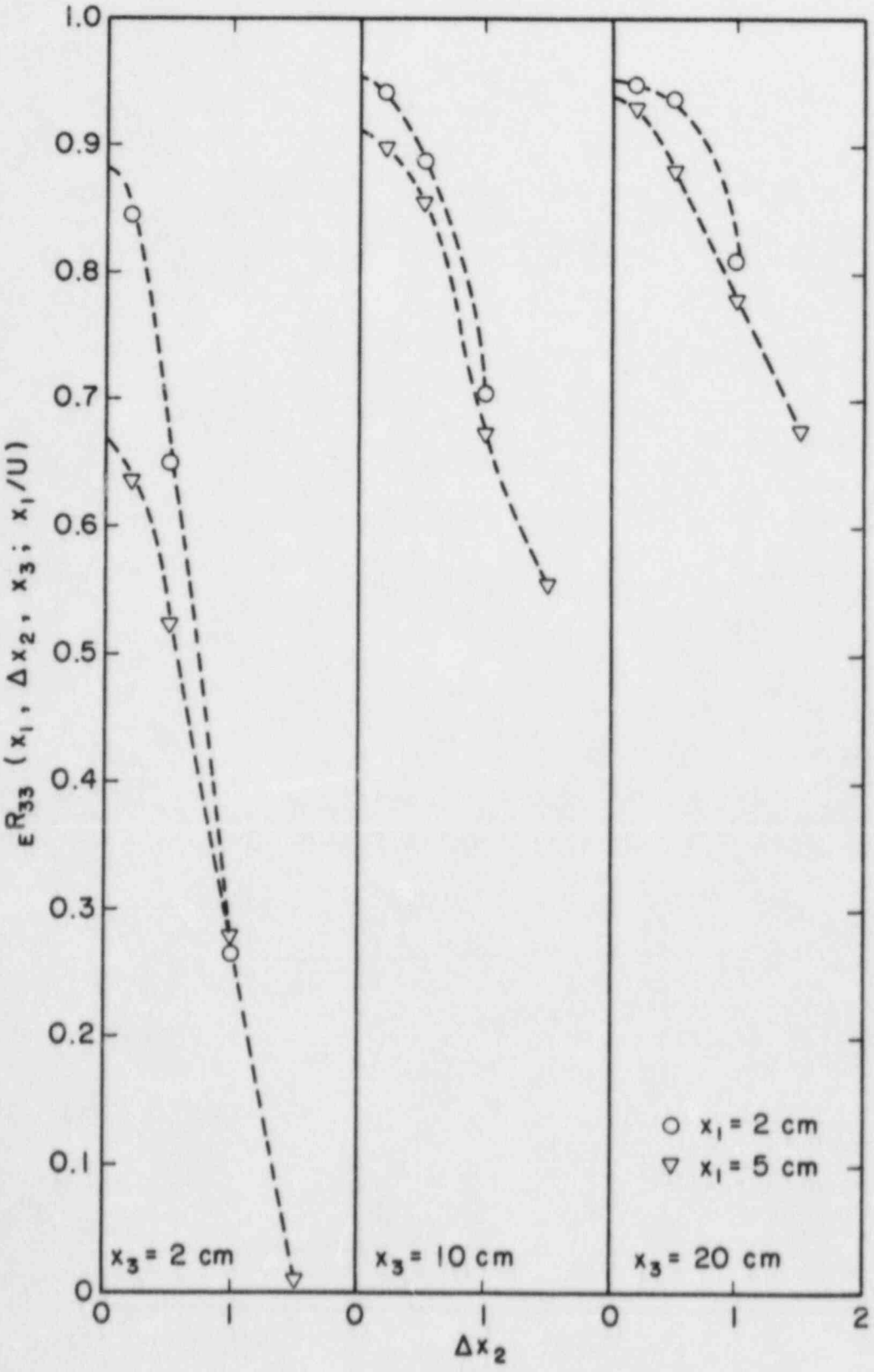

Figure 5.31. Extrapolation to zero separation to correct for probe wake effect of space-time correlation (continued).

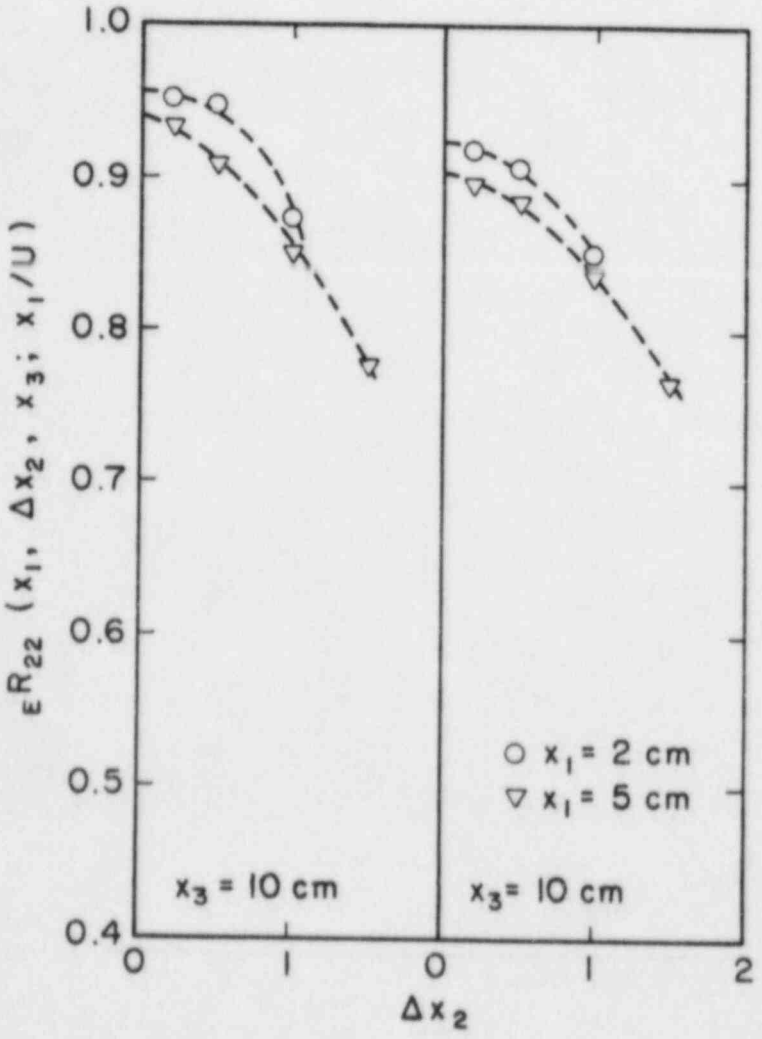

Figure 5.31. Extrapolation to zero separation to correct for probe wake effect of space-time correlation (continued).

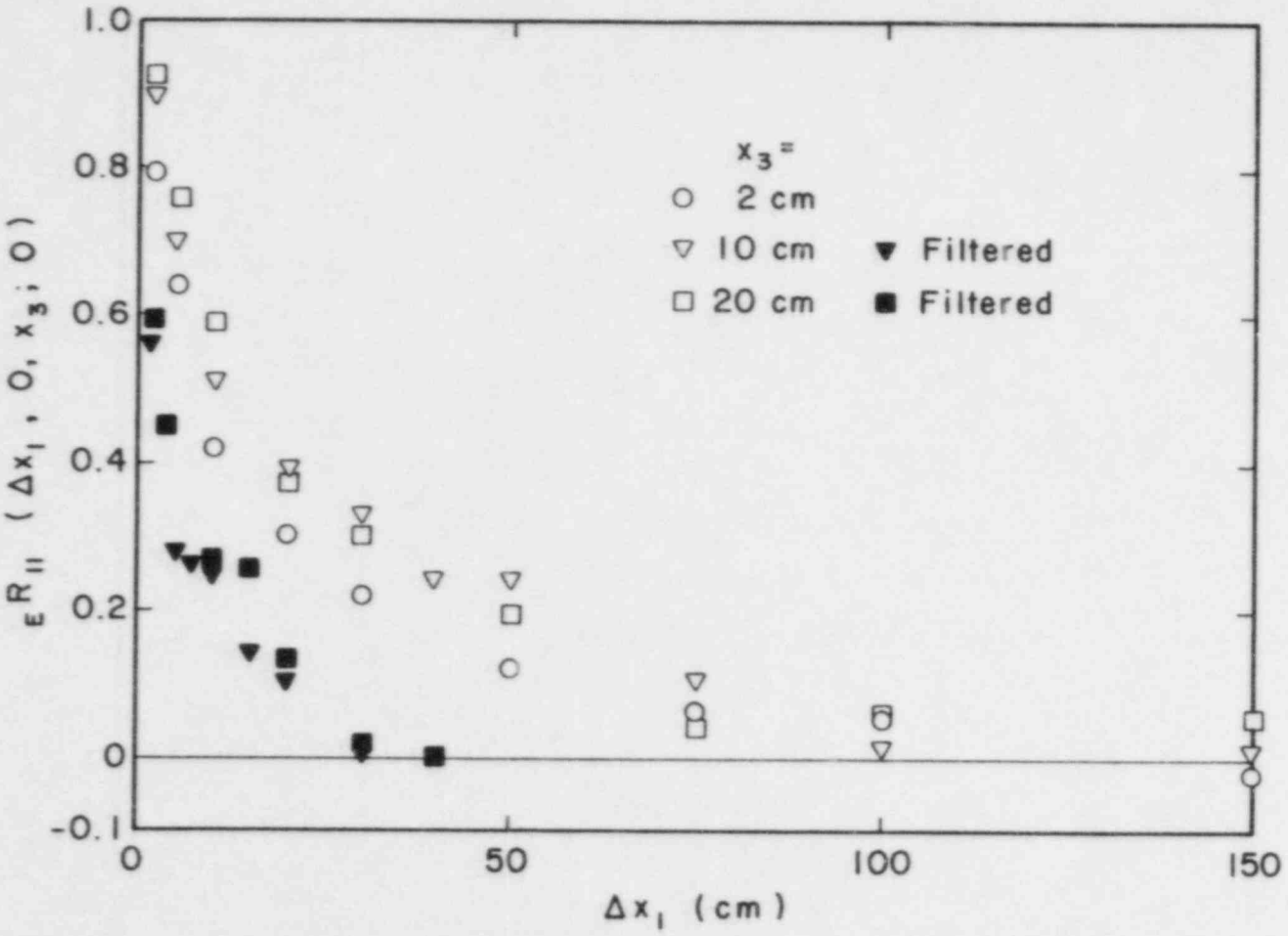

Figure 5.32. Longitudinal Eulerian space correlation.

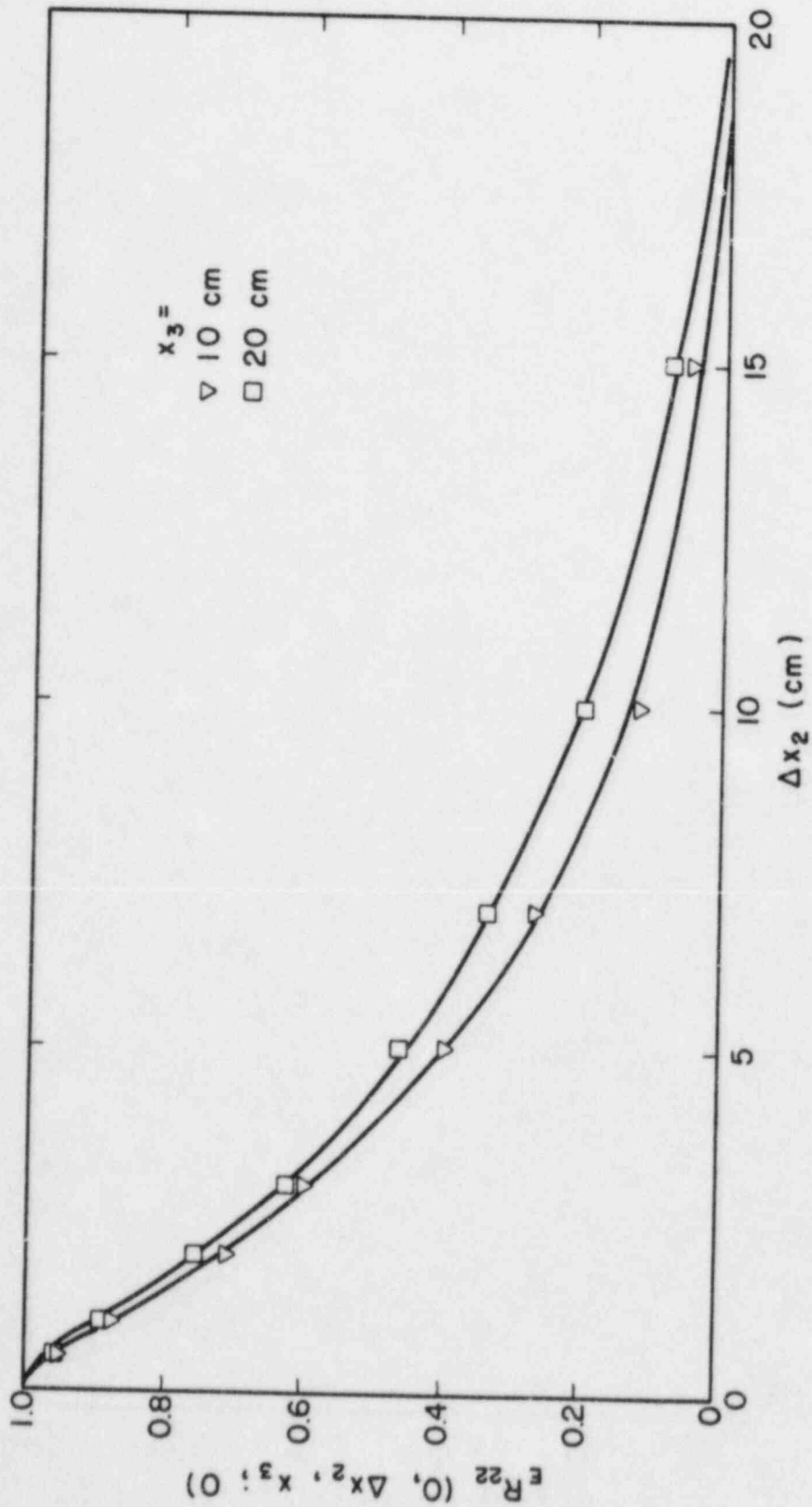

Figure 5.33. Lateral Eulerian space correlation.

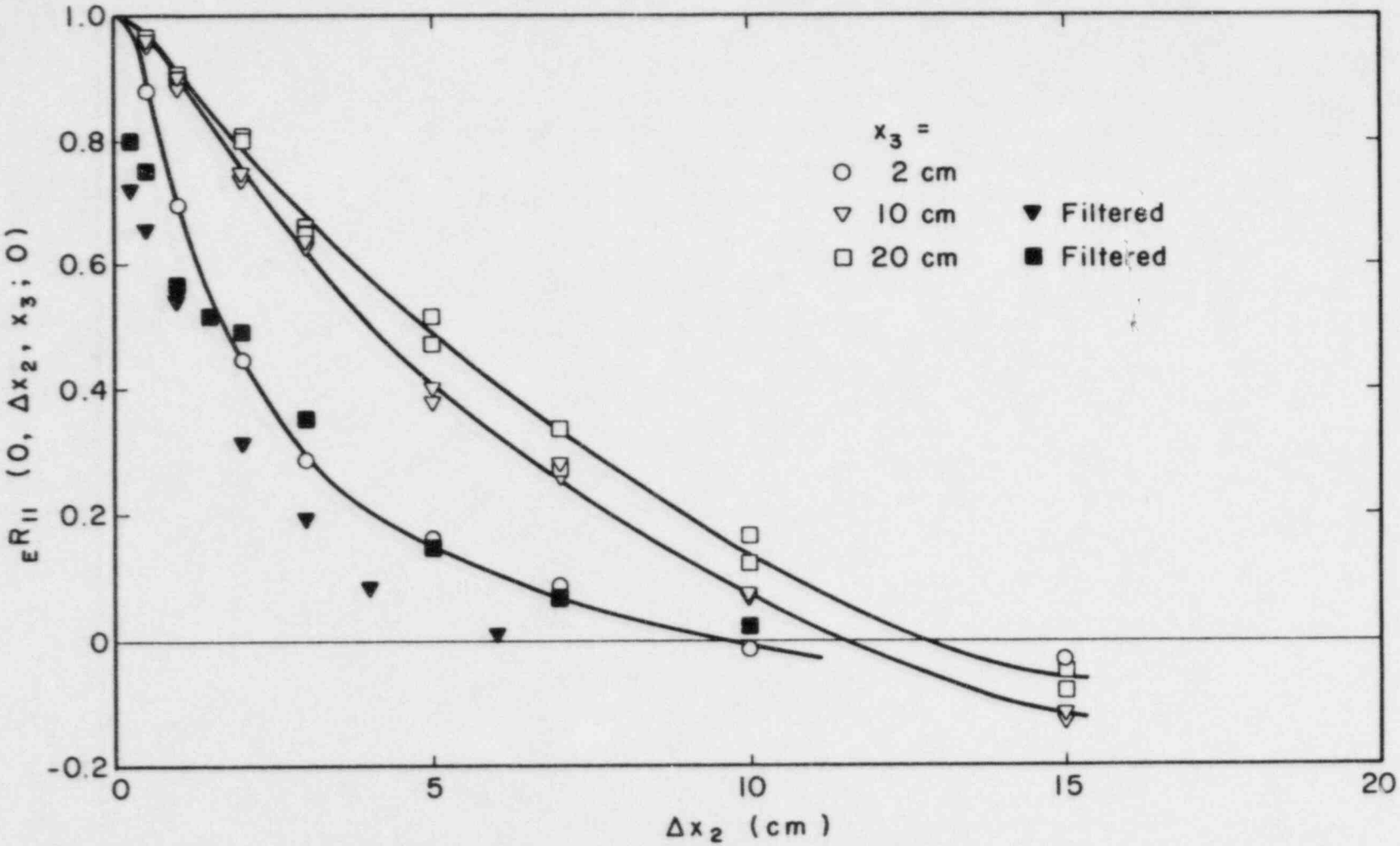

Figure 5.34. Longitudinal two-point velocity correlation with transverse separations.

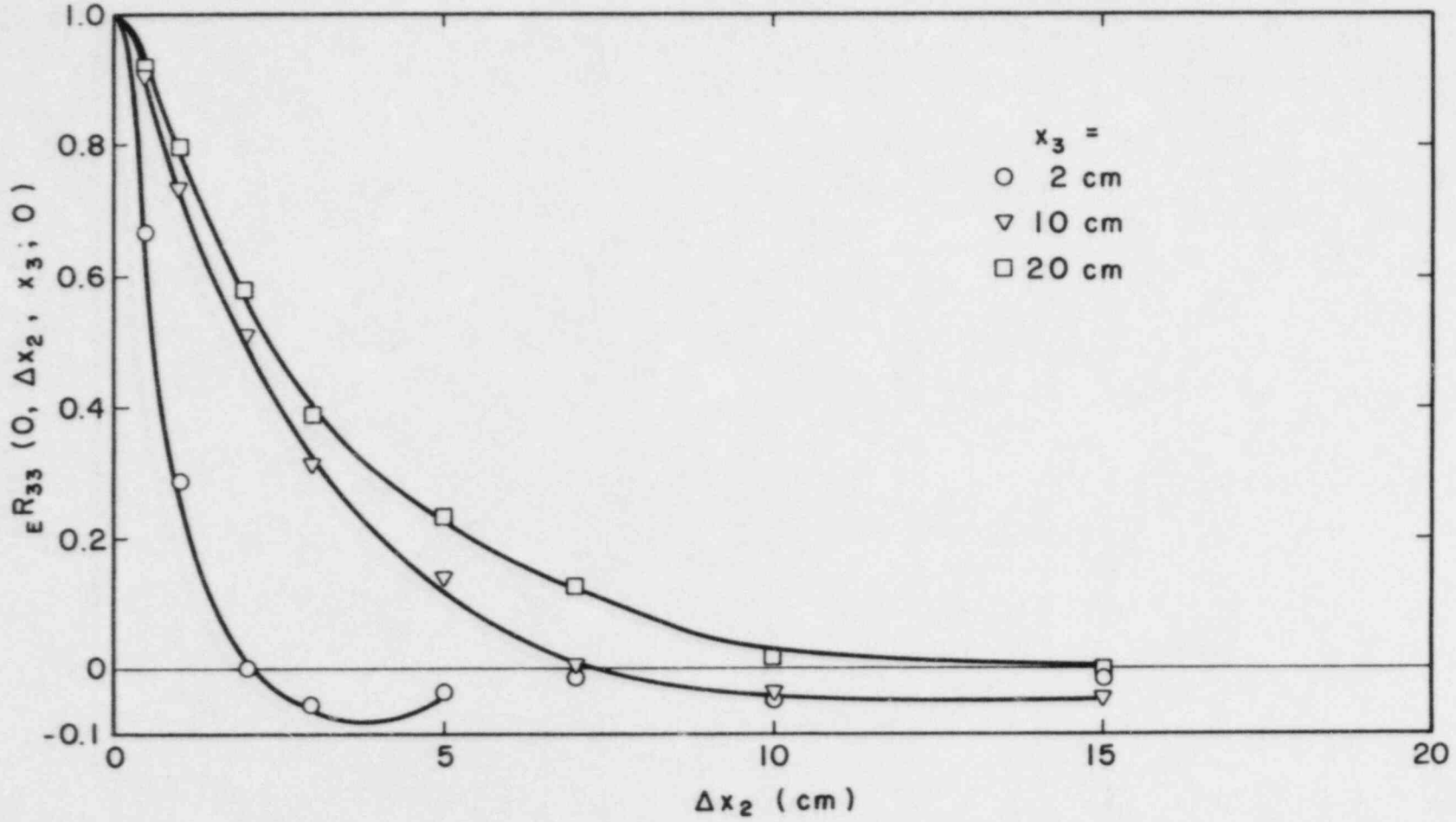

Figure 5.35. Vertical two-point velocity correlation with transverse separations.

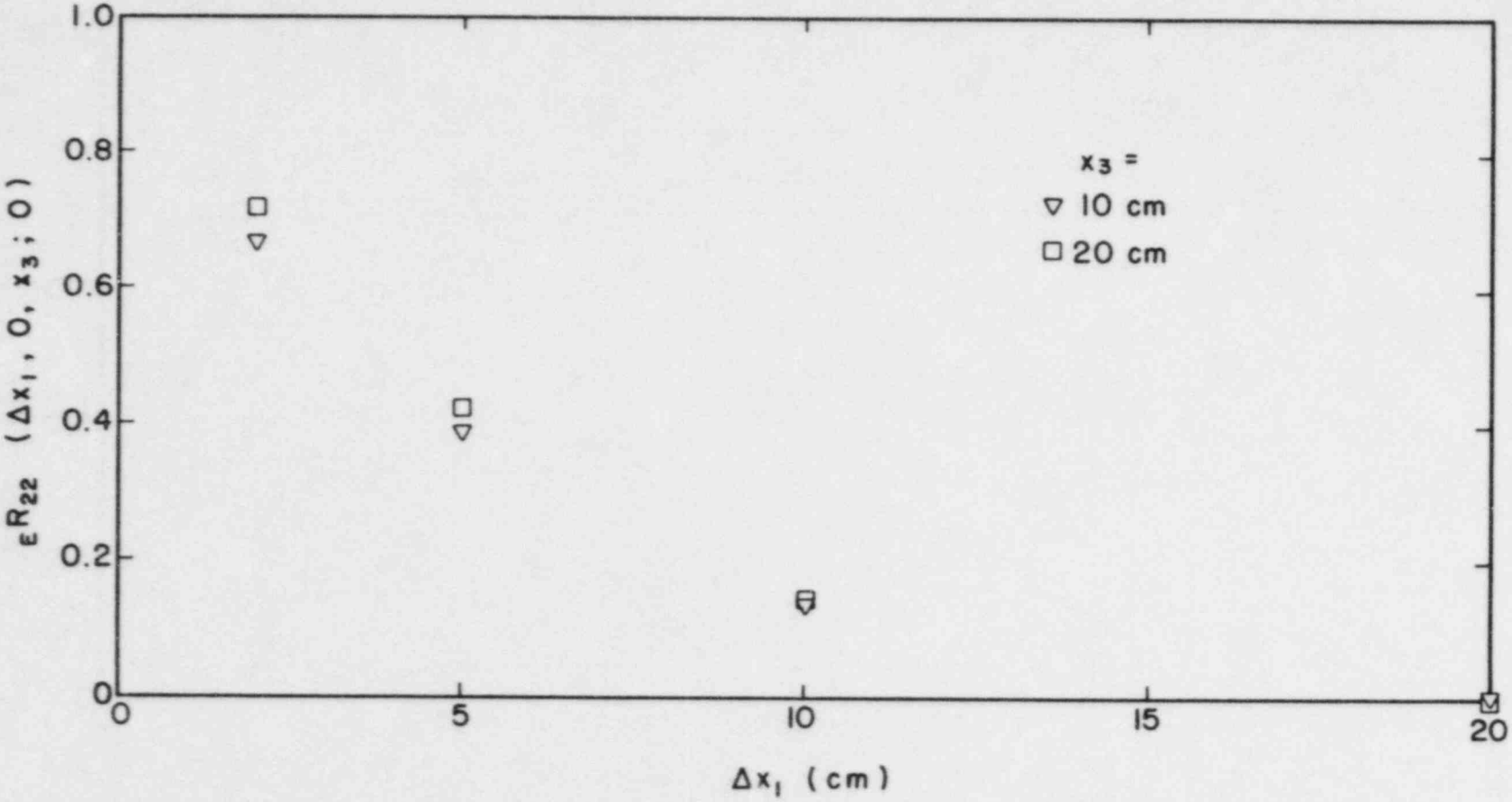

Figure 5.36. Lateral two-point velocity correlation with longitudinal separations.

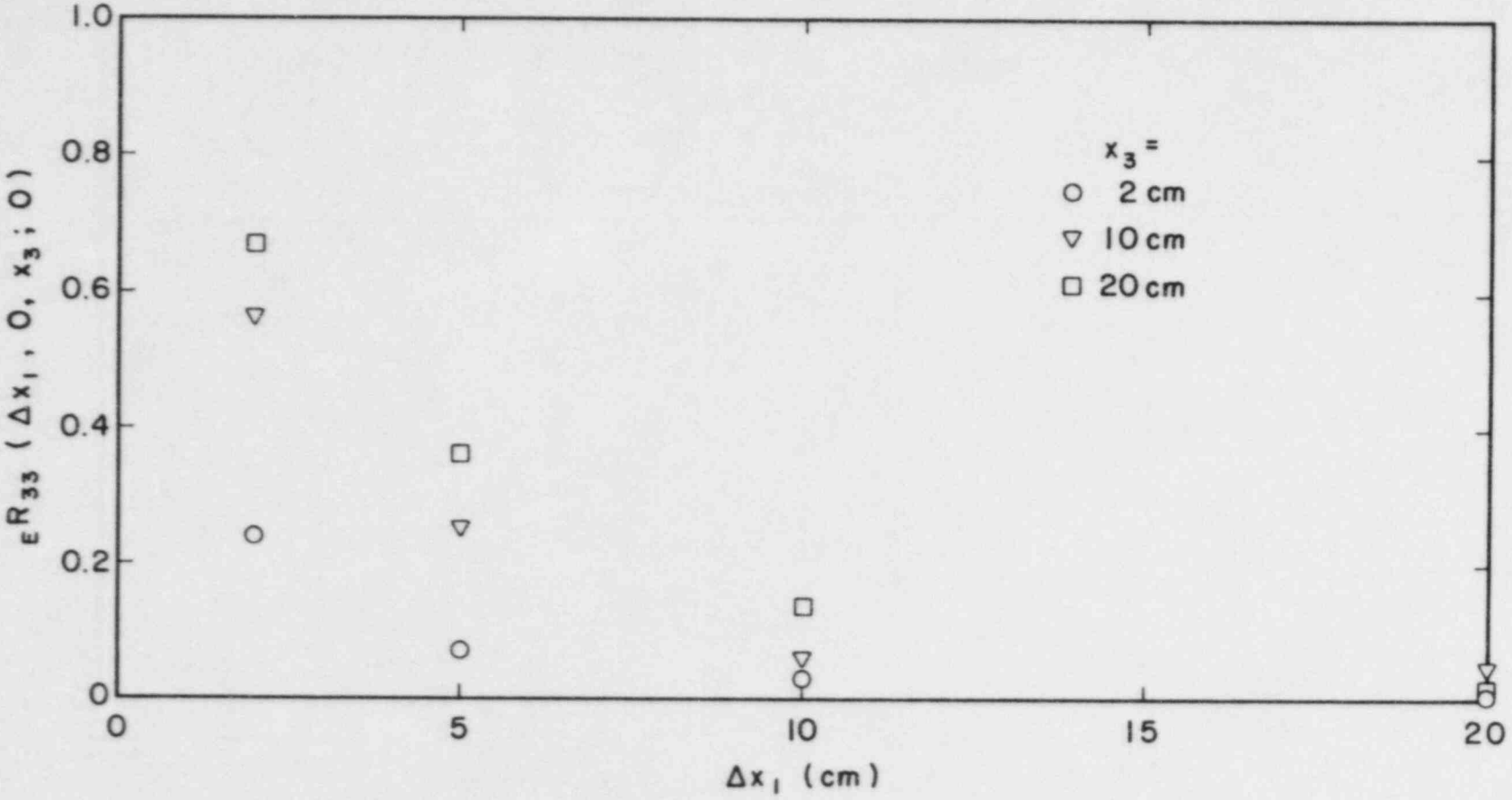

Figure 5.37. Vertical two-point velocity correlation with longitudinal separations.

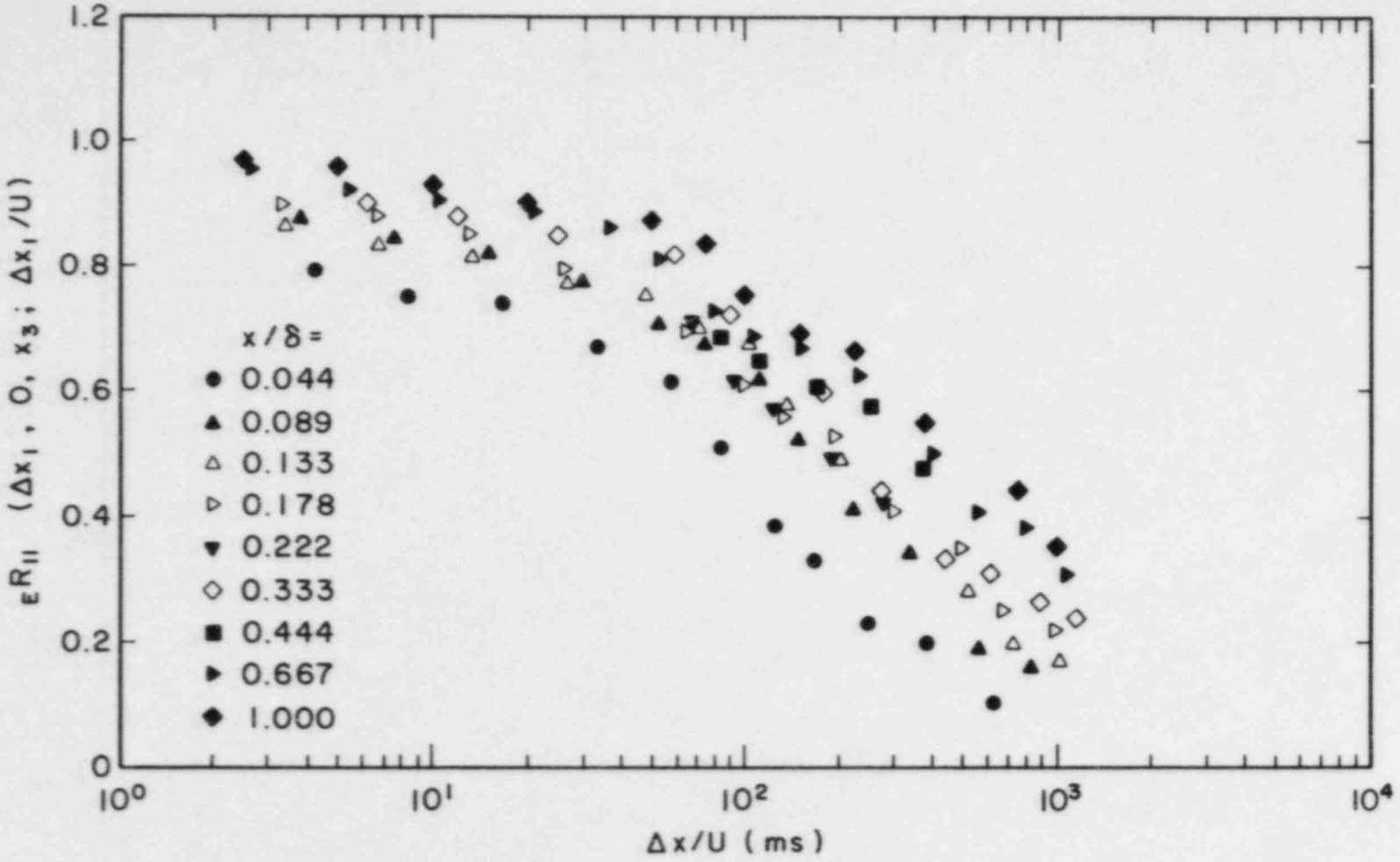

Figure 5.38. Longitudinal Eulerian space-time correlation in a neutral stratified boundary layer (filtered).

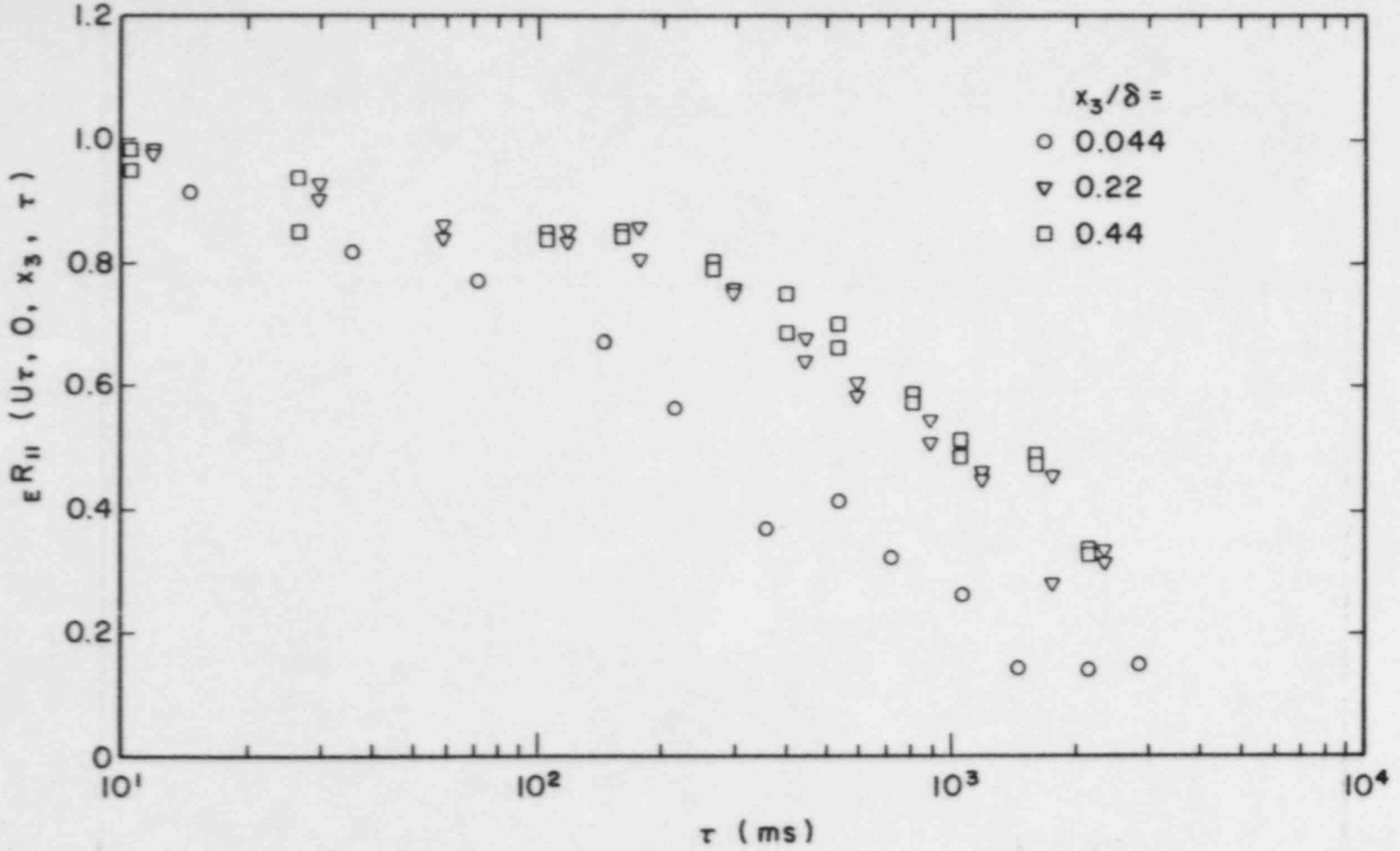

Figure 5.39. Longitudinal Eulerian space-time correlation in a neutral stratified boundary layer (unfiltered).

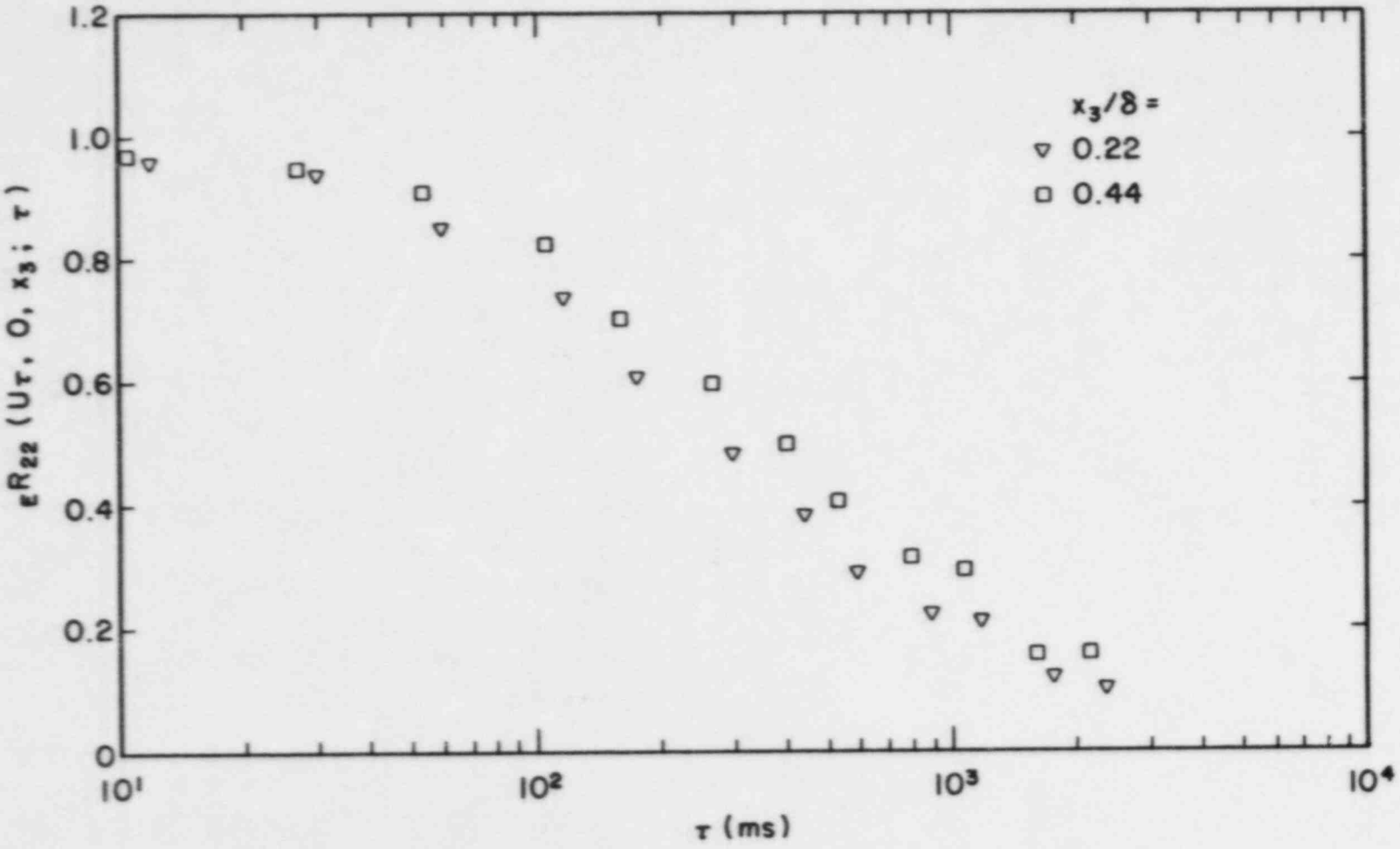

Figure 5.40. Transverse Eulerian space-time correlation in a neutral stratified boundary layer (unfiltered).

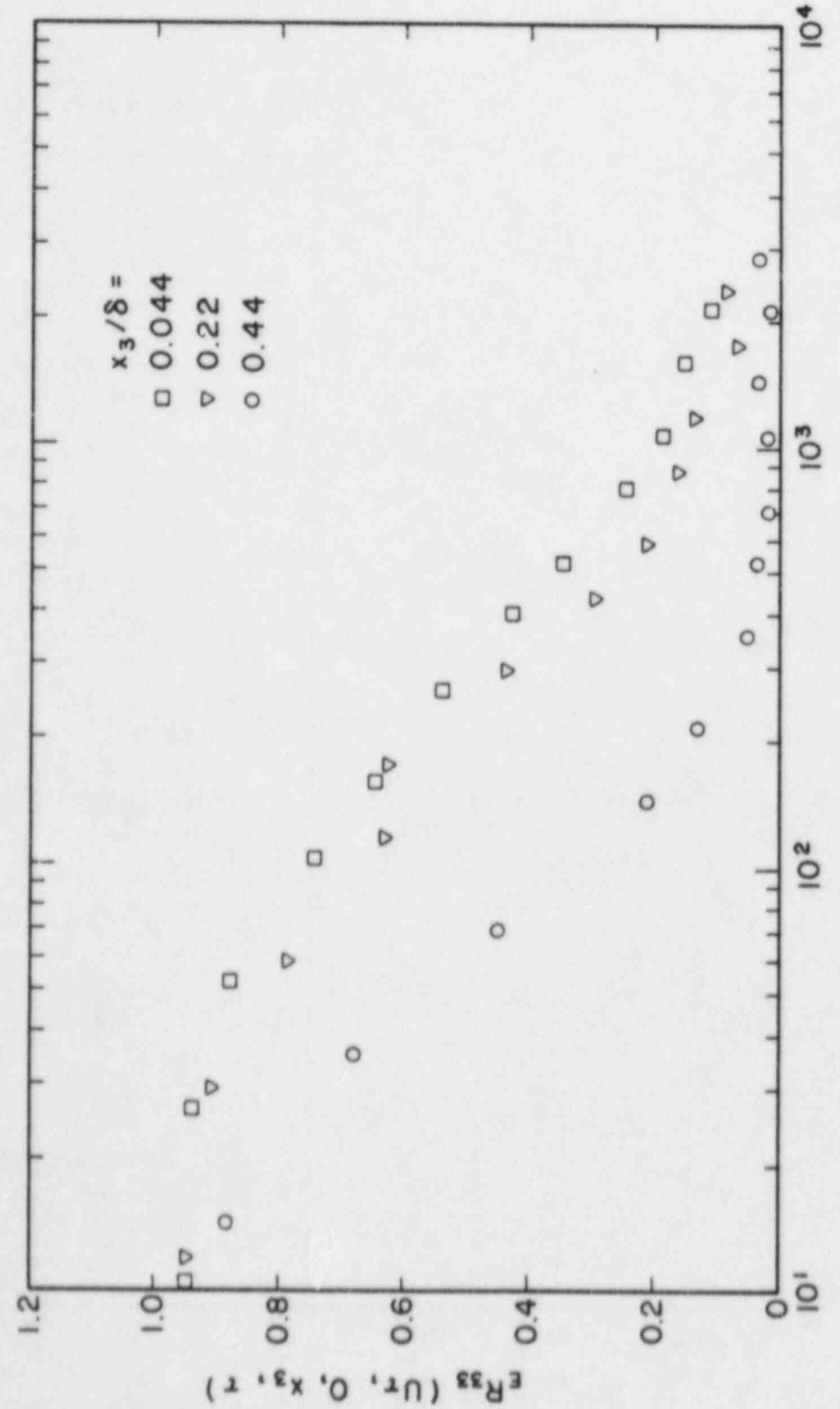

Figure 5.41. Vertical Eulerian space-time correlation in a neutral stratified boundary layer (unfiltered).

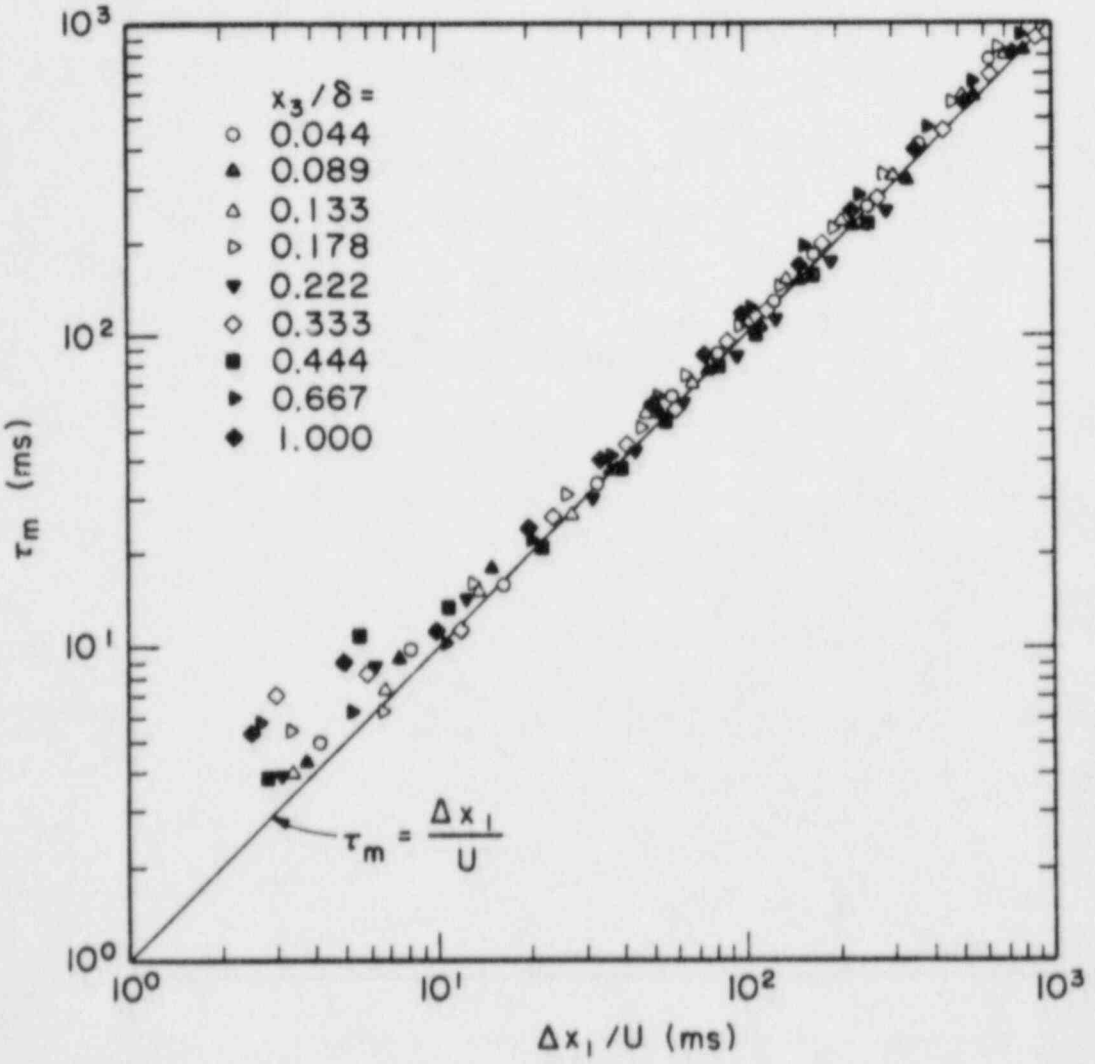

Figure 5.42. Convective velocity in a neutral stratified boundary layer.

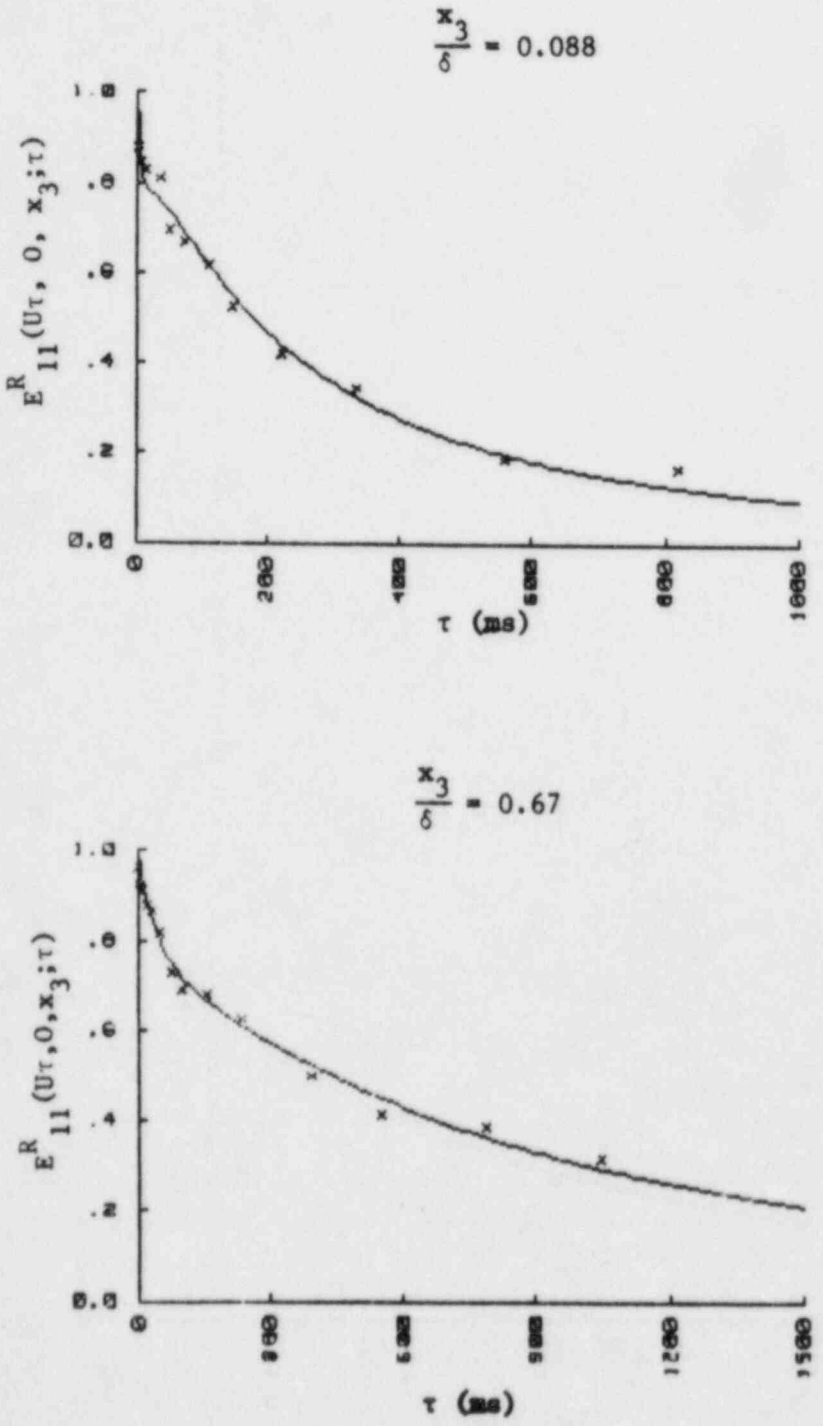

Figure 5.43. Estimation of the integral scale of the Eulerian space-time correlation.

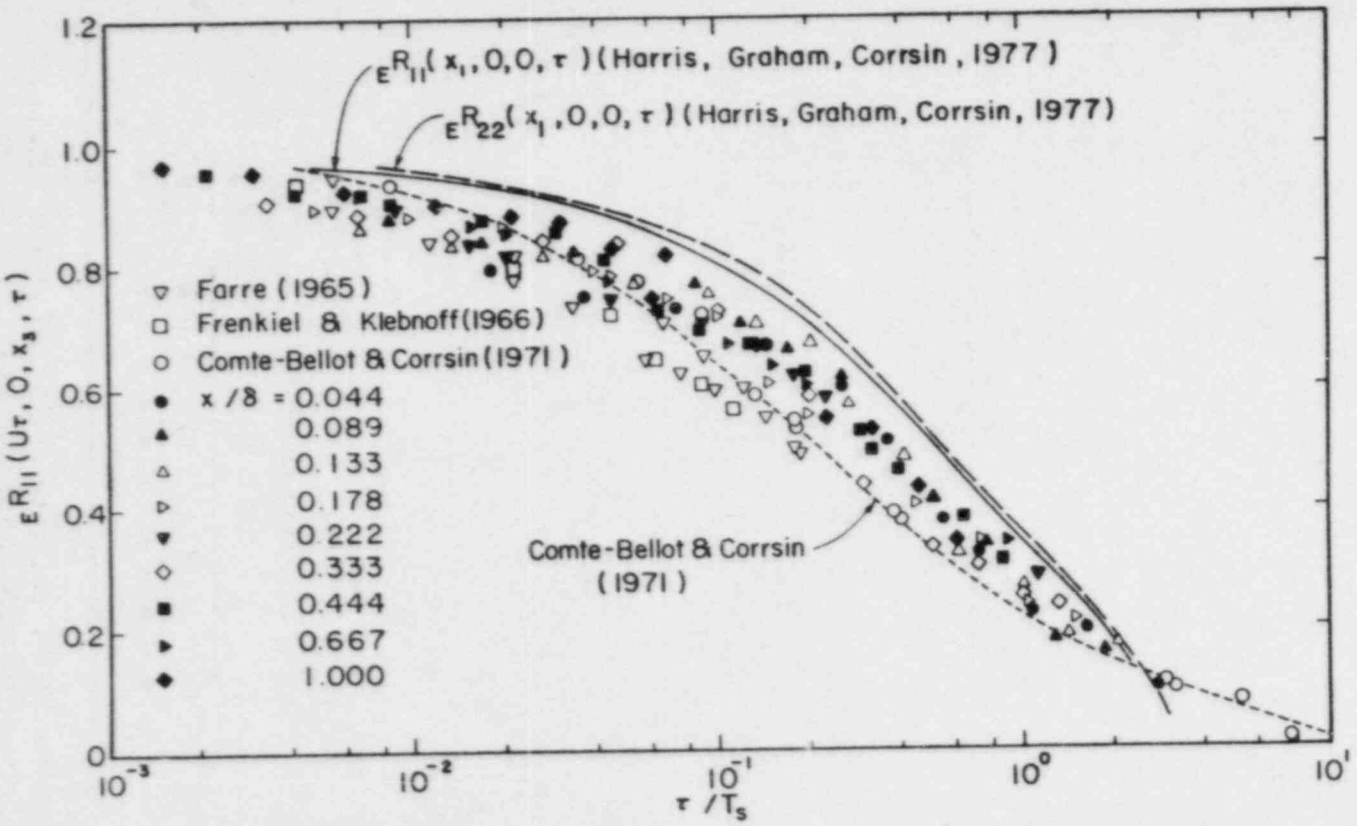

Figure 5.44. Normalized longitudinal space-time correlation in the boundary layer (filtered).

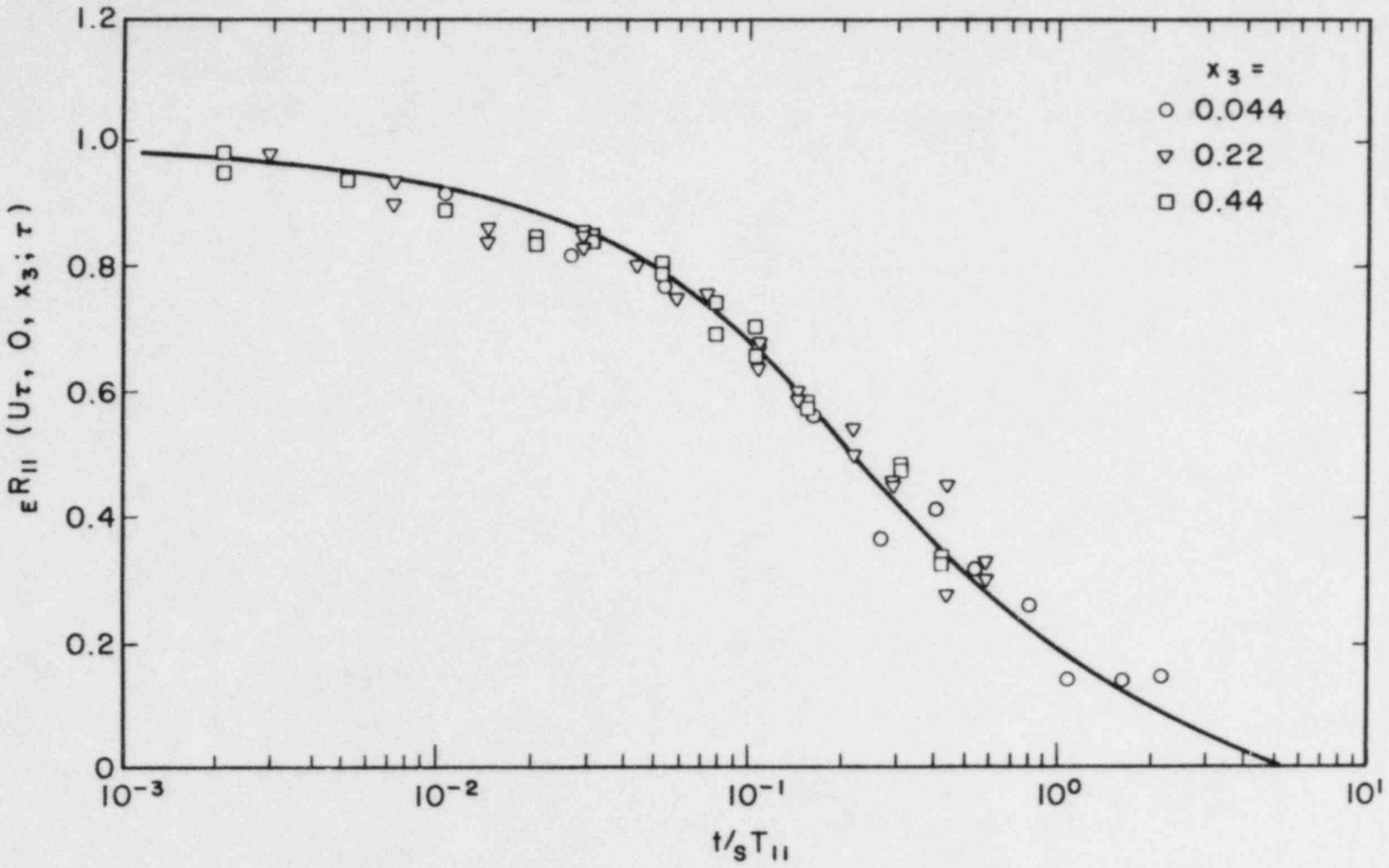

Figure 5.45. Normalized longitudinal space-time correlation in the boundary layer (unfiltered).

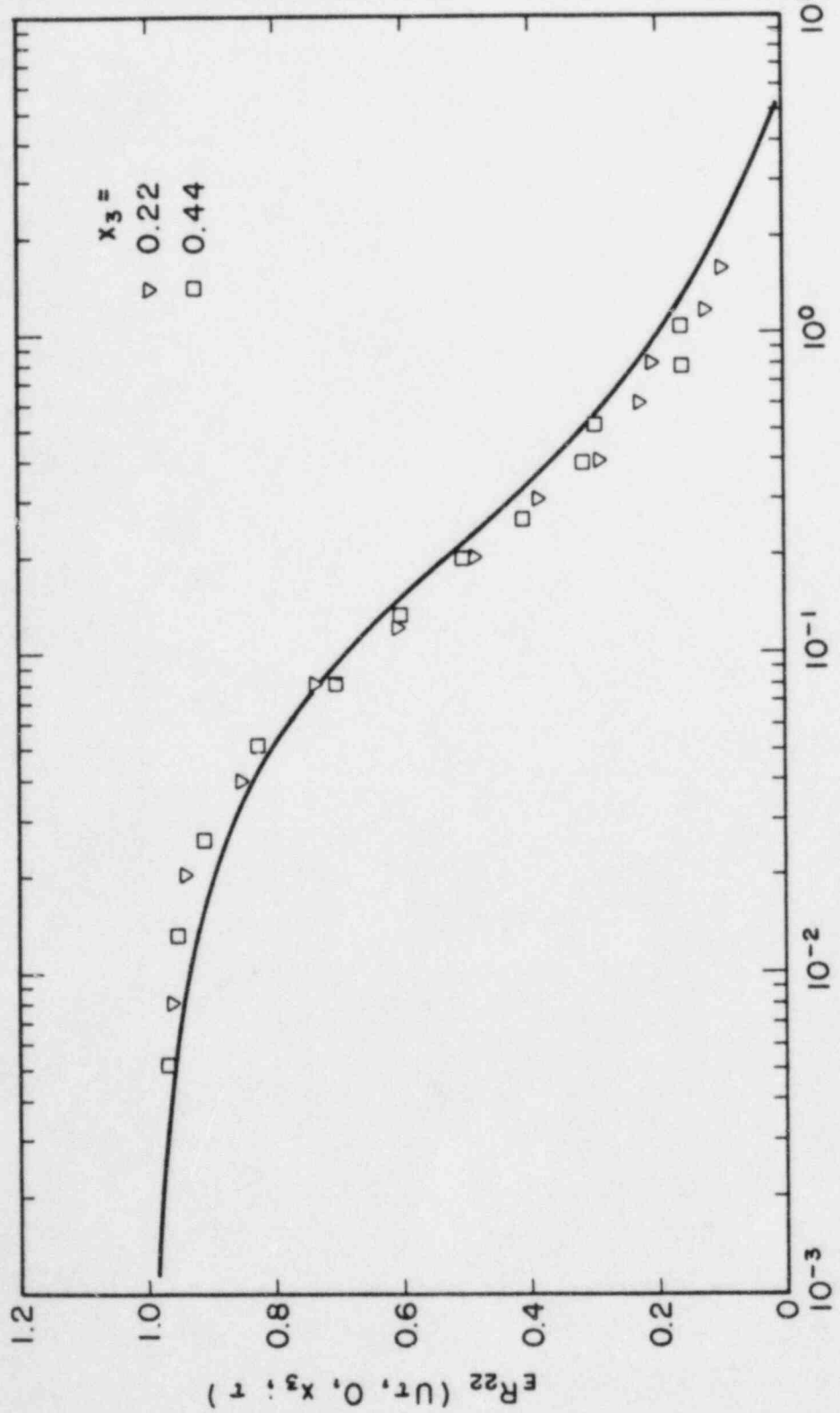

Figure 5.46. Normalized lateral space-time correlation in the boundary layer (unfiltered).

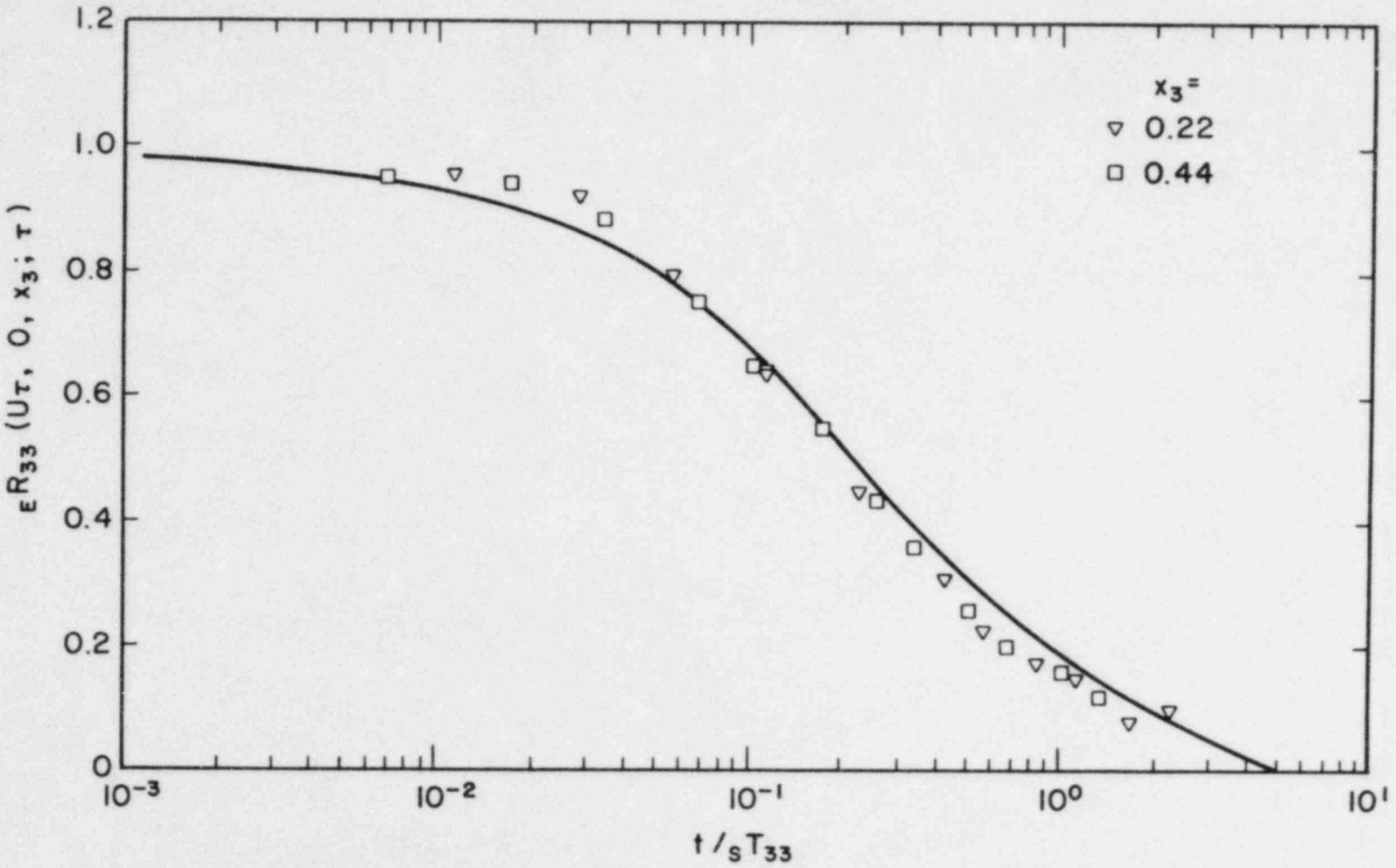

Figure 5.47. Normalized vertical space-time correlation in the boundary layer (unfiltered).

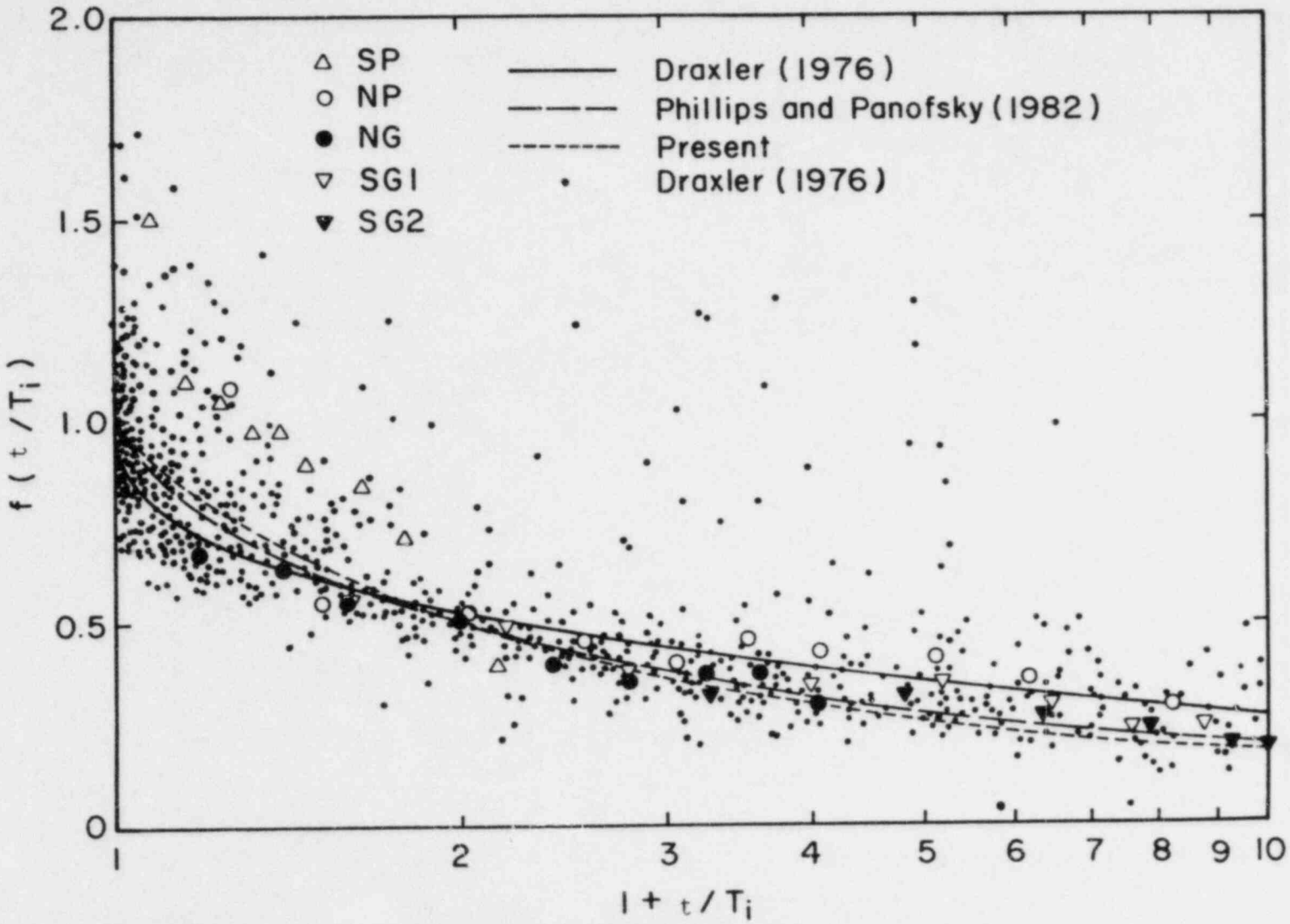

Figure 5.48. Lateral plume spread from a ground source vs. diffusion time.

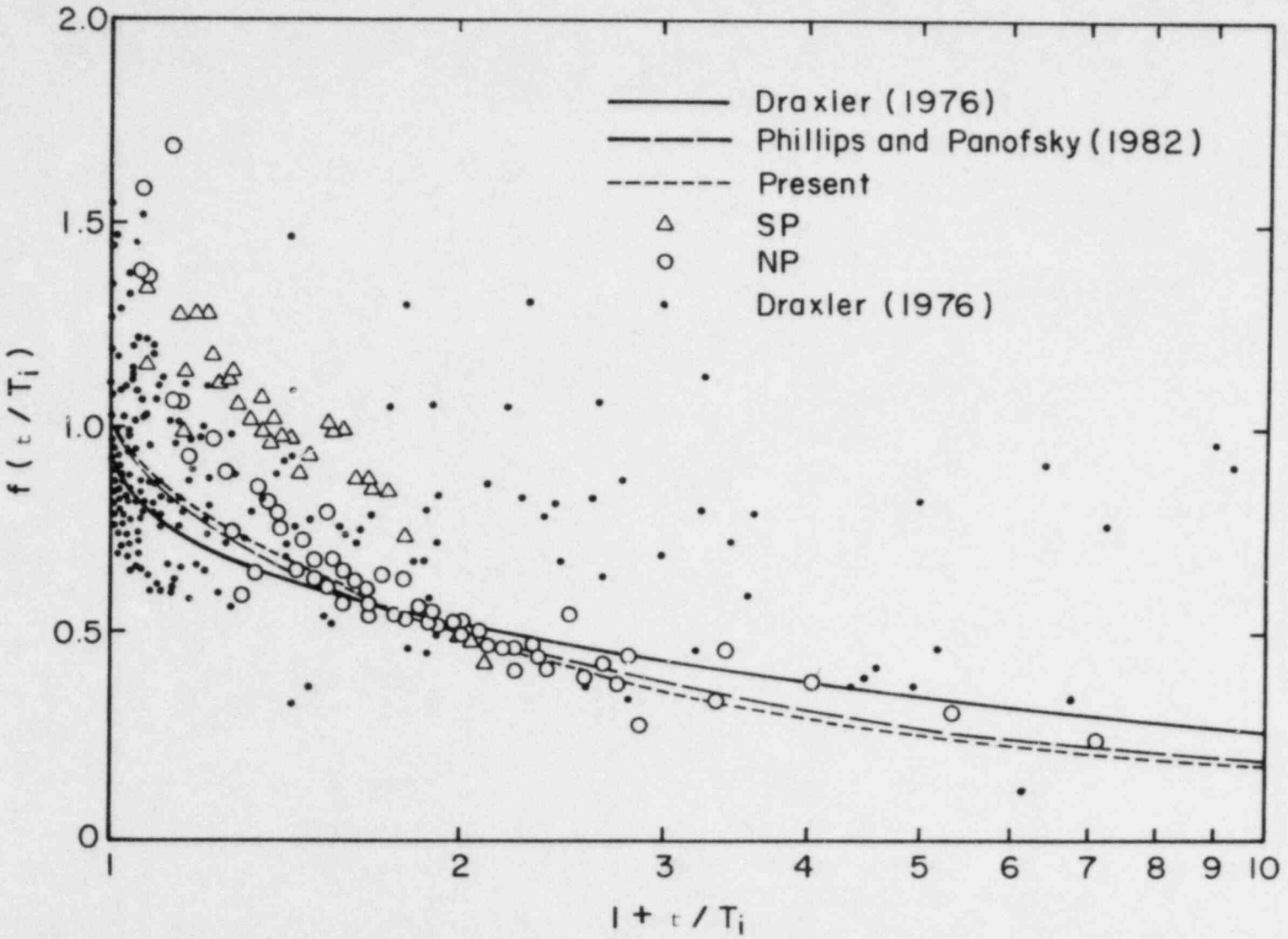

Figure 5.49. Lateral plume spread from an elevated source vs. diffusion time.

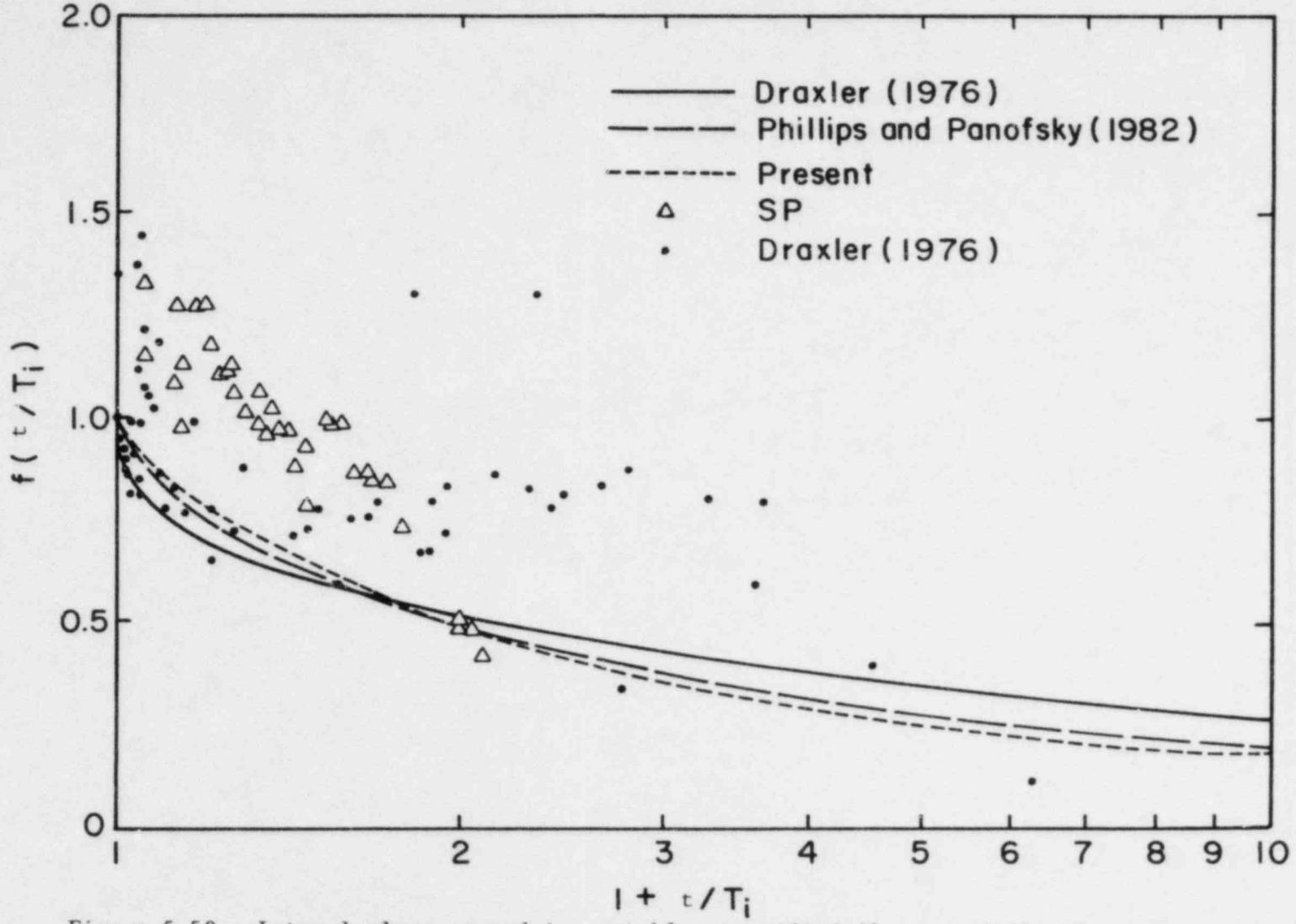

Figure 5.50. Lateral plume spread in a stable stratified flow vs. diffusion time.

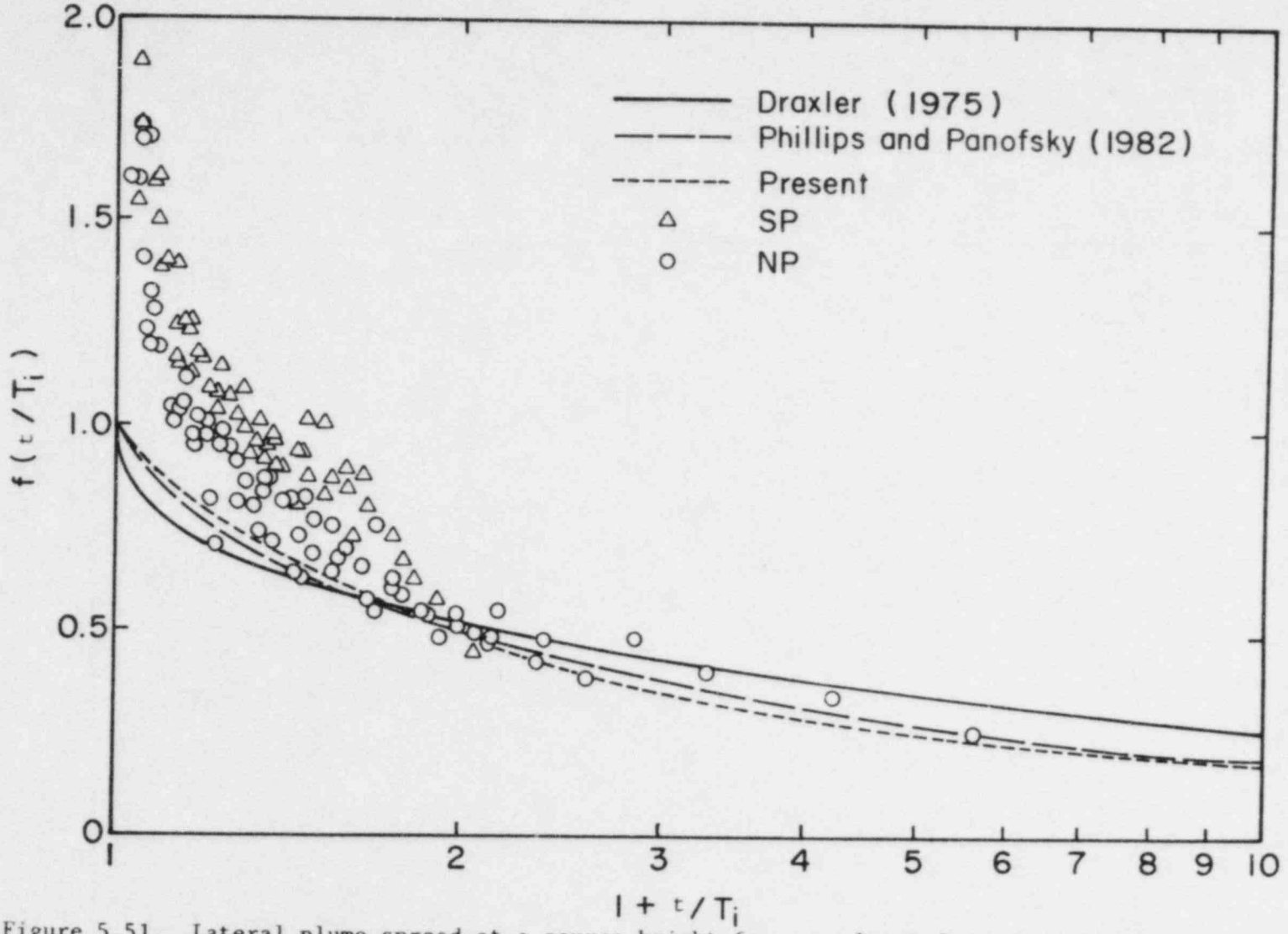

Figure 5.51. Lateral plume spread at a source height from an elevated source vs. diffusion time.

$$\text{(I)}\quad \text{Curve 1:}\quad f(t/T_i) = \frac{1}{1 + 0.9\sqrt{t/T_i}}$$

$$\text{(II)}\quad \text{Curve 2:}\quad f(t/T_i) = 0.617\left[\frac{T_i}{t} - \frac{(T_i/T)^2}{5.25}\ln\left(1 + 5.25\,\frac{t}{T_i}\right)\right]^{1/2}$$

$$\text{(III)}\quad \text{Dash Curve:}\quad f(t/T_i) = 0.541\left[\frac{T_i}{t} - \frac{(T_i/T)^2}{6.83}\left(1 - \exp\left(-6.83\ t/T_i\right)\right)\right]^{1/2}$$

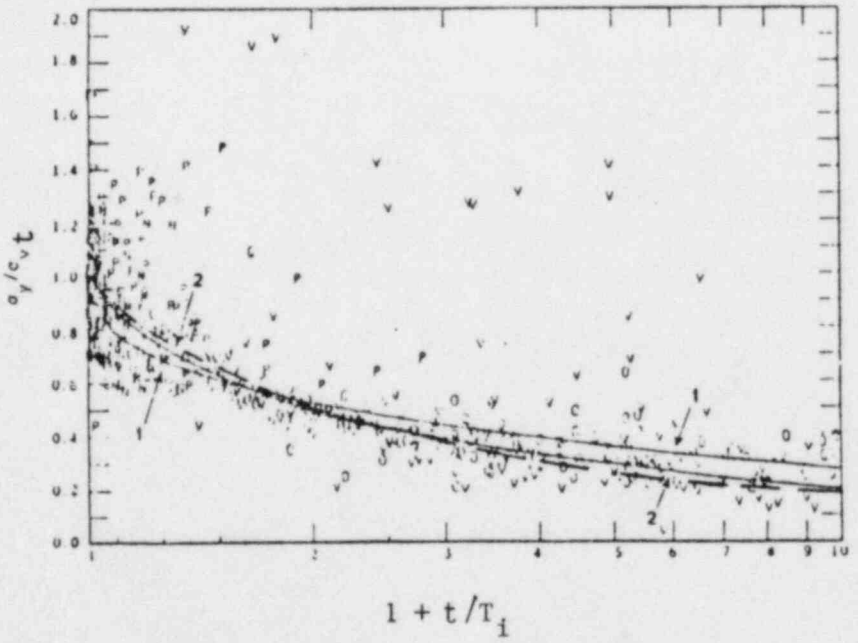

Figure 5.52. f curve for diffusion in the atmospheric boundary layer (from Phillips and Panofsky, 1982).

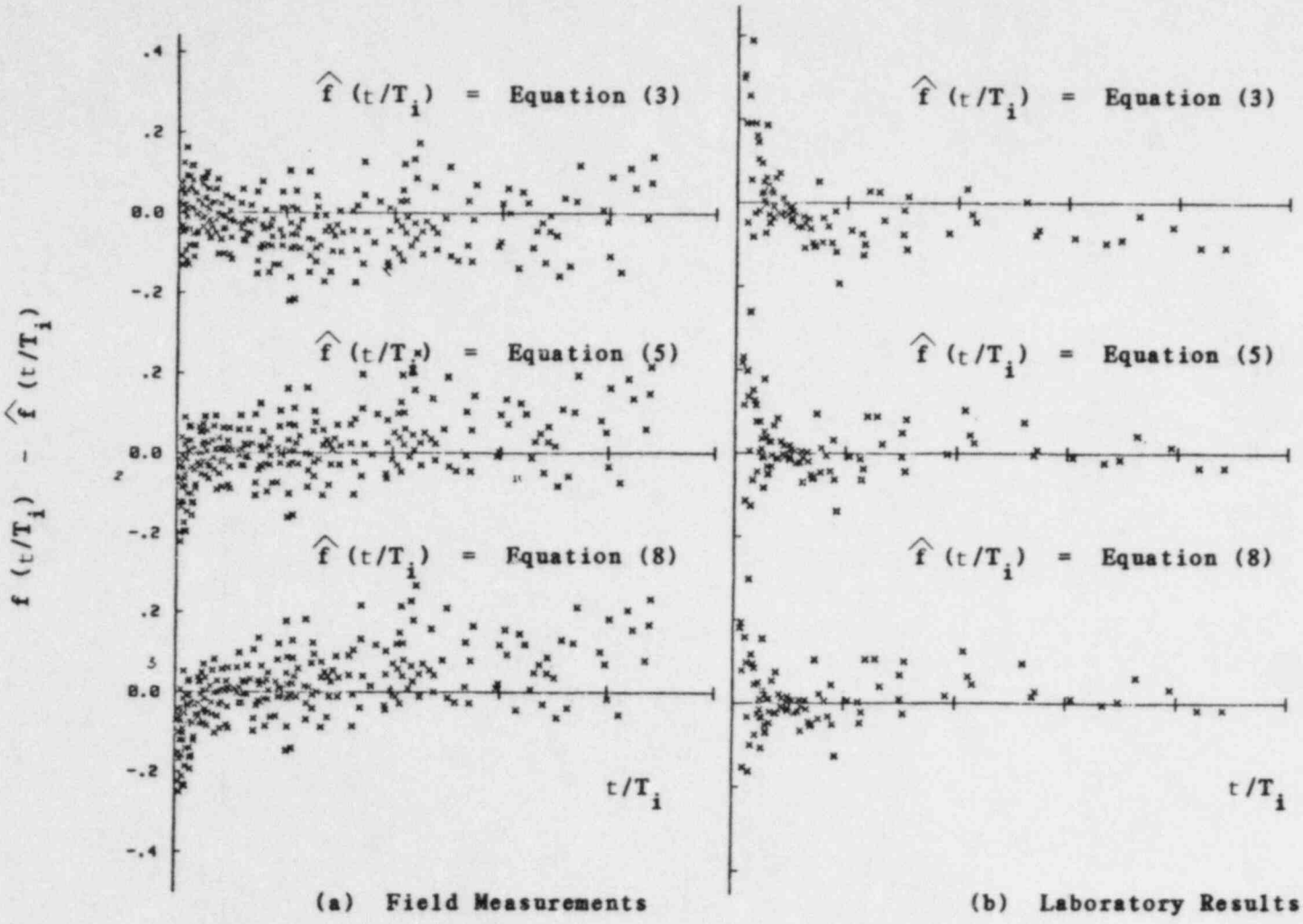

Figure 5.53. Residual analysis for predictive schemes.

Chapter 6

PREDICTIONS FOR LAGRANGIAN STATISTICS AND TURBULENT DIFFUSION

6.1 Introduction

The estimated Lagrangian statistics obtained from the present analysis are given in this chapter. These Lagrangian estimates are used to predict dispersion from a continuous point source; then comparisons are made between the predicted and measured dispersion in a simulated boundary layer.

The Lagrangian autocorrelation functions and integral scales for a uniform turbulent flow are presented in Section 6.2. Discussions are extended to a uniform sheared turbulence field in Section 6.3. Section 6.4 compares the Lagrangian estimates calculated from the Independence Hypothesis approach with other analytical methods. Section 6.5 examines the integral scale ratios between the present data and previous experimental results. Predictions of turbulent dispersion based on the Lagrangian estimates are presented in Section 6.6 for comparison with experimental data.

6.2 Lagrangian Estimates for Homogeneous Isotropic Turbulent Flow

6.2.1 Turbulent flow with uniform velocity

Lagrangian autocorrelation functions are computed according to Equation 3.12 for various α via the numerical iterative procedure described in Section 3.5. Four different functional forms for $F_1(t_*)$ are employed in the analysis of homogeneous isotropic turbulence with uniform velocity. The four cases are:

Model I (Exponential) : $F_1(t_*) = \exp(-t_*)$

Model II (Gaussian) : $F_1(t_*) = \exp(-\frac{\pi t_*^2}{4})$

Model III (Empirical) : $F_1(t_*)$ = dotted curve in Figure 5.44

Model IV (Empirical) : $F_1(t_*)$ = solid curve in Figure 5.45

Results computed from Equation 3.15 have been compared with results computed from Equation 3.12. Increasing the number of Gauss-Legendre quadrature points improves the accuracy of the double integral in

Equation 3.16. In order to reduce the computational time, the number of weighting points is limited to 400 in calculating the double integral. The maximum error resulting from the double integration is 0.5 percent in ${}_{L}T_{11}/{}_{S}T_{11}$.

Figure 6.1 presents the estimated Lagrangian autocorrelation function computed from four different models in terms of t_*. Figures are reproduced in the coordinates of $t/{}_{L}T_{11}$ in Figure 6.2. It is designed in the numerical procedure so that the Lagrangian and Eulerian space-time correlation functions are identical in the limit of $\alpha=0$. In each case, the shape of ${}_{L}R_{11}(t_*)$ strongly depends on the model selected and bears resemblance to the functional form of $F_1(t_*)$ at small α. For large α, the resultant ${}_{L}R_{11}(t_*)$ is less affected by $F_1(t_*)$ in all models. ${}_{L}R_{11}(t_*)$ decreases as the Eulerian parameter increases but preserves similarity, except Model II, when plotted in terms of $t/{}_{L}T_{11}$. ${}_{L}R_{11}(t_*)$ predicted from measured $F_1(t_*)$, Model III and Model IV, decays faster than predicted from analytical $F_1(t_*)$, Model I and Model II, at small t_* but retains higher correlation at large t_*. ${}_{L}T_{11}/{}_{S}T_{11}$ can be evaluated from Figure 6.1 and is plotted in Figure 6.3 against various α for all models. Figure 6.3 also presents results reported by other researchers. Discussions of those data are deferred to Section 6.5.

The fixed-point Eulerian autocorrelation can be obtained as a result of Equation 3.9 by substituting $r = -U\tau$ and $\theta = \pi$. Therefore, ${}_{E}T_{11}$ may be determined as

$$ {}_{E}T_{11} = {}_{S}T_{11} \int_{o}^{\infty} e^{-\left|\frac{\alpha}{i}\right| t_*} F_1(t_*)dt_* \quad . $$

The ratio ${}_{S}T_{11}/{}_{E}T_{11}$ calculated from the above relationship is shown in Figure 6.4. Another ratio of time scale, $\beta = {}_{L}T_{11}/{}_{E}T_{11}$ (the Pasquill's Beta), is readily evaluated by multiplying ${}_{L}T_{11}/{}_{S}T_{11}$ by ${}_{S}T_{11}/{}_{E}T_{11}$. Figure 6.5 is produced from Figures 6.3 and 6.4 with selected α.

Baldwin and Johnson (1972) have indicated that the bracket term in Equation 3.12, $G(\alpha,t_*)$, is rather insensitive to the functional form of $F_1(t_*)$. In the present analysis, cases considered are further extended to a general turbulence which includes non-isotropy and uniform shear strain. Figure 6.6 displays the results for various flow configurations. $G(\alpha,t_*)$ is presented in Figure 6.6a for an isotropic homogeneous uniform flow while Figures 6.6b,c,d present the same calculation for an isotropic uniform shear flow, a non-isotropic uniform flow, and a non-isotropic uniform shear flow, respectively. Under each turbulence category, all models yield similar estimation for a short diffusion time but diverge from one another for a long diffusion time. The shape of

$G(\alpha,t_*)$ is not much affected by different models as seen in the figures. ${}_LR_{11}(t_*)$ is obtained as the product of $G(\alpha,t_*)$ and $F_1(t_*)$. After multiplying with $F_1(t_*)$, the deviation in $G(\alpha,t_*)$ due to different $F_1(t_*)$ only accounts for a small percentage of error in estimating ${}_LR_{11}(t_*)$. Hence, it will be of practical interest to tabulate the calculation of $G(\alpha,t_*)$ with respect to α in each turbulence category. The tabulated results may be used in conjunction with a measured $F_1(t_*)$ without going through all the numerical computation as the first approximation to ${}_LR_{11}(t_*)$.

$F_1(t_*)$ will be limited to Model IV during subsequent predictions of ${}_LR_{11}(t_*)$ in some generalized turbulent fields.

6.2.2 Turbulent flow with uniform shear

Figure 6.7 presents ${}_LR_{11}(t_*)$ for various values of α and $\Gamma_S T_{11}$. The existence of mean shear does not change the Lagrangian autocorrelation function at small t_* ($t_* < 0.25$) but results in a faster decay at larger t_*. The ratio ${}_LT_{11}/{}_ST_{11}$ is plotted in terms of $\Gamma_S T_{11}$ for different α in Figure 6.8 to emphasize the shear effect. The ratio ${}_LT_{11}/{}_ST_{11}$ decreases faster for small value of α due to the shear strain. Increase of shear causes little change in ${}_LT_{11}/{}_ST_{11}$ after $\Gamma_S T_{11}$ approaches 5.0 for large α. Figure 6.8 may be used together with Figure 6.4 to predict β in an isotropic homogeneous uniform shear flow as long as such turbulence parameters as $[u_1^2]$, L, Γ and ${}_ST_{11}$ are specified in the turbulence field. Figure 6.9 displays the predicted β contours for i=0.1. Note that β falls between 3.0 and 5.0 for a wider range of α with the presence of shear than without the presence of shear (e.g., β = 3.0~5.0 for α = 0.35~3.3 and $\Gamma_S T_{11}$ = 2.0 while β = 3.0~5.0 for α = 0.19~1.0 and $\Gamma_S T_{11}$ = 0.0). For atmospheric turbulence, $\frac{\alpha}{i} \simeq \frac{1.0}{0.1} = 10.0$, an averaged β = 4.0 for various strain rates agrees very well with field observations.

6.3 Lagrangian Estimates for Homogeneous Non-Isotropic Turbulent Flow

It is difficult to provide complete information on the estimated Lagrangian statistics for a non-isotropic turbulent flow since there are four parameters involved, namely, α_1, α_2, α_3 and $\Gamma_S T_{11}$. However the numerical procedure can perform the estimation for any specified combination of these four parameters. Figure 6.10 presents results for ${}_LT_{11}/{}_ST_{11}$ in an ideal one-dimensional non-isotropic uniform turbulent flow by assuming $\alpha_2 = \alpha_3 = 0$. The magnitude of the Lagrangian autocorrelation function as well as the scale ratio is gradually reduced once the turbulence field is expanded from one-dimension to three-dimension. Figure 6.11 presents the resultant ${}_LT_{11}/{}_ST_{11}$ for two-dimensional turbulent flow with uniform velocity. ${}_LT_{11}/{}_ST_{11}$ for a

designated three-dimensional turbulence with $\alpha_2 = \alpha_3$ is given in Figure 6.12. Reduction of ${}_L^T{}_{11}/{}_S^T{}_{11}$ due to the redistribution of turbulent energy to other directions is clearly observed through Figures 6.10 to 6.12. Variation in ${}_L^T{}_{11}/{}_S^T{}_{11}$ resulting from different α_2 and α_3 values plotted in Figure 6.13 for an $\alpha_1 = 1.0$. ${}_L^T{}_{11}/{}_S^T{}_{11}$ may be obtained without significant error by using the averaged value of α_2 and α_3 from Figure 6.12. Figure 6.12 or Figure 6.13 can be used in connection with Figure 6.8 as the first approximation for ${}_L^T{}_{11}/{}_S^T{}_{11}$ in a non-isotropic uniform shear flow. Similarly, β may be estimated from Figure 6.12 in conjunction with Figure 6.4.

6.4 Comparison with Analytical Predictions

6.4.1 Numerical simulation of particle motion

In a recent paper prepared by Lee and Stone (1983), Monte Carlo techniques were used to predict one-dimensional diffusion in a stationary, homogeneous field of turbulence. An analytical expression to predict the Lagrangian statistics from Eulerian statistics was also presented. The analytical solution for cloud growth compared favorably with the results from the Monte Carlo simulation, and both results agreed with Lagrangian statistics estimated from the present analysis. It is indeed impressive that a one-dimensional turbulence model approximated cloud dispersion as well as a full three-dimensional model. Hence, their expressions are re-examined here.

Lee and Stone approximated the Lagrangian autocorrelation function at a short time increment by the Eulerian space-time correlation. They assumed that the velocity fluctuations is normally distributed with zero mean and standard deviation $[u_1^2]^{\frac{1}{2}}$. They used the expression

$$ {}_L^R{}_{11}(\delta t) = (\frac{2}{\pi})^{\frac{1}{2}} \exp(-\frac{\delta t}{{}_S^T{}_{11}}) \int_o^\infty n^2 e^{-an} e^{-\frac{n^2}{2}} dn \qquad (6.1) $$

where $a = \frac{[u^2]^{\frac{1}{2}}\delta t}{L}$ and $n = N(0,1)$.

The Lagrangian autocorrelation function at δt can be obtained as

$$ {}_L^R{}_{11}(\delta t) = e^{-\frac{\delta t}{{}_S^T{}_{11}}} \{ e^{\frac{a^2}{2}} (1+a^2)(1-\mathrm{erf}(\frac{a}{\sqrt{2}})) - \frac{\sqrt{2}}{\sqrt{\pi}} a \} . \qquad (6.2) $$

Since a first order autoregressive process successfully describes the motion of a diffusion air particle, the autocorrelation function must satisfy the following relationship (Box and Jenkin, 1976)

$$ {}_{L}R_{11}(t) = \{{}_{L}R_{11}(\delta t)\}^{k} \quad , \quad t = k\delta t \ . \tag{6.3} $$

Therefore ${}_{L}R_{11}(t)$ can be expressed as

$$ {}_{L}R_{11}(t) = e^{-\frac{t}{{}_{S}T_{11}}} \{e^{\frac{a^2}{2}}(1+a^2)(1-\mathrm{erf}(\frac{a}{\sqrt{2}})) - \frac{\sqrt{2}}{\sqrt{\pi}}\, a\}^{\frac{t}{\delta t}} \tag{6.4} $$

and

$$ \frac{{}_{L}T_{11}}{{}_{S}T_{11}} = \{1 - \frac{{}_{S}T_{11}}{\delta t} \ln(e^{\frac{a^2}{2}}(1+a^2)(1-\mathrm{erf}(\frac{a}{\sqrt{2}})) - \frac{\sqrt{2}}{\sqrt{\pi}}\, a)\}^{-1} \tag{6.5} $$

or

$$ \frac{{}_{L}T_{11}}{{}_{S}T_{11}} = \{1 - \frac{1}{\Delta t_{*}} \ln\{e^{\frac{\alpha^2 \Delta t_{*}^2}{2}}(1+\alpha^2 \Delta t_{*}^2)(1-\mathrm{erf}(\frac{\alpha \Delta t_{*}}{\sqrt{2}})) - \frac{\sqrt{2}}{\sqrt{\pi}}\, \alpha\, \Delta t_{*}\}\}^{-1} \ , \tag{6.6} $$

where $a = \alpha \Delta t_{*}$ and

$\Delta t_{*} = \delta t / {}_{S}T_{11}$.

Lee and Stone obtained ${}_{L}R_{11}(\delta t)$ by expanding the exponentials, $\exp(-\delta t/{}_{S}T_{11})$ and $\exp(-an)$, in Equation 6.1 for small value of $\delta t \to 0$. ${}_{L}T_{11}/{}_{S}T_{11}$ was obtained in conjunction with the random force model suggested by Gifford (1982). Their result is

$$ {}_{L}T_{11}/{}_{S}T_{11} = (1 + (\frac{8}{\pi})^{\frac{1}{2}}\, \alpha)^{-1} \ . \tag{6.7} $$

Equation 6.6 is a more exact solution to the Monte Carlo simulation, yet the differences found are negligible. Table 6.1 displays values calculated from Equations 6.6 and 6.7. It is not surprising that Equation 6.6 successfully predicts results from a Monte Carlo simulation since it is the natural consequence of the Markov process. Table 6.1 also lists ${}_{L}T_{11}/{}_{S}T_{11}$ computed from Equation 3.12 by adopting $F_1(t_{*}) = \exp(-t/{}_{S}T_{11})$. For a small value of α, the estimated ${}_{L}T_{11}/{}_{S}T_{11}$ agrees with the Monte Carlo simulation predictions. As α increases, the deviation becomes appreciable. Lee and Stone warned of the possibility that the one-dimensional model inadequately represents the spatial

variation of the correlation function in three-dimensional homogeneous turbulence. Indeed their results agree with these more exact calculations at small α.

Suppose that instead of using Equation 3.9, ${}_{E}R_{11}(r,\theta,t)$ is replaced with $\exp(-t_{\star})\exp(-r/L)$ as utilized by Lee and Stone. The Lagrangian autocorrelation function is then

$$ {}_{L}R_{11}(t_{\star}) = e^{-\tau_{\star}} \{e^{\alpha^2 I}(1 + 2\alpha^2 I)(1-\mathrm{erf}(\sqrt{\alpha^2 I})) - \frac{2}{\sqrt{\pi}}\sqrt{\alpha^2 I}\} \quad . \qquad (6.8) $$

If $\delta t_{\star}$ is a small value such that $\delta t_{\star} \to 0$, $I(t_{\star})$ will approximate its asymptotic value,

$$ I(\delta t_{\star}) = \frac{\delta t_{\star}^2}{2} \quad . $$

Substituting this approximation for $I(\delta t_{\star})$ into Equation 6.8 recovers Equation 6.2 with $\sigma = \alpha\delta t_{\star}$. Values for ${}_{L}T_{11}/{}_{S}T_{11}$ calculated from Equation 6.8 are also included in Table 6.1. The results are significantly larger than estimates from Equations 6.4 and 3.12. Deviations between estimates result solely from the simplification introduced for the general Eulerian space correlation function. ${}_{L}T_{11}/{}_{S}T_{11}$ is overestimated when one assumes that the g-correlation is the same as the f-correlation in an isotropic homogeneous turbulence field.

The difference between estimates from Equations 6.4 and 6.8 is due to the different approaches employed. By virtue of the Lagrangian kinematics of a fluid particle, the Independence Hypothesis is applicable only when t is so large that there is no relation between the fluctuating velocity and the particle position. Equation 3.12 represents results based on such a theory.

Equation 6.2 may be interpreted in terms of the present approach by ignoring the influence of fluctuating velocities on particle position when t is small. For small δt, see Figure 3.1; particles released at t=0 are most likely to arrive at $x_1=U\delta t$, but they will actually scatter about $x_1=U\delta t$. When one assumes ${}_{L}R_{11}(2\delta t) = {}_{L}R_{11}{}^{2}(\delta t)$, the Independence Hypothesis is essentially utilized twice. Hence, the assumption neglects the contribution to the autocorrelation from those fluid particles which scattered about $x_1=Ut$. At large t, Equation 6.4 underestimates the Lagrangian autocorrelation as compared to Equation 6.8. Table 6.1 shows that ${}_{L}T_{11}/{}_{S}T_{11}$ values derived from Equation 6.8 are larger than time ratios calculated from Equation 6.6. The resultant overestimations and underestimations tend to compensate; hence, Lee and Stone's expressions result in close agreement with present analysis for $F_1(t_{\star}) = \exp(-t_{\star})$ as shown in Figures 6.3 and 6.4.

Indeed, the Monte Carlo simulation is mathematically and physically similar to the present approach despite the fact that the numerical simulation is fundamentally incorrect for three-dimensional turbulence.

6.4.2 Prediction from estimated space-time correlation

Favre (1965) has proposed a method for calculating the Eulerian space-time correlation from the space correlation through the Independence Hypothesis. Townsend (1976) also developed an analysis to obtain the space-time correlation starting from the space-time structure function. Both analyses took into account the mean particle displacement in the first approximation and resembled the other. Instead of using the exact form, the mean square particle displacement is assumed to have its asymptotic value as

$$[X_1^2(t)] = [u_1^2]t^2 \ .$$

Such approximation automatically limits the validity of the approach to short diffusion time. Their estimated Eulerian space-time correlation may be expressed in terms of the present derivation as

$$F_1(t_*) = G(\alpha,t_*) \ . \tag{6.9}$$

If one applied their estimated $F_1(t_*)$ to the present analysis, the Lagrangian autocorrelation function is found to be

$$_L R_{11}(t_*) = G^2(\alpha,t_*) \tag{6.10}$$

and $$\int_0^\infty G(\alpha,t_*)dt_* = 1 \ .$$

$F_1(t_*)$ calculated from Equation 6.9 has been compared with the measured results from Favre et al. (1962) by Townsend. For a time delay of $U_1 t/M = 7.57$, the effective value of $\alpha^2 I(t_*)$ is found to be 0.0648, and the estimated value of $F_1(t_*)$ is 0.48 compared to the measured maximum correlation coefficient 0.41 in Favre's experiment. The value 0.48 is different from Townsend's calculation of 0.85 but consistent with Favre's computation. A possible error may exist in Townsend's calculation.

A consequence of the form of $[X_1^2(t_*)]$ adopted in Favre's analysis, the predicted $F_1(t_*)$ has a higher correlation at small t and lower correlation at large t than the measured results reported by Favre. Equation 6.9 predicts $F_1(t_*)$ based on the knowledge of knowing mean square particle displacement (equivalently, the Lagrangian autocorrelation function). Hence the methodology employed in their analysis is quite similar to the present approach except the unknown

in their analysis is the known variable in the present study and vice versa. In order to satisfy $\int_0^\infty G(\alpha,t_*)dt_* = 1$, the present analysis yields $\alpha \tilde{\sim} 1.1$ and ${}_L T_{11}/{}_S T_{11} = 0.336$ according to Equation 6.10. The data point marked as Favre and Townsend in Figure 6.2 shows their result is close to the prediction using Comte-Bellot and Corrsin's measured $F_1(t_*)$.

6.4.3 Comparison with analysis using Independence Hypothesis

Philip (1967) and Saffman (1963) employed the Independence Hypothesis to estimate Lagrangian autocorrelation functions and integral scales. Both analyses, closely related to the present approach, have been discussed thoroughly by Baldwin and Johnson. Their results are briefly summarized in this section.

Philip's results for ${}_L T_{11}/{}_S T_{11}$, derived from Equation 2.26 are reproduced and presented in Figure 6.3. His results are comparable to Model II by using a Gaussian form for $F_1(t_*)$. The deviations result from his use of an averaged integral length scale regardless of the variation in the space correlation. The averaging process for L becomes more accurate in the region in Figure 6.3 where the two curves intercept.

Saffman assumed a functional form of an Eulerian spectral density function rather than an equivalent general space-time correlation function. Baldwin and Johnson were able to transform the spectral density function into the Eulerian space-time correlation function as

$$ {}_E R_{11}(r,\theta,\tau) = e^{-\frac{1}{2}\eta^2}\{1 - \frac{1}{2}\eta^2(1-\cos^2\theta)\}\left(\frac{L}{\sqrt{\pi}\Lambda}\right)^5 , \qquad (6.11) $$

where $\eta = \frac{r}{\sqrt{2}\Lambda}$ and $\Lambda = \left\{\frac{L^2}{\pi} + \frac{1}{2}[u^2]\tau^2\right\}^{\frac{1}{2}}$.

Based on Equation 6.11, Baldwin and Johnson reduced two time-scale ratios from Saffman's analysis. The results are reproduced in Figures 6.3 and 6.4. One notices that models with analytical $F_1(t_*)$ approach the Taylor's hypothesis asymptotic, 45 degree line in Figure 6.3 more rapidly than models using emperical $F_1(t_*)$.

To avoid repetition, comparison made by Baldwin and Johnson with previous work are summarized in Figure 6.14 without further discussion. This figure is compatible with Figure 6.5 but separated for clarity.

6.5 Comparison with Experimental Data

Simultaneous measurements leading to confirmation of the integral scales (${}_{E}T_{ii}$, ${}_{S}T_{ii}$ and ${}_{L}T_{ii}$) are rare both in the laboratory and in the atmosphere. Nevertheless, there were several Eulerian measurements reported while examining the production of turbulent energy. The following comparisons are made in a qualitative sense despite the fact that variations in the different experiments preclude similarity.

6.5.1 ${}_{S}T_{11}/{}_{L}T_{11}$

In a nearly homogeneous turbulent shear flow, Champagne et al. (1970) demonstrated that the temporal history of turbulence at a fixed position is well approximated with convective spatial structure in a low turbulence field. Based on this, ${}_{E}T_{11}$ was found to be 0.00335 sec in their measurement. ${}_{S}T_{11}$ was estimated through the relationship, ${}_{S}T_{11} = (\frac{u_1}{L} + \frac{dU}{dx_3})^{-1}$, which resulted in a value of ${}_{S}T_{11} = 0.056$ sec for $i = 0.018$. The following parameters are obtained from their results

$$\alpha_1 = 0.3 \quad ; \quad \alpha_2 = 0.23 \quad ; \quad \alpha_3 = 0.22 \quad ;$$

$$\Gamma = 12.9 \text{ sec}^{-1} \quad \text{and} \quad {}_{S}T_{11}/{}_{L}T_{11} = 16.7 \ .$$

After correcting for decaying turbulence, the following properties in a homogeneous isotropic uniform turbulent flow were obtained by Comte-Bellot and Corrsin (1971)

$$i = 0.0175 \quad ; \quad L = 2.4 \text{ cm}$$

$${}_{E}T_{11} = 0.00189 \text{ sec} \quad ; \quad {}_{S}T_{11} = 0.084 \text{ sec}$$

$$\alpha = 0.78 \quad \text{and} \quad \Gamma = 0 \text{ sec}^{-1} \ .$$

The term ${}_{S}T_{11}/{}_{E}T_{11}$ is then found to be 44.4.

The above two experiments emphasize the uniform shear effect on ${}_{S}T_{11}/{}_{E}T_{11}$. It seems that ${}_{S}T_{11}/{}_{E}T_{11}$ was significantly reduced when a uniform shear was introduced.

The turbulent shear effect was further investigated by Harris et al. (1977). An experiment was performed in the same wind tunnel facility used by Champagne et al. with stronger strain rate and the same free stream velocity. The turbulence levels were slightly changed to $\sqrt{\overline{u_1^2}}/U = 0.052$, $\sqrt{\overline{u_2^2}}/U = 0.040$, and $\sqrt{\overline{u_3^2}}/U = 0.033$. Both integral and micro length scales were reduced a significant amount, but ${}_{S}T_{11}$ remained about the same, 0.061 sec. Their conditions may be written as

*Results were adopted in conjunction with an errata sheet later issued by Harris et al.

$\Gamma = 48.0\ \text{sec}^{-1}$* ; ${}_{E}T_{11} = 0.00169$ sec

$\alpha_1 = 1.86$; $\alpha_2 = 1.43$; $\alpha_3 = 1.17$

and ${}_{S}T_{11}/{}_{E}T_{11} = 36.1$.

Unfortunately, both turbulence levels and strain rate were different from measurements by Champagne et al.; thus the separate effect on the scale ratio due to turbulent parameters cannot be compared.

Tavoularis and Corrsin (1981) extended the shear flow measurements to a turbulent field with a uniform mean temperature gradient. The velocity measurements were made under a neutral thermal stratification which was identical to the configuration employed by Harris et al. Paradoxically, they reported an integral scale which is about twice the value reported by Harris et al. and assumed ${}_{S}T_{11}$ was the same as in their earlier finding. Consequently ${}_{S}T_{11}/{}_{E}T_{11}$ was found to be 15.1 in their report.

Blackwelder and Kovasznay (1972) conducted measurements of space-time correlation in a turbulent boundary layer. As in their earlier paper, Kovasznay et al. (1970), the turbulence statistics at $x_3/\delta = 0.45$ may be summarized as

$\sqrt{\overline{u_1^2}}/U = 0.57$; ${}_{E}T_{11} = 0.0137$ sec ; $\delta = 10$ cm

$\alpha_1 = 0.87$; ${}_{S}T_{11} = 0.185$ sec ; $\Gamma = 34.5\ \text{sec}^{-1}$

and ${}_{S}T_{11}/{}_{E}T_{11} = 13.2$.

Sabot et al. (1973) performed a space-time correlation measurement in a pipe flow. Measurements were made at $r/R = 0.5$ where R is the radius of the pipe and R = 5 cm. The corresponding mean velocity gradient is 95 sec^{-2} and

$\sqrt{u_1^2}/U = 0.061$; $\alpha = 1.09$

${}_{S}T_{11} = 0.048$; ${}_{E}T_{11} = 0.00268$

and ${}_{S}T_{11}/{}_{E}T_{11} = 17.9$

Turbulent statistics obtained from previous experiments are summarized in Table 6.2. The scale ratios are referred to in Table 6.3, where results from present measurements are tabulated for comparison. Present measurements in a filtered (without large eddies) and in an unfiltered turbulence gives consistent results for α_1 and ${}_{S}T_{11}/{}_{E}T_{11}$. But these two parameters have higher magnitudes than data reported either in a pipe flow or in a thin boundary layer.

6.5.2 The Lagrangian integral scale

In Snyder and Lumley's measurements (see Section 2.3.1), they reported that ${}_{L}T_{22} = 0.1$ at $x_1/M = 73$ sec after a correction for decay adjusted. The corresponding RMS velocity fluctuations were tabulated as

$$\sqrt{\overline{u_1^2}} = \sqrt{\overline{u_2^2}} = 13.1 \text{ cm/sec} .$$

The time scale ${}_{E}T_{11}$ can be approximated as

$${}_{E}T_{11} = \frac{L_{11}}{U} = \frac{3.1 \text{ (cm)}}{655 \text{ (cm/sec)}} = 0.0047 \text{ sec.}$$

They suggested that the Lagrangian integral time scale may be approximated by $L_{22}/\sqrt{\overline{u_2^2}}$.

The quantity $L_{11}/\sqrt{\overline{u_1^2}}$ reflects the persistent time of the turbulent structure during the destruction by self-scrambling and is referred as the "eddy turnover time." This time scale has been found to be roughly the same as ${}_{S}T_{11}$ by Comte-Bellot and Corrsin in grid turbulence and has been confirmed by Sabot et al. in pipe flow and turbulent boundary layer. If one approximates ${}_{S}T_{11}$ by $L_{11}/\sqrt{\overline{u_1^2}}$, then ${}_{S}T_{11} = {}_{S}T_{22} = 0.237$ in Snyder and Lumley's homogeneous isotropic turbulent field. The corresponding α in their measurements is 1.0 which yields ${}_{L}T_{22}/{}_{S}T_{22} = 0.36$ from present analysis. Therefore ${}_{L}T_{22}$ is found to be 0.085 sec which closely agrees with their estimated ${}_{L}T_{22}$ (0.09 sec from Figure 14 in their report). ${}_{L}T_{22}$ was reported to have an asymptotic value of 0.10 sec. Snyder and Lumley mistakenly adopt L_{21} as L_{22} since $L_{21} = 1.2$ cm is implied in their results (Figure 7 in their report). Based on the estiated ${}_{S}T_{11}$, one also obtains

$${}_{L}T_{11}/{}_{S}T_{11} = 0.09/0.237 = 0.38$$

and

$${}_{S}T_{11}/{}_{E}T_{11} = 50.4 .$$

Baldwin and Walsh (1961) performed turbulent diffusion experiments in the core of a fully developed pipe flow. They reported that the pipe core turbulence departed from isotropy by about 30 percent and $\sqrt{u_2^2}/\sqrt{u_1^2} \tilde{\sim} 0.7$ to 0.8. If the eddy turnover time is adopted as an approximation to the integral time scale for Eulerian space-time correlation, one one obtains ${}_{S}T_{22} = \frac{L_{22}}{\sqrt{\overline{u_2^2}}} \tilde{\sim} \frac{L_{11}}{\sqrt{\overline{u_1^2}}}$. ${}_{S}T_{22}$ is calculated from their results and tabulated in Table 6.4 for various velocities. ${}_{S}T_{22}$ ranges from 0.038 to 0.027 sec which agrees with Baldwin and Johnson's (1972)

estimation, by fitting the Eulerian space-time correlaton data to $F_1(t_*)$ (0.045 to 0.019 sec).

A consequence of using the eddy turnover time as an approximation to ${}_S T_{22}$ is that α automatically becomes unity. ${}_L T_{22}$ is estimated from ${}_S T_{22}$ in connection with the present analysis. The estimated ${}_L T_{22}$ is displayed in Table 6.4 for comparison with experimental values. ${}_S T_{22}$ is found to be greater than ${}_L T_{22}$, and ${}_L T_{22}$ qualitatively agrees with the prediction. ${}_S T_{11}/{}_E T_{11}$ is obtained as 28.6 for various mean velocities.

The most recent experiment identified was made by Shlein and Corrsin (1974). They conducted diffusion measurements in a similar turbulent field to that used Comte-Bellot and Corrsin. Shlein and Corrsin reported that ${}_L T_{22}$ is larger than ${}_S T_{22}$ (0.11 sec and 0.084 sec, respectively). The Eulerian parameter may be evaluated as $\alpha = 0.78$. The present analysis cannot be made consistent with their results.

Lagrangian integral time scales calculated from both turbulence and dispersion measurements are included in Table 6.5. Table 6.5a lists the Lagrangian integral time scale as ${}_L T_{11}$ since the Eulerian longitudinal length scale L_{11} is adopted as the turbulence length scale in the analysis. The non-isotropic turbulence proposed in the present approach is considered as a "pseudo" anisotropic turbulence because the isotropic Karman-Howarth relationship is still employed as the general Eulerian space correlation in the non-isotropic analysis. This remains a shortcoming in the present approach until further information is obtained about the general Eulerian space-time correlation in a non-isotropic turbulence field. Similarly, Table 6.5b lists the Lagrangian integral time scale as ${}_L T_{22}$ since L_{22} is used for the prediction. ${}_L T_{22}$ obtained from lateral plume growth is based on the assumption that ${}_L R_{22}(t)$ is either an exponential function or equal to the inverse of $(1 + t/{}_L T_{22})^2$. The predicted ${}_L T_{11}$ agrees with ${}_L T_{22}$ from dispersion measurements and ${}_L T_{11}/{}_E T_{11}$ averages to a value of 4.0. ${}_L T_{22}$ obtained from ${}_S T_{22}$ and L_{22} apparently underestimates the lateral plume growth which implies the longitudinal length scale may be the dominant length scale even in a non-isotropic turbulent field.

${}_L T_{11}$ estimated from the isotropic uniform flow approach is also displayed in Table 6.5. The prediction generally agrees with estimates based on the non-isotropic uniform shear flow approach. It is encouraging to see that an isotropic approach can approximate a more sophisticated approach so well. This implies that an overestimation in the transverse dispersion which resulted from the isotropic assumption compensates the additional dispersion caused by uniform shear in a non-isotropic turbulence.

6.6 Turbulent Dispersion Predicted from the Lagrangian Estimates

The Lagrangian statistics obtained from velocity correlation measurements are utilized to predict the concentration distributions from a continuous point source in the boundary layer. The predicted concentrations are compared to dispersion data for three elevated point-source releases under thermally neutral stratification. The measured dispersion data are listed in Table 6.6 to Table 6.8, Part (A). Predictions resulting from Equation 2.43 with uniform velocity gradients, $\Gamma = U/H$, and constant K_{33} are tabulated in (B). Parts (C), (D), and (E) of Tables 6.6 through 6.8 present predictions based on Equation 2.45: (C) is based on a constant K_{33}; (D) is based on a reflected Gaussian model; (E) is based on a power law K_{33} profile. One notices that neither Equation 2.43 nor 2.45 predicts the ground concentrations downwind from an elevated point source successfully because a Neuman boundary condition was employed in solving the diffusion equation. A Neuman boundary condition specifies that a zero mass flux occurs at the impermeable boundary but leaves the concentration at the boundary as an undetermined constant. Smith (1957) disclosed this deficiency in the analytical solution of turbulent diffusion, and thereafter provided a method to predict the ground concentrations from an elevated point source through the Reciprocal Theorem. The Reciprocal Theorem states that "the concentration at x_i'' due to a source at x_i''' with the flow in the position x_1-direction, is equal to the concentration at x_i''' due to an identical source at x_i'' when the direction of flow is reversed." Smith proved the theorem with Neuman boundary conditions. The methodology is adopted in the present analysis. Hence, the ground concentrations are evaluated from Equation 2.46 with the Reciprocal Theorem for (C), (D), and (E). Such estimation for ground concentration was found identical (error < 0.1%) to prediction from Equation 2.45 with $x_3 = 0.2$ cm. Thus $x_3 = 0.2$ cm was used instead of $x_3 = 0.0$ cm in Equation 2.43 to predict the ground concentration because Lauwerier did not provide a solution for ground source releases.

K_{22} was approximated by its asymptotic value, $[u_2^2]_L T_{11}$, and $[x_2^2(t)]$ was approximated by $2[u_2^2]_L T_{11}\, x_1/U$ for all predictions, where $_L T_{11}$ is the value measured at source height. Similarly, $[u_3^2]_L T_{11}$ was adopted as K_{33} for the constant eddy diffusivity cases. For the varying eddy diffusivity case, K_{33} was assumed to vary in the x_3 direction and fitted to a power law profile. Such approximations inevitably introduced significant errors in predicting turbulent dispersion, especially for short distance observations.

Tables 6.6 through 6.8 show that concentration predictions are roughly fall within a 30 percent error range when compared to the measured values at downwind distances greater than 5 L_{11}. For an elevated point source at $x_3 = 10$ cm, the maximum concentration drops to

the ground much faster in the predicted cases. Farther downwind from the source, the predicted concentrations agree better with measured data. For H = 20 cm, the concentration predictions are made for distances up to 700 cm where the maximum concentration still occurs above the ground but tends to drop to the ground level before the observed data drops. Figures 6.15, 6.16, and 6.17 display concentration contours at x_3 = 700 cm for sources located at x_3 = 2 cm, 10 cm, and 20 cm, respectively. Predicted concentration contours presented in these figures are obtained from Equation 2.45 with a constant K_{33} and a power law velocity profile. Figure 6.15 shows that the predicted concentrations agree with measured dispersion data from a near ground elevated source release. The measured data in Table 6.7j were displaced to the left to compare with predicted data due to lateral plume drift in the wind tunnel. Satisfactory results are still reflected in Figure 6.16, as the source height increases to x_3 = 10 cm. The assumption that the plume spreads at a constant rate with respect to height is appropriate only at distances where the maximum concentration occurred on the ground as shown in Figure 6.17. This is attributed to the simplified assumptions of K_{22} and K_{33} employed in Equation 2.45.

Comparison between the measured and estimated lateral plume spread is displayed in Figure 6.18. Based on an analysis of variance, the lateral plume spread predicted from the Lagrangian estimates agrees with observations from the dispersion measurements to a correlation coefficient of 0.90. This suggested that the statistical model explains 81% of the variance found in the wind tunnel experiments.

The major thrust of this research was to reveal the importance of the Lagrangian velocity statistics in atmospheric dispersion phenomenon and to provide a method to estimate plume dispersion from fixed-point Eulerian turbulence measurements via the Independence Hypothesis. Therefore, this report does not attempt to select the best solution to the diffusion equation. Equations 2.43 and 2.45 were chosen to examine the turbulent dispersion because they cover most of the analytical solutions proposed in the literature. A better prediction might be obtained if more Eulerian measurements were performed to evaluate K_{ij} for the boundary layer and if a more sophisticated numerical approach to solve the diffusion equation were pursued. Nevertheless, the above comparisons indicate that plume dispersion can be correctly predicted with simple dispersion formulae if the Lagrangian integral scale is correctly estimated.

Table 6.1. Summary of predicted Lagrangian-Eulerian time scale from Monte-Carlo particle simulation and Independence Hypothesis

	α	0.1	0.3	0.5	1.0	1.5	2.0	4.0
$\frac{L^T_{11}}{S^T_{11}}$	Eqn. 6.6	0.8624	0.6764	0.5564	0.3856	0.2977	0.2391	0.1378
	Eqn. 6.7	0.8624	0.6763	0.5562	0.3852	0.2947	0.2386	0.1354
	Eqn. 3.12	0.8635	0.6837	0.5702	0.4087	0.3216	0.2664	0.1612
	Eqn. 6.8	0.8946	0.7439	0.6417	0.4853	0.3949	0.3350	0.2140

Table 6.2. Turbulent statistics of previous measurements.

Property	Experiment CHC	CBC	HGC	SRC	BK
FLOW	low shear	grid turbulence	high shear	boundary layer	pipe flow
U (cm/sec)	1240	1270	1240	1850	374
$\frac{\sqrt{\overline{u_1^2}}}{U}$	.018	.022	.050	.061	.057
L	4.2	2.4	2.1	.50	5.1
Γ (1/sec)	12.9	0	48	95	34.4
S^T_{11} (sec)	.056	.084	.061	.048	.182
E^T_{11} (sec)	.00348	.00189	.00169	.00268	.0137
$\frac{S^T_{11}}{E^T_{11}}$	16.7	44.4	36.1	17.9	13.2
α_1	0.3	0.78	1.86	1.09	0.87
α_2	0.23	0.78	1.43	-	-
α_3	0.22	0.78	1.17	-	-

CHC = Champagne et al. (1970)
CBC = Comte-Bellot and Corrsin (1971)
HGC = Harris et al. (1977)
SRC = Sabot et al. (1973), r/R = 0.5
BK = Blackwelder and Kovasznay (1973), $x_3/\delta = 0.45$

Table 6.3. Turbulent statistics from neutral stratified boundary layer.

$\frac{x_3}{\delta}$	$\frac{\sqrt{\overline{u_1^2}}}{U}$	Γ (sec^{-1})	Filtered Turbulence		Unfiltered Turbulence			
			α_1	$\frac{S^T_{11}}{E^T_{11}}$	$\alpha 1$	$\frac{S^T_{11}}{E^T_{11}}$	$\frac{S^T_{21}}{E^T_{22}}$	$\frac{S^T_{31}}{E^T_{33}}$
.044	.15	9.7	1.37	9.2	1.09	9.5	-	13.7
.222	.096	2.5	1.96	20.5	2.25	25.5	52.8	41.6
.444	.066	1.4	1.85	27.6	2.27	36.5	61.1	59.8

Table 6.4. Re-examination of Baldwin and Walsh's turbulent statistics

Baldwin and Walsh's result				Estimation based on eddy turnover time			
U (ft)	$\frac{\sqrt{\overline{u_1^2}}}{U}$	L_{11} (ft)	L^T_{22} (sec)	$S^T_{22} \simeq \frac{L_{11}}{\sqrt{\overline{u_1^2}}}$ (sec)	α	$\frac{L^T_{22}}{S^T_{22}}$	$\frac{L^T_{22}}{L^T_{22}}$ (sec)
72.6	.035	.0978	.014	.038	1	.36	.014
106	.035	.116	.0075	.031	1	.36	.011
135	.035	.142	.0062	.030	1	.36	.011
160	.035	.154	.0046	.027	1	.36	.0097

Table 6.5. Comparison of Lagrangian integral time scale from predictions and dispersion measurements.

(a)

	Turbulence Measurement					Non-isotropic shear flow (prediction)			Isotropic uniform flow (prediction)		Dispersion Measurement	
$\frac{x_3}{\delta}$	S^T_{11} (sec)	α_1	α_2	α_3	$\Gamma_{S^T_{11}}$	$\frac{L^T_{11}}{S^T_{11}}$	L^T_{11} (sec)	$\frac{L^T_{11}}{E^T_{11}}$	$\frac{L^T_{11}}{S^T_{11}}$	L^T_{11} (sec)	$L^T_{22} = \frac{Ti}{5.25}$ (sec)	$L^T_{22} = \frac{Ti}{6.83}$ (sec)
.044	1.33	1.09	0.54	0.54	12.9	0.28	0.37	2.7	0.35	0.46	0.34	0.26
.222	4.03	2.25	1.20	1.20	10.1	0.21	0.84	5.2	0.22	0.89	0.80	0.62
.444	5.13	2.27	1.58	1.58	7.2	0.20	1.03	7.3	0.22	1.13	0.85	0.65

(b)

	Turbulence Measurement					Non-isotropic shear flow (prediction)			Isotropic uniform flow (prediction)		Dispersion Measurement	
$\frac{x_3}{\delta}$	S^T_{22} (sec)	α_1	α_2	α_3	$\Gamma_{S^T_{22}}$	$\frac{L^T_{22}}{S^T_{22}}$	L^T_{22} (sec)	$\frac{L^T_{22}}{E^T_{22}}$	$\frac{L^T_{22}}{S^T_{22}}$	L^T_{22} (sec)	$L^T_{22} = \frac{Ti}{5.25}$ (sec)	$L^T_{22} = \frac{Ti}{6.83}$ (sec)
.222	1.48	4.32	2.30	2.30	3.7	0.17	0.25	8.8	0.14	0.21	0.80	0.62
.444	2.05	3.93	2.73	2.73	2.9	0.16	0.33	9.7	0.15	0.31	0.85	0.65

Table 6.6. Comparison of turbulent dispersion between measured and predicted concentration distribution, H = 2 cm.

(a)

U(FREE STREAM) = 200.0 CM/SEC	U1RMS= 18.3 CM/SEC	U(LOCAL VEL.) = 125.4 CM/SEC	
RELEASE HEIGHT = 2.0 CM	U2RMS= 9.0 CM/SEC	VEL. GRADIENT = 9.400 1/SEC	
DOWNWIND DIST. = 25.0 CM	U3RMS= 6.0 CM/SEC	SOURCE STRENGTH = 10 % METHANE	

(A) DIFFUSION MEASUREMENTS IN THE WIND TUNNEL (PPM/C.C.)

8.0	.1040E+03	.8245E+02	.6243E+02	.2719E+02	.1047E+02	.3652E+01	.1950E+01	.1974E+01
6.0	.6599E+03	.4716E+03	.3101E+03	.1435E+03	.6436E+02	.2214E+02	.8014E+01	.1813E+01
4.0	.1692E+04	.1209E+04	.7466E+03	.3392E+03	.1363E+03	.4652E+02	.1771E+02	.7523E+01
2.0	.2173E+04	.1669E+04	.9352E+03	.4092E+03	.1708E+03	.5892E+02	.3365E+02	.7326E+01
0.0	.2140E+04	.1483E+04	.8343E+03	.4614E+03	.2714E+03	.1141E+03	.6151E+02	.2165E+02
X3/X2(CM)	0.0	1.0	2.0	3.0	4.0	5.0	6.0	7.0

(B) EQUATION 2-44 WITH CONSTANT DIFFUSIVITIES IN X3-DIRECTION (PPM/C.C.)

8.0	.4790E+01	.4586E+01	.4046E+01	.3258E+01	.2456E+01	.1691E+01	.1070E+01	.6234E+00
6.0	.1055E+03	.1012E+03	.8935E+02	.7258E+02	.5425E+02	.3732E+02	.2302E+02	.1376E+02
4.0	.5005E+03	.4801E+03	.4238E+03	.3443E+03	.2574E+03	.1770E+03	.1121E+03	.6527E+02
2.0	.8815E+03	.8456E+03	.7465E+03	.6064E+03	.4533E+03	.3118E+03	.1974E+03	.1150E+03
0.0	.9553E+03	.9164E+03	.8089E+03	.6571E+03	.4912E+03	.3379E+03	.2139E+03	.1246E+03
X3/X2(CM)	0.0	1.0	2.0	3.0	4.0	5.0	6.0	7.0

(C) EQUATION 2-45 WITH CONSTANT DIFFUSIVITIES IN X3-DIRECTION (PPM/C.C.)

8.0	.6917E+02	.6638E+02	.5859E+02	.4759E+02	.3557E+02	.2447E+02	.1549E+02	.9021E+01
6.0	.2909E+03	.2407E+03	.2125E+03	.1726E+03	.1290E+03	.8875E+02	.5615E+02	.3272E+02
4.0	.5730E+03	.5497E+03	.4852E+03	.3941E+03	.2946E+03	.2027E+03	.1283E+03	.7473E+02
2.0	.8838E+03	.8478E+03	.7484E+03	.6079E+03	.4544E+03	.3126E+03	.1979E+03	.1153E+03
0.0	.9977E+03	.9571E+03	.8449E+03	.6863E+03	.5130E+03	.3529E+03	.2234E+03	.1301E+03
X3/X2(CM)	0.0	1.0	2.0	3.0	4.0	5.0	6.0	7.0

(D) GAUSSIAN DIFFUSION EQUATION (PPM/C.C.)

8.0	.9257E+02	.8880E+02	.7839E+02	.6367E+02	.4760E+02	.3274E+02	.2072E+02	.1207E+02
6.0	.2768E+03	.2655E+03	.2344E+03	.1904E+03	.1423E+03	.9791E+02	.6197E+02	.3610E+02
4.0	.5714E+03	.5481E+03	.4838E+03	.3930E+03	.2938E+03	.2021E+03	.1279E+03	.7451E+02
2.0	.8511E+03	.8164E+03	.7207E+03	.5854E+03	.4376E+03	.3010E+03	.1905E+03	.1110E+03
0.0	.9638E+03	.9245E+03	.8161E+03	.6630E+03	.4956E+03	.3409E+03	.2156E+03	.1257E+03
X3/X2(CM)	0.0	1.0	2.0	3.0	4.0	5.0	6.0	7.0

(E) EQUATION 2-45 WITH VARYING DIFFUSIVITIES IN X3-DIRECTION (PPM/C.C.)

8.0	.1213E+03	.1164E+03	.1027E+03	.8343E+02	.6237E+02	.4290E+02	.2716E+02	.1582E+02
6.0	.2825E+03	.2710E+03	.2392E+03	.1943E+03	.1452E+03	.9990E+02	.6324E+02	.3684E+02
4.0	.5232E+03	.5076E+03	.4481E+03	.3640E+03	.2721E+03	.1872E+03	.1185E+03	.6901E+02
2.0	.7955E+03	.7631E+03	.6736E+03	.5472E+03	.4090E+03	.2814E+03	.1781E+03	.1037E+03
0.0	.9440E+03	.9055E+03	.7993E+03	.6493E+03	.4854E+03	.3339E+03	.2113E+03	.1231E+03
X3/X2(CM)	0.0	1.0	2.0	3.0	4.0	5.0	6.0	7.0

Table 6.6. Comparison of turbulent dispersion between measured and predicted concentration distribution, H = 2 cm.

(b)

U(FREE STREAM) = 200.0 CM/SEC U1RMS= 19.3 CM/SEC U(LOCAL VEL.) = 125.4 CM/SEC
RELEASE HEIGHT = 2.0 CM U2RMS= 9.0 CM/SEC VEL. GRADIENT = 9.400 1/SEC
DOWNWIND DIST. = 50.0 CM U3RMS= 8.0 CM/SEC SOURCE STRENGTH = 10 % METHANE

(A) DIFFUSION MEASUREMENTS IN THE WIND TUNNEL (PPM/C.C.)

8.0	.2055E+03	.1300E+03	.4369E+02	.2273E+02	.7268E+01	.2237E+01	.1211E+01	.1037E+01
6.0	.4575E+03	.2900E+03	.1409E+03	.4685E+02	.1039E+02	.3329E+01	.1371E+01	.1206E+01
4.0	.7143E+03	.4313E+03	.1920E+03	.5596E+02	.1606E+02	.4043E+01	.1333E+01	.1031E+01
2.0	.8199E+03	.4586E+03	.1839E+03	.5200E+02	.1483E+02	.4554E+01	.1631E+01	.1002E+01
0.0	.8999E+03	.3629E+03	.1249E+03	.3900E+02	.1295E+02	.3575E+01	.1693E+01	.9741E+00
X3/X2(CM)	0.0	2.0	4.0	6.0	8.0	10.0	12.0	14.0

(B) EQUATION 2-44 WITH CONSTANT DIFFUSIVITIES IN X3-DIRECTION (PPM/C.C.)

8.0	.2725E+02	.2507E+02	.1754E+02	.1299E+02	.7204E+01	.3409E+01	.1366E+01	.4634E+00
6.0	.1375E+03	.1265E+03	.9861E+02	.6507E+02	.3636E+02	.1720E+02	.6693E+01	.2339E+01
4.0	.3149E+03	.2897E+03	.2258E+03	.1490E+03	.8324E+02	.3939E+02	.1578E+02	.5355E+01
2.0	.4270E+03	.3929E+03	.3062E+03	.2020E+03	.1129E+03	.5341E+02	.2140E+02	.7262E+01
0.0	.4459E+03	.4103E+03	.3198E+03	.2110E+03	.1179E+03	.5573E+02	.2235E+02	.7584E+01
X3/X2(CM)	0.0	2.0	4.0	6.0	8.0	10.0	12.0	14.0

(C) EQUATION 2-45 WITH CONSTANT DIFFUSIVITIES IN X3-DIRECTION (PPM/C.C.)

8.0	.1173E+03	.1079E+03	.8412E+02	.5551E+02	.3102E+02	.1466E+02	.5880E+01	.1995E+01
6.0	.2373E+03	.2184E+03	.1702E+03	.1123E+03	.6274E+02	.2969E+02	.1190E+02	.4036E+01
4.0	.3903E+03	.3505E+03	.2731E+03	.1802E+03	.1007E+03	.4765E+02	.1909E+02	.6473E+01
2.0	.4945E+03	.4551E+03	.3546E+03	.2340E+03	.1307E+03	.6187E+02	.2479E+02	.8411E+01
0.0	.5334E+03	.4908E+03	.3825E+03	.2524E+03	.1410E+03	.6673E+02	.2674E+02	.9071E+01
X3/X2(CM)	0.0	2.0	4.0	6.0	8.0	10.0	12.0	14.0

(D) GAUSSIAN DIFFUSION EQUATION (PPM/C.C.)

8.0	.1353E+03	.1259E+03	.9807E+02	.6471E+02	.3616E+02	.1711E+02	.6856E+01	.2326E+01
6.0	.2504E+03	.2305E+03	.1796E+03	.1185E+03	.6621E+02	.3133E+02	.1255E+02	.4259E+01
4.0	.3930E+03	.3525E+03	.2747E+03	.1812E+03	.1013E+03	.4792E+02	.1920E+02	.6515E+01
2.0	.4926E+03	.4533E+03	.3532E+03	.2331E+03	.1302E+03	.6163E+02	.2469E+02	.8378E+01
0.0	.5354E+03	.4926E+03	.3839E+03	.2533E+03	.1415E+03	.6696E+02	.2684E+02	.9105E+01
X3/X2(CM)	0.0	2.0	4.0	6.0	8.0	10.0	12.0	14.0

(E) EQUATION 2-45 WITH VARYING DIFFUSIVITIES IN X3-DIRECTION (PPM/C.C.)

8.0	.1420E+03	.1307E+03	.1013E+03	.6720E+02	.3755E+02	.1777E+02	.7119E+01	.2415E+01
6.0	.2787E+03	.2104E+03	.1643E+03	.1082E+03	.6047E+02	.2861E+02	.1146E+02	.3893E+01
4.0	.3319E+03	.3054E+03	.2380E+03	.1570E+03	.8775E+02	.4152E+02	.1664E+02	.5645E+01
2.0	.4296E+03	.3954E+03	.3081E+03	.2033E+03	.1136E+03	.5375E+02	.2154E+02	.7307E+01
0.0	.4820E+03	.4436E+03	.3456E+03	.2281E+03	.1274E+03	.6030E+02	.2416E+02	.8198E+01
X3/X2(CM)	0.0	2.0	4.0	6.0	8.0	10.0	12.0	14.0

Table 6.6. Comparison of turbulent dispersion between measured and predicted concentration distribution, H = 2 cm.

(c)

U(FREE STREAM) = 200.0 CM/SEC U1RMS= 19.3 CM/SEC U(LOCAL VEL.) = 125.4 CM/SEC
RELEASE HEIGHT = 2.0 CM U2RMS= 9.0 CM/SEC VEL. GRADIENT = 5.400 1/SEC
DOWNWIND DIST. = 100.0 CM U3RMS= 8.0 CM/SEC SOURCE STRENGTH = 10 X MILLIMAN

(A) DIFFUSION MEASUREMENTS IN THE WIND TUNNEL (PPM/C.C.)

8.0	.1982E+03	.1611E+03	.9415E+02	.7814E+02	.4706E+02	.2414E+02	.1214E+02	.6305E+01
6.0	.2773E+03	.2225E+03	.1617E+03	.9854E+02	.5262E+02	.2971E+02	.1466E+02	.6133E+01
4.0	.3319E+03	.2612E+03	.1783E+03	.1035E+03	.6379E+02	.3213E+02	.1563E+02	.8512E+01
2.0	.3567E+03	.2701E+03	.1815E+03	.1026E+03	.5999E+02	.3196E+02	.1632E+02	.6653E+01
0.0	.3767E+03	.2562E+03	.1603E+03	.9448E+02	.5622E+02	.2909E+02	.1670E+02	.7112E+01
X3/X2(CM)	0.0	2.0	4.0	6.0	8.0	10.0	12.0	14.0

(B) EQUATION 2-44 WITH CONSTANT DIFFUSIVITIES IN X3-DIRECTION (PPM/C.C.)

8.0	.4794E+02	.4599E+02	.4060E+02	.3298E+02	.2465E+02	.1696E+02	.1073E+02	.6252E+01
6.0	.1136E+03	.1061E+03	.9362E+02	.7605E+02	.5685E+02	.3910E+02	.2475E+02	.1442E+02
4.0	.1699E+03	.1628E+03	.1438E+03	.1169E+03	.8729E+02	.6004E+02	.3801E+02	.2214E+02
2.0	.1983E+03	.1907E+03	.1684E+03	.1369E+03	.1022E+03	.7032E+02	.4451E+02	.2593E+02
0.0	.2033E+03	.1951E+03	.1722E+03	.1399E+03	.1046E+03	.7192E+02	.4553E+02	.2652E+02
X3/X2(CM)	0.0	2.0	4.0	6.0	8.0	10.0	12.0	14.0

(C) EQUATION 2-45 WITH CONSTANT DIFFUSIVITIES IN X3-DIRECTION (PPM/C.C.)

8.0	.1197E+03	.1148E+03	.1014E+03	.8235E+02	.6156E+02	.4235E+02	.2680E+02	.1561E+02
6.0	.1750E+03	.1679E+03	.1482E+03	.1204E+03	.8995E+02	.6190E+02	.3918E+02	.2282E+02
4.0	.2264E+03	.2172E+03	.1917E+03	.1558E+03	.1164E+03	.8009E+02	.5070E+02	.2953E+02
2.0	.2613E+03	.2507E+03	.2213E+03	.1799E+03	.1344E+03	.9243E+02	.5851E+02	.3408E+02
0.0	.2724E+03	.2613E+03	.2307E+03	.1874E+03	.1401E+03	.9636E+02	.6100E+02	.3553E+02
X3/X2(CM)	0.0	2.0	4.0	6.0	8.0	10.0	12.0	14.0

(D) GAUSSIAN DIFFUSION EQUATION (PPM/C.C.)

8.0	.1325E+03	.1271E+03	.1122E+03	.9115E+02	.6814E+02	.4687E+02	.2967E+02	.1728E+02
6.0	.1945E+03	.1770E+03	.1563E+03	.1269E+03	.9489E+02	.6527E+02	.4132E+02	.2407E+02
4.0	.2337E+03	.2242E+03	.1979E+03	.1607E+03	.1202E+03	.8265E+02	.5232E+02	.3047E+02
2.0	.2593E+03	.2502E+03	.2279E+03	.1852E+03	.1384E+03	.9520E+02	.6026E+02	.3510E+02
0.0	.2691E+03	.2707E+03	.2349E+03	.1941E+03	.1451E+03	.9979E+02	.6317E+02	.3680E+02
X3/X2(CM)	0.0	2.0	4.0	6.0	8.0	10.0	12.0	14.0

(E) EQUATION 2-45 WITH VARYING DIFFUSIVITIES IN X3-DIRECTION (PPM/C.C.)

8.0	.1158E+03	.1111E+03	.9808E+02	.7966E+02	.5955E+02	.4096E+02	.2573E+02	.1510E+02
6.0	.1504E+03	.1446E+03	.1275E+03	.1036E+03	.7743E+02	.5326E+02	.3371E+02	.1964E+02
4.0	.1853E+03	.1778E+03	.1569E+03	.1275E+03	.9530E+02	.6555E+02	.4149E+02	.2417E+02
2.0	.2143E+03	.2056E+03	.1815E+03	.1474E+03	.1102E+03	.7581E+02	.4799E+02	.2795E+02
0.0	.2288E+03	.2195E+03	.1937E+03	.1574E+03	.1176E+03	.8092E+02	.5122E+02	.2984E+02
X3/X2(CM)	0.0	2.0	4.0	6.0	8.0	10.0	12.0	14.0

Table 6.6. Comparison of turbulent dispersion between measured and predicted concentration distribution, H = 2 cm.

(d)

U(FREE STREAM) = 200.0 CM/SEC U1RMS= 18.3 CM/SEC U(LOCAL VEL.) = 125.4 CM/SEC
RELEASE HEIGHT = 2.0 CM U2RMS= 9.0 CM/SEC VEL. GRADIENT = 9.400 1/SEC
DOWNWIND DIST. = 150.0 CM U3RMS= 9.0 CM/SEC SOURCE STRENGTH = 10 % METHANE

(A) DIFFUSION MEASUREMENTS IN THE WIND TUNNEL (PPM/C.C.)

8.0	.1640E+03	.1166E+03	.5316E+02	.3562E+02	.1603E+02	.6133E+01	.2852E+01	.1351E+01
6.0	.1990E+03	.1547E+03	.6444E+02	.4907E+02	.2201E+02	.9559E+01	.3849E+01	.1554E+01
4.0	.2497E+03	.1c59E+03	.1095E+03	.5559E+02	.2588E+02	.1149E+02	.4782E+01	.1c14E+01
2.0	.2708E+03	.2011E+03	.1227E+03	.6462E+02	.2968E+02	.1311E+02	.5409E+01	.1867E+01
0.0	.2957E+03	.2108E+03	.1266E+03	.6795E+02	.3277E+02	.1340E+02	.5429E+01	.1887E+01
X3/X2(CM)	0.0	3.0	6.0	9.0	12.0	15.0	18.0	21.0

(B) EQUATION 2-44 WITH CONSTANT DIFFUSIVITIES IN X3-DIRECTION (PPM/C.C.)

8.0	.6819E+02	.4527E+02	.3755E+02	.2749E+02	.1777E+02	.1014E+02	.5105E+01	.2269E+01
6.0	.8455E+02	.7453E+02	.6596E+02	.4729E+02	.3121E+02	.1701E+02	.8988E+01	.3987E+01
4.0	.1191E+03	.1062E+03	.8810E+02	.6450E+02	.4168E+02	.2378E+02	.1196E+02	.5324E+01
2.0	.1358E+03	.1182E+03	.9800E+02	.7175E+02	.4637E+02	.2646E+02	.1332E+02	.5923E+01
0.0	.1377E+03	.1200E+03	.9950E+02	.7285E+02	.4708E+02	.2686E+02	.1353E+02	.6014E+01
X3/X2(CM)	0.0	3.0	6.0	9.0	12.0	15.0	18.0	21.0

(C) EQUATION 2-45 WITH CONSTANT DIFFUSIVITIES IN X3-DIRECTION (PPM/C.C.)

8.0	.1034E+03	.9716E+02	.8058E+02	.5900E+02	.3813E+02	.2175E+02	.1096E+02	.4870E+01
6.0	.1342E+03	.1261E+03	.1045E+03	.7654E+02	.4947E+02	.2822E+02	.1422E+02	.6319E+01
4.0	.1401E+03	.1504E+03	.1248E+03	.9135E+02	.5904E+02	.3366E+02	.1696E+02	.7541E+01
2.0	.1767E+03	.1660E+03	.1377E+03	.1008E+03	.6514E+02	.3717E+02	.1872E+02	.8321E+01
0.0	.1918E+03	.1706E+03	.1417E+03	.1037E+03	.6704E+02	.3824E+02	.1926E+02	.8563E+01
X3/X2(CM)	0.0	3.0	6.0	9.0	12.0	15.0	18.0	21.0

(D) GAUSSIAN DIFFUSION EQUATION (PPM/C.C.)

8.0	.1135E+03	.1067E+03	.8847E+02	.6477E+02	.4188E+02	.2388E+02	.1203E+02	.5347E+01
6.0	.1427E+03	.1341E+03	.1112E+03	.8141E+02	.5262E+02	.3002E+02	.1512E+02	.6721E+01
4.0	.1693E+03	.1592E+03	.1309E+03	.9585E+02	.6197E+02	.3534E+02	.1780E+02	.7912E+01
2.0	.1793E+03	.1741E+03	.1444E+03	.1057E+03	.6831E+02	.3897E+02	.1963E+02	.8726E+01
0.0	.1814E+03	.1798E+03	.1492E+03	.1092E+03	.7058E+02	.4027E+02	.2028E+02	.9015E+01
X3/X2(CM)	0.0	3.0	6.0	9.0	12.0	15.0	18.0	21.0

(E) EQUATION 2-45 WITH VARYING DIFFUSIVITIES IN X3-DIRECTION (PPM/C.C.)

8.0	.9048E+02	.8520E+02	.7066E+02	.5173E+02	.3343E+02	.1907E+02	.9606E+01	.4271E+01
6.0	.1087E+03	.1022E+03	.8472E+02	.6203E+02	.4004E+02	.2287E+02	.1152E+02	.5121E+01
4.0	.1255E+03	.1179E+03	.9782E+02	.7162E+02	.4626E+02	.2641E+02	.1330E+02	.5917E+01
2.0	.1339E+03	.1304E+03	.1082E+03	.7921E+02	.5115E+02	.2920E+02	.1471E+02	.6539E+01
0.0	.1453E+03	.1365E+03	.1132E+03	.8287E+02	.5356E+02	.3056E+02	.1539E+02	.6841E+01
X3/X2(CM)	0.0	3.0	6.0	9.0	12.0	15.0	18.0	21.0

Table 6.6. Comparison of turbulent dispersion between measured and predicted concentration distribution, H = 2 cm.

(e)

U(FREE STREAM) = 200.0 CM/SEC U1RMS= 18.3 CM/SEC U(LOCAL VEL.) = 125.4 CM/SEC
RELEASE HEIGHT = 2.0 CM U2RMS= 0.0 CM/SEC VEL. GRADIENT = 0.400 1/SEC
DOWNWIND DIST. = 200.0 CM U3RMS= 0.0 CM/SEC SOURCE STRENGTH = 10 % METHANE

(A) DIFFUSION MEASUREMENTS IN THE WIND TUNNEL (PPM/C.C.)

12.0	.7723E+02	.5851E+02	.3211E+02	.2410E+02	.1204E+02	.6490E+01	.3625E+01	.2056E+01
9.0	.1035E+03	.8278E+02	.5624E+02	.3149E+02	.1696E+02	.8739E+01	.4714E+01	.2765E+01
6.0	.1444E+03	.1089E+03	.7467E+02	.4498E+02	.2565E+02	.1259E+02	.6712E+01	.3469E+01
3.0	.1566E+03	.1292E+03	.8876E+02	.5983E+02	.3013E+02	.1616E+02	.8116E+01	.4150E+01
0.0	.1930E+03	.1443E+03	.9769E+02	.6991E+02	.3433E+02	.1809E+02	.9311E+01	.4314E+01
X3/X2(CM)	0.0	3.0	6.0	9.0	12.0	15.0	18.0	21.0

(B) EQUATION 2-44 WITH CONSTANT DIFFUSIVITIES IN X3-DIRECTION (PPM/C.C.)

12.0	.7661E+01	.7311E+01	.6354E+01	.5029E+01	.3625E+01	.2360E+01	.1423E+01	.7745E+00
9.0	.3217E+02	.3070E+02	.2668E+02	.2112E+02	.1522E+02	.9993E+01	.5774E+01	.3252E+01
6.0	.6721E+02	.6414E+02	.5574E+02	.4412E+02	.3180E+02	.2087E+02	.1248E+02	.6774E+01
3.0	.8918E+02	.8513E+02	.7312E+02	.5787E+02	.4171E+02	.2736E+02	.1637E+02	.8913E+01
0.0	.9164E+02	.8746E+02	.7601E+02	.6016E+02	.4336E+02	.2847E+02	.1702E+02	.9265E+01
X3/X2(CM)	0.0	3.0	6.0	9.0	12.0	15.0	18.0	21.0

(C) EQUATION 2-45 WITH CONSTANT DIFFUSIVITIES IN X3-DIRECTION (PPM/C.C.)

12.0	.4870E+02	.4643E+02	.4039E+02	.3197E+02	.2304E+02	.1513E+02	.9044E+01	.4924E+01
9.0	.7223E+02	.7466E+02	.6486E+02	.5135E+02	.3702E+02	.2430E+02	.1453E+02	.7909E+01
6.0	.1073E+03	.1030E+03	.8952E+02	.7085E+02	.5107E+02	.3353E+02	.2004E+02	.1091E+02
3.0	.1291E+03	.1232E+03	.1071E+03	.8478E+02	.6109E+02	.4011E+02	.2398E+02	.1305E+02
0.0	.1360E+03	.1298E+03	.1128E+03	.8929E+02	.6436E+02	.4225E+02	.2526E+02	.1375E+02
X3/X2(CM)	0.0	3.0	6.0	9.0	12.0	15.0	18.0	21.0

(D) GAUSSIAN DIFFUSION EQUATION (PPM/C.C.)

12.0	.5900E+02	.5630E+02	.4893E+02	.3873E+02	.2792E+02	.1833E+02	.1096E+02	.5965E+01
9.0	.8741E+02	.8342E+02	.7250E+02	.5738E+02	.4136E+02	.2715E+02	.1623E+02	.8837E+01
6.0	.1157E+03	.1104E+03	.9596E+02	.7597E+02	.5476E+02	.3594E+02	.2149E+02	.1170E+02
3.0	.1369E+03	.1307E+03	.1136E+03	.8989E+02	.6479E+02	.4253E+02	.2543E+02	.1384E+02
0.0	.1448E+03	.1382E+03	.1201E+03	.9507E+02	.6853E+02	.4499E+02	.2689E+02	.1464E+02
X3/X2(CM)	0.0	3.0	6.0	9.0	12.0	15.0	18.0	21.0

(E) EQUATION 2-45 WITH VARYING DIFFUSIVITIES IN X3-DIRECTION (PPM/C.C.)

12.0	.5124E+02	.4890E+02	.4249E+02	.3363E+02	.2424E+02	.1591E+02	.9514E+01	.5180E+01
9.0	.6747E+02	.6439E+02	.5598E+02	.4429E+02	.3193E+02	.2096E+02	.1253E+02	.6821E+01
6.0	.8391E+02	.8007E+02	.6959E+02	.5508E+02	.3970E+02	.2606E+02	.1559E+02	.8493E+01
3.0	.9776E+02	.9329E+02	.8108E+02	.6417E+02	.4626E+02	.3036E+02	.1815E+02	.9883E+01
0.0	.1067E+03	.9991E+02	.8683E+02	.6873E+02	.4954E+02	.3252E+02	.1944E+02	.1059E+02
X3/X2(CM)	0.0	3.0	6.0	9.0	12.0	15.0	18.0	21.0

Table 6.6. Comparison of turbulent dispersion between measured and predicted concentration distribution, H = 2 cm.

(f)

U(FREE STREAM) : 200.0 CM/SEC U1RMS: 18.3 CM/SEC U(LOCAL VEL.) : 125.4 CM/SEC
RELEASE HEIGHT : 2.0 CM U2RMS: 9.0 CM/SEC VEL. GRADIENT : 9.400 1/SEC
DOWNWIND DIST. : 250.0 CM U3RMS: 8.0 CM/SEC SOURCE STRENGTH : 10 % METHANE

(A) DIFFUSION MEASUREMENTS IN THE WIND TUNNEL (PPM/C.C.)

12.0	.6123E+02	.5008E+02	.3569E+02	.2494E+02	.1577E+02	.7935E+01	.4017E+01	.2001E+01
9.0	.8799E+02	.8256E+02	.6222E+02	.3978E+02	.2296E+02	.1146E+02	.5095E+01	.2743E+01
6.0	.1097E+03	.1031E+03	.7686E+02	.5181E+02	.2939E+02	.1476E+02	.7236E+01	.3276E+01
3.0	.1294E+03	.1216E+03	.9245E+02	.6236E+02	.3470E+02	.1774E+02	.8534E+01	.3759E+01
0.0	.1492E+03	.1356E+03	.1009E+03	.6779E+02	.3878E+02	.2007E+02	.9537E+01	.4060E+01
X3/X2(CM)	0.0	4.0	8.0	12.0	16.0	20.0	24.0	28.0

(B) EQUATION 2-44 WITH CONSTANT DIFFUSIVITIES IN X3-DIRECTION (PPM/C.C.)

12.0	.9456E+01	.9035E+01	.7401E+01	.5307E+01	.3331E+01	.1631E+01	.6506E+00	.3710E+00
9.0	.3055E+02	.2859E+02	.2342E+02	.1679E+02	.1054E+02	.5793E+01	.2787E+01	.1174E+01
6.0	.5520E+02	.5165E+02	.4230E+02	.3033E+02	.1904E+02	.1046E+02	.5035E+01	.2121E+01
3.0	.6963E+02	.6422E+02	.5260E+02	.3772E+02	.2366E+02	.1301E+02	.6260E+01	.2637E+01
0.0	.7080E+02	.6625E+02	.5426E+02	.3891E+02	.2443E+02	.1342E+02	.6458E+01	.2720E+01
X3/X2(CM)	0.0	4.0	8.0	12.0	16.0	20.0	24.0	28.0

(C) EQUATION 2-45 WITH CONSTANT DIFFUSIVITIES IN X3-DIRECTION (PPM/C.C.)

12.0	.4736E+02	.4431E+02	.3629E+02	.2603E+02	.1634E+02	.8479E+01	.4320E+01	.1819E+01
9.0	.6741E+02	.6495E+02	.5320E+02	.3815E+02	.2395E+02	.1316E+02	.6331E+01	.2667E+01
6.0	.9009E+02	.8421E+02	.6897E+02	.4946E+02	.3105E+02	.1706E+02	.8209E+01	.3457E+01
3.0	.1040E+03	.9731E+02	.7971E+02	.5715E+02	.3586E+02	.1972E+02	.9486E+01	.3995E+01
0.0	.1085E+03	.1015E+03	.8313E+02	.5961E+02	.3742E+02	.2056E+02	.9894E+01	.4167E+01
X3/X2(CM)	0.0	4.0	8.0	12.0	16.0	20.0	24.0	28.0

(D) GAUSSIAN DIFFUSION EQUATION (PPM/C.C.)

12.0	.5435E+02	.5272E+02	.4319E+02	.3097E+02	.1944E+02	.1068E+02	.5140E+01	.2165E+01
9.0	.7743E+02	.7244E+02	.5934E+02	.4255E+02	.2671E+02	.1468E+02	.7062E+01	.2975E+01
6.0	.9715E+02	.9090E+02	.7445E+02	.5339E+02	.3351E+02	.1842E+02	.8861E+01	.3732E+01
3.0	.1113E+03	.1041E+03	.8531E+02	.6117E+02	.3840E+02	.2110E+02	.1015E+02	.4276E+01
0.0	.1165E+03	.1090E+03	.8927E+02	.6401E+02	.4018E+02	.2206E+02	.1062E+02	.4475E+01
X3/X2(CM)	0.0	4.0	8.0	12.0	16.0	20.0	24.0	28.0

(E) EQUATION 2-45 WITH VARYING DIFFUSIVITIES IN X3-DIRECTION (PPM/C.C.)

12.0	.4547E+02	.4254E+02	.3485E+02	.2499E+02	.1569E+02	.8620E+01	.4147E+01	.1747E+01
9.0	.5490E+02	.5315E+02	.4353E+02	.3122E+02	.1960E+02	.1077E+02	.5181E+01	.2182E+01
6.0	.6775E+02	.6339E+02	.5193E+02	.3723E+02	.2337E+02	.1285E+02	.6180E+01	.2603E+01
3.0	.7667E+02	.7173E+02	.5876E+02	.4213E+02	.2645E+02	.1454E+02	.6993E+01	.2945E+01
0.0	.8194E+02	.7583E+02	.6211E+02	.4454E+02	.2796E+02	.1536E+02	.7392E+01	.3113E+01
X3/X2(CM)	0.0	4.0	8.0	12.0	16.0	20.0	24.0	28.0

Table 6.6. Comparison of turbulent dispersion between measured and predicted concentration distribution, H = 2 cm.

(g)

U(FREE STREAM) = 300.0 CM/SEC U1RMS= 18.3 CM/SEC U(LOCAL VEL.) = 125.4 CM/SEC
RELEASE HEIGHT = 2.0 CM U2RMS= 9.0 CM/SEC VEL. GRADIENT = 9.400 1/SEC
DOWNWIND DIST. = 300.0 CM U3RMS= 9.0 CM/SEC SOURCE STRENGTH = 10 % METHANE

(A) DIFFUSION MEASUREMENTS IN THE WIND TUNNEL (PPM/C.C.)

16.0	.3239E+02	.2639E+02	.1564E+02	.1741E+02	.7533E+01	.6133E+01	.3623E+01	.1435E+01
12.0	.5277E+02	.4474E+02	.3794E+02	.4692E+02	.1639E+02	.9570E+01	.4778E+01	.2677E+01
8.0	.7497E+02	.6922E+02	.5144E+02	.5776E+02	.2326E+02	.1338E+02	.6556E+01	.3114E+01
4.0	.9827E+02	.9289E+02	.7098E+02	.7221E+02	.3105E+02	.1269E+02	.6365E+01	.3656E+01
0.0	.1204E+03	.1075E+03	.8346E+02	.8061E+02	.3447E+02	.1894E+02	.8052E+01	.4376E+01
X3/X2(CM)	0.0	4.0	8.0	12.0	16.0	20.0	24.0	28.0

(B) EQUATION 2-44 WITH CONSTANT DIFFUSIVITIES IN X3-DIRECTION (PPM/C.C.)

16.0	.1109E+01	.1050E+01	.8868E+00	.6737E+00	.4570E+00	.2775E+00	.1509E+00	.7337E-01
12.0	.1076E+02	.1027E+02	.8697E+01	.6592E+01	.4472E+01	.2715E+01	.1476E+01	.7179E+00
8.0	.3501E+02	.3313E+02	.2805E+02	.2126E+02	.1442E+02	.8756E+01	.4760E+01	.2316E+01
4.0	.5390E+02	.5099E+02	.4318E+02	.3273E+02	.2220E+02	.1348E+02	.7329E+01	.3565E+01
0.0	.5733E+02	.5424E+02	.4593E+02	.3481E+02	.2362E+02	.1434E+02	.7794E+01	.3791E+01
X3/X2(CM)	0.0	4.0	8.0	12.0	16.0	20.0	24.0	28.0

(C) EQUATION 2-45 WITH CONSTANT DIFFUSIVITIES IN X3-DIRECTION (PPM/C.C.)

16.0	.2481E+02	.2348E+02	.1986E+02	.1507E+02	.1022E+02	.6207E+01	.3373E+01	.1641E+01
12.0	.4439E+02	.4256E+02	.3604E+02	.2731E+02	.1853E+02	.1125E+02	.6115E+01	.2975E+01
8.0	.6738E+02	.6375E+02	.5398E+02	.4092E+02	.2776E+02	.1685E+02	.9160E+01	.4456E+01
4.0	.8438E+02	.7983E+02	.6760E+02	.5124E+02	.3476E+02	.2111E+02	.1147E+02	.5581E+01
0.0	.9033E+02	.8523E+02	.7216E+02	.5470E+02	.3711E+02	.2254E+02	.1225E+02	.5955E+01
X3/X2(CM)	0.0	4.0	8.0	12.0	16.0	20.0	24.0	28.0

(D) GAUSSIAN DIFFUSION EQUATION (PPM/C.C.)

16.0	.3296E+02	.3118E+02	.2641E+02	.2001E+02	.1356E+02	.6245E+01	.4481E+01	.2180E+01
12.0	.5296E+02	.5010E+02	.4243E+02	.3216E+02	.2182E+02	.1325E+02	.7200E+01	.3502E+01
8.0	.7430E+02	.7029E+02	.5957E+02	.4511E+02	.3061E+02	.1858E+02	.1010E+02	.4914E+01
4.0	.9103E+02	.8612E+02	.7293E+02	.5527E+02	.3750E+02	.2277E+02	.1238E+02	.6020E+01
0.0	.9740E+02	.9215E+02	.7803E+02	.5915E+02	.4012E+02	.2436E+02	.1324E+02	.6442E+01
X3/X2(CM)	0.0	4.0	8.0	12.0	16.0	20.0	24.0	28.0

(E) EQUATION 2-45 WITH VARYING DIFFUSIVITIES IN X3-DIRECTION (PPM/C.C.)

16.0	.2983E+02	.2822E+02	.2390E+02	.1811E+02	.1229E+02	.7462E+01	.4056E+01	.1973E+01
12.0	.4842E+02	.4624E+02	.3879E+02	.2939E+02	.1995E+02	.1211E+02	.6582E+01	.3202E+01
8.0	.6914E+02	.6605E+02	.5542E+02	.4198E+02	.2849E+02	.1730E+02	.9401E+01	.4573E+01
4.0	.8698E+02	.8307E+02	.6972E+02	.5281E+02	.3585E+02	.2177E+02	.1183E+02	.5754E+01
0.0	.9357E+02	.8935E+02	.7499E+02	.5681E+02	.3856E+02	.2341E+02	.1272E+02	.6189E+01
X3/X2(CM)	0.0	4.0	8.0	12.0	16.0	20.0	24.0	28.0

Table 6.6. Comparison of turbulent dispersion between measured and predicted concentration distribution, H = 2 cm.

(h)

U(FREE STREAM) = 200.0 CM/SEC U1RMS= 19.3 CM/SEC U(LOCAL VEL.) = 125.4 CM/SEC
RELEASE HEIGHT = 2.0 CM U2RMS= 0.0 CM/SEC VEL. GRADIENT = 9.400 1/SEC
DOWNWIND DIST. = 400.0 CM U3RMS= 0.0 CM/SEC SOURCE STRENGTH = 10 % METHANE

(A) DIFFUSION MEASUREMENTS IN THE WIND TUNNEL (PPM/C.C.)

16.0	.3319E+02	.3281E+02	.2649E+02	.2152E+02	.1475E+02	.9014E+01	.5465E+01	.3650E+01
12.0	.4931E+02	.4813E+02	.4084E+02	.3109E+02	.2051E+02	.1209E+02	.7278E+01	.4214E+01
8.0	.6163E+02	.6261E+02	.5429E+02	.3935E+02	.2565E+02	.1601E+02	.8687E+01	.4766E+01
4.0	.7379E+02	.7398E+02	.6140E+02	.4520E+02	.2966E+02	.1807E+02	.9803E+01	.4990E+01
0.0	.8574E+02	.8219E+02	.6774E+02	.4918E+02	.3325E+02	.2011E+02	.1077E+02	.5257E+01
X3/X2(CM)	0.0	5.0	10.0	15.0	20.0	25.0	30.0	35.0

(B) EQUATION 2-44 WITH CONSTANT DIFFUSIVITIES IN X3-DIRECTION (PPM/C.C.)

16.0	.2113E+01	.1980E+01	.1629E+01	.1177E+01	.7472E+00	.4165E+00	.2036E+00	.8760E-01
12.0	.1174E+02	.1101E+02	.9057E+01	.6545E+01	.4154E+01	.2315E+01	.1133E+01	.4870E+00
8.0	.2934E+02	.2750E+02	.2265E+02	.1636E+02	.1002E+02	.5586E+01	.2734E+01	.1175E+01
4.0	.3920E+02	.3674E+02	.3023E+02	.2185E+02	.1387E+02	.7728E+01	.3782E+01	.1626E+01
0.0	.4106E+02	.3848E+02	.3167E+02	.2289E+02	.1452E+02	.8094E+01	.3962E+01	.1703E+01
X3/X2(CM)	0.0	5.0	10.0	15.0	20.0	25.0	30.0	35.0

(C) EQUATION 2-45 WITH CONSTANT DIFFUSIVITIES IN X3-DIRECTION (PPM/C.C.)

16.0	.2535E+02	.2376E+02	.1955E+02	.1413E+02	.8986E+01	.4998E+01	.2446E+01	.1051E+01
12.0	.3773E+02	.3724E+02	.3064E+02	.2214E+02	.1405E+02	.7833E+01	.3834E+01	.1648E+01
8.0	.5302E+02	.5053E+02	.4158E+02	.3005E+02	.1907E+02	.1063E+02	.5202E+01	.2236E+01
4.0	.6391E+02	.5989E+02	.4929E+02	.3563E+02	.2260E+02	.1260E+02	.6166E+01	.2650E+01
0.0	.6715E+02	.6292E+02	.5178E+02	.3743E+02	.2375E+02	.1324E+02	.6476E+01	.2784E+01
X3/X2(CM)	0.0	5.0	10.0	15.0	20.0	25.0	30.0	35.0

(D) GAUSSIAN DIFFUSION EQUATION (PPM/C.C.)

16.0	.3232E+02	.3029E+02	.2493E+02	.1801E+02	.1143E+02	.6371E+01	.3118E+01	.1340E+01
12.0	.4427E+02	.4336E+02	.3560E+02	.2579E+02	.1636E+02	.9121E+01	.4464E+01	.1919E+01
8.0	.5978E+02	.5602E+02	.4610E+02	.3332E+02	.2114E+02	.1178E+02	.5767E+01	.2479E+01
4.0	.6971E+02	.6533E+02	.5376E+02	.3885E+02	.2466E+02	.1374E+02	.6725E+01	.2891E+01
0.0	.7337E+02	.6876E+02	.5659E+02	.4089E+02	.2595E+02	.1446E+02	.7079E+01	.3043E+01
X3/X2(CM)	0.0	5.0	10.0	15.0	20.0	25.0	30.0	35.0

(E) EQUATION 2-45 WITH VARYING DIFFUSIVITIES IN X3-DIRECTION (PPM/C.C.)

16.0	.2589E+02	.2426E+02	.1997E+02	.1443E+02	.9158E+01	.5104E+01	.2498E+01	.1074E+01
12.0	.3769E+02	.3654E+02	.2913E+02	.1916E+02	.1153E+02	.6423E+01	.3144E+01	.1351E+01
8.0	.3810E+02	.3664E+02	.3015E+02	.2175E+02	.1383E+02	.7707E+01	.3772E+01	.1621E+01
4.0	.4442E+02	.4163E+02	.3426E+02	.2474E+02	.1571E+02	.8757E+01	.4288E+01	.1842E+01
0.0	.4704E+02	.4409E+02	.3629E+02	.2622E+02	.1664E+02	.9274E+01	.4539E+01	.1951E+01
X3/X2(CM)	0.0	5.0	10.0	15.0	20.0	25.0	30.0	35.0

Table 6.6. Comparison of turbulent dispersion between measured and predicted concentration distribution, H = 2 cm.

(i)

U(FREE STREAM) = 200.0 CM/SEC U1RMS= 18.3 CM/SEC U(LOCAL VEL.) = 125.4 CM/SEC
RELEASE HEIGHT = 2.0 CM U2RMS= 9.0 CM/SEC VEL. GRADIENT = 5.400 1/SEC
DOWNWIND DIST. = 500.0 CM U3RMS= 9.0 CM/SEC SOURCE STRENGTH = 10 % METHANE

(A) DIFFUSION MEASUREMENTS IN THE WIND TUNNEL (PPM/C.C.)

20.0	.2087E+02	.1975E+02	.1419E+02	.1239E+02	.6751E+01	.5770E+01	.3865E+01	.1409E+01
15.0	.3322E+02	.3094E+02	.2570E+02	.2007E+02	.1358E+02	.6830E+01	.5550E+01	.3439E+01
10.0	.4503E+02	.4304E+02	.3617E+02	.2669E+02	.1822E+02	.1201E+02	.7291E+01	.4124E+01
5.0	.5553E+02	.5200E+02	.4412E+02	.3292E+02	.2265E+02	.1450E+02	.8545E+01	.4550E+01
0.0	.6372E+02	.5887E+02	.4843E+02	.3661E+02	.2534E+02	.1616E+02	.9510E+01	.4822E+01
X3/X2(CM)	0.0	5.0	10.0	15.0	20.0	25.0	30.0	35.0

(B) EQUATION 2-44 WITH CONSTANT DIFFUSIVITIES IN X3-DIRECTION (PPM/C.C.)

20.0	.3047E+00	.2893E+00	.2475E+00	.1903E+00	.1327E+00	.6311E-01	.4693E-01	.2385E-01
15.0	.4467E+01	.4241E+01	.3626E+01	.2738E+01	.1945E+01	.1219E+01	.6879E+00	.3501E+00
10.0	.1773E+02	.1683E+02	.1440E+02	.1111E+02	.7721E+01	.4837E+01	.2731E+01	.1390E+01
5.0	.2947E+02	.2798E+02	.2394E+02	.1848E+02	.1283E+02	.8036E+01	.4537E+01	.2310E+01
0.0	.3169E+02	.3008E+02	.2574E+02	.1985E+02	.1380E+02	.8643E+01	.4880E+01	.2483E+01
X3/X2(CM)	0.0	5.0	10.0	15.0	20.0	25.0	30.0	35.0

(C) EQUATION 2-45 WITH CONSTANT DIFFUSIVITIES IN X3-DIRECTION (PPM/C.C.)

20.0	.1509E+02	.1432E+02	.1226E+02	.9452E+01	.6570E+01	.4116E+01	.2324E+01	.1103E+01
15.0	.2704E+02	.2567E+02	.2196E+02	.1694E+02	.1177E+02	.7374E+01	.4164E+01	.2119E+01
10.0	.4019E+02	.3815E+02	.3264E+02	.2517E+02	.1750E+02	.1096E+02	.6180E+01	.3149E+01
5.0	.5010E+02	.4757E+02	.4070E+02	.3139E+02	.2182E+02	.1367E+02	.7716E+01	.3927E+01
0.0	.5342E+02	.5072E+02	.4340E+02	.3347E+02	.2326E+02	.1457E+02	.8223E+01	.4187E+01
X3/X2(CM)	0.0	5.0	10.0	15.0	20.0	25.0	30.0	35.0

(D) GAUSSIAN DIFFUSION EQUATION (PPM/C.C.)

20.0	.2100E+02	.1994E+02	.1706E+02	.1316E+02	.9146E+01	.5729E+01	.3235E+01	.1646E+01
15.0	.3297E+02	.3130E+02	.2678E+02	.2065E+02	.1436E+02	.8993E+01	.5077E+01	.2584E+01
10.0	.4549E+02	.4319E+02	.3695E+02	.2850E+02	.1981E+02	.1241E+02	.7006E+01	.3565E+01
5.0	.5518E+02	.5239E+02	.4483E+02	.3457E+02	.2403E+02	.1505E+02	.8499E+01	.4325E+01
0.0	.5885E+02	.5587E+02	.4781E+02	.3687E+02	.2563E+02	.1605E+02	.9064E+01	.4612E+01
X3/X2(CM)	0.0	5.0	10.0	15.0	20.0	25.0	30.0	35.0

(E) EQUATION 2-45 WITH VARYING DIFFUSIVITIES IN X3-DIRECTION (PPM/C.C.)

20.0	.1901E+02	.1710E+02	.1463E+02	.1130E+02	.7842E+01	.4913E+01	.2774E+01	.1411E+01
15.0	.2959E+02	.2239E+02	.1916E+02	.1478E+02	.1027E+02	.6433E+01	.3632E+01	.1848E+01
10.0	.3929E+02	.2772E+02	.2372E+02	.1829E+02	.1272E+02	.7966E+01	.4496E+01	.2288E+01
5.0	.3392E+02	.3220E+02	.2756E+02	.2125E+02	.1477E+02	.9253E+01	.5224E+01	.2659E+01
0.0	.3429E+02	.3445E+02	.2947E+02	.2273E+02	.1580E+02	.9897E+01	.5586E+01	.2844E+01
X3/X2(CM)	0.0	5.0	10.0	15.0	20.0	25.0	30.0	35.0

Table 6.6. Comparison of turbulent dispersion between measured and predicted concentration distribution, H = 2 cm.

(j)

U(FREE STREAM) = 200.0 CM/SEC U1RMS= 18.3 CM/SEC U(LOCAL VEL.) = 125.4 CM/SEC
RELEASE HEIGHT = 2.0 CM U2RMS= 9.0 CM/SEC VEL. GRADIENT = 9.400 1/SEC
DOWNWIND DIST. = 700.0 CM U3RMS= 9.0 CM/SEC SOURCE STRENGTH = 10 % METHANE

(A) DIFFUSION MEASUREMENTS IN THE WIND TUNNEL (PPM/C.C.)

20.0	.1907E+02	.1677E+02	.1575E+02	.1215E+02	.9655E+01	.7405E+01	.5324E+01	.3752E+01
15.0	.2440E+02	.2322E+02	.2105E+02	.1691E+02	.1319E+02	.9734E+01	.7116E+01	.4935E+01
10.0	.3093E+02	.2876E+02	.2463E+02	.2019E+02	.1556E+02	.1197E+02	.8398E+01	.6006E+01
5.0	.3494E+02	.3235E+02	.2753E+02	.2259E+02	.1763E+02	.1307E+02	.9330E+01	.6548E+01
0.0	.3819E+02	.3325E+02	.2837E+02	.2344E+02	.1843E+02	.1422E+02	.1004E+02	.6749E+01
X3/X2(CM)	0.0	5.0	10.0	15.0	20.0	25.0	30.0	35.0

(B) EQUATION 2-44 WITH CONSTANT DIFFUSIVITIES IN X3-DIRECTION (PPM/C.C.)

20.0	.7716E+00	.7435E+00	.6652E+00	.5525E+00	.4261E+00	.3051E+00	.2028E+00	.1252E+00
15.0	.5727E+01	.5080E+01	.4545E+01	.3775E+01	.2911E+01	.2084E+01	.1385E+01	.8553E+00
10.0	.1414E+02	.1363E+02	.1219E+02	.1013E+02	.7810E+01	.5592E+01	.3717E+01	.2294E+01
5.0	.2034E+02	.1960E+02	.1754E+02	.1457E+02	.1123E+02	.8043E+01	.5347E+01	.3300E+01
0.0	.2143E+02	.2065E+02	.1847E+02	.1534E+02	.1183E+02	.8472E+01	.5632E+01	.3476E+01
X3/X2(CM)	0.0	5.0	10.0	15.0	20.0	25.0	30.0	35.0

(C) EQUATION 2-45 WITH CONSTANT DIFFUSIVITIES IN X3-DIRECTION (PPM/C.C.)

20.0	.1535E+02	.1470E+02	.1315E+02	.1093E+02	.8426E+01	.6033E+01	.4010E+01	.2475E+01
15.0	.2319E+02	.2235E+02	.1996E+02	.1660E+02	.1281E+02	.9169E+01	.6095E+01	.3762E+01
10.0	.3092E+02	.2970E+02	.2657E+02	.2207E+02	.1702E+02	.1219E+02	.8100E+01	.5000E+01
5.0	.3611E+02	.3479E+02	.3113E+02	.2589E+02	.1994E+02	.1428E+02	.9491E+01	.5858E+01
0.0	.3781E+02	.3643E+02	.3259E+02	.2707E+02	.2088E+02	.1495E+02	.9933E+01	.6134E+01
X3/X2(CM)	0.0	5.0	10.0	15.0	20.0	25.0	30.0	35.0

(D) GAUSSIAN DIFFUSION EQUATION (PPM/C.C.)

20.0	.2011E+02	.1938E+02	.1734E+02	.1440E+02	.1110E+02	.7951E+01	.5285E+01	.3262E+01
15.0	.2783E+02	.2679E+02	.2397E+02	.1991E+02	.1535E+02	.1099E+02	.7307E+01	.4510E+01
10.0	.3504E+02	.3376E+02	.3021E+02	.2508E+02	.1935E+02	.1385E+02	.9210E+01	.5684E+01
5.0	.4026E+02	.3879E+02	.3470E+02	.2883E+02	.2223E+02	.1592E+02	.1058E+02	.6531E+01
0.0	.4217E+02	.4063E+02	.3635E+02	.3019E+02	.2328E+02	.1667E+02	.1108E+02	.6840E+01
X3/X2(CM)	0.0	5.0	10.0	15.0	20.0	25.0	30.0	35.0

(E) EQUATION 2-45 WITH VARYING DIFFUSIVITIES IN X3-DIRECTION (PPM/C.C.)

20.0	.1490E+02	.1426E+02	.1276E+02	.1060E+02	.8175E+01	.5853E+01	.3891E+01	.2402E+01
15.0	.1797E+02	.1732E+02	.1549E+02	.1287E+02	.9923E+01	.7105E+01	.4723E+01	.2915E+01
10.0	.2095E+02	.2019E+02	.1806E+02	.1500E+02	.1157E+02	.8284E+01	.5507E+01	.3399E+01
5.0	.2334E+02	.2240E+02	.2012E+02	.1671E+02	.1289E+02	.9226E+01	.6133E+01	.3786E+01
0.0	.2449E+02	.2360E+02	.2111E+02	.1754E+02	.1352E+02	.9683E+01	.6437E+01	.3973E+01
X3/X2(CM)	0.0	5.0	10.0	15.0	20.0	25.0	30.0	35.0

Table 6.6. Comparison of turbulent dispersion between measured and predicted concentration distribution, H = 2 cm.

(k)

JEFFS STREAM) : 200.0 CM/SEC U1RMS: 1?.3 CM/SEC VERTICAL VEL.) : 125.4 CM/SEC
RELEASE HEIGHT : 2.0 CM U2RMS: 9.0 CM/SEC VEL. GRADIENT : 9.403 1/SEC
DOWNWIND DIST. :1000.0 CM U3RMS: 6.0 CM/SEC SOURCE STRENGTH : 10 % METHANE

(A) DIFFUSION MEASUREMENTS IN THE WIND TUNNEL (PPM/C.C.)

20.0	.1391E+02	.1291E+02	.1159E+02	.1010E+02	.8800E+01	.7396E+01	.5889E+01	.4476E+01
15.0	.1720E+02	.1633E+02	.1502E+02	.1291E+02	.1073E+02	.9065E+01	.7288E+01	.5667E+01
10.0	.2069E+02	.1970E+02	.1671E+02	.1446E+02	.1247E+02	.1024E+02	.8230E+01	.6636E+01
5.0	.2171E+02	.2046E+02	.1819E+02	.1598E+02	.1361E+02	.1134E+02	.8908E+01	.7038E+01
0.0	.2285E+02	.2089E+02	.1890E+02	.1644E+02	.1436E+02	.1160E+02	.9473E+01	.7259E+01
X3/X2(CM)	0.0	5.0	10.0	15.0	20.0	25.0	30.0	35.0

(B) EQUATION 2-44 WITH CONSTANT DIFFUSIVITIES IN X3-DIRECTION (PPM/C.C.)

20.0	.1376E+01	.1341E+01	.1240E+01	.1082E+01	.9031E+00	.7180E+00	.5401E+00	.3853E+00
15.0	.5294E+01	.5158E+01	.4771E+01	.4190E+01	.3493E+01	.2705E+01	.2077E+01	.1462E+01
10.0	.1057E+02	.1030E+02	.9529E+01	.8369E+01	.6977E+01	.5522E+01	.4149E+01	.2960E+01
5.0	.1364E+02	.1329E+02	.1230E+02	.1080E+02	.9002E+01	.7125E+01	.5354E+01	.3819E+01
0.0	.1415E+02	.1379E+02	.1275E+02	.1120E+02	.9338E+01	.7389E+01	.5552E+01	.3961E+01
X3/X2(CM)	0.0	5.0	10.0	15.0	20.0	25.0	30.0	35.0

(C) EQUATION 2-45 WITH CONSTANT DIFFUSIVITIES IN X3-DIRECTION (PPM/C.C.)

20.0	.1394E+02	.1349E+02	.1248E+02	.1096E+02	.9136E+01	.7231E+01	.5433E+01	.3876E+01
15.0	.1758E+02	.1710E+02	.1674E+02	.1470E+02	.1226E+02	.9703E+01	.7291E+01	.5201E+01
10.0	.2269E+02	.2211E+02	.2045E+02	.1794E+02	.1497E+02	.1185E+02	.8903E+01	.6351E+01
5.0	.2536E+02	.2471E+02	.2286E+02	.2007E+02	.1673E+02	.1324E+02	.9952E+01	.7099E+01
0.0	.2719E+02	.2652E+02	.2361E+02	.2073E+02	.1728E+02	.1368E+02	.1028E+02	.7332E+01
X3/X2(CM)	0.0	5.0	10.0	15.0	20.0	25.0	30.0	35.0

(D) GAUSSIAN DIFFUSION EQUATION (PPM/C.C.)

20.0	.1759E+02	.1713E+02	.1584E+02	.1391E+02	.1160E+02	.9180E+01	.6898E+01	.4920E+01
15.0	.2207E+02	.2151E+02	.1989E+02	.1747E+02	.1456E+02	.1153E+02	.8662E+01	.6179E+01
10.0	.2597E+02	.2531E+02	.2341E+02	.2056E+02	.1714E+02	.1356E+02	.1019E+02	.7271E+01
5.0	.2864E+02	.2790E+02	.2581E+02	.2266E+02	.1889E+02	.1496E+02	.1124E+02	.8016E+01
0.0	.2959E+02	.2882E+02	.2666E+02	.2341E+02	.1952E+02	.1545E+02	.1161E+02	.8282E+01
X3/X2(CM)	0.0	5.0	10.0	15.0	20.0	25.0	30.0	35.0

(E) EQUATION 2-45 WITH VARYING DIFFUSIVITIES IN X3-DIRECTION (PPM/C.C.)

20.0	.1133E+02	.1103E+02	.1020E+02	.8959E+01	.7468E+01	.5911E+01	.4442E+01	.3168E+01
15.0	.1297E+02	.1264E+02	.1169E+02	.1027E+02	.8559E+01	.6774E+01	.5090E+01	.3631E+01
10.0	.1445E+02	.1408E+02	.1302E+02	.1144E+02	.9535E+01	.7547E+01	.5671E+01	.4045E+01
5.0	.1559E+02	.1519E+02	.1405E+02	.1235E+02	.1029E+02	.8140E+01	.6117E+01	.4363E+01
0.0	.1613E+02	.1571E+02	.1453E+02	.1277E+02	.1064E+02	.8422E+01	.6328E+01	.4514E+01
X3/X2(CM)	0.0	5.0	10.0	15.0	20.0	25.0	30.0	35.0

Table 6.7. Comparison of turbulent dispersion between measured and predicted concentration distribution, H = 10 cm.

(a)

U(FREE STREAM) : 200.0 CM/SEC	U1RMS: 15.0 CM/SEC	U(LOCAL VEL.) : 156.6 CM/SEC	
RELEASE HEIGHT : 10.0 CM	U2RMS: 7.5 CM/SEC	VEL. GRADIENT : 2.400 1/SEC	
DOWNWIND DIST. : 25.0 CM	U3RMS: 6.0 CM/SEC	SOURCE STRENGTH : 10 % METHANE	

(A) DIFFUSION MEASUREMENTS IN THE WIND TUNNEL (PPM/C.C.)

14.0	.1652E+03	.1670E+03	.1310E+03	.6543E+02	.3387E+02	.1463E+02	.5432E+01	.2473E+01
12.0	.2474E+03	.8160E+03	.6256E+03	.3607E+03	.2181E+03	.1166E+03	.4250E+02	.1269E+02
10.0	.1964E+04	.1751E+04	.1342E+04	.8774E+03	.4600E+03	.2417E+03	.8419E+02	.2624E+02
8.0	.9093E+03	.1017E+04	.7710E+03	.5260E+03	.3324E+03	.1654E+03	.6600E+02	.2196E+02
6.0	.1599E+03	.1452E+03	.1167E+03	.1315E+03	.8186E+02	.3620E+02	.1750E+02	.8946E+01
X3/X2(CM)	0.0	1.0	2.0	3.0	4.0	5.0	6.0	7.0

(B) EQUATION 2-44 WITH CONSTANT DIFFUSIVITIES IN X3-DIRECTION (PPM/C.C.)

14.0	.1433E+03	.1385E+03	.1253E+03	.1052E+03	.8377E+02	.6195E+02	.4264E+02	.2771E+02
12.0	.3209E+03	.3104E+03	.2907E+03	.2374E+03	.1877E+03	.1355E+03	.9600E+02	.6238E+02
10.0	.4749E+03	.4100E+03	.3708E+03	.3135E+03	.2460E+03	.1834E+03	.1268E+03	.8201E+02
8.0	.3757E+03	.3634E+03	.3286E+03	.2779E+03	.2197E+03	.1625E+03	.1124E+03	.7268E+02
6.0	.2593E+03	.2504E+03	.2264E+03	.1915E+03	.1514E+03	.1120E+03	.7744E+02	.5003E+02
X3/X2(CM)	0.0	1.0	2.0	3.0	4.0	5.0	6.0	7.0

(C) EQUATION 2-45 WITH CONSTANT DIFFUSIVITIES IN X3-DIRECTION (PPM/C.C.)

14.0	.1757E+03	.1699E+03	.1536E+03	.1290E+03	.1027E+03	.7598E+02	.5254E+02	.3398E+02
12.0	.3959E+03	.3247E+03	.2937E+03	.2494E+03	.1964E+03	.1452E+03	.1004E+03	.6496E+02
10.0	.4175E+03	.4037E+03	.3651E+03	.3087E+03	.2442E+03	.1806E+03	.1249E+03	.8076E+02
8.0	.3434E+03	.3321E+03	.3003E+03	.2540E+03	.2009E+03	.1485E+03	.1027E+03	.6643E+02
6.0	.1913E+03	.1850E+03	.1673E+03	.1414E+03	.1119E+03	.8272E+02	.5721E+02	.3700E+02
X3/X2(CM)	0.0	1.0	2.0	3.0	4.0	5.0	6.0	7.0

(D) GAUSSIAN DIFFUSION EQUATION (PPM/C.C.)

14.0	.1917E+03	.1757E+03	.1569E+03	.1344E+03	.1063E+03	.7859E+02	.5435E+02	.3515E+02
12.0	.3956E+03	.3274E+03	.2961E+03	.2514E+03	.1980E+03	.1464E+03	.1013E+03	.6550E+02
10.0	.4167E+03	.4029E+03	.3644E+03	.3081E+03	.2437E+03	.1802E+03	.1246E+03	.8060E+02
8.0	.3396E+03	.3274E+03	.2961E+03	.2514E+03	.1980E+03	.1464E+03	.1013E+03	.6550E+02
6.0	.1917E+03	.1757E+03	.1569E+03	.1344E+03	.1063E+03	.7859E+02	.5435E+02	.3515E+02
X3/X2(CM)	0.0	1.0	2.0	3.0	4.0	5.0	6.0	7.0

(E) EQUATION 2-45 WITH VARYING DIFFUSIVITIES IN X3-DIRECTION (PPM/C.C.)

14.0	.1773E+03	.1712E+03	.1546E+03	.1309E+03	.1035E+03	.7656E+02	.5295E+02	.3424E+02
12.0	.3997E+03	.3285E+03	.2971E+03	.2517E+03	.1987E+03	.1469E+03	.1016E+03	.6571E+02
10.0	.4341E+03	.4198E+03	.3796E+03	.3210E+03	.2539E+03	.1877E+03	.1298E+03	.8397E+02
8.0	.3570E+03	.3452E+03	.3122E+03	.2644E+03	.2091E+03	.1544E+03	.1068E+03	.6910E+02
6.0	.1993E+03	.1743E+03	.1576E+03	.1333E+03	.1054E+03	.7786E+02	.5391E+02	.3487E+02
X3/X2(CM)	0.0	1.0	2.0	3.0	4.0	5.0	6.0	7.0

Table 6.7. Comparison of turbulent dispersion between measured and predicted concentration distribution, H = 10 cm.

(b)

U(FREE STREAM) = 200.0 CM/SEC U1RMS= 15.0 CM/SEC U(LOCAL VEL.) = 159.6 CM/SEC
RELEASE HEIGHT = 10.0 CM U2RMS= 7.5 CM/SEC VEL. GRADIENT = 2.400 1/SEC
DOWNWIND DIST. = 50.0 CM U3RMS= 6.0 CM/SEC SOURCE STRENGTH = 10 % METHANE

(A) DIFFUSION MEASUREMENTS IN THE WIND TUNNEL (PPM/C.C.)

20.0	.6299E+01	.5343E+01	.2553E+01	.1466E+01	.8039E+00	.6404E+00	.6384E+00	.7046E+00
15.0	.9421E+03	.2621E+03	.1524E+03	.8951E+02	.1608E+02	.4506E+01	.1419E+01	.8039E+00
10.0	.5096E+03	.4383E+03	.2831E+03	.1266E+03	.4706E+02	.1276E+02	.3570E+01	.1702E+01
5.0	.3580E+02	.4156E+02	.2927E+02	.1471E+02	.6431E+01	.2660E+01	.1092E+01	.6667E+00
0.0	.1702E+01	.1098E+01	.8984E+00	.7566E+00	.6620E+00	.7140E+00	.6715E+00	.6147E+00
X3/X2(CM)	0.0	2.0	4.0	6.0	8.0	10.0	12.0	14.0

(B) EQUATION 2-44 WITH CONSTANT DIFFUSIVITIES IN X3-DIRECTION (PPM/C.C.)

20.0	.3760E+01	.3516E+01	.2875E+01	.2058E+01	.1286E+01	.7033E+00	.3364E+00	.1407E+00
15.0	.8559E+02	.3003E+02	.6545E+02	.4480E+02	.2427E+02	.1601E+02	.7656E+01	.3202E+01
10.0	.2139E+03	.2048E+03	.1675E+03	.1198E+03	.7496E+02	.4096E+02	.1959E+02	.8194E+01
5.0	.1927E+03	.1802E+03	.1474E+03	.1054E+03	.6590E+02	.3604E+02	.1724E+02	.7210E+01
0.0	.1764E+03	.1649E+03	.1349E+03	.9646E+02	.6033E+02	.3299E+02	.1578E+02	.6600E+01
X3/X2(CM)	0.0	2.0	4.0	6.0	8.0	10.0	12.0	14.0

(C) EQUATION 2-45 WITH CONSTANT DIFFUSIVITIES IN X3-DIRECTION (PPM/C.C.)

20.0	.1302E+02	.1217E+02	.9953E+01	.7119E+01	.4452E+01	.2435E+01	.1164E+01	.4870E+00
15.0	.1053E+03	.9846E+02	.8052E+02	.5758E+02	.3601E+02	.1970E+02	.9420E+01	.3940E+01
10.0	.2093E+03	.1957E+03	.1600E+03	.1144E+03	.7157E+02	.3914E+02	.1872E+02	.7830E+01
5.0	.1190E+03	.1103E+03	.9023E+02	.6453E+02	.4036E+02	.2207E+02	.1056E+02	.4419E+01
0.0	.4951E+02	.4536E+02	.3710E+02	.2653E+02	.1659E+02	.9074E+01	.4340E+01	.1815E+01
X3/X2(CM)	0.0	2.0	4.0	6.0	8.0	10.0	12.0	14.0

(D) GAUSSIAN DIFFUSION EQUATION (PPM/C.C.)

20.0	.1559E+02	.1457E+02	.1191E+02	.8520E+01	.5326E+01	.2914E+01	.1394E+01	.5829E+00
15.0	.1083E+03	.1019E+03	.8331E+02	.5958E+02	.3726E+02	.2036E+02	.9747E+01	.4076E+01
10.0	.2093E+03	.1968E+03	.1593E+03	.1139E+03	.7126E+02	.3897E+02	.1864E+02	.7796E+01
5.0	.1096E+03	.1024E+03	.8378E+02	.5991E+02	.3747E+02	.2049E+02	.9801E+01	.4099E+01
0.0	.3114E+02	.2914E+02	.2383E+02	.1704E+02	.1066E+02	.5828E+01	.2787E+01	.1166E+01
X3/X2(CM)	0.0	2.0	4.0	6.0	8.0	10.0	12.0	14.0

(E) EQUATION 2-45 WITH VARYING DIFFUSIVITIES IN X3-DIRECTION (PPM/C.C.)

20.0	.1444E+02	.1537E+02	.1257E+02	.8980E+01	.5622E+01	.3075E+01	.1471E+01	.6150E+00
15.0	.1065E+03	.9963E+02	.8147E+02	.5827E+02	.3644E+02	.1993E+02	.9531E+01	.3986E+01
10.0	.2139E+03	.2040E+03	.1669E+03	.1193E+03	.7463E+02	.4081E+02	.1952E+02	.8164E+01
5.0	.1137E+03	.1063E+03	.8695E+02	.6213E+02	.3886E+02	.2127E+02	.1017E+02	.4255E+01
0.0	.1494E+02	.1367E+02	.1135E+02	.8114E+01	.5074E+01	.2775E+01	.1327E+01	.5551E+00
X3/X2(CM)	0.0	2.0	4.0	6.0	8.0	10.0	12.0	14.0

Table 6.7. Comparison of turbulent dispersion between measured and predicted concentration distribution, H = 10 cm.

(c)

U(FREE STREAM) = 200.0 CM/SEC U1RMS= 15.0 CM/SEC U(LOCAL VEL.) = 159.6 CM/SEC
RELEASE HEIGHT = 10.0 CM U2RMS= 7.5 CM/SEC VEL. GRADIENT = 2.400 1/SEC
DOWNWIND DIST. = 100.0 CM U3RMS= 6.0 CM/SEC SOURCE STRENGTH = 10 % METHANE

(A) DIFFUSION MEASUREMENTS IN THE WIND TUNNEL (PPM/C.C.)

20.0	.4140E+02	.3781E+02	.2717E+02	.2594E+02	.1934E+02	.9920E+01	.5428E+01	.3376E+01
15.0	.1889E+03	.1817E+03	.1634E+03	.1251E+03	.7393E+02	.4532E+02	.2388E+02	.1044E+02
10.0	.2025E+03	.1987E+03	.1768E+03	.1406E+03	.1019E+03	.5984E+02	.3352E+02	.1674E+02
5.0	.6353E+02	.6665E+02	.5926E+02	.4973E+02	.3554E+02	.2220E+02	.1302E+02	.6045E+01
0.0	.8724E+01	.2498E+01	.7256E+01	.5887E+01	.4705E+01	.3277E+01	.2407E+01	.1532E+01
X3/X2(CM)	0.0	2.0	4.0	6.0	8.0	10.0	12.0	14.0

(B) EQUATION 2-44 WITH CONSTANT DIFFUSIVITIES IN X3-DIRECTION (PPM/C.C.)

20.0	.1312E+02	.1269E+02	.1147E+02	.9701E+01	.7672E+01	.5674E+01	.3924E+01	.2538E+01
15.0	.4661E+02	.6442E+02	.5325E+02	.4926E+02	.3896E+02	.2861E+02	.1992E+02	.1269E+02
10.0	.1218E+03	.1178E+03	.1065E+03	.9005E+02	.7121E+02	.5266E+02	.3642E+02	.2355E+02
5.0	.1383E+03	.1337E+03	.1209E+03	.1023E+03	.8087E+02	.5981E+02	.4136E+02	.2675E+02
0.0	.1388E+03	.1352E+03	.1223E+03	.1034E+03	.8179E+02	.6046E+02	.4182E+02	.2704E+02
X3/X2(CM)	0.0	2.0	4.0	6.0	8.0	10.0	12.0	14.0

(C) EQUATION 2-45 WITH CONSTANT DIFFUSIVITIES IN X3-DIRECTION (PPM/C.C.)

20.0	.2579E+02	.2493E+02	.2255E+02	.1907E+02	.1508E+02	.1115E+02	.7712E+01	.4967E+01
15.0	.7390E+02	.7146E+02	.6463E+02	.5465E+02	.4322E+02	.3196E+02	.2210E+02	.1430E+02
10.0	.1044E+03	.1029E+03	.9306E+02	.7870E+02	.6223E+02	.4602E+02	.3183E+02	.2058E+02
5.0	.8930E+02	.8635E+02	.7809E+02	.6604E+02	.5223E+02	.3862E+02	.2671E+02	.1727E+02
0.0	.7273E+02	.7032E+02	.6359E+02	.5378E+02	.4253E+02	.3145E+02	.2175E+02	.1407E+02
X3/X2(CM)	0.0	2.0	4.0	6.0	8.0	10.0	12.0	14.0

(D) GAUSSIAN DIFFUSION EQUATION (PPM/C.C.)

20.0	.2849E+02	.2755E+02	.2491E+02	.2107E+02	.1666E+02	.1232E+02	.8520E+01	.5510E+01
15.0	.7934E+02	.7287E+02	.6590E+02	.5573E+02	.4407E+02	.3259E+02	.2254E+02	.1459E+02
10.0	.1047E+03	.1013E+03	.9160E+02	.7746E+02	.6126E+02	.4530E+02	.3133E+02	.2028E+02
5.0	.8096E+02	.7829E+02	.7080E+02	.5987E+02	.4735E+02	.3502E+02	.2422E+02	.1568E+02
0.0	.5497E+02	.5509E+02	.4982E+02	.4213E+02	.3332E+02	.2464E+02	.1704E+02	.1103E+02
X3/X2(CM)	0.0	2.0	4.0	6.0	8.0	10.0	12.0	14.0

(E) EQUATION 2-45 WITH VARYING DIFFUSIVITIES IN X3-DIRECTION (PPM/C.C.)

20.0	.2850E+02	.2756E+02	.2493E+02	.2108E+02	.1667E+02	.1233E+02	.8526E+01	.5514E+01
15.0	.7939E+02	.7193E+02	.6505E+02	.5501E+02	.4350E+02	.3217E+02	.2225E+02	.1439E+02
10.0	.1105E+03	.1068E+03	.9662E+02	.8171E+02	.6462E+02	.4779E+02	.3305E+02	.2137E+02
5.0	.8867E+02	.8382E+02	.7580E+02	.6410E+02	.5069E+02	.3749E+02	.2592E+02	.1677E+02
0.0	.4610E+02	.4459E+02	.4032E+02	.3410E+02	.2696E+02	.1994E+02	.1379E+02	.8918E+01
X3/X2(CM)	0.0	2.0	4.0	6.0	8.0	10.0	12.0	14.0

Table 6.7. Comparison of turbulent dispersion between measured and predicted concentration distribution, H = 10 cm.

(d)

U(FREE STREAM) = 200.0 CM/SEC U1RMS= 15.0 CM/SEC U(LOCAL VEL.) = 159.6 CM/SEC
RELEASE HEIGHT = 10.0 CM U2RMS= 7.5 CM/SEC VEL. GRADIENT = 2.400 1/SEC
DOWNWIND DIST. = 150.0 CM U3RMS= 6.0 CM/SEC SOURCE STRENGTH = 10 % METHANE

(A) DIFFUSION MEASUREMENTS IN THE WIND TUNNEL (PPM/C.C.)

20.0	.6329E+02	.6519E+02	.4123E+02	.3785E+02	.2182E+02	.1110E+02	.5177E+01	.2115E+01
15.0	.1259E+03	.1287E+03	.1115E+03	.8291E+02	.4790E+02	.2467E+02	.1095E+02	.4134E+01
10.0	.1100E+03	.1091E+03	.9749E+02	.7219E+02	.4592E+02	.2466E+02	.1161E+02	.4594E+01
5.0	.5451E+02	.5756E+02	.4823E+02	.3848E+02	.2544E+02	.1434E+02	.6621E+01	.3433E+01
0.0	.1791E+02	.1743E+02	.1538E+02	.1245E+02	.8156E+01	.4708E+01	.2463E+01	.1458E+01
X3/X2(CM)	0.0	3.0	6.0	9.0	12.0	15.0	18.0	21.0

(B) EQUATION 2-44 WITH CONSTANT DIFFUSIVITIES IN X3-DIRECTION (PPM/C.C.)

20.0	.1709E+02	.1625E+02	.1397E+02	.1097E+02	.7642E+01	.4660E+01	.2795E+01	.1454E+01
15.0	.5396E+02	.5127E+02	.4405E+02	.3426E+02	.2409E+02	.1532E+02	.8811E+01	.4583E+01
10.0	.8852E+02	.8418E+02	.7239E+02	.5629E+02	.3959E+02	.2516E+02	.1448E+02	.7531E+01
5.0	.1034E+03	.9834E+02	.8457E+02	.6576E+02	.4625E+02	.2941E+02	.1692E+02	.8796E+01
0.0	.1056E+03	.1004E+03	.8632E+02	.6713E+02	.4721E+02	.3002E+02	.1727E+02	.8981E+01
X3/X2(CM)	0.0	3.0	6.0	9.0	12.0	15.0	18.0	21.0

(C) EQUATION 2-45 WITH CONSTANT DIFFUSIVITIES IN X3-DIRECTION (PPM/C.C.)

20.0	.2730E+02	.2596E+02	.2232E+02	.1736E+02	.1221E+02	.7764E+01	.4465E+01	.2322E+01
15.0	.5579E+02	.5305E+02	.4562E+02	.3549E+02	.2495E+02	.1587E+02	.9126E+01	.4746E+01
10.0	.7404E+02	.7041E+02	.6055E+02	.4709E+02	.3311E+02	.2106E+02	.1211E+02	.6299E+01
5.0	.7912E+02	.6953E+02	.5979E+02	.4650E+02	.3270E+02	.2080E+02	.1196E+02	.6221E+01
0.0	.6948E+02	.6607E+02	.5682E+02	.4419E+02	.3107E+02	.1976E+02	.1137E+02	.5911E+01
X3/X2(CM)	0.0	3.0	6.0	9.0	12.0	15.0	18.0	21.0

(D) GAUSSIAN DIFFUSION EQUATION (PPM/C.C.)

20.0	.2929E+02	.2785E+02	.2395E+02	.1862E+02	.1310E+02	.8330E+01	.4791E+01	.2492E+01
15.0	.5626E+02	.5350E+02	.4601E+02	.3578E+02	.2516E+02	.1600E+02	.9203E+01	.4787E+01
10.0	.7163E+02	.6812E+02	.5858E+02	.4556E+02	.3204E+02	.2037E+02	.1172E+02	.6094E+01
5.0	.6598E+02	.6265E+02	.5387E+02	.4190E+02	.2946E+02	.1874E+02	.1078E+02	.5605E+01
0.0	.5851E+02	.5564E+02	.4785E+02	.3721E+02	.2617E+02	.1664E+02	.9572E+01	.4978E+01
X3/X2(CM)	0.0	3.0	6.0	9.0	12.0	15.0	18.0	21.0

(E) EQUATION 2-45 WITH VARYING DIFFUSIVITIES IN X3-DIRECTION (PPM/C.C.)

20.0	.2900E+02	.2748E+02	.2364E+02	.1838E+02	.1293E+02	.8221E+01	.4728E+01	.2459E+01
15.0	.5593E+02	.5309E+02	.4566E+02	.3551E+02	.2497E+02	.1588E+02	.9133E+01	.4750E+01
10.0	.7211E+02	.7143E+02	.6143E+02	.4777E+02	.3359E+02	.2137E+02	.1229E+02	.6390E+01
5.0	.6951E+02	.6610E+02	.5685E+02	.4421E+02	.3109E+02	.1977E+02	.1137E+02	.5914E+01
0.0	.5476E+02	.5208E+02	.4478E+02	.3483E+02	.2449E+02	.1558E+02	.8958E+01	.4659E+01
X3/X2(CM)	0.0	3.0	6.0	9.0	12.0	15.0	18.0	21.0

Table 6.7. Comparison of turbulent dispersion between measured and predicted concentration distribution, H = 10 cm.

(e)

U(FREE STREAM) = 200.0 CM/SEC U1RMS= 15.0 CM/SEC U(LOCAL VEL.) = 159.6 CM/SEC
RELEASE HEIGHT = 10.0 CM U2RMS= 7.5 CM/SEC VEL. GRADIENT = 2.400 1/SEC
DOWNWIND DIST. = 200.0 CM U3RMS= 6.0 CM/SEC SOURCE STRENGTH = 10 % METHANE

(A) DIFFUSION MEASUREMENTS IN THE WIND TUNNEL (PPM/C.C.)

20.0	.5685E+02	.5516E+02	.3468E+02	.3459E+02	.2314E+02	.1247E+02	.6659E+01	.2920E+01
15.0	.8036E+02	.8640E+02	.7370E+02	.5477E+02	.3685E+02	.2155E+02	.1191E+02	.5727E+01
10.0	.8912E+02	.7698E+02	.6626E+02	.5716E+02	.3642E+02	.2196E+02	.1262E+02	.6360E+01
5.0	.5052E+02	.5207E+02	.4434E+02	.3623E+02	.2473E+02	.1624E+02	.8750E+01	.4351E+01
0.0	.2855E+02	.2633E+02	.2222E+02	.1826E+02	.1296E+02	.7837E+01	.4752E+01	.2347E+01
X3/X2(CM)	0.0	3.0	6.0	9.0	12.0	15.0	18.0	21.0

(B) EQUATION 2-44 WITH CONSTANT DIFFUSIVITIES IN X3-DIRECTION (PPM/C.C.)

20.0	.1833E+02	.1765E+02	.1576E+02	.1305E+02	.1002E+02	.7139E+01	.4715E+01	.2837E+01
15.0	.4575E+02	.4407E+02	.3936E+02	.3259E+02	.2503E+02	.1782E+02	.1177E+02	.7209E+01
10.0	.7022E+02	.6762E+02	.6039E+02	.5001E+02	.3841E+02	.2735E+02	.1806E+02	.1106E+02
5.0	.8138E+02	.7837E+02	.6999E+02	.5794E+02	.4451E+02	.3170E+02	.2093E+02	.1282E+02
0.0	.8307E+02	.7996E+02	.7144E+02	.5916E+02	.4543E+02	.3235E+02	.2137E+02	.1309E+02
X3/X2(CM)	0.0	3.0	6.0	9.0	12.0	15.0	18.0	21.0

(C) EQUATION 2-45 WITH CONSTANT DIFFUSIVITIES IN X3-DIRECTION (PPM/C.C.)

20.0	.2633E+02	.2504E+02	.2236E+02	.1851E+02	.1422E+02	.1013E+02	.6673E+01	.4045E+01
15.0	.4534E+02	.4366E+02	.3899E+02	.3229E+02	.2480E+02	.1766E+02	.1166E+02	.7142E+01
10.0	.5861E+02	.5644E+02	.5040E+02	.4174E+02	.3205E+02	.2283E+02	.1507E+02	.9233E+01
5.0	.6225E+02	.5994E+02	.5353E+02	.4433E+02	.3404E+02	.2425E+02	.1601E+02	.9806E+01
0.0	.6220E+02	.5990E+02	.5349E+02	.4429E+02	.3402E+02	.2422E+02	.1600E+02	.9798E+01
X3/X2(CM)	0.0	3.0	6.0	9.0	12.0	15.0	18.0	21.0

(D) GAUSSIAN DIFFUSION EQUATION (PPM/C.C.)

20.0	.2739E+02	.2637E+02	.2355E+02	.1950E+02	.1498E+02	.1067E+02	.7045E+01	.4314E+01
15.0	.4520E+02	.4352E+02	.3887E+02	.3219E+02	.2472E+02	.1760E+02	.1163E+02	.7120E+01
10.0	.5588E+02	.5381E+02	.4814E+02	.3986E+02	.3061E+02	.2180E+02	.1440E+02	.8818E+01
5.0	.5640E+02	.5431E+02	.4859E+02	.4027E+02	.3094E+02	.2203E+02	.1456E+02	.8918E+01
0.0	.5647E+02	.5435E+02	.4863E+02	.4029E+02	.3095E+02	.2204E+02	.1456E+02	.8918E+01
X3/X2(CM)	0.0	3.0	6.0	9.0	12.0	15.0	18.0	21.0

(E) EQUATION 2-45 WITH VARYING DIFFUSIVITIES IN X3-DIRECTION (PPM/C.C.)

20.0	.2697E+02	.2587E+02	.2310E+02	.1913E+02	.1469E+02	.1046E+02	.6911E+01	.4232E+01
15.0	.4492E+02	.4317E+02	.3855E+02	.3192E+02	.2452E+02	.1746E+02	.1153E+02	.7061E+01
10.0	.5791E+02	.5577E+02	.4980E+02	.4124E+02	.3167E+02	.2256E+02	.1490E+02	.9123E+01
5.0	.5879E+02	.5661E+02	.5055E+02	.4186E+02	.3215E+02	.2289E+02	.1512E+02	.9260E+01
0.0	.5893E+02	.5199E+02	.4643E+02	.3845E+02	.2953E+02	.2103E+02	.1389E+02	.8504E+01
X3/X2(CM)	0.0	3.0	6.0	9.0	12.0	15.0	18.0	21.0

Table 6.7. Comparison of turbulent dispersion between measured and predicted concentration distribution, H = 10 cm.

(f)

U(FREE STREAM) = 200.0 CM/SEC U1RMS= 15.0 CM/SEC U(LOCAL VEL.) = 154.5 CM/SEC
RELEASE HEIGHT = 10.0 CM U2RMS= 7.5 CM/SEC VEL. GRADIENT = 2.400 1/SEC
DOWNWIND DIST. = 250.0 CM U3RMS= 6.0 CM/SEC SOURCE STRENGTH = 10 % METHANE

(A) DIFFUSION MEASUREMENTS IN THE WIND TUNNEL (PPM/C.C.)

20.0	.4033E+02	.4412E+02	.3905E+02	.3410E+02	.2446E+02	.1447E+02	.7361E+01	.3519E+01
15.0	.4164E+02	.6661E+02	.6171E+02	.5032E+02	.3461E+02	.2080E+02	.1092E+02	.4796E+01
10.0	.6792E+02	.7064E+02	.6425E+02	.5258E+02	.3732E+02	.2249E+02	.1160E+02	.5250E+01
5.0	.5593E+02	.5752E+02	.5142E+02	.3995E+02	.2859E+02	.1704E+02	.9191E+01	.3930E+01
0.0	.4446E+02	.4693E+02	.4053E+02	.3070E+02	.2141E+02	.1249E+02	.7269E+01	.3223E+01
X3/X2(CM)	0.0	4.0	8.0	12.0	16.0	20.0	24.0	28.0

(B) EQUATION 7-44 WITH CONSTANT DIFFUSIVITIES IN X3-DIRECTION (PPM/C.C.)

20.0	.1849E+02	.1752E+02	.1492E+02	.1141E+02	.7837E+01	.4636E+01	.2691E+01	.1335E+01
15.0	.4008E+02	.3791E+02	.3227E+02	.2468E+02	.1695E+02	.1046E+02	.5799E+01	.2887E+01
10.0	.5933E+02	.5518E+02	.4698E+02	.3593E+02	.2468E+02	.1523E+02	.8442E+01	.4203E+01
5.0	.6455E+02	.6303E+02	.5371E+02	.4107E+02	.2821E+02	.1741E+02	.9650E+01	.4805E+01
0.0	.6793E+02	.6428E+02	.5473E+02	.4186E+02	.2875E+02	.1774E+02	.9834E+01	.4896E+01
X3/X2(CM)	0.0	4.0	8.0	12.0	16.0	20.0	24.0	28.0

(C) EQUATION 7-45 WITH CONSTANT DIFFUSIVITIES IN X3-DIRECTION (PPM/C.C.)

20.0	.2426E+02	.2299E+02	.1957E+02	.1497E+02	.1028E+02	.6345E+01	.3517E+01	.1751E+01
15.0	.3974E+02	.3671E+02	.3126E+02	.2390E+02	.1642E+02	.1013E+02	.5616E+01	.2796E+01
10.0	.4944E+02	.4605E+02	.3902E+02	.3051E+02	.2096E+02	.1293E+02	.7167E+01	.3569E+01
5.0	.5422E+02	.5139E+02	.4375E+02	.3346E+02	.2298E+02	.1416E+02	.7861E+01	.3914E+01
0.0	.5524E+02	.5235E+02	.4457E+02	.3408E+02	.2341E+02	.1445E+02	.8004E+01	.3987E+01
X3/X2(CM)	0.0	4.0	8.0	12.0	16.0	20.0	24.0	28.0

(D) GAUSSIAN DIFFUSION EQUATION (PPM/C.C.)

20.0	.2520E+02	.2386E+02	.2033E+02	.1555E+02	.1066E+02	.6591E+01	.3653E+01	.1819E+01
15.0	.3933E+02	.3623E+02	.3085E+02	.2359E+02	.1620E+02	.9999E+01	.5543E+01	.2760E+01
10.0	.4639E+02	.4445E+02	.3786E+02	.2894E+02	.1986E+02	.1227E+02	.6800E+01	.3386E+01
5.0	.4957E+02	.4698E+02	.4000E+02	.3055E+02	.2101E+02	.1297E+02	.7187E+01	.3579E+01
0.0	.4941E+02	.4702E+02	.4003E+02	.3061E+02	.2103E+02	.1298E+02	.7193E+01	.3581E+01
X3/X2(CM)	0.0	4.0	8.0	12.0	16.0	20.0	24.0	28.0

(E) EQUATION 7-45 WITH VARYING DIFFUSIVITIES IN X3-DIRECTION (PPM/C.C.)

20.0	.2459E+02	.2331E+02	.1984E+02	.1517E+02	.1042E+02	.6432E+01	.3565E+01	.1775E+01
15.0	.3773E+02	.3575E+02	.3044E+02	.2328E+02	.1599E+02	.9868E+01	.5473E+01	.2723E+01
10.0	.4794E+02	.4534E+02	.3860E+02	.2952E+02	.2028E+02	.1251E+02	.6937E+01	.3454E+01
5.0	.5121E+02	.4854E+02	.4132E+02	.3160E+02	.2171E+02	.1340E+02	.7425E+01	.3697E+01
0.0	.5043E+02	.4779E+02	.4069E+02	.3112E+02	.2138E+02	.1319E+02	.7311E+01	.3640E+01
X3/X2(CM)	0.0	4.0	8.0	12.0	16.0	20.0	24.0	28.0

Table 6.7. Comparison of turbulent dispersion between measured and predicted concentration distribution, H = 10 cm.

(g)

U(FREE STREAM) = 200.0 CM/SEC U1RMS= 15.0 CM/SEC U(LOCAL VEL.) = 159.6 CM/SEC
RELEASE HEIGHT = 10.0 CM U2RMS= 7.5 CM/SEC VEL. GRADIENT = 2.400 1/SEC
DOWNWIND DIST. = 300.0 CM U3RMS= 6.0 CM/SEC SOURCE STRENGTH = 10 % METHANE

(A) DIFFUSION MEASUREMENTS IN THE WIND TUNNEL (PPM/C.C.)

20.0	.4060E+02	.3866E+02	.3194E+02	.2409E+02	.1705E+02	.1077E+02	.5842E+01	.3207E+01
15.0	.5121E+02	.4857E+02	.4179E+02	.3144E+02	.2197E+02	.1372E+02	.8062E+01	.4206E+01
10.0	.5943E+02	.5024E+02	.4346E+02	.3367E+02	.2324E+02	.1469E+02	.9263E+01	.4597E+01
5.0	.4778E+02	.4566E+02	.3814E+02	.2918E+02	.2032E+02	.1289E+02	.7535E+01	.3853E+01
0.0	.4432E+02	.4056E+02	.3340E+02	.2568E+02	.1819E+02	.1116E+02	.6729E+01	.3305E+01
X3/X2(CM)	0.0	4.0	8.0	12.0	16.0	20.0	24.0	28.0

(B) EQUATION 2-44 WITH CONSTANT DIFFUSIVITIES IN X3-DIRECTION (PPM/C.C.)

20.0	.1918E+02	.1739E+02	.1520E+02	.1216E+02	.8892E+01	.5946E+01	.3637E+01	.2034E+01
15.0	.3557E+02	.3402E+02	.2975E+02	.2379E+02	.1746E+02	.1164E+02	.7116E+01	.3980E+01
10.0	.4965E+02	.4749E+02	.4152E+02	.3321E+02	.2428E+02	.1624E+02	.9932E+01	.5555E+01
5.0	.5401E+02	.5356E+02	.4686E+02	.3748E+02	.2739E+02	.1832E+02	.1120E+02	.6266E+01
0.0	.5698E+02	.5449E+02	.4765E+02	.3811E+02	.2787E+02	.1864E+02	.1140E+02	.6374E+01
X3/X2(CM)	0.0	4.0	8.0	12.0	16.0	20.0	24.0	28.0

(C) EQUATION 2-45 WITH CONSTANT DIFFUSIVITIES IN X3-DIRECTION (PPM/C.C.)

20.0	.2264E+02	.2165E+02	.1893E+02	.1514E+02	.1107E+02	.7405E+01	.4528E+01	.2533E+01
15.0	.3419E+02	.3270E+02	.2859E+02	.2287E+02	.1672E+02	.1118E+02	.6840E+01	.3825E+01
10.0	.4319E+02	.4130E+02	.3612E+02	.2889E+02	.2112E+02	.1413E+02	.8640E+01	.4832E+01
5.0	.4800E+02	.4591E+02	.4014E+02	.3210E+02	.2346E+02	.1570E+02	.9602E+01	.5370E+01
0.0	.4929E+02	.4714E+02	.4122E+02	.3298E+02	.2411E+02	.1612E+02	.9860E+01	.5514E+01
X3/X2(CM)	0.0	4.0	8.0	12.0	16.0	20.0	24.0	28.0

(D) GAUSSIAN DIFFUSION EQUATION (PPM/C.C.)

20.0	.2375E+02	.2223E+02	.1944E+02	.1555E+02	.1137E+02	.7604E+01	.4650E+01	.2601E+01
15.0	.3350E+02	.3203E+02	.2801E+02	.2240E+02	.1638E+02	.1096E+02	.6700E+01	.3747E+01
10.0	.4258E+02	.3910E+02	.3419E+02	.2734E+02	.2000E+02	.1337E+02	.8178E+01	.4574E+01
5.0	.4430E+02	.4236E+02	.3704E+02	.2963E+02	.2166E+02	.1448E+02	.8861E+01	.4956E+01
0.0	.4507E+02	.4310E+02	.3769E+02	.3014E+02	.2204E+02	.1474E+02	.9016E+01	.5043E+01
X3/X2(CM)	0.0	4.0	8.0	12.0	16.0	20.0	24.0	28.0

(E) EQUATION 2-45 WITH VARYING DIFFUSIVITIES IN X3-DIRECTION (PPM/C.C.)

20.0	.2254E+02	.2157E+02	.1887E+02	.1509E+02	.1103E+02	.7379E+01	.4513E+01	.2524E+01
15.0	.3282E+02	.3139E+02	.2745E+02	.2196E+02	.1605E+02	.1074E+02	.6566E+01	.3672E+01
10.0	.4119E+02	.3939E+02	.3445E+02	.2755E+02	.2015E+02	.1347E+02	.8240E+01	.4608E+01
5.0	.4545E+02	.4346E+02	.3800E+02	.3039E+02	.2223E+02	.1486E+02	.9091E+01	.5084E+01
0.0	.4631E+02	.4429E+02	.3873E+02	.3097E+02	.2265E+02	.1515E+02	.9264E+01	.5181E+01
X3/X2(CM)	0.0	4.0	8.0	12.0	16.0	20.0	24.0	28.0

Table 6.7. Comparison of turbulent dispersion between measured and predicted concentration distribution, H = 10 cm.

(h)

U(FREE STREAM) = 200.0 CM/SEC U1RMS= 15.0 CM/SEC CELERITY VEL.) = 159.6 CM/SEC
RELEASE HEIGHT = 10.0 CM U2RMS= 7.5 CM/SEC VEL. GRADIENT = 2.400 1/SEC
DOWNWIND DIST. = 400.0 CM U3RMS= 6.0 CM/SEC SOURCE STRENGTH = 10 % METHANE

(A) DIFFUSION MEASUREMENTS IN THE WIND TUNNEL (PPM/C.C.)

20.0	.2762E+02	.2664E+02	.2287E+02	.1749E+02	.1194E+02	.7713E+01	.4766E+01	.2732E+01
15.0	.3714E+02	.3675E+02	.3174E+02	.2480E+02	.1640E+02	.1001E+02	.6196E+01	.3503E+01
10.0	.4308E+02	.4230E+02	.3653E+02	.2888E+02	.2003E+02	.1266E+02	.7821E+01	.4020E+01
5.0	.4669E+02	.4524E+02	.3919E+02	.3013E+02	.2192E+02	.1417E+02	.8079E+01	.4016E+01
0.0	.4854E+02	.4643E+02	.3956E+02	.3085E+02	.2225E+02	.1502E+02	.8476E+01	.3969E+01
X3/X2(CM)	0.0	5.0	10.0	15.0	20.0	25.0	30.0	35.0

(B) EQUATION 2-44 WITH CONSTANT DIFFUSIVITIES IN X3-DIRECTION (PPM/C.C.)

20.0	.1703E+02	.1616E+02	.1381E+02	.1063E+02	.7366E+01	.4597E+01	.2504E+01	.1308E+01
15.0	.2910E+02	.2762E+02	.2360E+02	.1814E+02	.1259E+02	.7855E+01	.4413E+01	.2234E+01
10.0	.3816E+02	.3621E+02	.3095E+02	.2382E+02	.1651E+02	.1030E+02	.5769E+01	.2930E+01
5.0	.4214E+02	.3999E+02	.3417E+02	.2630E+02	.1822E+02	.1137E+02	.6372E+01	.3235E+01
0.0	.4374E+02	.4056E+02	.3466E+02	.2667E+02	.1848E+02	.1154E+02	.6483E+01	.3291E+01
X3/X2(CM)	0.0	5.0	10.0	15.0	20.0	25.0	30.0	35.0

(C) EQUATION 2-45 WITH CONSTANT DIFFUSIVITIES IN X3-DIRECTION (PPM/C.C.)

20.0	.2033E+02	.1900E+02	.1624E+02	.1250E+02	.8661E+01	.5405E+01	.3035E+01	.1538E+01
15.0	.2923E+02	.2679E+02	.2289E+02	.1762E+02	.1221E+02	.7620E+01	.4283E+01	.2167E+01
10.0	.3494E+02	.3315E+02	.2833E+02	.2180E+02	.1511E+02	.9430E+01	.5300E+01	.2682E+01
5.0	.3898E+02	.3699E+02	.3161E+02	.2433E+02	.1686E+02	.1052E+02	.5914E+01	.2993E+01
0.0	.4013E+02	.3814E+02	.3259E+02	.2508E+02	.1738E+02	.1085E+02	.6096E+01	.3085E+01
X3/X2(CM)	0.0	5.0	10.0	15.0	20.0	25.0	30.0	35.0

(D) GAUSSIAN DIFFUSION EQUATION (PPM/C.C.)

20.0	.2024E+02	.1921E+02	.1641E+02	.1263E+02	.8754E+01	.5463E+01	.3070E+01	.1554E+01
15.0	.2745E+02	.2605E+02	.2226E+02	.1713E+02	.1187E+02	.7409E+01	.4164E+01	.2107E+01
10.0	.3314E+02	.3147E+02	.2689E+02	.2070E+02	.1434E+02	.8951E+01	.5031E+01	.2546E+01
5.0	.3657E+02	.3471E+02	.2966E+02	.2282E+02	.1582E+02	.9872E+01	.5548E+01	.2808E+01
0.0	.3766E+02	.3574E+02	.3054E+02	.2351E+02	.1629E+02	.1017E+02	.5713E+01	.2892E+01
X3/X2(CM)	0.0	5.0	10.0	15.0	20.0	25.0	30.0	35.0

(E) EQUATION 2-45 WITH VARYING DIFFUSIVITIES IN X3-DIRECTION (PPM/C.C.)

20.0	.1930E+02	.1846E+02	.1573E+02	.1210E+02	.8388E+01	.5235E+01	.2942E+01	.1493E+01
15.0	.2640E+02	.2514E+02	.2148E+02	.1653E+02	.1146E+02	.7151E+01	.4021E+01	.2034E+01
10.0	.3276E+02	.3109E+02	.2657E+02	.2045E+02	.1417E+02	.8844E+01	.4970E+01	.2516E+01
5.0	.3704E+02	.3516E+02	.3005E+02	.2313E+02	.1603E+02	.1000E+02	.5621E+01	.2845E+01
0.0	.3838E+02	.3642E+02	.3147E+02	.2423E+02	.1678E+02	.1047E+02	.5887E+01	.2979E+01
X3/X2(CM)	0.0	5.0	10.0	15.0	20.0	25.0	30.0	35.0

Table 6.7. Comparison of turbulent dispersion between measured and predicted concentration distribution, H = 10 cm.

(i)

U(FREE STREAM) = 200.0 CM/SEC U1RMS= 15.0 CM/SEC L(LOCAL VEL.) = 159.6 CM/SEC
RELEASE HEIGHT = 10.0 CM U2RMS= 7.5 CM/SEC VEL. GRADIENT = 2.400 1/SEC
DOWNWIND DIST. = 500.0 CM U3RMS= 6.0 CM/SEC SOURCE STRENGTH = 10 % METHANE

(A) DIFFUSION MEASUREMENTS IN THE WIND TUNNEL (PPM/C.C.)

20.0	.2461E+02	.2397E+02	.2087E+02	.1622E+02	.1217E+02	.8359E+01	.5690E+01	.3434E+01
15.0	.3017E+02	.2906E+02	.2546E+02	.2110E+02	.1594E+02	.1063E+02	.7246E+01	.4629E+01
10.0	.3912E+02	.3247E+02	.2840E+02	.2330E+02	.1789E+02	.1234E+02	.8402E+01	.5157E+01
5.0	.3459E+02	.3422E+02	.3045E+02	.2527E+02	.1932E+02	.1366E+02	.9570E+01	.5300E+01
0.0	.3723E+02	.3545E+02	.3154E+02	.2615E+02	.2067E+02	.1442E+02	.9894E+01	.5291E+01
X3/X2(CM)	0.0	5.0	10.0	15.0	20.0	25.0	30.0	35.0

(B) EQUATION 2-44 WITH CONSTANT DIFFUSIVITIES IN X3-DIRECTION (PPM/C.C.)

20.0	.1570E+02	.1506E+02	.1326E+02	.1077E+02	.8031E+01	.5508E+01	.3473E+01	.2014E+01
15.0	.2454E+02	.2354E+02	.2076E+02	.1693E+02	.1255E+02	.8609E+01	.5429E+01	.3149E+01
10.0	.3092E+02	.2955E+02	.2606E+02	.2114E+02	.1576E+02	.1081E+02	.6817E+01	.3954E+01
5.0	.3350E+02	.3213E+02	.2833E+02	.2298E+02	.1713E+02	.1175E+02	.7411E+01	.4298E+01
0.0	.3390E+02	.3251E+02	.2867E+02	.2325E+02	.1734E+02	.1189E+02	.7500E+01	.4350E+01
X3/X2(CM)	0.0	5.0	10.0	15.0	20.0	25.0	30.0	35.0

(C) EQUATION 2-45 WITH CONSTANT DIFFUSIVITIES IN X3-DIRECTION (PPM/C.C.)

20.0	.1834E+02	.1732E+02	.1527E+02	.1239E+02	.9237E+01	.6334E+01	.3995E+01	.2317E+01
15.0	.2435E+02	.2335E+02	.2059E+02	.1670E+02	.1245E+02	.8540E+01	.5386E+01	.3123E+01
10.0	.2954E+02	.2833E+02	.2496E+02	.2026E+02	.1511E+02	.1036E+02	.6534E+01	.3789E+01
5.0	.3274E+02	.3142E+02	.2770E+02	.2247E+02	.1675E+02	.1149E+02	.7246E+01	.4203E+01
0.0	.3374E+02	.3236E+02	.2853E+02	.2314E+02	.1726E+02	.1183E+02	.7463E+01	.4328E+01
X3/X2(CM)	0.0	5.0	10.0	15.0	20.0	25.0	30.0	35.0

(D) GAUSSIAN DIFFUSION EQUATION (PPM/C.C.)

20.0	.1808E+02	.1735E+02	.1530E+02	.1241E+02	.9254E+01	.6346E+01	.4002E+01	.2321E+01
15.0	.2365E+02	.2267E+02	.2000E+02	.1622E+02	.1209E+02	.8293E+01	.5230E+01	.3033E+01
10.0	.2933E+02	.2706E+02	.2386E+02	.1935E+02	.1443E+02	.9897E+01	.6242E+01	.3620E+01
5.0	.3115E+02	.2987E+02	.2634E+02	.2136E+02	.1593E+02	.1093E+02	.6890E+01	.3996E+01
0.0	.3215E+02	.3083E+02	.2719E+02	.2205E+02	.1644E+02	.1128E+02	.7111E+01	.4124E+01
X3/X2(CM)	0.0	5.0	10.0	15.0	20.0	25.0	30.0	35.0

(E) EQUATION 2-45 WITH VARYING DIFFUSIVITIES IN X3-DIRECTION (PPM/C.C.)

20.0	.1713E+02	.1642E+02	.1448E+02	.1174E+02	.8755E+01	.6004E+01	.3787E+01	.2196E+01
15.0	.2251E+02	.2159E+02	.1904E+02	.1544E+02	.1151E+02	.7896E+01	.4980E+01	.2888E+01
10.0	.2744E+02	.2634E+02	.2322E+02	.1883E+02	.1405E+02	.9632E+01	.6075E+01	.3523E+01
5.0	.2911E+02	.2790E+02	.2637E+02	.2139E+02	.1595E+02	.1094E+02	.6897E+01	.4000E+01
0.0	.3257E+02	.3153E+02	.2780E+02	.2255E+02	.1681E+02	.1153E+02	.7272E+01	.4217E+01
X3/X2(CM)	0.0	5.0	10.0	15.0	20.0	25.0	30.0	35.0

Table 6.7. Comparison of turbulent dispersion between measured and predicted concentration distribution, H = 10 cm.

(j)

FREE STREAM) = 200.0 CM/SEC	U1RMS= 15.0 CM/SEC	U(LOCAL VEL.) = 159.6 CM/SEC	
RELEASE HEIGHT = 10.0 CM	U2RMS= 7.5 CM/SEC	VEL. GRADIENT = 2.400 1/SEC	
DOWNWIND DIST. = 700.0 CM	U3RMS= 6.0 CM/SEC	SOURCE STRENGTH = 10 % METHANE	

(A) DIFFUSION MEASUREMENTS IN THE WIND TUNNEL (PPM/C.C.)

20.0	.1996E+02	.1962E+02	.1807E+02	.1477E+02	.1481E+02	.1220E+02	.9840E+01	.7604E+01
15.0	.2260E+02	.2269E+02	.2223E+02	.2025E+02	.1736E+02	.1454E+02	.1155E+02	.8727E+01
10.0	.2419E+02	.2516E+02	.2439E+02	.2295E+02	.1956E+02	.1579E+02	.1250E+02	.9417E+01
5.0	.2533E+02	.2633E+02	.2570E+02	.2358E+02	.2018E+02	.1675E+02	.1294E+02	.9637E+01
0.0	.2695E+02	.2777E+02	.2693E+02	.2447E+02	.2156E+02	.1777E+02	.1370E+02	.9892E+01
X3/X2(CM)	0.0	5.0	10.0	15.0	20.0	25.0	30.0	35.0

(B) EQUATION 2-46 WITH CONSTANT DIFFUSIVITIES IN X3-DIRECTION (PPM/C.C.)

20.0	.1326E+02	.1287E+02	.1176E+02	.1013E+02	.8214E+01	.6274E+01	.4514E+01	.3059E+01
15.0	.1956E+02	.1900E+02	.1645E+02	.1414E+02	.1149E+02	.8773E+01	.6312E+01	.4277E+01
10.0	.2202E+02	.2137E+02	.1953E+02	.1692E+02	.1364E+02	.1042E+02	.7496E+01	.5078E+01
5.0	.2365E+02	.2276E+02	.2060E+02	.1791E+02	.1453E+02	.1110E+02	.7983E+01	.5407E+01
0.0	.2464E+02	.2297E+02	.2069E+02	.1807E+02	.1466E+02	.1120E+02	.8055E+01	.5458E+01
X3/X2(CM)	0.0	5.0	10.0	15.0	20.0	25.0	30.0	35.0

(C) EQUATION 2-45 WITH CONSTANT DIFFUSIVITIES IN X3-DIRECTION (PPM/C.C.)

20.0	.1523E+02	.1476E+02	.1351E+02	.1163E+02	.9432E+01	.7204E+01	.5183E+01	.3512E+01
15.0	.1934E+02	.1877E+02	.1716E+02	.1477E+02	.1198E+02	.9150E+01	.6583E+01	.4461E+01
10.0	.2268E+02	.2201E+02	.2012E+02	.1733E+02	.1405E+02	.1073E+02	.7721E+01	.5232E+01
5.0	.2476E+02	.2403E+02	.2197E+02	.1891E+02	.1534E+02	.1172E+02	.8429E+01	.5712E+01
0.0	.2560E+02	.2485E+02	.2253E+02	.1940E+02	.1573E+02	.1202E+02	.8645E+01	.5858E+01
X3/X2(CM)	0.0	5.0	10.0	15.0	20.0	25.0	30.0	35.0

(D) GAUSSIAN DIFFUSION EQUATION (PPM/C.C.)

20.0	.1517E+02	.1473E+02	.1346E+02	.1159E+02	.9399E+01	.7180E+01	.5165E+01	.3500E+01
15.0	.1889E+02	.1833E+02	.1675E+02	.1442E+02	.1170E+02	.8934E+01	.6428E+01	.4356E+01
10.0	.2197E+02	.2133E+02	.1949E+02	.1678E+02	.1361E+02	.1040E+02	.7480E+01	.5069E+01
5.0	.2402E+02	.2331E+02	.2131E+02	.1834E+02	.1488E+02	.1136E+02	.8175E+01	.5540E+01
0.0	.2473E+02	.2400E+02	.2194E+02	.1888E+02	.1532E+02	.1170E+02	.8418E+01	.5704E+01
X3/X2(CM)	0.0	5.0	10.0	15.0	20.0	25.0	30.0	35.0

(E) EQUATION 2-45 WITH VARYING DIFFUSIVITIES IN X3-DIRECTION (PPM/C.C.)

20.0	.1494E+02	.1362E+02	.1245E+02	.1077E+02	.8695E+01	.6642E+01	.4770E+01	.3238E+01
15.0	.1758E+02	.1706E+02	.1560E+02	.1343E+02	.1084E+02	.8317E+01	.5984E+01	.4055E+01
10.0	.2098E+02	.2028E+02	.1852E+02	.1595E+02	.1293E+02	.9879E+01	.7104E+01	.4816E+01
5.0	.2347E+02	.2278E+02	.2082E+02	.1793E+02	.1454E+02	.1111E+02	.7989E+01	.5414E+01
0.0	.2471E+02	.2398E+02	.2192E+02	.1887E+02	.1530E+02	.1169E+02	.8410E+01	.5699E+01
X3/X2(CM)	0.0	5.0	10.0	15.0	20.0	25.0	30.0	35.0

Table 6.8. Comparison of turbulent dispersion between measured and predicted concentration distribution, H = 20 cm.

(a)

JETOFF STREAM) = 700.0 CM/SEC	U1RMS= 11.4 CM/SEC	LELOCAL VEL.)	= 179.7 CM/SEC
RELEASE HEIGHT = 21.5 CM	U2RMS= 7.0 CM/SEC	VEL. GRADIENT	= 1.200 1/SEC
DOWNWIND DIST. = 25.0 CM	U3RMS= 5.5 CM/SEC	SOURCE STRENGTH	= 10 % METHANE

(A) DIFFUSION MEASUREMENTS IN THE WIND TUNNEL (PPM/C.C.)

22.5	.1049E+04	.6344E+03	.1852E+03	.1220E+02	.8578E+00	.7269E+00	.6957E+00	.6748E+00
20.0	.1654E+04	.1231E+04	.3329E+03	.3036E+02	.1530E+01	.7963E+00	.6957E+00	.7038E+00
17.5	.1144E+03	.1222E+03	.4606E+02	.6450E+01	.4596E+00	.7293E+00	.6874E+00	.7460E+00
15.0	.3223E+01	.3349E+01	.1812E+01	.1224E+01	.7712E+00	.7460E+00	.7167E+00	.6455E+00
12.5	.8760E+00	.8299E+00	.7335E+00	.7125E+00	.6974E+00	.6664E+00	.6560E+00	.5993E+00
X3/X2(CM)	0.0	2.0	4.0	6.0	8.0	10.0	12.0	14.0

(B) EQUATION 2-44 WITH CONSTANT DIFFUSIVITIES IN X3-DIRECTION (PPM/C.C.)

22.5	.3722E+03	.3270E+03	.2129E+03	.1042E+03	.3029E+02	.1057E+02	.2194E+01	.3420E+00
20.0	.3437E+03	.3153E+03	.2053E+03	.1004E+03	.3892E+02	.1020E+02	.2115E+01	.3297E+00
17.5	.1943E+03	.1598E+03	.1041E+03	.5091E+02	.1971E+02	.5167E+01	.1072E+01	.1671E+00
15.0	.5598E+02	.4852E+02	.3160E+02	.1544E+02	.5862E+01	.1569E+01	.3256E+00	.5075E-01
12.5	.1147E+02	.1011E+02	.6516E+01	.3223E+01	.1104E+01	.3271E+00	.6795E-01	.1059E-01
X3/X2(CM)	0.0	2.0	4.0	6.0	8.0	10.0	12.0	14.0

(C) EQUATION 2-45 WITH CONSTANT DIFFUSIVITIES IN X3-DIRECTION (PPM/C.C.)

22.5	.3922E+03	.3296E+03	.2146E+03	.1050E+03	.3860E+02	.1066E+02	.2211E+01	.3447E+00
20.0	.3546E+03	.3091E+03	.2013E+03	.9946E+02	.3614E+02	.9995E+01	.2074E+01	.3232E+00
17.5	.1643E+03	.1424E+03	.9271E+02	.4538E+02	.1667E+02	.4604E+01	.9553E+00	.1489E+00
15.0	.3810E+02	.3303E+02	.2151E+02	.1052E+02	.3886E+01	.1086E+01	.2216E+00	.3454E-01
12.5	.4573E+01	.3964E+01	.2581E+01	.1263E+01	.4642E+00	.1282E+00	.2660E-01	.4146E-02
X3/X2(CM)	0.0	2.0	4.0	6.0	8.0	10.0	12.0	14.0

(D) GAUSSIAN DIFFUSION EQUATION (PPM/C.C.)

22.5	.3640E+03	.3155E+03	.2054E+03	.1005E+03	.3694E+02	.1020E+02	.2117E+01	.3300E+00
20.0	.3537E+03	.3057E+03	.1991E+03	.9741E+02	.3581E+02	.9886E+01	.2052E+01	.3198E+00
17.5	.1598E+03	.1385E+03	.9022E+02	.4414E+02	.1622E+02	.4481E+01	.9296E+00	.1449E+00
15.0	.3497E+02	.3031E+02	.1974E+02	.9657E+01	.3550E+01	.9802E+00	.2034E+00	.3170E-01
12.5	.3709E+01	.3215E+01	.2094E+01	.1024E+01	.3765E+00	.1040E+00	.2157E-01	.3363E-02
X3/X2(CM)	0.0	2.0	4.0	6.0	8.0	10.0	12.0	14.0

(E) EQUATION 2-45 WITH VARYING DIFFUSIVITIES IN X3-DIRECTION (PPM/C.C.)

22.5	.1520E+03	.1317E+03	.8579E+02	.4197E+02	.1543E+02	.4261E+01	.8840E+00	.1378E+00
20.0	.2534E+03	.2198E+03	.1432E+03	.7004E+02	.2574E+02	.7110E+01	.1475E+01	.2299E+00
17.5	.1564E+03	.1355E+03	.8823E+02	.4318E+02	.1587E+02	.4383E+01	.9093E+00	.1417E+00
15.0	.3567E+02	.3092E+02	.2013E+02	.9849E+01	.3625E+01	.1004E+01	.2249E+00	.3506E-01
12.5	.4130E+01	.3580E+01	.2331E+01	.1141E+01	.4193E+00	.1161E+00	.2402E-01	.3744E-02
X3/X2(CM)	0.0	2.0	4.0	6.0	8.0	10.0	12.0	14.0

Table 6.8. Comparison of turbulent dispersion between measured and predicted concentration distribution, H = 20 cm.

(b)

FREE STREAM U : 700.0 CM/SEC	U1RMS: 11.6 CM/SEC	U(LOCAL VEL.) : 179.7 CM/SEC	
RELEASE HEIGHT : 21.5 CM	U2RMS: 7.0 CM/SEC	VEL. GRADIENT : 1.200 1/SEC	
DOWNWIND DIST. : 50.0 CM	U3RMS: 5.5 CM/SEC	SOURCE STRENGTH : 10 P METHANE	

(A) DIFFUSION MEASUREMENTS IN THE WIND TUNNEL (PPM/C.C.)

30.0	.1430E+01	.1111E+01	.5179E+00	.2047E+00	.8047E+00	.4808E+00	.7502E+00	.6664E+00
25.0	.1473E+03	.1223E+03	.5215E+02	.1919E+02	.4288E+01	.1513E+01	.9766E+00	.8257E+00
20.0	.7189E+03	.6000E+03	.3210E+03	.1091E+03	.2215E+02	.3567E+01	.1296E+01	.7754E+00
15.0	.3769E+02	.3357E+02	.2817E+02	.1400E+02	.4501E+01	.1555E+01	.1044E+01	.7712E+00
10.0	.8676E+00	.8944E+00	.9640E+00	.8715E+00	.8089E+00	.7754E+00	.7093E+00	.6957E+00
X3/X2(CM)	0.0	2.0	4.0	6.0	8.0	10.0	12.0	14.0

(B) EQUATION 2-44 WITH CONSTANT DIFFUSIVITIES IN X3-DIRECTION (PPM/C.C.)

30.0	.1531E+02	.1425E+02	.1150E+02	.8064E+01	.4678E+01	.2563E+01	.1168E+01	.4610E+00
25.0	.1331E+03	.1240E+03	.1000E+03	.6993E+02	.4262E+02	.2229E+02	.1015E+02	.4009E+01
20.0	.1943E+03	.1809E+03	.1460E+03	.1021E+03	.6192E+02	.3254E+02	.1482E+02	.5852E+01
15.0	.7929E+02	.7381E+02	.5956E+02	.4156E+02	.2526E+02	.1327E+02	.6046E+01	.2387E+01
10.0	.1562E+03	.1454E+02	.1174E+02	.8210E+01	.4977E+01	.2616E+01	.1191E+01	.4704E+00
X3/X2(CM)	0.0	2.0	4.0	6.0	8.0	10.0	12.0	14.0

(C) EQUATION 2-45 WITH CONSTANT DIFFUSIVITIES IN X3-DIRECTION (PPM/C.C.)

30.0	.2352E+02	.2189E+02	.1767E+02	.1236E+02	.7493E+01	.3937E+01	.1793E+01	.7081E+00
25.0	.1407E+03	.1310E+03	.1057E+03	.7396E+02	.4484E+02	.2356E+02	.1073E+02	.4238E+01
20.0	.1903E+03	.1771E+03	.1429E+03	.9998E+02	.6062E+02	.3185E+02	.1451E+02	.5729E+01
15.0	.6754E+02	.5823E+02	.4699E+02	.3287E+02	.1993E+02	.1047E+02	.4770E+01	.1883E+01
10.0	.5535E+01	.5153E+01	.4156E+01	.2905E+01	.1763E+01	.9266E+00	.4221E+00	.1666E+00
X3/X2(CM)	0.0	2.0	4.0	6.0	8.0	10.0	12.0	14.0

(D) GAUSSIAN DIFFUSION EQUATION (PPM/C.C.)

30.0	.2493E+02	.2321E+02	.1873E+02	.1310E+02	.7942E+01	.4173E+01	.1901E+01	.7505E+00
25.0	.1416E+03	.1319E+03	.1064E+03	.7441E+02	.4511E+02	.2371E+02	.1080E+02	.4263E+01
20.0	.1981E+03	.1761E+03	.1421E+03	.9939E+02	.6026E+02	.3167E+02	.1442E+02	.5695E+01
15.0	.5941E+02	.5531E+02	.4463E+02	.3122E+02	.1893E+02	.9947E+01	.4531E+01	.1789E+01
10.0	.4389E+01	.4086E+01	.3297E+01	.2306E+01	.1398E+01	.7347E+00	.3347E+00	.1321E+00
X3/X2(CM)	0.0	2.0	4.0	6.0	8.0	10.0	12.0	14.0

(E) EQUATION 2-45 WITH VARYING DIFFUSIVITIES IN X3-DIRECTION (PPM/C.C.)

30.0	.3919E+02	.2810E+02	.2268E+02	.1586E+02	.5618E+01	.3054E+01	.2302E+01	.9089E+00
25.0	.1382E+03	.1276E+03	.1038E+03	.7261E+02	.4402E+02	.2313E+02	.1054E+02	.4160E+01
20.0	.1967E+03	.1723E+03	.1386E+03	.9708E+02	.5886E+02	.3093E+02	.1409E+02	.5563E+01
15.0	.6321E+02	.5385E+02	.4349E+02	.3122E+02	.2014E+02	.1058E+02	.4821E+01	.1903E+01
10.0	.4535E+01	.4194E+01	.3384E+01	.2367E+01	.1435E+01	.7542E+00	.3435E+00	.1356E+00
X3/X2(CM)	0.0	2.0	4.0	6.0	8.0	10.0	12.0	14.0

Table 6.8. Comparison of turbulent dispersion between measured and predicted concentration distribution, H = 20 cm.

(c)

U(FREE STREAM) = 200.0 CM/SEC U1RMS= 11.6 CM/SEC LOCAL VEL.) = 179.7 CM/SEC
RELEASE HEIGHT = 21.5 CM U2RMS= 7.0 CM/SEC VEL. GRADIENT = 1.200 1/SEC
DOWNWIND DIST. = 100.0 CM U3RMS= 5.5 CM/SEC SOLENOID STRENGTH = 10 % METHANE

(A) DIFFUSION MEASUREMENTS IN THE WIND TUNNEL (PPM/C.C.)

40.0	.5391E+00	.5769E+00	0.	.5769E+00	0.	.5769E+00	.6053E+00	.9032E+00
30.0	.1419E+02	.1202E+02	.9750E+01	.6771E+01	.3130E+01	.1712E+01	.1162E+01	.7519E+00
20.0	.2559E+03	.2239E+03	.1759E+03	.1140E+03	.6938E+02	.3514E+02	.1636E+02	.6942E+01
10.0	.6139E+01	.4691E+01	.3225E+01	.3130E+01	.2466E+01	.1759E+01	.1261E+01	.8133E+00
0.0	.5769E+00	.4923E+00	.6715E+00	.5769E+00	.4350E+00	.6147E+00	.5532E+00	.5063E+00
X3/X2(CM)	0.0	2.0	4.0	6.0	8.0	10.0	12.0	14.0

(B) EQUATION 2-44 WITH CONSTANT DIFFUSIVITIES IN X3-DIRECTION (PPM/C.C.)

40.0	.7677E-01	.7406E-01	.6653E-01	.5564E-01	.4332E-01	.3141E-01	.2120E-01	.1332E-01
30.0	.2631E+02	.2567E+02	.2324E+02	.1944E+02	.1514E+02	.1097E+02	.7405E+01	.4653E+01
20.0	.1911E+03	.9751E+02	.8759E+02	.7326E+02	.5704E+02	.4135E+02	.2791E+02	.1754E+02
10.0	.3291E+02	.3166E+02	.2844E+02	.2377E+02	.1852E+02	.1343E+02	.9062E+01	.5694E+01
0.0	.1613E+02	.1563E+02	.1404E+02	.1174E+02	.9141E+01	.6626E+01	.4472E+01	.2810E+01
X3/X2(CM)	0.0	2.0	4.0	6.0	8.0	10.0	12.0	14.0

(C) EQUATION 2-45 WITH CONSTANT DIFFUSIVITIES IN X3-DIRECTION (PPM/C.C.)

40.0	.5472E+00	.5280E+00	.4743E+00	.3967E+00	.3096E+00	.2239E+00	.1511E+00	.9494E-01
30.0	.3499E+02	.3309E+02	.2973E+02	.2486E+02	.1936E+02	.1403E+02	.9471E+01	.5951E+01
20.0	.9933E+02	.9493E+02	.8523E+02	.7129E+02	.5550E+02	.4024E+02	.2716E+02	.1706E+02
10.0	.1702E+02	.1642E+02	.1475E+02	.1234E+02	.9606E+01	.6964E+01	.4700E+01	.2953E+01
0.0	.7172E+01	.6920E+01	.6216E+00	.5198E+00	.4046E+00	.2934E+00	.1980E+00	.1244E+00
X3/X2(CM)	0.0	2.0	4.0	6.0	8.0	10.0	12.0	14.0

(D) GAUSSIAN DIFFUSION EQUATION (PPM/C.C.)

40.0	.7171E+00	.6670E+00	.6172E+00	.5167E+00	.4019E+00	.2914E+00	.1966E+00	.1236E+00
30.0	.3547E+02	.3422E+02	.3074E+02	.2571E+02	.2002E+02	.1451E+02	.9795E+01	.6154E+01
20.0	.9770E+02	.9427E+02	.8468E+02	.7082E+02	.5514E+02	.3998E+02	.2698E+02	.1695E+02
10.0	.1499E+02	.1436E+02	.1293E+02	.1079E+02	.8400E+01	.6089E+01	.4110E+01	.2582E+01
0.0	.2597E+00	.2419E+00	.2173E+00	.1817E+00	.1415E+00	.1026E+00	.6924E-01	.4350E-01
X3/X2(CM)	0.0	2.0	4.0	6.0	8.0	10.0	12.0	14.0

(E) EQUATION 2-45 WITH VARYING DIFFUSIVITIES IN X3-DIRECTION (PPM/C.C.)

40.0	.1507E+01	.1454E+01	.1300E+01	.1092E+01	.8504E+00	.6165E+00	.4151E+00	.2614E+00
30.0	.3737E+02	.3605E+02	.3234E+02	.2709E+02	.2109E+02	.1529E+02	.1032E+02	.6494E+01
20.0	.9942E+02	.9207E+02	.8271E+02	.6917E+02	.5386E+02	.3904E+02	.2635E+02	.1656E+02
10.0	.1576E+02	.1520E+02	.1366E+02	.1143E+02	.8894E+01	.6447E+01	.4351E+01	.2734E+01
0.0	.7714E-01	.7059E-01	.6341E-01	.5304E-01	.4130E-01	.2994E-01	.2020E-01	.1269E-01
X3/X2(CM)	0.0	2.0	4.0	6.0	8.0	10.0	12.0	14.0

Table 6.8. Comparison of turbulent dispersion between measured and predicted concentration distribution, H = 20 cm.

(d)

FREE STREAM U = 200.0 CM/SEC	U1RMS= 11.5 CM/SEC	CENTERLINE VEL. = 179.7 CM/SEC	
RELEASE HEIGHT = 21.5 CM	U2RMS= 7.0 CM/SEC	VEL. GRADIENT = 1.203 1/SEC	
DOWNWIND DIST. = 150.0 CM	U3RMS= 4.5 CM/SEC	SOURCE STRENGTH = 10 % METHANE	

(A) DIFFUSION MEASUREMENTS IN THE WIND TUNNEL (PPM/C.C.)

40.0	.1014E+01	.1048E+01	.4201E+00	.1994E+01	.9030E+00	.5175E+00	.6692E+00	.9079E+00
30.0	.7616E+02	.2761E+02	.2141E+02	.1358E+02	.6567E+01	.3013E+01	.1671E+01	.1115E+01
20.0	.1370E+03	.1323E+03	.1077E+03	.7185E+02	.3954E+02	.1870E+02	.7644E+01	.3120E+01
10.0	.2017E+02	.1935E+02	.1517E+02	.1180E+02	.8688E+01	.4658E+01	.2564E+01	.1313E+01
0.0	.1193E+01	.8644E+00	.8740E+00	.9745E+00	.6592E+00	.6342E+00	.8016E+00	.7920E+00
X3/X2(CM)	0.0	3.0	6.0	9.0	12.0	15.0	18.0	21.0

(B) EQUATION 2-44 WITH CONSTANT DIFFUSIVITIES IN X3-DIRECTION (PPM/C.C.)

40.0	.9345E+00	.5066E+00	.4313E+00	.3230E+00	.2267E+00	.1399E+00	.7757E-01	.3854E-01
30.0	.2723E+02	.2508E+02	.2197E+02	.1450E+02	.1155E+02	.7126E+01	.3951E+01	.1908E+01
20.0	.6876E+02	.6517E+02	.5549E+02	.4244E+02	.2916E+02	.1800E+02	.9978E+01	.4970E+01
10.0	.3713E+02	.3519E+02	.2997E+02	.2292E+02	.1575E+02	.9719E+01	.5386E+01	.2684E+01
0.0	.2719E+02	.2577E+02	.2194E+02	.1677E+02	.1153E+02	.7117E+01	.3946E+01	.1965E+01
X3/X2(CM)	0.0	3.0	6.0	9.0	12.0	15.0	18.0	21.0

(C) EQUATION 2-45 WITH CONSTANT DIFFUSIVITIES IN X3-DIRECTION (PPM/C.C.)

40.0	.2063E+01	.1955E+01	.1665E+01	.1277E+01	.8749E+00	.5400E+00	.2994E+00	.1491E+00
30.0	.3268E+02	.3097E+02	.2637E+02	.2017E+02	.1386E+02	.8553E+01	.4742E+01	.2362E+01
20.0	.6633E+02	.6286E+02	.5352E+02	.4094E+02	.2813E+02	.1736E+02	.9625E+01	.4794E+01
10.0	.2095E+02	.1976E+02	.1682E+02	.1287E+02	.8840E+01	.5456E+01	.3025E+01	.1507E+01
0.0	.3225E+01	.3056E+01	.2602E+01	.1990E+01	.1367E+01	.8440E+00	.4680E+00	.2331E+00
X3/X2(CM)	0.0	3.0	6.0	9.0	12.0	15.0	18.0	21.0

(D) GAUSSIAN DIFFUSION EQUATION (PPM/C.C.)

40.0	.2475E+01	.2346E+01	.1997E+01	.1529E+01	.1050E+01	.6476E+00	.3592E+00	.1789E+00
30.0	.3351E+02	.3176E+02	.2704E+02	.2068E+02	.1421E+02	.8770E+01	.4863E+01	.2422E+01
20.0	.6594E+02	.6248E+02	.5318E+02	.4068E+02	.2792E+02	.1723E+02	.9555E+01	.4759E+01
10.0	.1979E+02	.1868E+02	.1590E+02	.1215E+02	.7966E+01	.4917E+01	.2726E+01	.1358E+01
0.0	.1555E+01	.1474E+01	.1255E+01	.9597E+00	.6594E+00	.4070E+00	.2257E+00	.1124E+00
X3/X2(CM)	0.0	3.0	6.0	9.0	12.0	15.0	18.0	21.0

(E) EQUATION 2-45 WITH VARYING DIFFUSIVITIES IN X3-DIRECTION (PPM/C.C.)

40.0	.3907E+01	.3703E+01	.3152E+01	.2411E+01	.1657E+01	.1023E+01	.5669E+00	.2824E+00
30.0	.3379E+02	.3197E+02	.2722E+02	.2082E+02	.1431E+02	.8829E+01	.4895E+01	.2438E+01
20.0	.6642E+02	.6291E+02	.5354E+02	.4097E+02	.2812E+02	.1736E+02	.9624E+01	.4795E+01
10.0	.2016E+02	.1911E+02	.1627E+02	.1244E+02	.8549E+01	.5276E+01	.2926E+01	.1457E+01
0.0	.7951E+00	.7441E+00	.6336E+00	.4844E+00	.3329E+00	.2055E+00	.1139E+00	.5675E-01
X3/X2(CM)	0.0	3.0	6.0	9.0	12.0	15.0	18.0	21.0

Table 6.8. Comparison of turbulent dispersion between measured and predicted concentration distribution, H = 20 cm.

(e)

DIRECT STREAM : 200.0 CM/SEC U1RMS: 11.6 CM/SEC CELLULAR VEL. : 179.7 CM/SEC
RELEASE HEIGHT : 21.5 CM U2RMS: 7.0 CM/SEC VEL. GRADIENT : 1.200 1/SEC
DOWNWIND DIST. : 200.0 CM U3RMS: 5.5 CM/SEC SOURCE STRENGTH : 10 % METHANE

(A) DIFFUSION MEASUREMENTS IN THE WIND TUNNEL (PPM/C.C.)

40.0	.9803E+00	.9175E+00	.8270E+00	.7032E+00	.5616E+00	.5167E+00	.4508E+00	.3650E+00
30.0	.2020E+02	.3136E+02	.2869E+02	.2048E+02	.1179E+02	.6056E+01	.2786E+01	.1492E+01
20.0	.9051E+02	.9098E+02	.8557E+02	.7148E+02	.5136E+02	.3021E+02	.1507E+02	.7084E+01
10.0	.2100E+02	.2315E+02	.2274E+02	.2017E+02	.1838E+02	.1305E+02	.7070E+01	.3675E+01
0.0	.8258E+00	.9223E+00	.9656E+00	.9417E+00	.7340E+00	.6161E+00	.5264E+00	.4029E+00
X3/X2(CM)	0.0	3.0	6.0	9.0	12.0	15.0	18.0	21.0

(B) EQUATION 2-44 WITH CONSTANT DIFFUSIVITIES IN X3-DIRECTION (PPM/C.C.)

40.0	.1297E+01	.1246E+01	.1105E+01	.9035E+00	.6816E+00	.4748E+00	.3051E+00	.1809E+00
30.0	.2536E+02	.2427E+02	.2151E+02	.1759E+02	.1326E+02	.9244E+01	.5940E+01	.3522E+01
20.0	.5257E+02	.5056E+02	.4476E+02	.3661E+02	.2763E+02	.1924E+02	.1236E+02	.7329E+01
10.0	.3727E+02	.3580E+02	.3173E+02	.2595E+02	.1956E+02	.1364E+02	.8763E+01	.5196E+01
0.0	.3191E+02	.3065E+02	.2717E+02	.2222E+02	.1677E+02	.1168E+02	.7502E+01	.4448E+01
X3/X2(CM)	0.0	3.0	6.0	9.0	12.0	15.0	18.0	21.0

(C) EQUATION 2-45 WITH CONSTANT DIFFUSIVITIES IN X3-DIRECTION (PPM/C.C.)

40.0	.3690E+01	.3535E+01	.3134E+01	.2563E+01	.1934E+01	.1347E+01	.8654E+00	.5131E+00
30.0	.2931E+02	.2815E+02	.2495E+02	.2041E+02	.1540E+02	.1073E+02	.6891E+01	.4086E+01
20.0	.5098E+02	.4899E+02	.4342E+02	.3548E+02	.2681E+02	.1832E+02	.1177E+02	.6979E+01
10.0	.2132E+02	.2048E+02	.1815E+02	.1485E+02	.1120E+02	.7802E+01	.5013E+01	.2972E+01
0.0	.8263E+01	.6615E+01	.5932E+01	.4861E+01	.3691E+01	.2592E+01	.1672E+01	.1730E+00
X3/X2(CM)	0.0	3.0	6.0	9.0	12.0	15.0	18.0	21.0

(D) GAUSSIAN DIFFUSION EQUATION (PPM/C.C.)

40.0	.4239E+01	.4072E+01	.3609E+01	.2953E+01	.2227E+01	.1551E+01	.9966E+00	.5909E+00
30.0	.2992E+02	.2874E+02	.2547E+02	.2083E+02	.1572E+02	.1095E+02	.7034E+01	.4170E+01
20.0	.4965E+02	.4769E+02	.4227E+02	.3457E+02	.2609E+02	.1817E+02	.1167E+02	.6921E+01
10.0	.1943E+02	.1865E+02	.1653E+02	.1352E+02	.1020E+02	.7105E+01	.4565E+01	.2707E+01
0.0	.3957E+01	.3417E+01	.3029E+01	.2477E+01	.1869E+01	.1302E+01	.8363E+00	.4959E+00
X3/X2(CM)	0.0	3.0	6.0	9.0	12.0	15.0	18.0	21.0

(E) EQUATION 2-45 WITH VARYING DIFFUSIVITIES IN X3-DIRECTION (PPM/C.C.)

40.0	.5782E+01	.5554E+01	.4923E+01	.4026E+01	.3039E+01	.2116E+01	.1360E+01	.8060E+00
30.0	.2947E+02	.2831E+02	.2509E+02	.2052E+02	.1549E+02	.1078E+02	.6929E+01	.4106E+01
20.0	.4968E+02	.4676E+02	.4145E+02	.3390E+02	.2558E+02	.1781E+02	.1145E+02	.6786E+01
10.0	.2101E+02	.2018E+02	.1788E+02	.1463E+02	.1104E+02	.7688E+01	.4946E+01	.2929E+01
0.0	.3326E+01	.2235E+01	.1981E+01	.1620E+01	.1223E+01	.8513E+00	.5470E+00	.3243E+00
X3/X2(CM)	0.0	3.0	6.0	9.0	12.0	15.0	18.0	21.0

Table 6.8. Comparison of turbulent dispersion between measured and predicted concentration distribution, H = 20 cm.

(f)

HEIGHT STREAM) = 200.0 CM/SEC U1RMS= 11.4 CM/SEC U(LOCAL VEL.) = 179.7 CM/SEC
RELEASE HEIGHT = 21.5 CM U2RMS= 7.0 CM/SEC VEL. GRADIENT = 1.200 1/SEC
DOWNWIND DIST. = 350.0 CM U3RMS= 5.5 CM/SEC SOLACE STRENGTH = 10 % METHANE

(A) DIFFUSION MEASUREMENTS IN THE WIND TUNNEL (PPM/C.C.)

40.0	.2188E+01	.2289E+01	.1140E+01	.1917E+01	.1661E+01	.1149E+01	.8644E+00	.7726E+00
30.0	.3132E+02	.3284E+02	.3140E+02	.2531E+02	.1830E+02	.1192E+02	.6920E+01	.4114E+01
20.0	.6395E+02	.6380E+02	.6230E+02	.5544E+02	.4478E+02	.3253E+02	.2167E+02	.1163E+02
10.0	.2144E+02	.2302E+02	.2258E+02	.2121E+02	.2014E+02	.1576E+02	.1064E+02	.6621E+01
0.0	.2274E+01	.2516E+01	.2487E+01	.2535E+01	.2173E+01	.1621E+01	.1415E+01	.1236E+01
X3/X2(CM)	0.0	3.0	6.0	9.0	12.0	15.0	18.0	21.0

(B) EQUATION 2-44 WITH CONSTANT DIFFUSIVITIES IN X3-DIRECTION (PPM/C.C.)

40.0	.2103E+01	.2036E+01	.1849E+01	.1574E+01	.1257E+01	.9407E+00	.6604E+00	.4347E+00
30.0	.2102E+02	.2229E+02	.2024E+02	.1723E+02	.1376E+02	.1030E+02	.7230E+01	.4759E+01
20.0	.4299E+02	.4163E+02	.3780E+02	.3218E+02	.2569E+02	.1923E+02	.1350E+02	.8887E+01
10.0	.3692E+02	.3479E+02	.3156E+02	.2689E+02	.2147E+02	.1607E+02	.1128E+02	.7427E+01
0.0	.3311E+02	.3206E+02	.2911E+02	.2479E+02	.1979E+02	.1482E+02	.1040E+02	.6846E+01
X3/X2(CM)	0.0	3.0	6.0	9.0	12.0	15.0	18.0	21.0

(C) EQUATION 2-45 WITH CONSTANT DIFFUSIVITIES IN X3-DIRECTION (PPM/C.C.)

40.0	.4953E+01	.4796E+01	.4355E+01	.3708E+01	.2960E+01	.2216E+01	.1556E+01	.1024E+01
30.0	.2611E+02	.2526E+02	.2296E+02	.1955E+02	.1561E+02	.1168E+02	.8231E+01	.5398E+01
20.0	.4023E+02	.3895E+02	.3537E+02	.3012E+02	.2404E+02	.1800E+02	.1263E+02	.8317E+01
10.0	.2073E+02	.2007E+02	.1823E+02	.1552E+02	.1239E+02	.9275E+01	.6511E+01	.4286E+01
0.0	.8950E+01	.8670E+01	.7882E+01	.6716E+01	.5360E+01	.3960E+01	.2780E+01	.1830E+01
X3/X2(CM)	0.0	3.0	6.0	9.0	12.0	15.0	18.0	21.0

(D) GAUSSIAN DIFFUSION EQUATION (PPM/C.C.)

40.0	.5565E+01	.5389E+01	.4893E+01	.4164E+01	.3326E+01	.2490E+01	.1749E+01	.1151E+01
30.0	.2657E+02	.2573E+02	.2336E+02	.1989E+02	.1588E+02	.1189E+02	.8345E+01	.5493E+01
20.0	.3985E+02	.3859E+02	.3504E+02	.2983E+02	.2382E+02	.1783E+02	.1252E+02	.8239E+01
10.0	.1890E+02	.1830E+02	.1662E+02	.1415E+02	.1130E+02	.8457E+01	.5937E+01	.3906E+01
0.0	.5556E+01	.5380E+01	.4885E+01	.4159E+01	.3321E+01	.2486E+01	.1745E+01	.1149E+01
X3/X2(CM)	0.0	3.0	6.0	9.0	12.0	15.0	18.0	21.0

(E) EQUATION 2-45 WITH VARYING DIFFUSIVITIES IN X3-DIRECTION (PPM/C.C.)

40.0	.6959E+01	.6739E+01	.6119E+01	.5210E+01	.4159E+01	.3114E+01	.2186E+01	.1439E+01
30.0	.2595E+02	.2503E+02	.2273E+02	.1935E+02	.1545E+02	.1157E+02	.8120E+01	.5345E+01
20.0	.3917E+02	.3793E+02	.3444E+02	.2933E+02	.2341E+02	.1753E+02	.1230E+02	.8098E+01
10.0	.2054E+02	.1989E+02	.1806E+02	.1538E+02	.1228E+02	.9191E+01	.6452E+01	.4247E+01
0.0	.4204E+01	.4073E+01	.3698E+01	.3149E+01	.2514E+01	.1882E+01	.1321E+01	.8695E+00
X3/X2(CM)	0.0	3.0	6.0	9.0	12.0	15.0	18.0	21.0

Table 6.8. Comparison of turbulent dispersion between measured and predicted concentration distribution, H = 20 cm.

(g)

U(FREE STREAM) = 200.0 CM/SEC U1RMS= 11.5 CM/SEC U(LOCAL VEL.) = 179.7 CM/SEC
RELEASE HEIGHT = 21.5 CM U2RMS= 7.0 CM/SEC VEL. GRADIENT = 1.230 1/SEC
DOWNWIND DIST. = 300.0 CM U3RMS= 5.5 CM/SEC SOURCE STRENGTH = 10 % METHANE

(A) DIFFUSION MEASUREMENTS IN THE WIND TUNNEL (PPM/C.C.)

40.0	.6223E+01	.6193E+01	.5253E+01	.4267E+01	.3400E+01	.2327E+01	.1612E+01	.1258E+01
30.0	.4195E+02	.4211E+02	.3631E+02	.2744E+02	.1825E+02	.5796E+01	.5422E+01	.2362E+01
20.0	.4491E+02	.4702E+02	.4351E+02	.3649E+02	.2725E+02	.1621E+02	.5115E+01	.4297E+01
10.0	.1313E+02	.1363E+02	.1313E+02	.1256E+02	.1087E+02	.7067E+01	.4379E+01	.2439E+01
0.0	.2711E+01	.2607E+01	.2474E+01	.2393E+01	.2073E+01	.1711E+01	.1323E+01	.1116E+01
X3/X2(CM)	0.0	4.0	8.0	12.0	16.0	20.0	24.0	28.0

(B) EQUATION 2-44 WITH CONSTANT DIFFUSIVITIES IN X3-DIRECTION (PPM/C.C.)

40.0	.2809E+01	.2678E+01	.2321E+01	.1928E+01	.1310E+01	.8531E+00	.5050E+00	.2716E+00
30.0	.2098E+02	.2001E+02	.1734E+02	.1366E+02	.9785E+01	.6374E+01	.3774E+01	.2031E+01
20.0	.3670E+02	.3499E+02	.3033E+02	.2390E+02	.1712E+02	.1115E+02	.6600E+01	.3552E+01
10.0	.3405E+02	.3247E+02	.2814E+02	.2217E+02	.1588E+02	.1034E+02	.6124E+01	.3296E+01
0.0	.3264E+02	.3112E+02	.2697E+02	.2125E+02	.1522E+02	.9914E+01	.5869E+01	.3159E+01
X3/X2(CM)	0.0	4.0	8.0	12.0	16.0	20.0	24.0	28.0

(C) EQUATION 2-45 WITH CONSTANT DIFFUSIVITIES IN X3-DIRECTION (PPM/C.C.)

40.0	.5939E+01	.5667E+01	.4825E+01	.3902E+01	.2724E+01	.1774E+01	.1050E+01	.5651E+00
30.0	.2333E+02	.2229E+02	.1932E+02	.1523E+02	.1091E+02	.7103E+01	.4205E+01	.2263E+01
20.0	.3366E+02	.3209E+02	.2781E+02	.2192E+02	.1570E+02	.1022E+02	.6052E+01	.3257E+01
10.0	.1984E+02	.1894E+02	.1642E+02	.1294E+02	.9266E+01	.6034E+01	.3572E+01	.1922E+01
0.0	.1077E+02	.1026E+02	.8897E+01	.7011E+01	.5022E+01	.3270E+01	.1936E+01	.1042E+01
X3/X2(CM)	0.0	4.0	8.0	12.0	16.0	20.0	24.0	28.0

(D) GAUSSIAN DIFFUSION EQUATION (PPM/C.C.)

40.0	.6453E+01	.6152E+01	.5333E+01	.4282E+01	.3010E+01	.1960E+01	.1160E+01	.6245E+00
30.0	.2374E+02	.2264E+02	.1962E+02	.1546E+02	.1107E+02	.7212E+01	.4269E+01	.2295E+01
20.0	.3729E+02	.3174E+02	.2751E+02	.2168E+02	.1553E+02	.1011E+02	.5986E+01	.3222E+01
10.0	.1895E+02	.1721E+02	.1492E+02	.1176E+02	.8422E+01	.5484E+01	.3247E+01	.1747E+01
0.0	.7233E+01	.6896E+01	.5977E+01	.4710E+01	.3374E+01	.2197E+01	.1301E+01	.7000E+00
X3/X2(CM)	0.0	4.0	8.0	12.0	16.0	20.0	24.0	28.0

(E) EQUATION 2-45 WITH VARYING DIFFUSIVITIES IN X3-DIRECTION (PPM/C.C.)

40.0	.7619E+01	.7264E+01	.6296E+01	.4961E+01	.3554E+01	.2314E+01	.1370E+01	.7373E+00
30.0	.2799E+02	.2668E+02	.2313E+02	.1823E+02	.1306E+02	.8504E+01	.5035E+01	.2709E+01
20.0	.3780E+02	.3127E+02	.2711E+02	.2136E+02	.1530E+02	.9964E+01	.5899E+01	.3175E+01
10.0	.1964E+02	.1873E+02	.1623E+02	.1279E+02	.9162E+01	.5966E+01	.3532E+01	.1901E+01
0.0	.5993E+01	.5720E+01	.4956E+01	.3907E+01	.2798E+01	.1822E+01	.1079E+01	.5806E+00
X3/X2(CM)	0.0	4.0	8.0	12.0	16.0	20.0	24.0	28.0

Table 6.8. Comparison of turbulent dispersion between measured and predicted concentration distribution, H = 20 cm.

(h)

U(FREE STREAM) = 200.0 CM/SEC U1RMS= 11.6 CM/SEC U(LOCAL VEL.) = 179.7 CM/SEC
RELEASE HEIGHT = 21.5 CM U2RMS= 7.0 CM/SEC VEL. GRADIENT = 1.200 1/SEC
DOWNWIND DIST. = 400.0 CM U3RMS= 5.5 CM/SEC SOURCE STRENGTH = 10 % METHANE

(A) DIFFUSION MEASUREMENTS IN THE WIND TUNNEL (PPM/C.C.)

40.0	.7239E+01	.7032E+01	.4586E+01	.3972E+01	.2426E+01	.1396E+01	.9609E+00	.8144E+00
30.0	.3100E+02	.3063E+02	.2497E+02	.1837E+02	.1031E+02	.5451E+01	.2663E+01	.1280E+01
20.0	.3397E+02	.3343E+02	.3099E+02	.2423E+02	.1603E+02	.9062E+01	.4447E+01	.2292E+01
10.0	.1495E+02	.1652E+02	.1657E+02	.1375E+02	.1023E+02	.6196E+01	.3295E+01	.1724E+01
0.0	.6739E+01	.6855E+01	.6351E+01	.5701E+01	.4244E+01	.3072E+01	.1844E+01	.1073E+01
X3/X2(CM)	0.0	5.0	10.0	15.0	20.0	25.0	30.0	35.0

(B) EQUATION 2-44 WITH CONSTANT DIFFUSIVITIES IN X3-DIRECTION (PPM/C.C.)

40.0	.3810E+01	.3603E+01	.3047E+01	.2305E+01	.1559E+01	.9431E+00	.5102E+00	.2461E+00
30.0	.1776E+02	.1680E+02	.1421E+02	.1075E+02	.7266E+01	.4397E+01	.2379E+01	.1151E+01
20.0	.2994E+02	.2736E+02	.2315E+02	.1751E+02	.1184E+02	.7164E+01	.3876E+01	.1875E+01
10.0	.3009E+02	.2846E+02	.2407E+02	.1820E+02	.1231E+02	.7448E+01	.4029E+01	.1950E+01
0.0	.2989E+02	.2827E+02	.2391E+02	.1808E+02	.1223E+02	.7396E+01	.4003E+01	.1937E+01
X3/X2(CM)	0.0	5.0	10.0	15.0	20.0	25.0	30.0	35.0

(C) EQUATION 2-45 WITH CONSTANT DIFFUSIVITIES IN X3-DIRECTION (PPM/C.C.)

40.0	.6759E+01	.6392E+01	.5406E+01	.4089E+01	.2766E+01	.1673E+01	.9051E+00	.4372E+00
30.0	.1920E+02	.1816E+02	.1536E+02	.1162E+02	.7857E+01	.4753E+01	.2571E+01	.1244E+01
20.0	.2548E+02	.2409E+02	.2037E+02	.1541E+02	.1042E+02	.6306E+01	.3411E+01	.1650E+01
10.0	.1814E+02	.1716E+02	.1451E+02	.1097E+02	.7423E+01	.4490E+01	.2429E+01	.1175E+01
0.0	.1393E+02	.1223E+02	.1034E+02	.7820E+01	.5296E+01	.3200E+01	.1731E+01	.8375E+00
X3/X2(CM)	0.0	5.0	10.0	15.0	20.0	25.0	30.0	35.0

(D) GAUSSIAN DIFFUSION EQUATION (PPM/C.C.)

40.0	.7313E+01	.6916E+01	.5949E+01	.4424E+01	.2992E+01	.1810E+01	.9792E+00	.4738E+00
30.0	.1943E+02	.1837E+02	.1554E+02	.1175E+02	.7950E+01	.4809E+01	.2602E+01	.1259E+01
20.0	.2508E+02	.2372E+02	.2006E+02	.1517E+02	.1026E+02	.6207E+01	.3356E+01	.1624E+01
10.0	.1433E+02	.1354E+02	.1306E+02	.9875E+01	.6683E+01	.4042E+01	.2187E+01	.1058E+01
0.0	.9674E+01	.8959E+01	.7577E+01	.5731E+01	.3876E+01	.2345E+01	.1269E+01	.6138E+00
X3/X2(CM)	0.0	5.0	10.0	15.0	20.0	25.0	30.0	35.0

(E) EQUATION 2-45 WITH VARYING DIFFUSIVITIES IN X3-DIRECTION (PPM/C.C.)

40.0	.8045E+01	.7608E+01	.6434E+01	.4867E+01	.3292E+01	.1991E+01	.1077E+01	.5212E+00
30.0	.1861E+02	.1760E+02	.1489E+02	.1126E+02	.7617E+01	.4607E+01	.2493E+01	.1206E+01
20.0	.2492E+02	.2348E+02	.1985E+02	.1502E+02	.1016E+02	.6144E+01	.3324E+01	.1608E+01
10.0	.1769E+02	.1673E+02	.1415E+02	.1070E+02	.7237E+01	.4375E+01	.2368E+01	.1146E+01
0.0	.9714E+01	.9241E+01	.6969E+01	.5271E+01	.3566E+01	.2157E+01	.1167E+01	.5646E+00
X3/X2(CM)	0.0	5.0	10.0	15.0	20.0	25.0	30.0	35.0

Table 6.8. Comparison of turbulent dispersion between measured and predicted concentration distribution, H = 20 cm.

(i)

U(FREE STREAM) = 200.0 CM/SEC U1RMS= 11.5 CM/SEC U(LOCAL VEL.) = 179.7 CM/SEC
RELEASE HEIGHT = 21.5 CM U2RMS= 7.0 CM/SEC VEL. GRADIENT = 1.200 1/SEC
DOWNWIND DIST. = 500.0 CM U3RMS= 5.5 CM/SEC SOURCE STRENGTH = 10 % METHANE

(A) DIFFUSION MEASUREMENTS IN THE WIND TUNNEL (PPM/C.C.)

40.0	.1000E+02	.9430E+01	.7616E+01	.5749E+01	.3382E+01	.2042E+01	.1359E+01	.1036E+01
30.0	.2544E+02	.2528E+02	.2184E+02	.1732E+02	.1100E+02	.6842E+01	.3924E+01	.2196E+01
20.0	.3885E+02	.2559E+02	.2414E+02	.2111E+02	.1537E+02	.9855E+01	.5332E+01	.3378E+01
10.0	.1549E+02	.1570E+02	.1524E+02	.1321E+02	.1036E+02	.7414E+01	.4796E+01	.3460E+01
0.0	.9107E+01	.9142E+01	.8394E+01	.7186E+01	.5974E+01	.4977E+01	.3142E+01	.2080E+01
X3/X2(CM)	0.0	5.0	10.0	15.0	20.0	25.0	30.0	35.0

(B) EQUATION 2-44 WITH CONSTANT DIFFUSIVITIES IN X3-DIRECTION (PPM/C.C.)

40.0	.4371E+01	.4180E+01	.3656E+01	.2994E+01	.2138E+01	.1430E+01	.8750E+00	.4695E+00
30.0	.1566E+02	.1479E+02	.1293E+02	.1034E+02	.7566E+01	.5061E+01	.3396E+01	.1732E+01
20.0	.2427E+02	.2320E+02	.2029E+02	.1623E+02	.1187E+02	.7941E+01	.4856E+01	.2716E+01
10.0	.2454E+02	.2538E+02	.2220E+02	.1776E+02	.1299E+02	.8686E+01	.5313E+01	.2972E+01
0.0	.2674E+02	.2557E+02	.2236E+02	.1788E+02	.1308E+02	.8749E+01	.5352E+01	.2994E+01
X3/X2(CM)	0.0	5.0	10.0	15.0	20.0	25.0	30.0	35.0

(C) EQUATION 2-45 WITH CONSTANT DIFFUSIVITIES IN X3-DIRECTION (PPM/C.C.)

40.0	.7019E+01	.6712E+01	.5870E+01	.4808E+01	.3434E+01	.2297E+01	.1405E+01	.7861E+00
30.0	.1625E+02	.1554E+02	.1359E+02	.1087E+02	.7950E+01	.5318E+01	.3253E+01	.1820E+01
20.0	.2045E+02	.1975E+02	.1727E+02	.1381E+02	.1010E+02	.6759E+01	.4134E+01	.2313E+01
10.0	.1668E+02	.1595E+02	.1395E+02	.1114E+02	.8156E+01	.5456E+01	.3336E+01	.1868E+01
0.0	.1369E+02	.1309E+02	.1145E+02	.9159E+01	.6699E+01	.4481E+01	.2741E+01	.1533E+01
X3/X2(CM)	0.0	5.0	10.0	15.0	20.0	25.0	30.0	35.0

(D) GAUSSIAN DIFFUSION EQUATION (PPM/C.C.)

40.0	.7495E+01	.7167E+01	.6268E+01	.5013E+01	.3667E+01	.2453E+01	.1500E+01	.8394E+00
30.0	.1639E+02	.1567E+02	.1370E+02	.1096E+02	.8017E+01	.5362E+01	.3280E+01	.1835E+01
20.0	.2310E+02	.2193E+02	.1918E+02	.1534E+02	.1122E+02	.7506E+01	.4590E+01	.2568E+01
10.0	.1491E+02	.1426E+02	.1247E+02	.9971E+01	.7293E+01	.4877E+01	.2984E+01	.1669E+01
0.0	.1059E+02	.1013E+02	.8857E+01	.7084E+01	.5181E+01	.3466E+01	.2120E+01	.1186E+01
X3/X2(CM)	0.0	5.0	10.0	15.0	20.0	25.0	30.0	35.0

(E) EQUATION 2-45 WITH VARYING DIFFUSIVITIES IN X3-DIRECTION (PPM/C.C.)

40.0	.7913E+01	.7565E+01	.6618E+01	.5293E+01	.3872E+01	.2590E+01	.1584E+01	.8862E+00
30.0	.1565E+02	.1496E+02	.1309E+02	.1047E+02	.7656E+01	.5121E+01	.3133E+01	.1753E+01
20.0	.2005E+02	.1916E+02	.1677E+02	.1341E+02	.9810E+01	.6562E+01	.4014E+01	.2246E+01
10.0	.1431E+02	.1368E+02	.1198E+02	.9581E+01	.7008E+01	.4688E+01	.2868E+01	.1605E+01
0.0	.1027E+02	.9822E+01	.8590E+01	.6870E+01	.5025E+01	.3361E+01	.2056E+01	.1150E+01
X3/X2(CM)	0.0	5.0	10.0	15.0	20.0	25.0	30.0	35.0

Table 6.8. Comparison of turbulent dispersion between measured and predicted concentration distribution, H = 20 cm.

(j)

U(FREE STREAM) = 700.0 CM/SEC U1RMS= 11.6 CM/SEC U(LOCAL VEL.) = 179.7 CM/SEC
RELEASE HEIGHT = 21.5 CM U2RMS= 7.0 CM/SEC VEL. GRADIENT = 1.200 1/SEC
DOWNWIND DIST. = 700.0 CM U3RMS= 5.5 CM/SEC SOURCE STRENGTH = 10 % METHANE

(A) DIFFUSION MEASUREMENTS IN THE WIND TUNNEL (PPM/C.C.)

40.0	.1012E+02	.9709E+01	.7994E+01	.7057E+01	.5493E+01	.4139E+01	.2789E+01	.1973E+01
30.0	.1763E+02	.1503E+02	.1676E+02	.1484E+02	.1167E+02	.8706E+01	.6060E+01	.3902E+01
20.0	.1779E+02	.1608E+02	.1769E+02	.1631E+02	.1369E+02	.1073E+02	.7973E+01	.5703E+01
10.0	.1360E+02	.1445E+02	.1414E+02	.1290E+02	.1101E+02	.8624E+01	.6761E+01	.4809E+01
0.0	.1160E+02	.1150E+02	.1087E+02	.1022E+02	.8966E+01	.7129E+01	.5574E+01	.4152E+01
X3/X2(CM)	0.0	5.0	10.0	15.0	20.0	25.0	30.0	35.0

(B) EQUATION 2-44 WITH CONSTANT DIFFUSIVITIES IN X3-DIRECTION (PPM/C.C.)

40.0	.4783E+01	.4633E+01	.4210E+01	.3588E+01	.2870E+01	.2154E+01	.1516E+01	.1001E+01
30.0	.1243E+02	.1209E+02	.1099E+02	.9365E+01	.7494E+01	.5623E+01	.3958E+01	.2614E+01
20.0	.1766E+02	.1708E+02	.1642E+02	.1400E+02	.1120E+02	.8403E+01	.5915E+01	.3907E+01
10.0	.2107E+02	.2040E+02	.1854E+02	.1581E+02	.1264E+02	.9486E+01	.6677E+01	.4410E+01
0.0	.2140E+02	.2073E+02	.1883E+02	.1606E+02	.1284E+02	.9636E+01	.6783E+01	.4480E+01
X3/X2(CM)	0.0	5.0	10.0	15.0	20.0	25.0	30.0	35.0

(C) EQUATION 2-45 WITH CONSTANT DIFFUSIVITIES IN X3-DIRECTION (PPM/C.C.)

40.0	.4772E+01	.6560E+01	.5961E+01	.5092E+01	.4064E+01	.3059E+01	.2147E+01	.1416E+01
30.0	.1247E+02	.1201E+02	.1098E+02	.9359E+01	.7485E+01	.5617E+01	.3954E+01	.2611E+01
20.0	.1533E+02	.1485E+02	.1349E+02	.1150E+02	.9199E+01	.6902E+01	.4859E+01	.3209E+01
10.0	.1439E+02	.1394E+02	.1267E+02	.1080E+02	.8638E+01	.6482E+01	.4563E+01	.3013E+01
0.0	.1344E+02	.1302E+02	.1183E+02	.1009E+02	.8066E+01	.6052E+01	.4260E+01	.2814E+01
X3/X2(CM)	0.0	5.0	10.0	15.0	20.0	25.0	30.0	35.0

(D) GAUSSIAN DIFFUSION EQUATION (PPM/C.C.)

40.0	.7111E+01	.6887E+01	.6259E+01	.5335E+01	.4267E+01	.3202E+01	.2254E+01	.1499E+01
30.0	.1249E+02	.1209E+02	.1098E+02	.9362E+01	.7488E+01	.5616E+01	.3955E+01	.2612E+01
20.0	.1476E+02	.1430E+02	.1299E+02	.1108E+02	.8856E+01	.6647E+01	.4679E+01	.3090E+01
10.0	.1282E+02	.1242E+02	.1128E+02	.9620E+01	.7694E+01	.5773E+01	.4064E+01	.2684E+01
0.0	.1109E+02	.1074E+02	.9759E+01	.8319E+01	.6654E+01	.4993E+01	.3514E+01	.2321E+01
X3/X2(CM)	0.0	5.0	10.0	15.0	20.0	25.0	30.0	35.0

(E) EQUATION 2-45 WITH VARYING DIFFUSIVITIES IN X3-DIRECTION (PPM/C.C.)

40.0	.7193E+01	.6959E+01	.6322E+01	.5390E+01	.4311E+01	.3235E+01	.2277E+01	.1504E+01
30.0	.1190E+02	.1153E+02	.1047E+02	.8929E+01	.7141E+01	.5358E+01	.3772E+01	.2491E+01
20.0	.1467E+02	.1421E+02	.1291E+02	.1101E+02	.8805E+01	.6607E+01	.4651E+01	.3071E+01
10.0	.1352E+02	.1310E+02	.1190E+02	.1014E+02	.8113E+01	.6088E+01	.4285E+01	.2830E+01
0.0	.1176E+02	.1090E+02	.9908E+01	.8446E+01	.6755E+01	.5069E+01	.3568E+01	.2356E+01
X3/X2(CM)	0.0	5.0	10.0	15.0	20.0	25.0	30.0	35.0

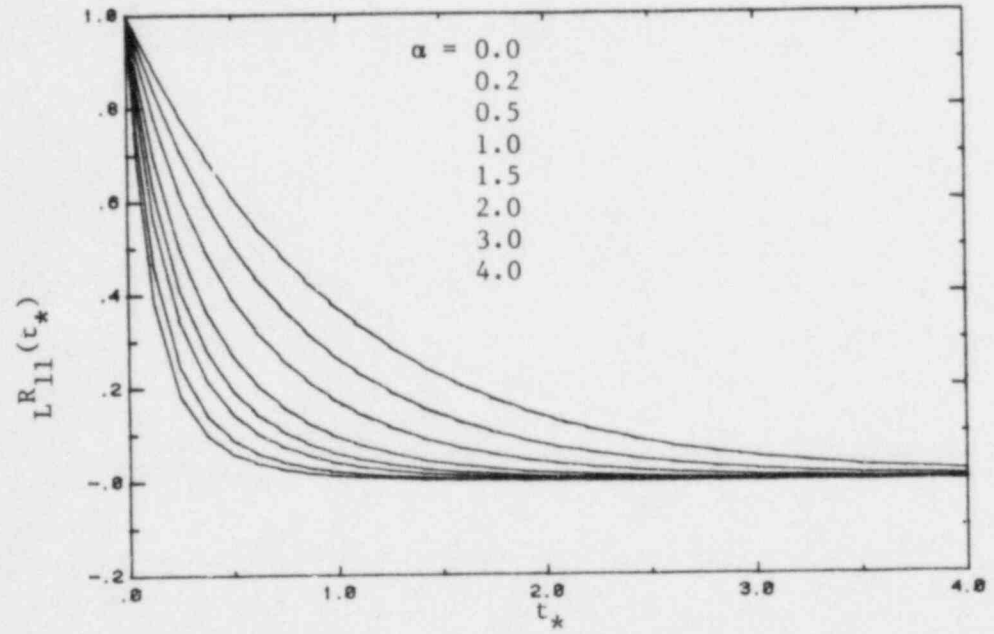

(a) Model I

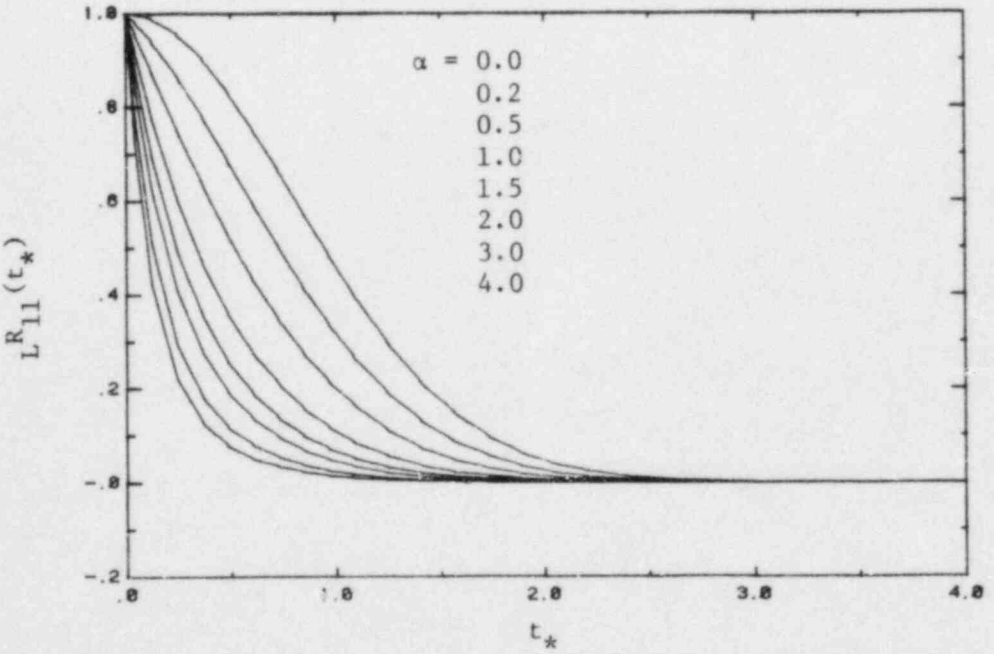

(b) Model II

Figure 6.1. Lagrangian autocorrelation function in a homogeneous isotropic uniform turbulent flow.

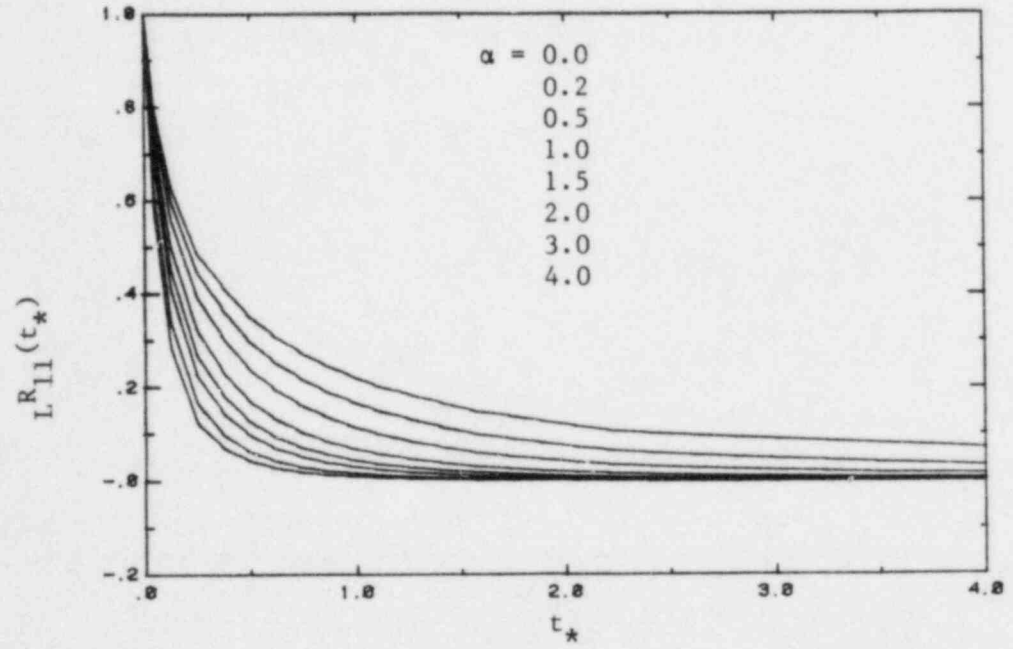

(c) Model III

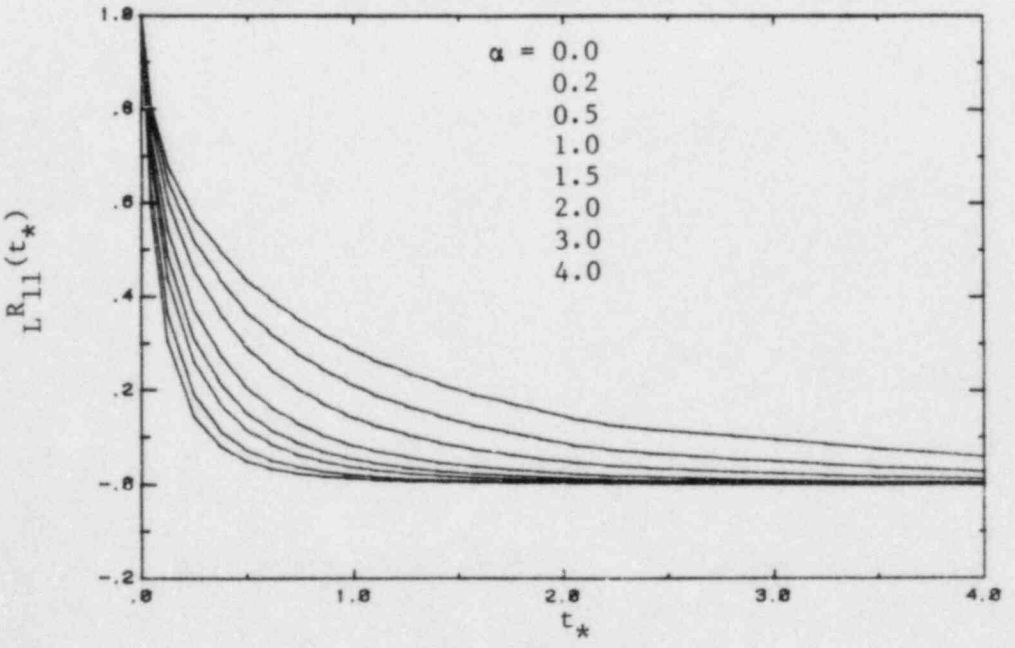

(d) Model IV

Figure 6.1. Lagrangian autocorrelation function in a homogeneous isotropic uniform turbulent flow (continued).

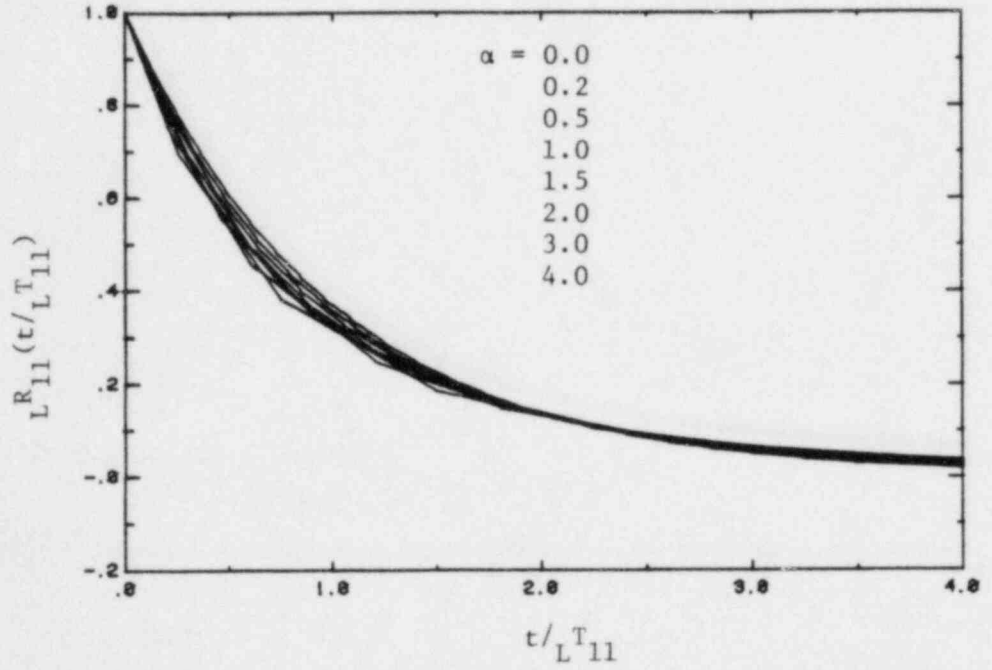

(a) Model I

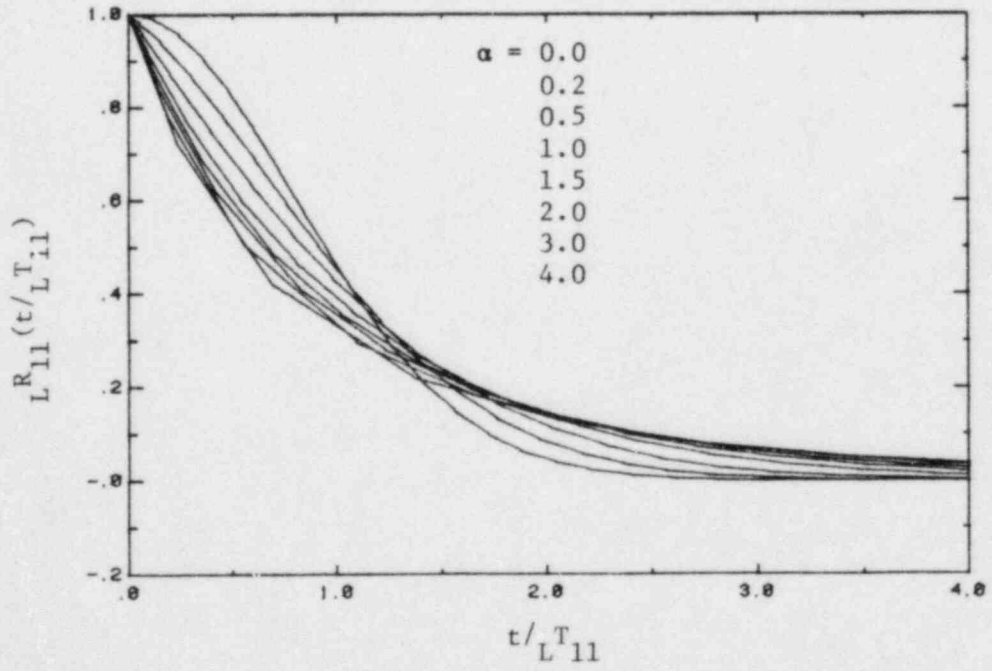

(b) Model II

Figure 6.2. Normalized Lagrangian autocorrelation function in a homogeneous isotropic uniform turbulent flow.

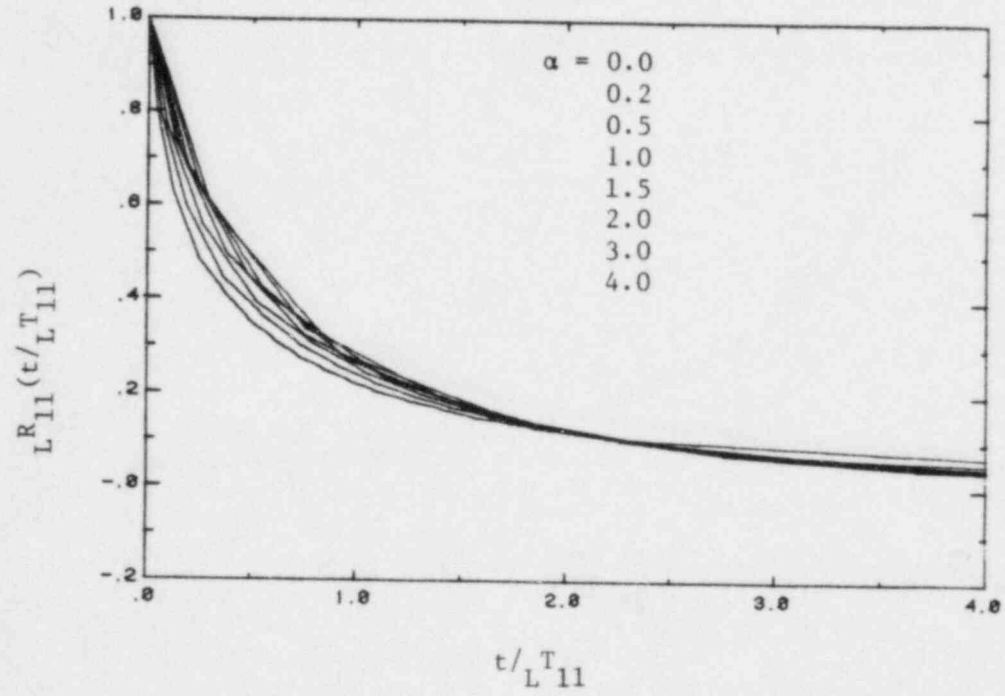

(c) Model III

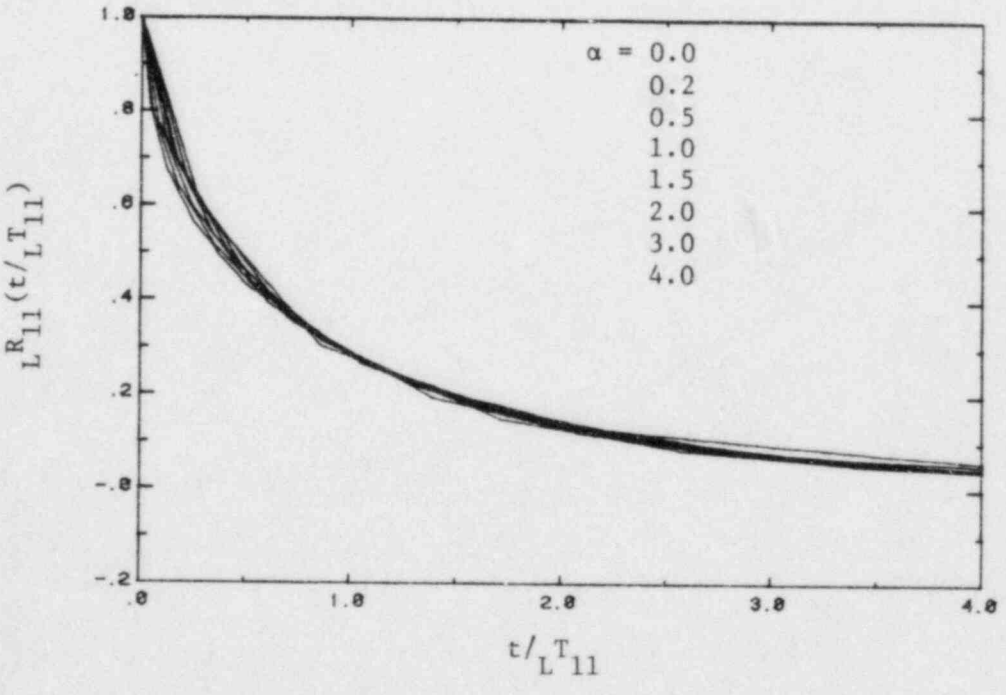

(d) Model IV

Figure 6.2. Normalized Lagrangian autocorrelation function in a homogeneous isotropic uniform turbulent flow (continued).

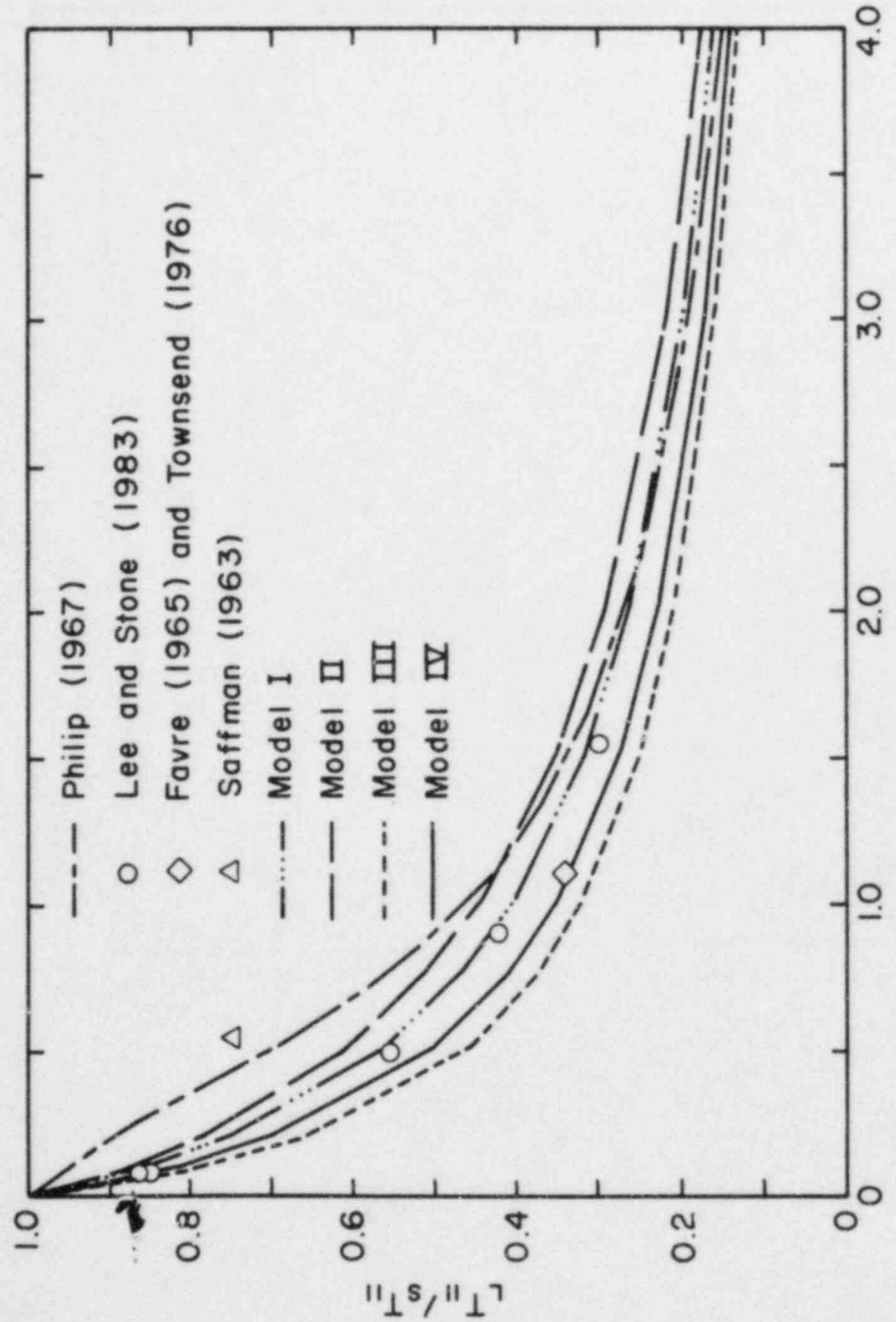

Figure 6.3. Lagrangian-Eulerian scale ratio vs. Eulerian parameter.

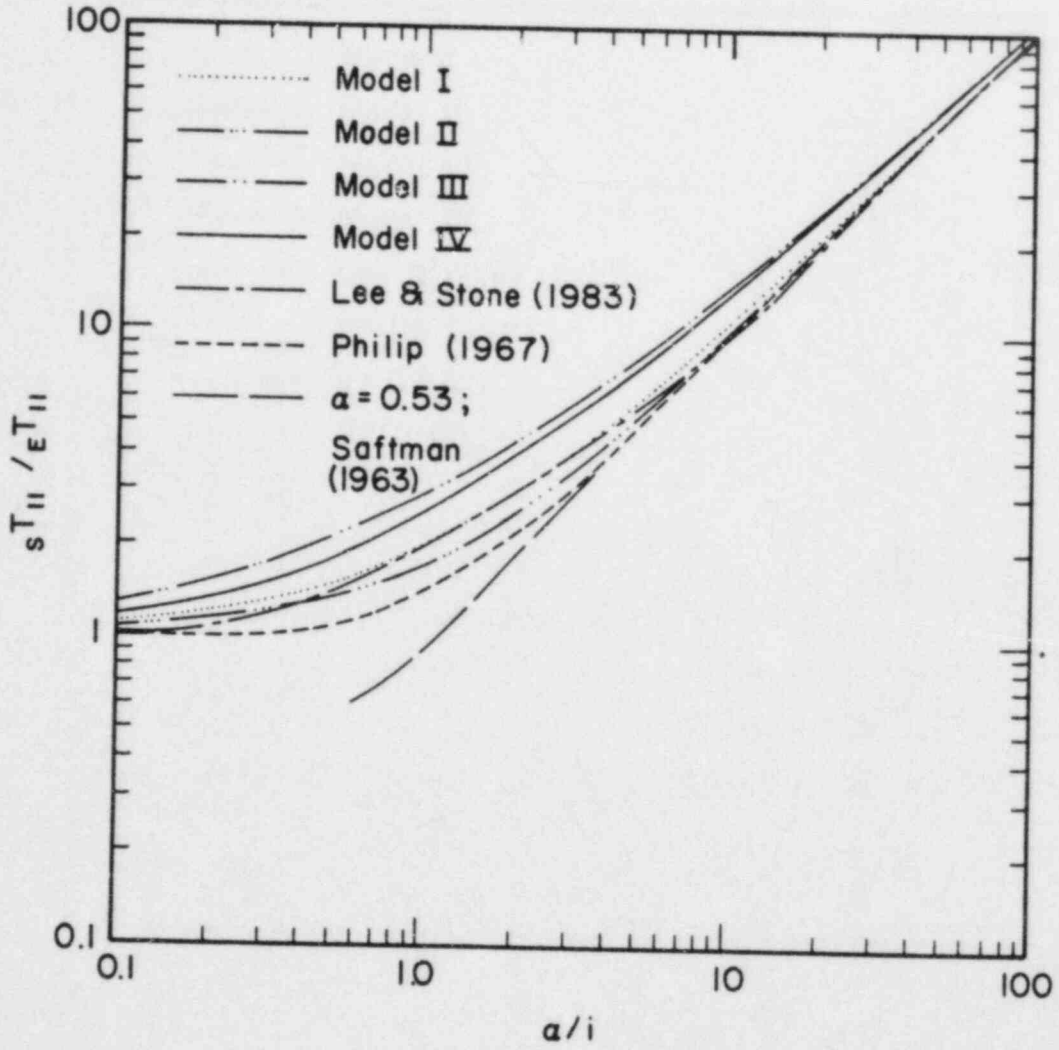

Figure 6.4. Properties of Eulerian statistics, $s^{T_{11}}/_{E}{}^{T_{11}}$, against α/i.

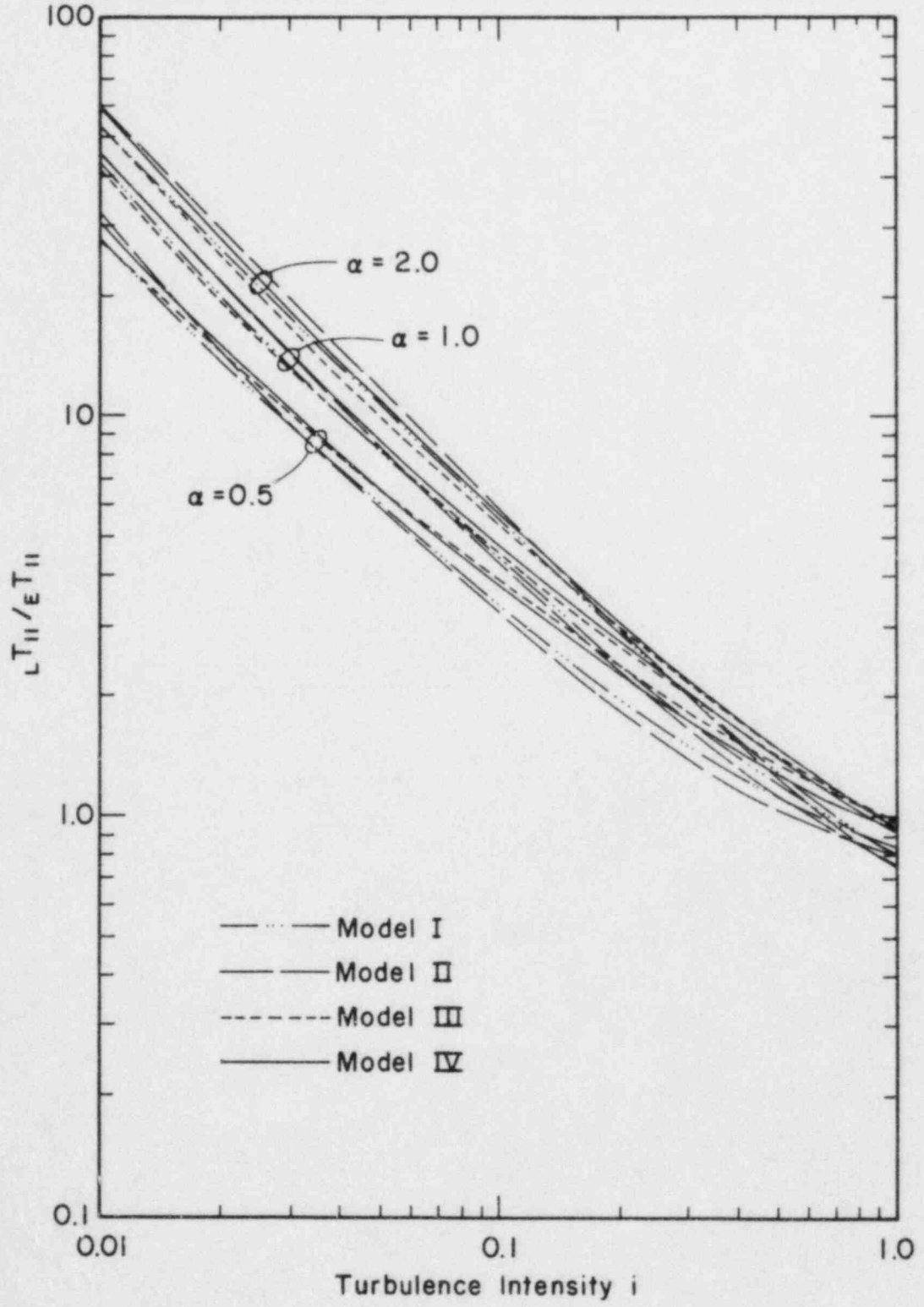

Figure 6.5. Scale ratio β predicted from different models.

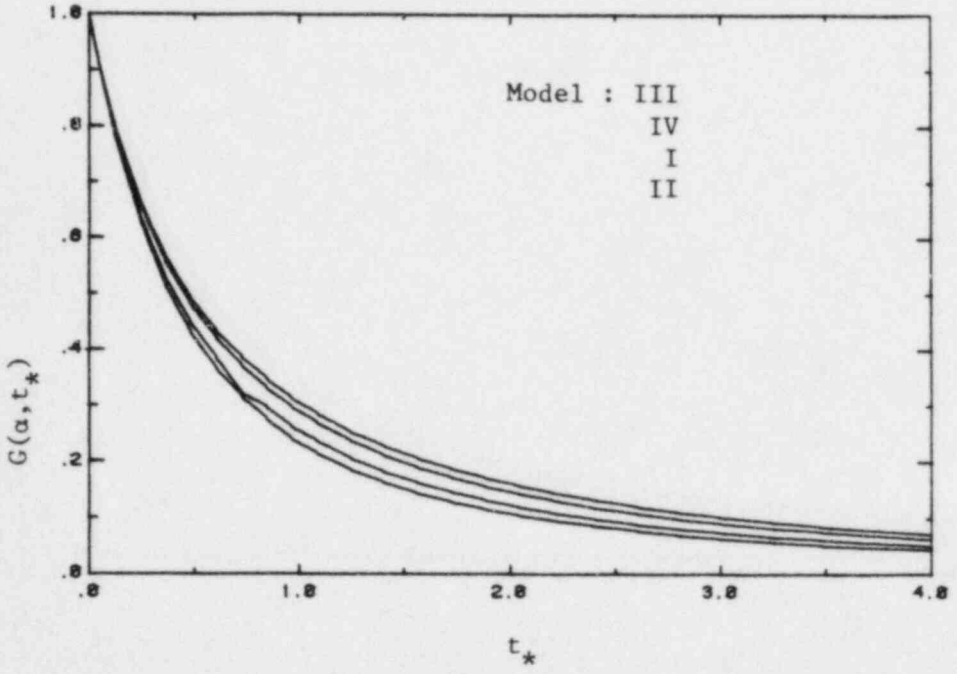

(a) $\alpha = 1.0$, $\Gamma_S T_{11} = 0.0$

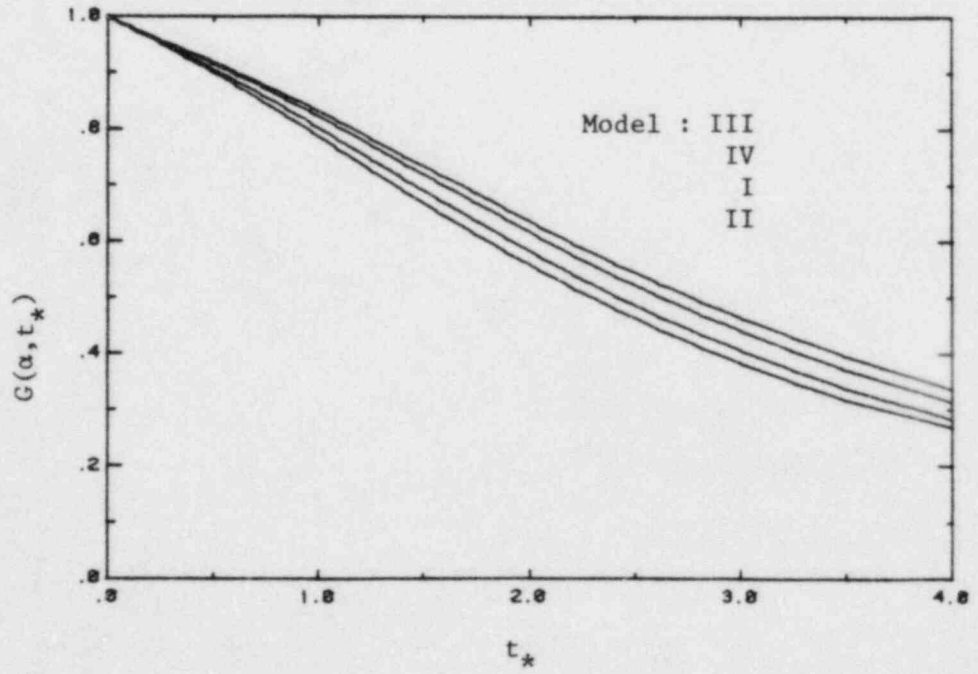

(b) $\alpha = 0.1$, $\Gamma_S T_{11} = 2.0$

Figure 6.6. Predicted $G(\alpha, t_*)$ in a turbulence field.

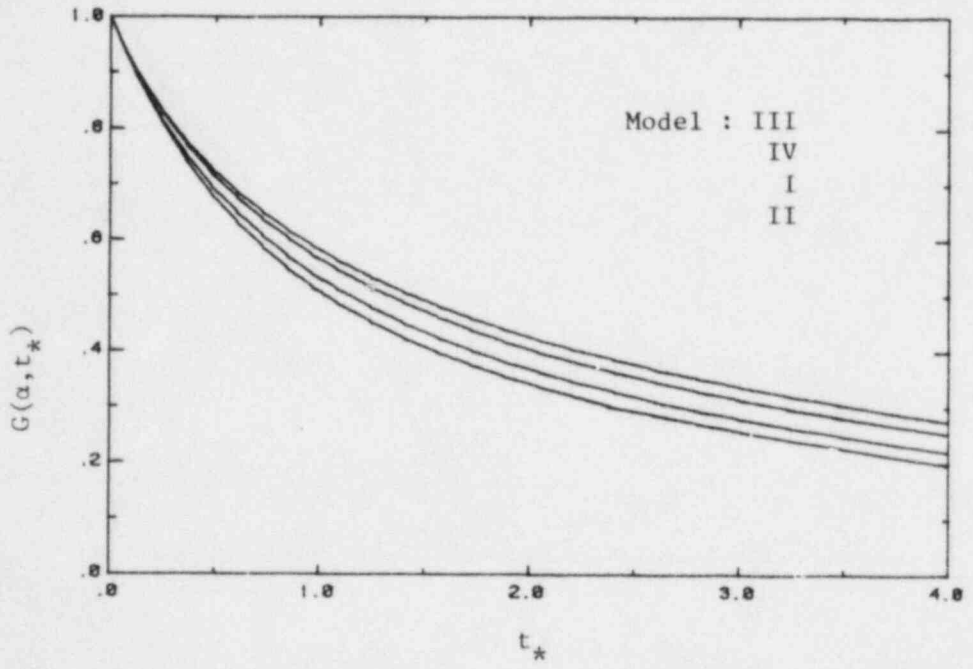

(a) $\alpha_1 = 1.0$, $\alpha_2 = \alpha_3 = 0.2$, $\Gamma_S T_{11} = 0.0$

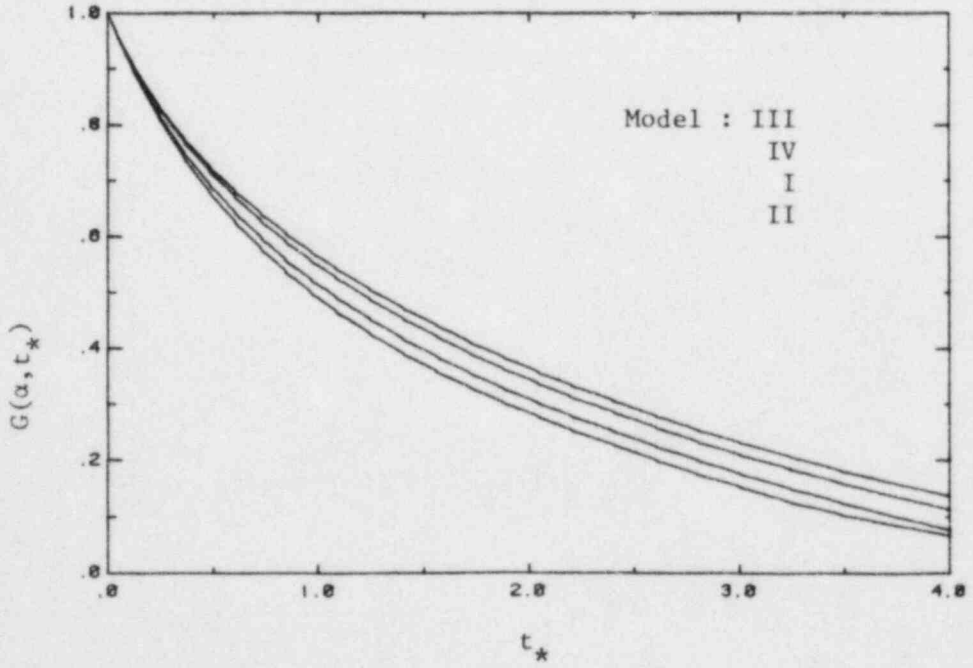

(b) $\alpha_1 = 1.0$, $\alpha_2 = \alpha_3 = 0.2$, $\Gamma_S T_{11} = 2.0$

Figure 6.6. Predicted $G(\alpha,t_*)$ in a turbulence field (continued).

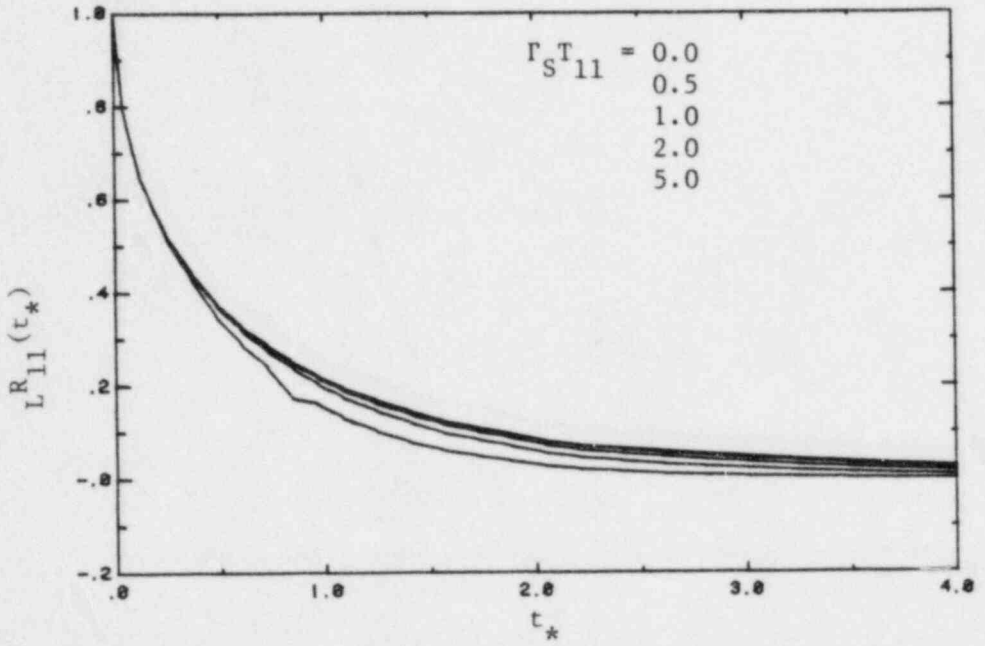

(a) $\alpha = 0.2$, $\Gamma_S T_{11} \neq 0$

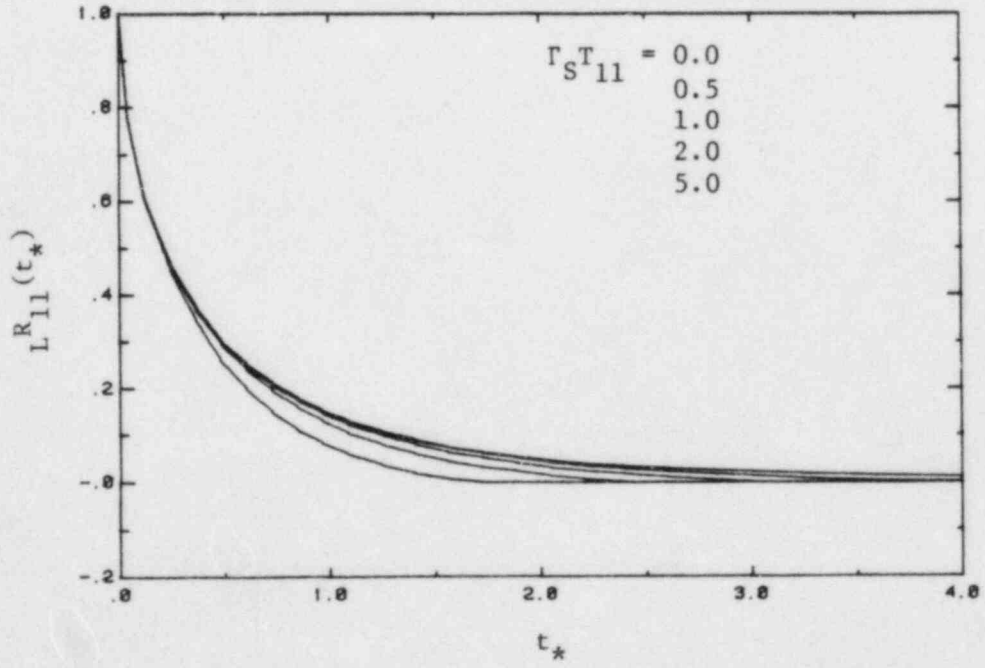

(b) $\alpha = 0.5$, $\Gamma_S T_{11} \neq 0$

Figure 6.7. Lagrangian autocorrelation function in a homogeneous isotropic uniform shear flow.

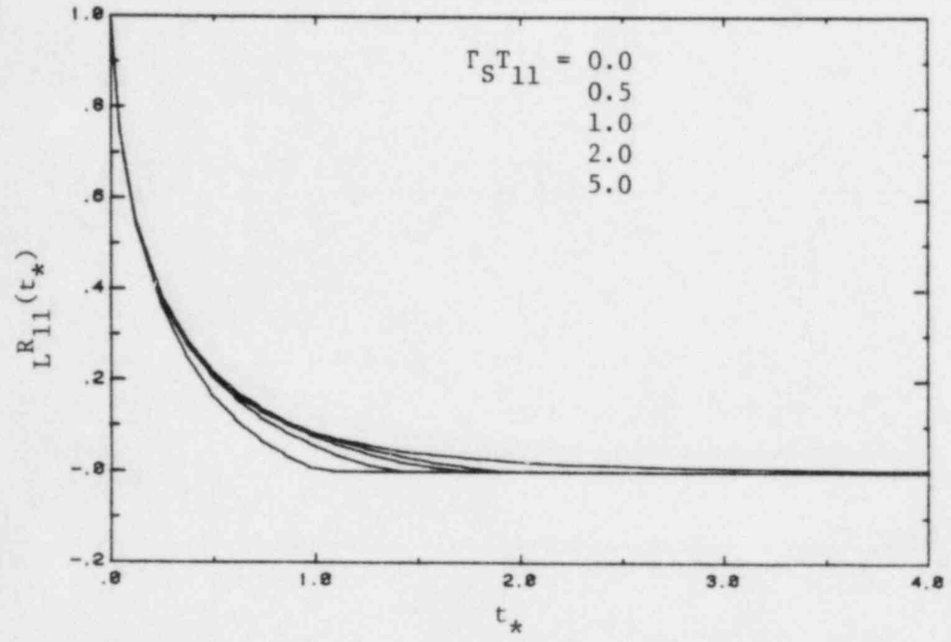

(c) $\alpha = 1.0$, $\Gamma_S T_{11} \neq 0$

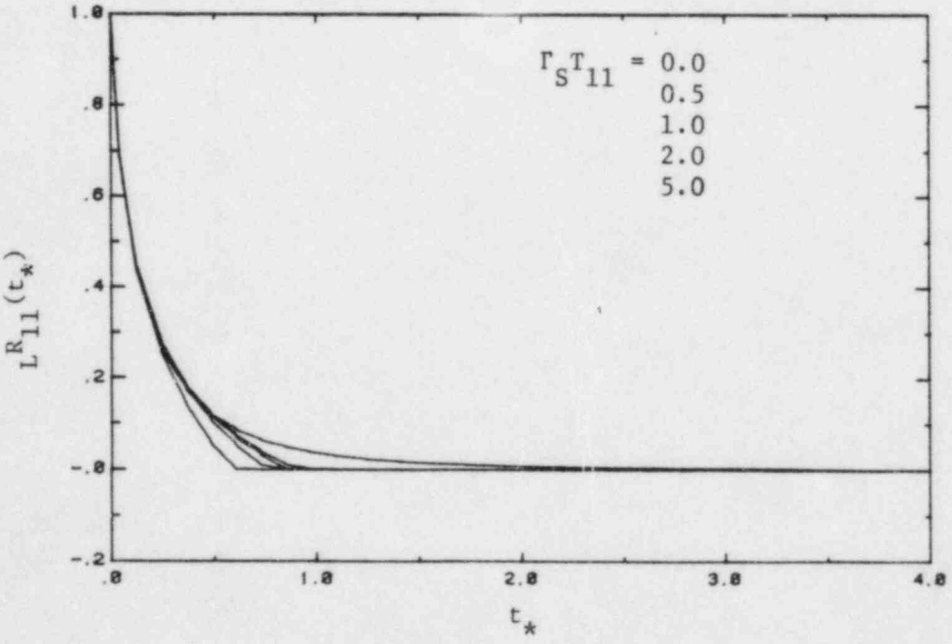

(d) $\alpha = 2.0$, $\Gamma_S T_{11} \neq 0$

Figure 6.7. Lagrangian autocorrelation function in a homogeneous isotropic uniform shear flow (continued).

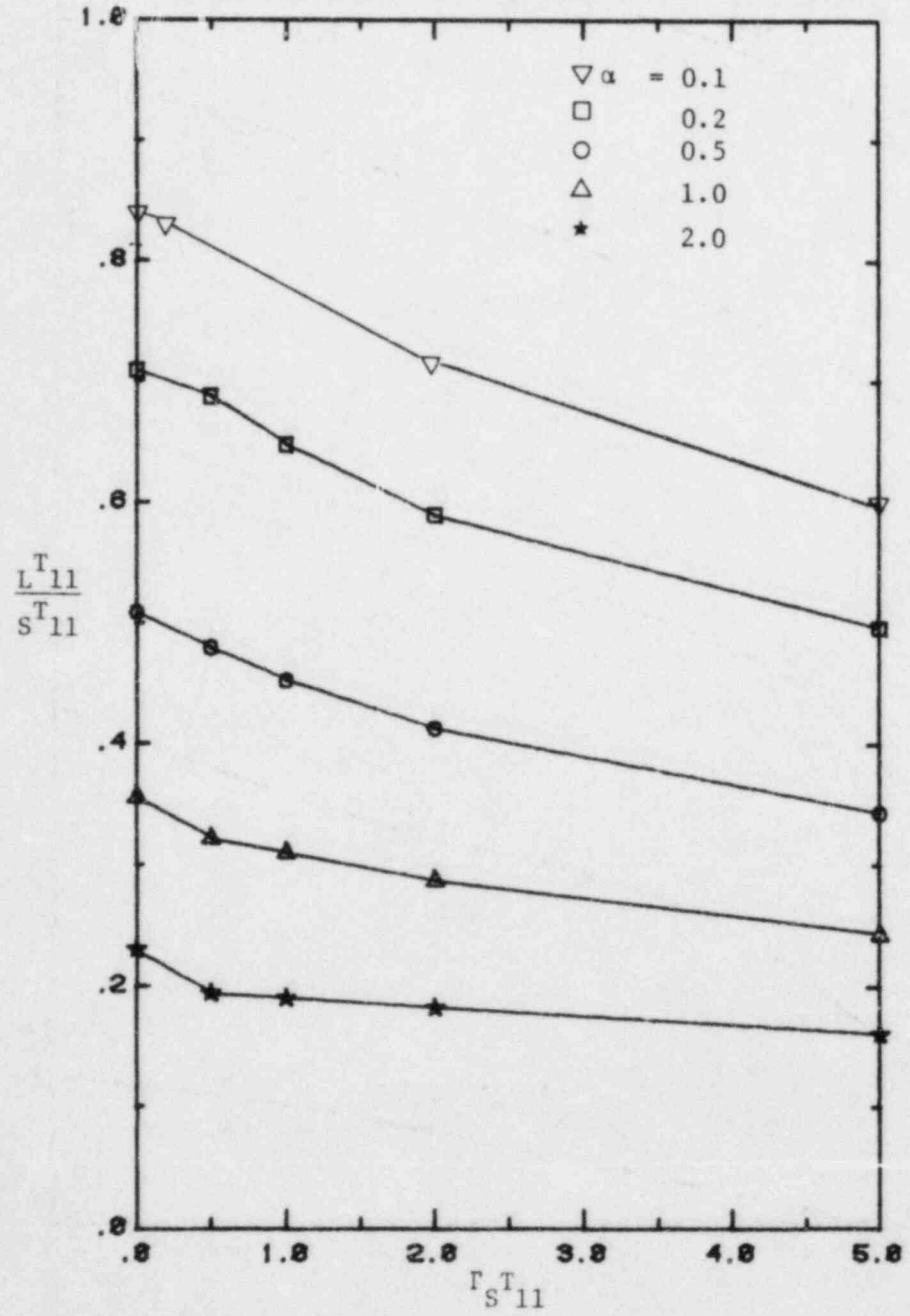

Figure 6.8. Effect of turbulent shear stress on the Lagrangian-Eulerian scale ratio.

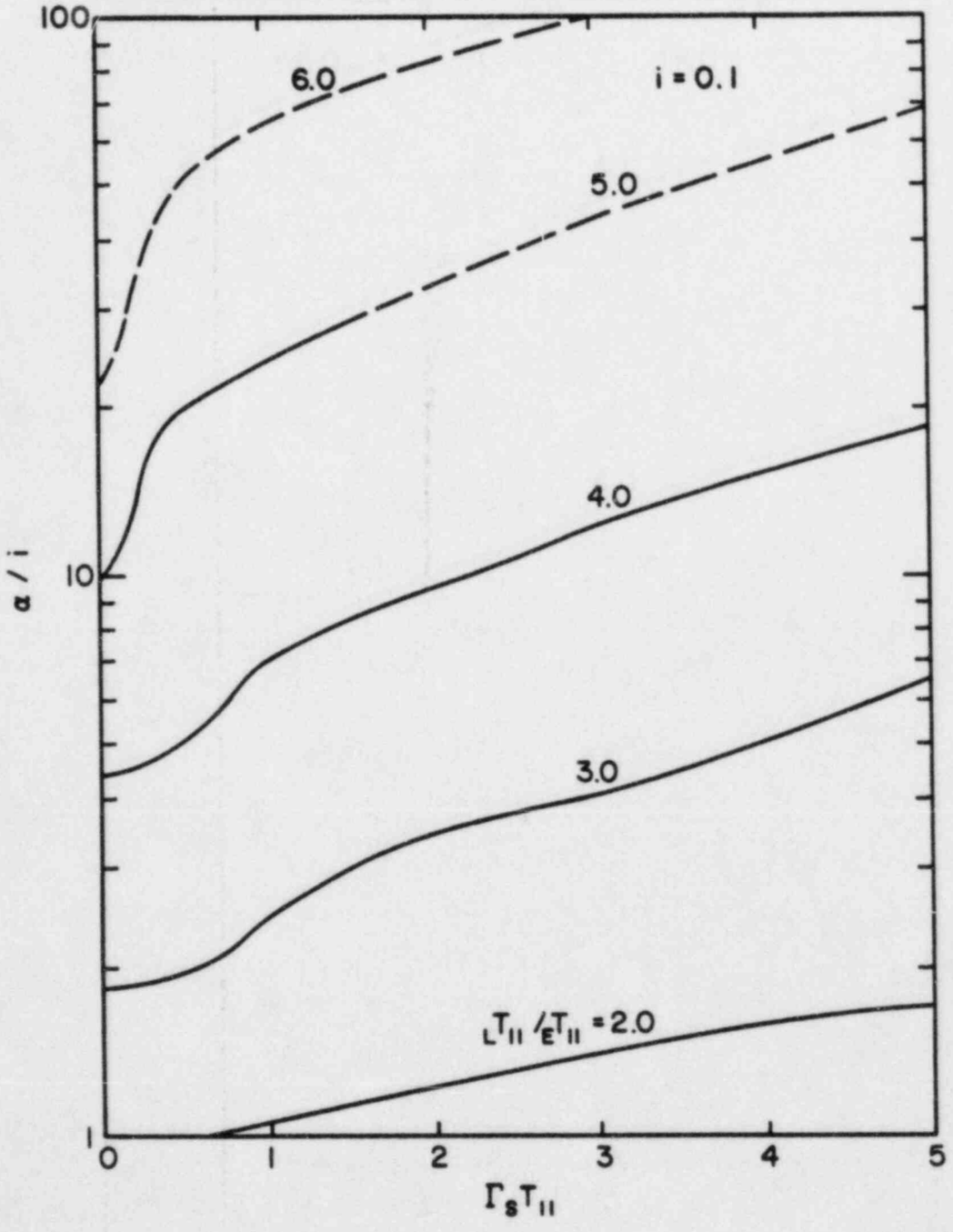

Figure 6.9. Effect of turbulent shear stress on the scale ratio β.

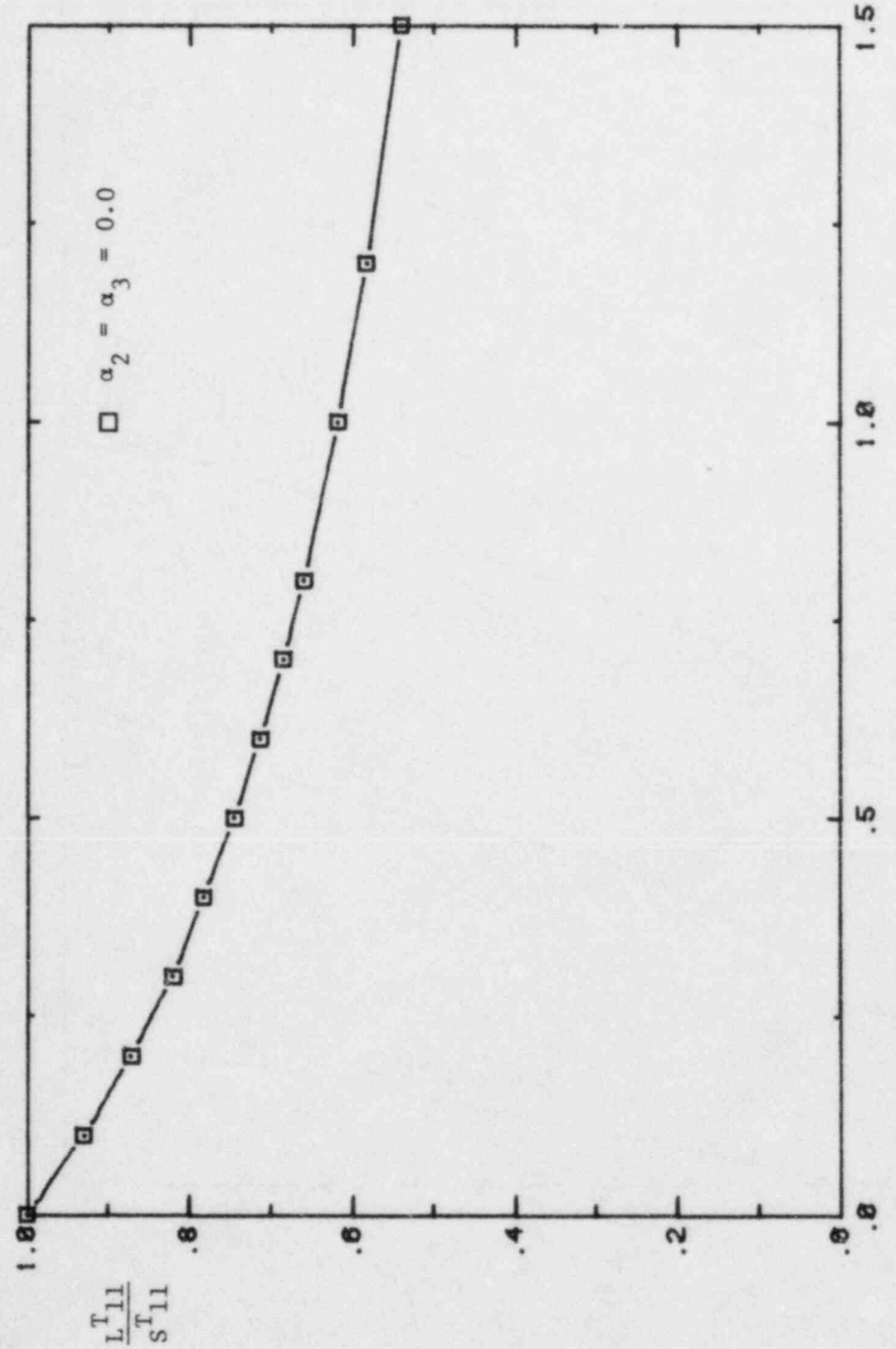

Figure 6.10. Lagrangian-Eulerian scale ratio in one-dimensional turbulence.

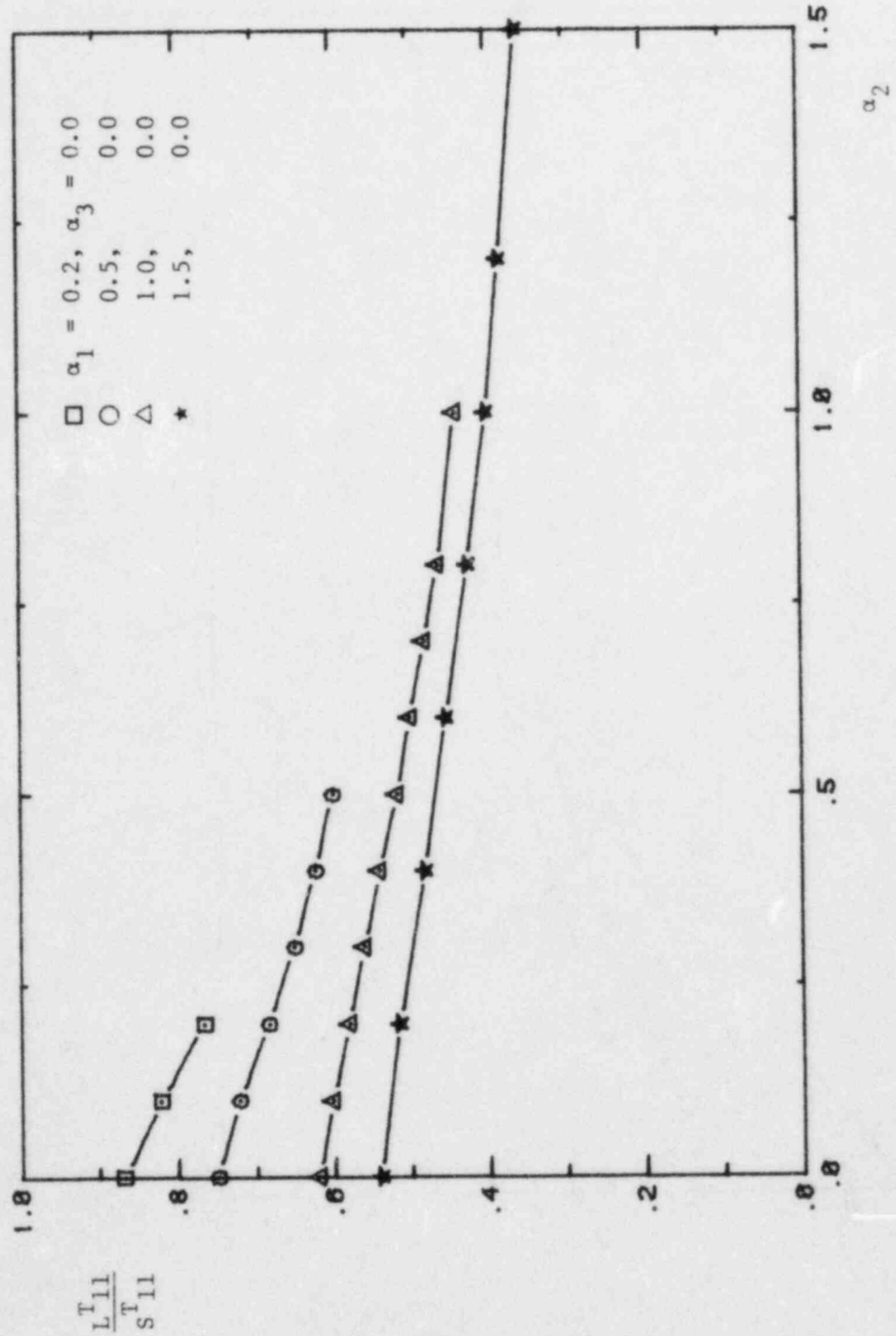

Figure 6.11. Lagrangian-Eulerian scale ratio in two-dimensional turbulence.

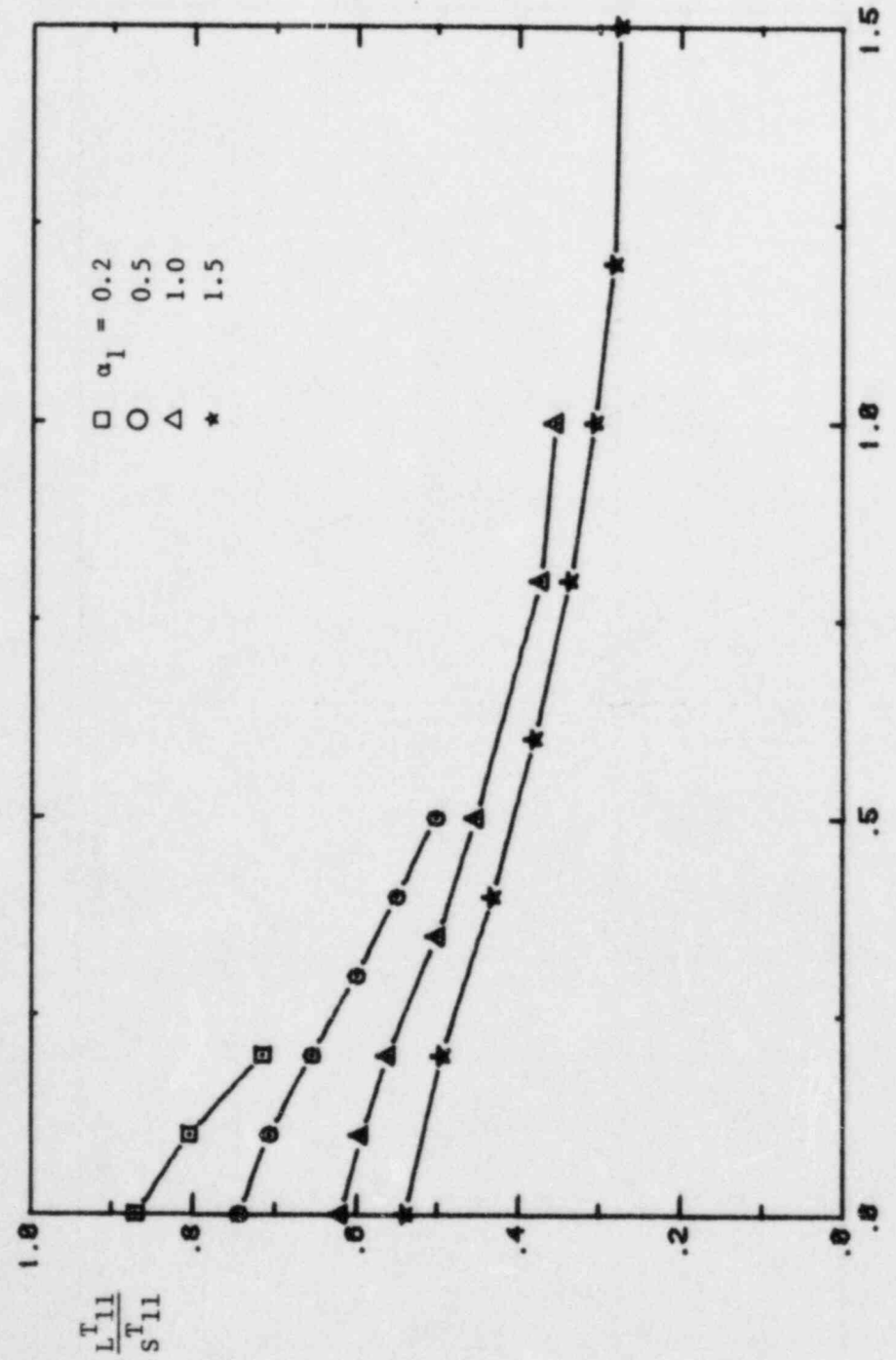

Figure 6.12. Lagrangian-Eulerian scale ratio in non-isotropic turbulence.

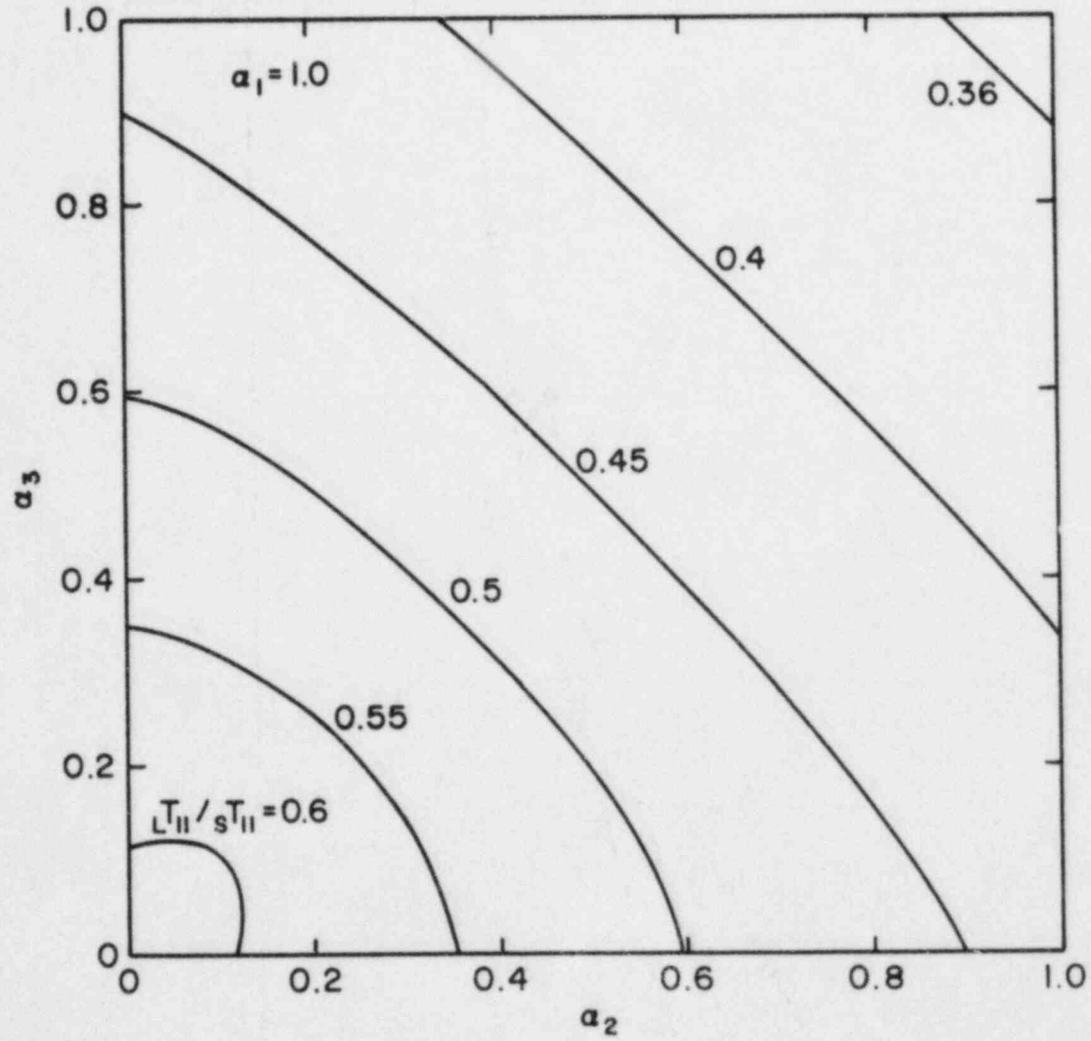

Figure 6.13. Contour of the Lagrangian-Eulerian scale ratio in non-isotropic turbulence.

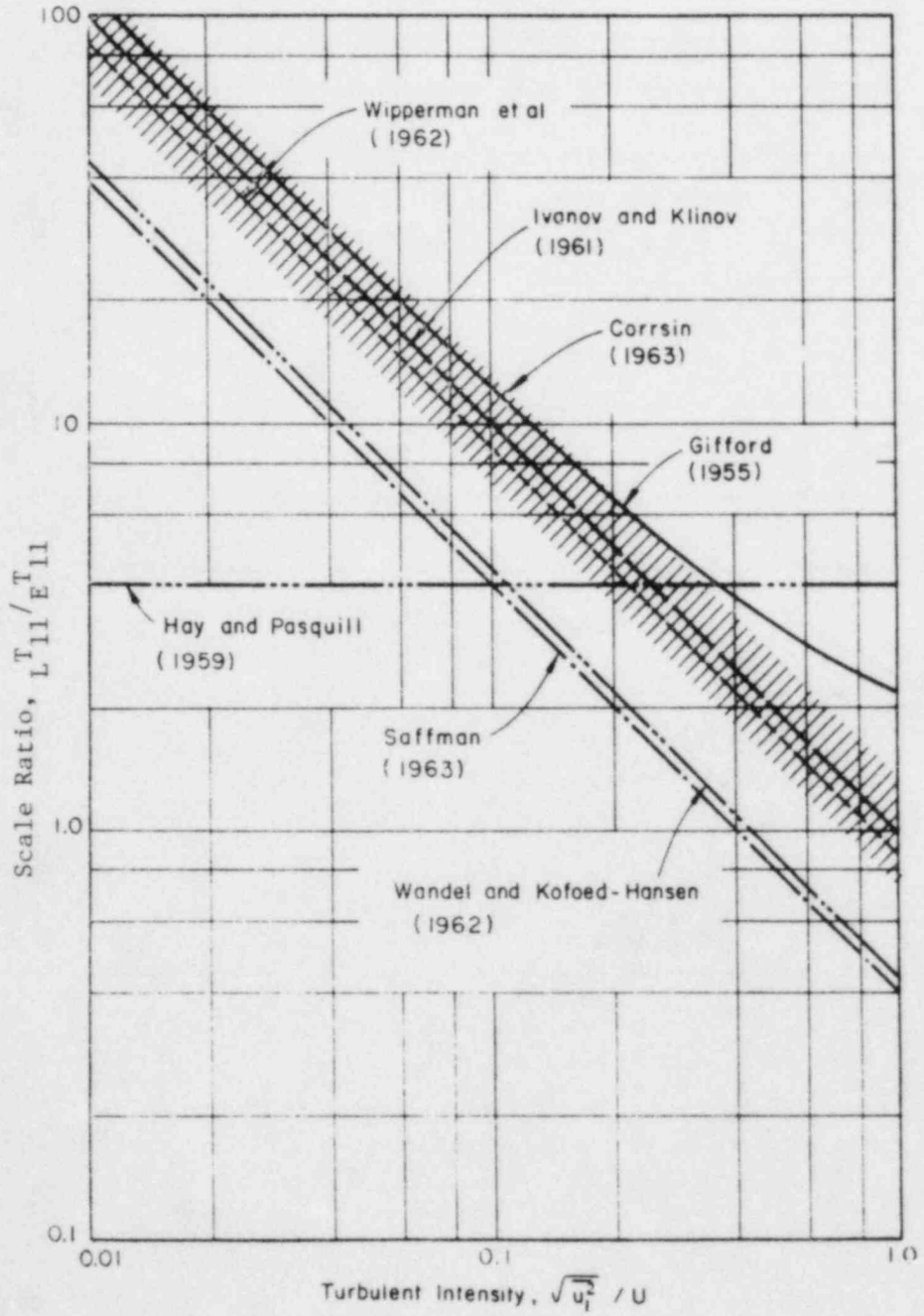

Figure 6.14. Scale ratio β predicted in Eulerian analysis.

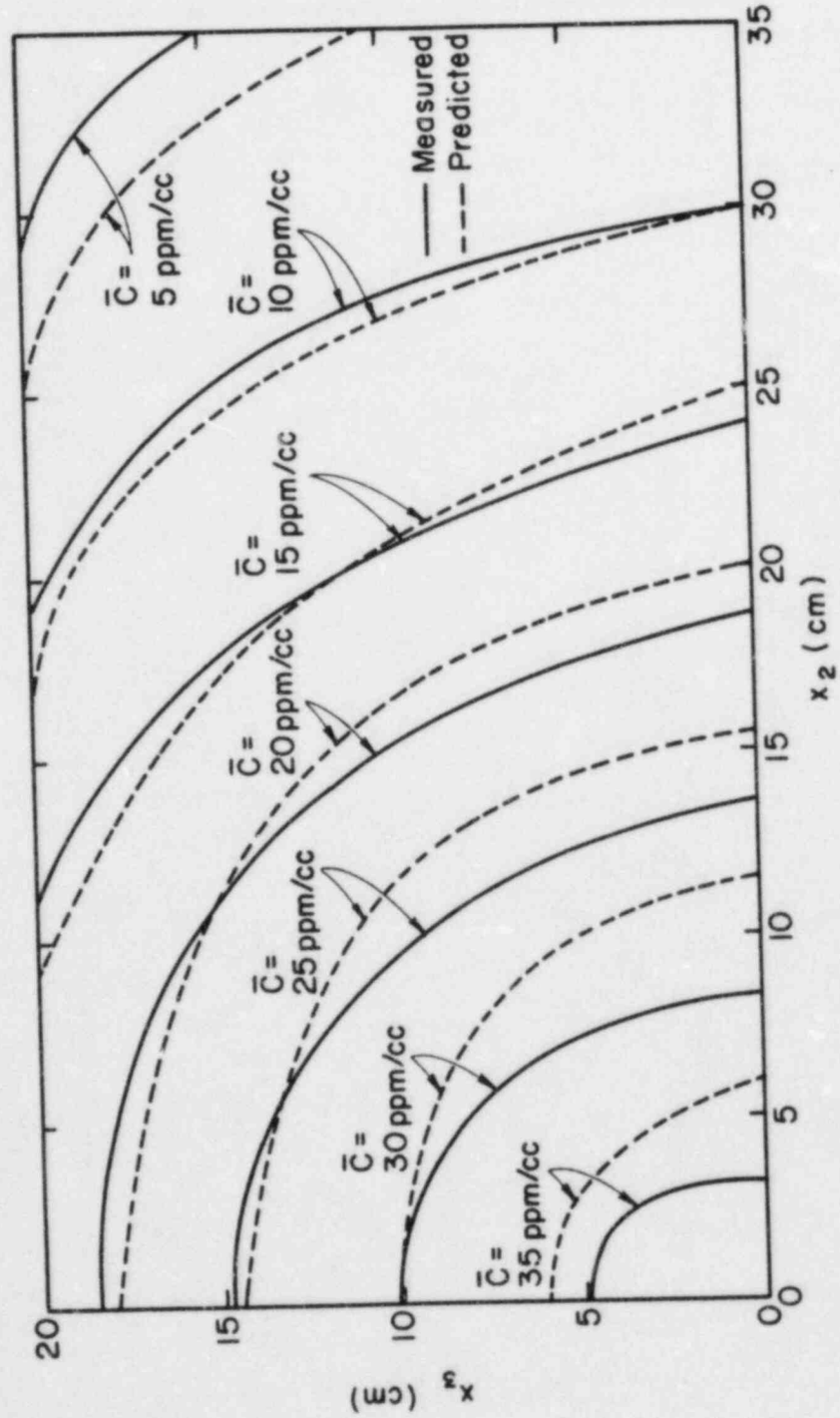

Figure 6.15. Predicted concentration distribution vs. measured concentration distribution, H = 2 cm, x_1 = 700 cm.

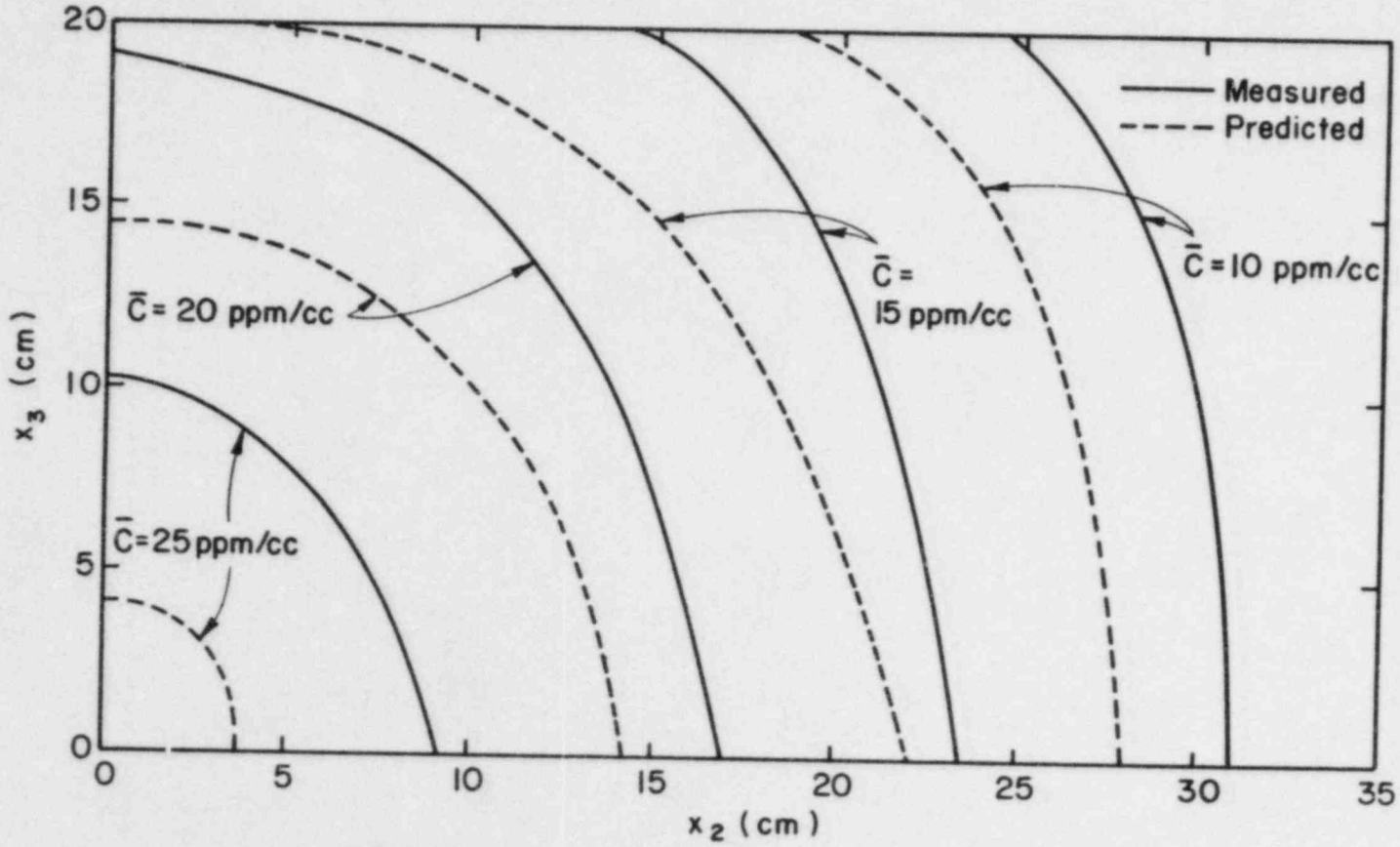

Figure 6.16. Predicted concentration distribution vs. measured concentration distribution, H = 10 cm, x_1 = 700 cm.

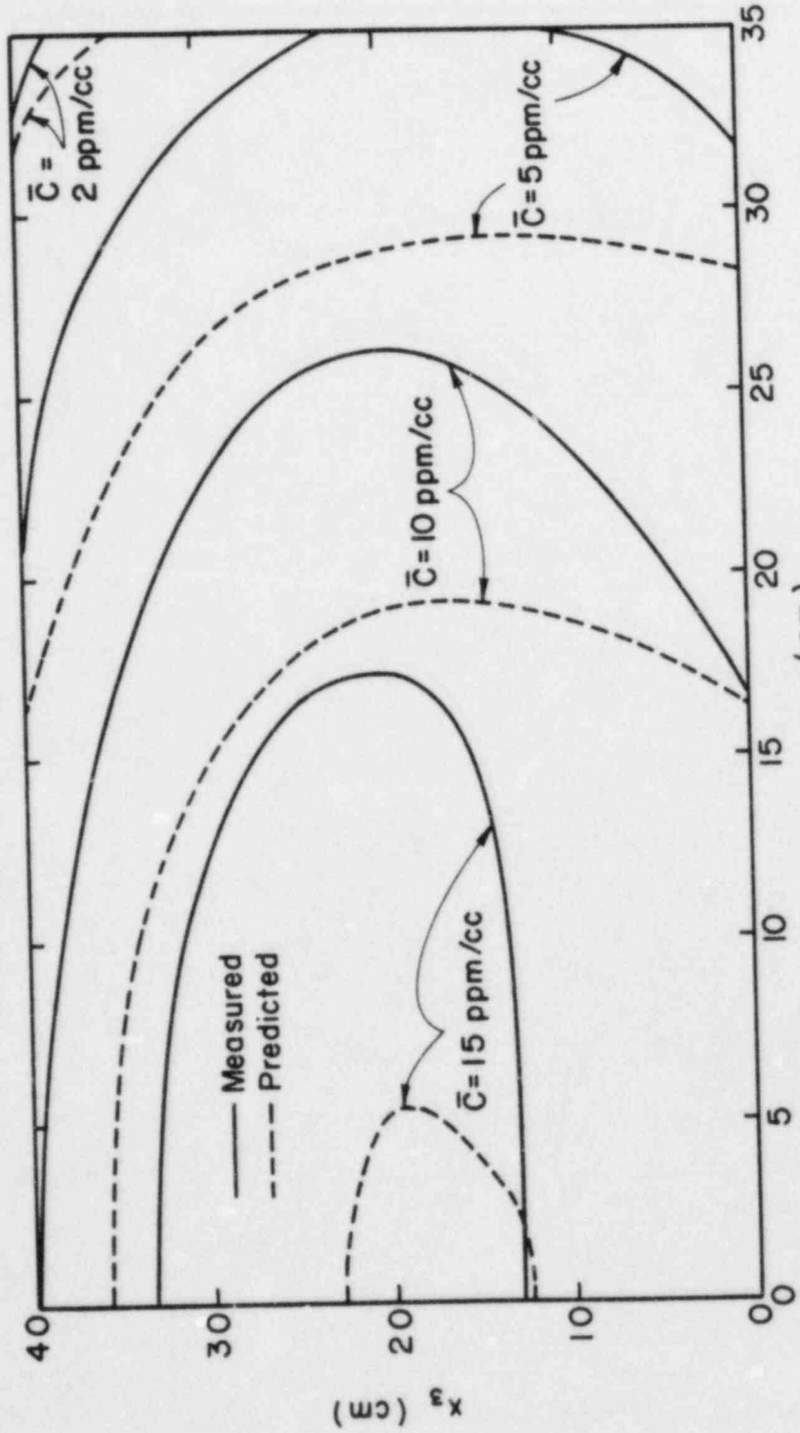

Figure 6.17. Predicted concentration distribution vs. measured concentration distribution, H = 20 cm, x_1 = 700 cm.

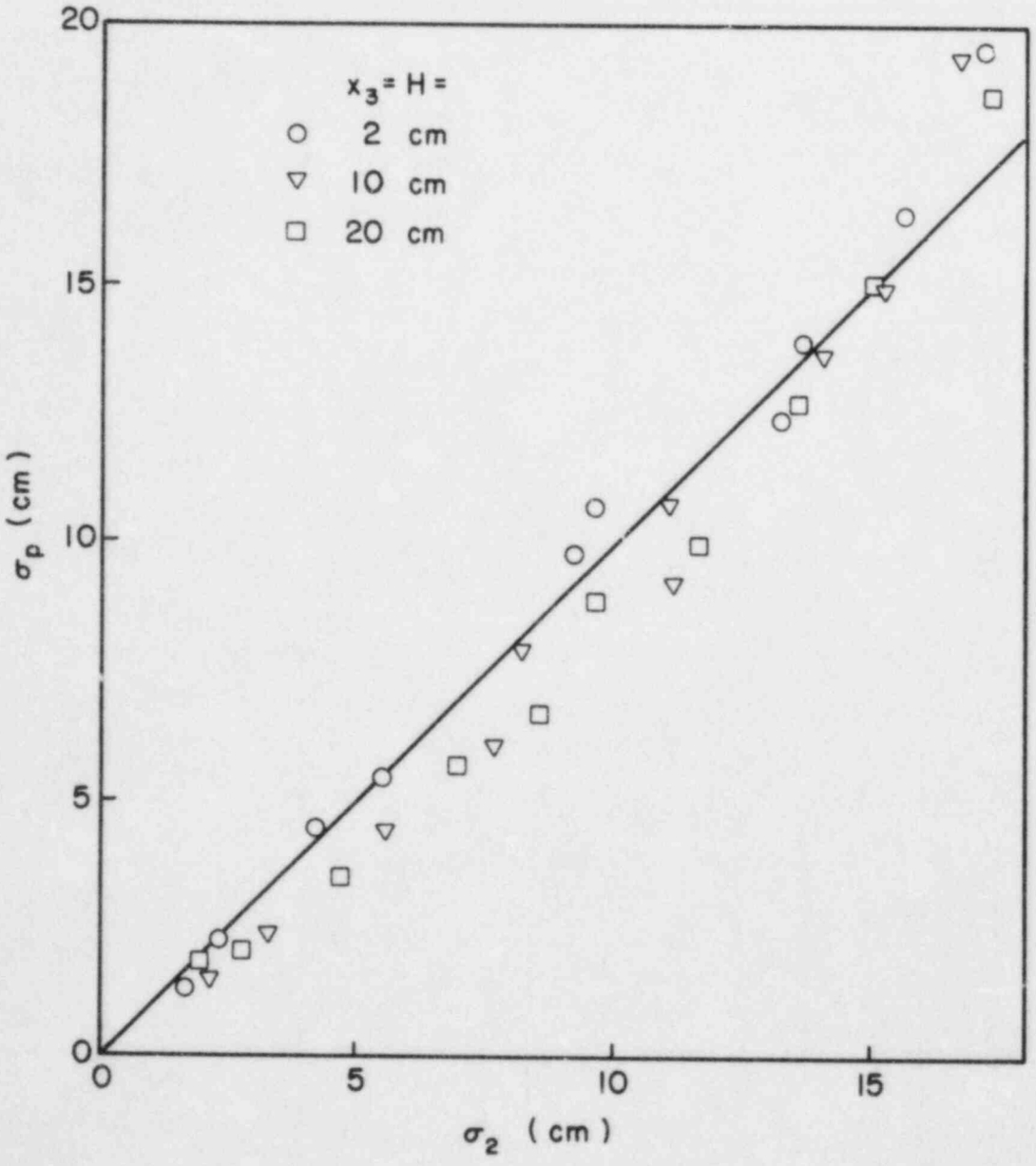

Figure 6.18. Comparison between predicted and measured lateral plume spread.

Chapter 7

CONCLUSIONS AND SUGGESTIONS FOR FURTHER RESEARCH

7.1 Conclusions

The purpose of this study was to reveal the importance of the Lagrangian statistics in the atmospheric dispersion phenomenon and to verify a methodology of estimating the Lagrangian statistics through some fixed-point Eulerian measurements. The evaluation process did not attempt to select a "best" predictive scheme from all existing dispersion models. The following conclusions may be made:

- Laboratory dispersion measurements were compared with 11 field experiments in terms of Pasquill's f curve for the lateral plume spread. It was found that the wind tunnel simulation replicates the characteristics of plume dispersion in the atmosphere. Both data statistically agree with one another through residual analysis.

  The dominant parameter in the f curve analysis and the most predictive scheme for the atmospheric dispersion is the Lagrangian integral time scale. The Lagrangian integral time scales obtained (or inferred) from six dispersion predictions display a wide range of variation. Such variation significantly depends upon the stratification condition and terrain topology. Hence, a good estimation of the Lagrangian integral time scale in the field will improve the accuracy of predicting the atmospheric dispersion in any of the suggested dispersion conditions.

- The Eulerian space-time correlations for $_{E}R_{ii}(\Delta x_1, x_2, x_3; \tau)$ with longitudinal separations were measured in the wind tunnel simulated boundary layer in the present study. These correlation functions were compared to previous measurements under other flow configurations. Laboratory measurements of the space-time correlation function suggest a unique form exists over a wide range of simulation.

- An Eulerian space-time correlation function and its integral time scale were adopted to estimate the Lagrangian velocity statistics through the Independence Hypothesis. A generalized approach which accounts for the fluid particle displacement tensors was proposed. A simplified model was developed which extended Baldwin and Johnson's isotropic homogeneous analysis to a homogeneous uniformly sheared turbulence field. The model requires the use of the isotropic Karman-Howarth kinematic relationship for the general Eulerian space correlation function in a non-isotropic turbulent field and

the assumption of an identical Lagrangian autocorrelation function for all three directions.

The presence of the turbulent shear decreases the magnitude of the Lagrangian autocorrelation function and its integral scale as the shear stress increases. The Lagrangian integral time scales estimated from turbulence measurements were compared to the estimated values obtained from dispersion measurements. The results agreed with one another within a 20% error.

- The Independence Hypothesis was found to be mathematically relevant to the one-dimensional Monte Carlo simulation of fluid particles even though the latter contradicts the basic assumption of the Independence Hypothesis and violates the isotropic Karman-Howarth kinetic relationship.

- The estimated Lagrangian integral time scale was employed in two analytical predictions for turbulent dispersion. The predicted dispersion data based on the estimated Lagrangian statistics were then compared to the wind tunnel dispersion measurements from a continuous point source. Short range dispersions predicted in the present study did not match the measurements in the wind tunnel. This was not unexpected since the asymptotic eddy diffusivities were utilized in the diffusion equation. The accuracy of the prediction improves as the downwind distance increases. At a distance farther downwind from the source, predictions agree with laboratory measurements within 30% error.

The present study supports Baldwin and Johnson's methodology as a good approximation for the atmospheric turbulent dispersion. Therefore, a set of two fixed-point Eulerian space-time correlation measurements in the field will provide an estimation of T_{ij} from the proposed universal Eulerian space-time correlation function. With a fixed-point Eulerian turbulence measurement for such parameters as $[u_i^2]$, T_{ii}, Γ and U, the atmospheric dispersion can be evaluated correctly from the present analysis.

7.2 Suggestions for Further Research

Further investigation should concentrate on modifying the Independence Hypothesis and on applying it to a more complicated turbulence field. Based on the summary described in Section 7.1, the following aspects are suggested for future research:

- It is necessary to establish the Eulerian space-time correlation functions in a boundary layer under different thermal stratifications and with various surface roughness characteristics. Construction of such functions will enable engineers to predict plume dispersion in all possible planetary boundary

layers. Construction of such functions can also be used to verify the proposed universal functional form of the Eulerian space-time correlation.

- The Karman-Howarth relationship for the general Eulerian spatial correlation may be inadequate for strong sheared turbulence. A theoretical or a semi-empirical expression of such a function in boundary layers would improve the accuracy of estimating the Lagrangian statistics.

- The analysis should be developed in a more general formulation which accounts for the correlated particle displacement, $[X_1(t_*)X_3(t_*)]$, in a uniform shear flow. This requires the knowledge of the cross-correlation function, ${}_E R_{13}(x_1,x_2,x_3;\tau)$, in a boundary layer. The numerical procedure could then consist of four integral equations iterated simultaneously with the Taylor's diffusion equation.

- It is desirable to verify the estimated Lagrangian velocity autocorrelation and the true Lagrangian velocity autocorrelation if the measuring technique is well conformed. Field experiments similar to the experimental procedures outlined in this study will ensure the availability of the present approach.

REFERENCES

Abramowitz, M. and Stegun, I. A., "Handbook of mathematical tables," 9th Edition, Dover Publishing Co., New York, 1972.

Angell, J. K., "Measurements of Lagrangian and Eulerian properties of turbulence at a height of 2500 ft." Quart. J. Roy. Meteor. Soc., Vol. 90, pp. 57-71, 1964.

Angell, J. K., Pack, D. H., Hoecker, W.H. and Delver, N., "Lagrangian-Eulerian time scale ratios estimated from constant volume balloon flights past a tall tower." Quart. J. Roy. Meteor. Soc., Vol. 97, pp. 87-92, 1971.

Baldwin, L. V. and Walsh, T. J., "Turbulent diffusion in the core of fully developed pipe flow." A.I.Ch.E.J., Vol. 7, pp. 53-61, 1961.

Baldwin, L. V. and Mickelsen, W. R., "Turbulent diffusion and anemometer measurements," Trans. ASCE, Vol. 128, pp. 1595-1627, 1963.

Baldwin, L. V. and Johnson, G. R., "The estimation of turbulent diffusivities from anemometer measurements. Part I: Fluid Particles." Colorado State University, CEP71-72LVB-GRJ42, 1972.

Batchelor, G. K., "Diffusion in a field of homogeneous turbulence," Austral. J. Sci. Res., Vol. 2, pp. 437-450, 1949.

Bienkiewicz, B., "Active modeling of turbulence for wind-tunnel studies of bridge models," Ph.D. dissertation, Civil Engineering Department, Colorado State University, 1981.

Blackwelder, R. F. and Kovaszhay, L. S. G., "Time scales and correlations in a turbulent boundary layer," Phy. Fluids, Vol. 15, pp. 1545-1554, 1972.

Briggs, G. A., "Diffusion estimation for small emissions," Air Resources Atmospheric Turbulence and Diffusion Laboratory, USAEC Report ATDL-106, NOAA, 60 pp., 1973.

Box, G. E. P. and Jenkins, G. M., "Time series analysis: forecasting and control." Revised Edition, Holden-Day Publication, Inc., San Francisco, 1976.

Burgers, J. M., "On turbulent fluid motion," Calif. Inst. Tech. Rep. No. E-34.1, 1951.

Cermak, J. E., "Physical modeling of the atmospheric boundary layer (ABL) in long boundary-layer wind tunnels (BLWT)," Wind Tunnel Modeling for Civil Engineering Applications, Ed. T. A. Reinhold, Cambridge University Press, pp. 97-125, 1982.

Champagne, F. H., Harris, V. G. and Corrsin, S., "Experiments on nearly homogeneous turbulent shear flow," J. Fluid Mech., Vol. 41, pp. 81-139, 1970.

Chaudhry, F. H. and Meroney, R. N., "A laboratory study of diffusion in stable stratified flow," Atmos. Environ., Vol. 7, pp. 443-454, 1973.

Chevray, R. and Tutu, N. K., "Simultaneous measurements of temperature and velocity in heated flow," Rev. of Sci. Instr., Vol. 43, pp. 1417-1421, 1972.

Comte-Bellot, G. and Corrsin, S., "Simple Eulerian time correlation of full- and narrow-band velocity signals in grid-generated, 'isotropic' turbulence," J. Fluid Mech., Vol. 48, pp. 273-337, 1971.

Conover, W. J., Practical nonparametric statistics. John Wiley and Sons, Inc., New York, 1971.

Corrsin, S., "Remarks on turbulent heat transfer," Proc. of the Iowa Thermodynamics Symposium, University of Iowa, Iowa City, pp. 5-30, 1953.

Corrsin, S., "Progress report on some turbulent diffusion research," Adv. Geophys., Vol. 6, pp. 161-164, 1959.

Corrsin, S., "Estimates of the relation between Eulrian and Lagrangian scales in large Reynolds number turbulence," J. Atmos. Sci., Vol. 20, pp. 115-119, 1963a.

Corrsin, S., "Discussion on turbulence measurements," Trans. ASCE, Vol. 128, pp. 1627-1631, 1963b.

Csanady, G. T., "Turbulent diffusion in the environment," D. Reidel Publishing Company, pp. 13, 1973.

Draxler, R. R., "Determination of atmospheric diffusion parameters," Atmos. Environ., Vol. 10, pp. 99-105, 1976.

Fackrell, J. E. and Robins, A. G., "Concentration fields associated with emissions from point sources in turbulent boundary layer, Part II: the effects of source size," Central Electricity Generating Board, Research Division MM/MECH/TF264, 1980.

Favre, A. J., Gaviglio, J. J., and Dumas, R. J., "Space-time double correlations and spectra in a turbulent boundary layer," J. Fluid Mech., Vol. 2, pp. 313-342, 1957.

Favre, A. J., Gaviglio, J. J. and Dumas, R. J., "Further space-time correlation of velocity in a turbulent boundary layer," J. Fluid Mech., Vol. 3, pp. 344-356, 1958.

Favre, A. J., "Review on space-time correlations in turbulent fluids," Trans. ASME, J. Applied Mech., Vol. 32, pp. 241-257, 1965.

Favre, A., Gaviglio, J. and Dumas, R., "Structure of velocity space-time correlations in a boundary layer," Phys. Fluids. Supplement, Vol. 10, pp. S138-S145, 1967.

Fisher, M. J. and Davies, P. O. A. L., "Correlation measurements in a non-frozen pattern of turbulence," J. Fluid Mech., Vol. 18, pp. 97-116, 1964.

Frenkiel, F. N., "Turbulent diffusion: mean concentration distribution in a flow field of homogeneous turbulence," Advances in Applied Mech., Vol. 3, Mises and von Karman (editors), Academic Press, pp. 61-107, 1953.

Frenkiel, F. N. and Klebanoff, P. S., "Space-time correlations in turbulence," Dynamics of Fluid and Plasmas, S. I. Pai (editor), Academic Press, pp. 257-274, 1966.

Gee, J. H. and Davies, D. R., "A further note on horizontal dispersion from an instantaneous ground source," Quart. J. Roy. Meteor. Soc., Vol. 90, pp. 478-480, 1964.

Gifford, F. A., "A simultaneous Lagrangian-Eulerian turbulent experiment," Mon. Wea. Rev., Vol. 83, pp. 293-301, 1955.

Gifford, F. A., "Preliminary communications, long range dispersion: comparison of the Mt. Isa data with theoretical and empirical formulas," Atmos. Environ. 16, pp. 1583-1586, 1982.

Hanna, S. R., "Lagrangian and Eulerian time-scale relations in the daytime boundary layer," J. of Appl. Meteor., Vol. 20, pp. 242-249, 1981.

Hanna, S. R., "Air quality modeling over short distance. Handbook of Applied Meteorology," John Wiley and Sons, Inc., New York, 1983.

Harris, V. G., Graham, J. A. H. and Corrsin, S., "Further experiments in nearly homogeneous turbulent shear flow," J. Fluid Mech., Vol. 81, pp. 657-687, 1977.

Hay, J. S. and Pasquill, F., "Diffusion from a continuous source in relation to the spectrum and scale of turbulence," Adv. Geophys., Vol. 6, pp. 345-365, 1959.

Hinze, J. O., "Turbulence," 2nd Edition, McGraw-Hill Book Co., 1975.

Huang, C. H., "A theory of dispersion in turbulent shear flow," Atmos. Environ., Vol. 13, pp. 453-463, 1979.

Inoue, E., "Interrelations between the structure of wind near the ground and its observation," J. Meteor. Soc. of Japan, Vol. 30, pp. 255-264, 1952.

Ivanov, V. N. and Klinov, F. Ya., "Some characteristics of a turbulent velocity field in the lower 300 meter layer of the atmosphere," Izv., Geoph. Ser., Ak Nauk, U.S.S.R., pp. 1570-1577, 1961.

Koper, C. A., Sadeh, W. Z. and Turner, R. E., "Investigation of turbulent diffusion in the extreme lower atmosphere," Fourth Symposium on Turbulence, Diffusion and Air Pollution, pp. 665-672, 1972.

Koper, C. A., Sadeh, W. Z. and Turner, R. E., "A relation between the Lagrangian and Eulerian turbulent velocity autocorrelation, AIAA J., Vol. 16, pp. 969-975, 1978.

Kovasznay, L. S. G., Kibens, V. and Blackwelder, R. F., "Large-scale motion in the intermittent region of a turbulent boundary layer," J. Fluid Mech., Vol. 41, pp. 283-325, 1970.

Kraichnan, R. H., "Relation between Lagrangian and Eulerian correlation times of a turbulent velocity field," Phys. Fluids, Vol. 7, pp. 142-143, 1963.

Kraichnan, R. H., "Diffusion by a random velocity field," Phys. Fluids, Vol. 13, pp. 22-31, 1970.

Lauwerier, H. A., "Diffusion from a source in a skew velocity field," Appl. Sci. Res., Vol. A4, pp. 153-156, 1953.

Lee, J. T. and Stone, G. L., "Eulerian-Lagrangian Relationships in Monte-Carlo simulations of turbulent diffusion," Atmos. Environ. Vol. 17, pp. 2483-2487, 1983.

Lumley, J. L. and Panofsky, H. A., "The structure of atmospheric turbulence," John Wiley and Sons, Inc., 239 pp., 1964.

Mickelsen, W. R., "An experimental comparison of the Lagrangian and Eulerian correlation coefficients in homogeneous isotropic turbulence," NAA TN3570, Washington, D.C., 1955.

Monin, A. S. and Yaglom, A. M., "Statistical Fluid Mechanics: Mechanics of Turbulence, Vol. 1," MIT Press, 1971.

Neumann, J., "Some observations on the simple exponential function as a Lagrangian velocity correlation function in turbulent diffusion," Atmos. Environ., Vol. 12, pp. 1965-1968, 1978.

Ogura, Y., "The relation between the space- and time-correlation functions in a turbulent flow," J. Meteor. Soc. of Japan, Vol. 31, pp. 355-369, 1953.

Pasquill, F., "Atmospheric dispersion of pollution," Quart. J. Roy. Met. Soc., Vol. 97, pp. 369-395, 1971.

Pasquill, F., "Atmospheric Diffusion," 2nd Edition, Halsted Press, 1974.

Peskin, R. L., "Numerical simulation of Lagrangian turbulent quantities in two and three dimensions." Adv. Geophys., Vol. 18A, pp. 141-163, 1974.

Philip, J. R., "Relation between Eulerian ... Lagrangian statistics," Phys. Fluids. Supplement, Vol. 10, pp. S69-S71, 1967.

Phillips, P. and Panofsky, H. A., "A re-exmination of lateral dispersion from continuous sources," Atmos. Environ., Vol. 16, pp. 1851-1859, 1982.

Plate, E. J. and Cermak, J. E., "Micrometeorological wind tunnel facility, description and characteristics," CER63EJP-JEC9, Colorado State University, 1963.

Riley, J. J. and Corrsin, S., "The relation of turbulent diffusivities to Lagrangian velocity statistics for the simplest shear flow," J. Geophys. Res., Vol. 79, pp. 1768-1771, 1974.

Sabot, J., Renault, J. and Comte-Bellot, G., "Space-time correlations of the transverse velocity fluctuation in pipe flow," Phys. Fluids, Vol. 16, pp. 1403-1405, 1973.

Saffman, P. G., "An approximate calculation of the Lagrangian auto-correlation coefficient for stationary homogeneous turbulence," Appl. Sci. Res., Vol. 11, pp. 245-255, 1963.

Sandborn, V. A., "Resistance temperature transducers," Meteorology Press, Fort Collins, Colorado, 1972.

Shlien, D. J. and Corrsin, S., "A measurement of Lagrangian velocity correlation in approximately isotropic turbulence," J. Fluid Mech., Vol. 62, pp. 255-271, 1974.

Smith, F. B., "The diffusion of smoke from a continuous elevated point source into a turbulent atmosphere," J. Fluid Mech., Vol. 2, pp. 49-76, 1957.

Snyder, W. H. and Lumley, J. L., "Some measurements of particle velocity autocorrelation functions in a turbulent flow," J. Fluid Mech., Vol. 48, pp. 41-71, 1971.

Sutton, O. G., "Micrometeorology," McGraw-Hill, New York, 1953.

Tavoularis, S. and Corrsin, S., "Experiments in nearly homogeneous turbulent shear flow with a uniform mean temperature gradient. Part I," J. Fluid Mech., Vol. 104, pp. 311-347, 1981.

Taylor, G. I., "Diffusion by continuous movements," Proc. London Math. Soc. Ser. A, Vol. 20, pp. 196-211, 1921.

Tennekes, H., "The exponential Lagrangian correlation function and turbulent diffusion in the inertial subrange." Atmos. Environ., Vol. 13, pp. 1565-1567, 1979.

Teunissen, H. W., "Structure of mean winds and turbulence in the planetary boundary layer over rural terrain," Boundary-Layer Meteorology, Vol. 19, pp. 187-221, 1980.

Townsend, A. A., "The structure of turbulent shear flow," 2nd Edition, Cambridge University Press, London, 1976.

Wacongne, S. and Babiano, A., "Space-time turbulent characteristics in the atmospheric surface layer," Boundary Layer Meteorology, Vol. 24, pp. 429-450, 1982.

Walters, T. S., "The effect of diffusion in the mean wind direction in atmospheric turbulence," Mathematia, Vol. 11, pp. 119-124, 1964.

Walters, T. S., "Diffusion from an elevated point source into a turbulent atmosphere," Mathematika, Vol. 12, pp. 49-57, 1964.

Wandel, C. F. and Kofoed-Hansen, O., "On the Eulerian-Lagrangian Transform in the Statistical Theory of Turbulence," J. Geophys. Res., Vol. 67, pp. 3089-3093, 1962.

Weinstock, J., "Lagrangian-Eulerian relation and the independence approximation," Phys. Fluids, Vol. 19, pp. 1702-1711, 1976.

Wipperman, F., Gburcik, P. and Klug, W., "On the Eulerian and Lagrangian statistics of very large-scale atmospheric motions," Tech. Note No. 1, Cont. No. AF61(052)-366, Inst. fur Meteor. Tech. Hochschule Darmstadt, 44 pp.

Yeh, G. T., "Green's function of a diffusion equation," Geophys. Res. Letter, Vol. 2, pp. 293-296, 1975.

APPENDIX A

DERIVATION OF EQUATION 3.16

Abramowitz and Stegun (1972) tabulated several important properties of the error function. Two integral formulae are utilized in the present derivation,

$$\int e^{-ax^2-2bx-c}\,dx = \frac{1}{2}\sqrt{\frac{\pi}{a}}\,e^{\frac{b^2-ac}{a}}\,\mathrm{erf}\left(\sqrt{a}\,x+\frac{b}{\sqrt{a}}\right) \tag{A-1}$$

$$\int \mathrm{erf}(x)\,dx = x\,\mathrm{erf}(x) + \frac{1}{\sqrt{\pi}}\,e^{-x^2} \tag{A-2}$$

Based on the above two integrals, the following relations are derived

$$\int x\,e^{-ax^2-2bx-c}\,dx = e^{\frac{b^2-ac}{a}}\left[-\frac{1}{2a}\,e^{-\left(\sqrt{a}\,x+\frac{b}{\sqrt{a}}\right)^2} - \frac{b\sqrt{\pi}}{2a\sqrt{a}}\,\mathrm{erf}\left(\sqrt{a}x+\frac{b}{\sqrt{a}}\right)\right] \tag{A-3}$$

$$\int x^2 e^{-ax^2-2bx-c}\,dx = e^{\frac{b^2-ac}{a}}\left\{\left(\frac{\sqrt{\pi}}{4a\sqrt{a}} + \frac{b^2\sqrt{\pi}}{2a^2\sqrt{a}}\right)\mathrm{erf}\left(\sqrt{a}\,x+\frac{b}{\sqrt{a}}\right) + \left(\frac{b}{2a^2}-\frac{x}{2a}\right)e^{-\left(\sqrt{a}\,x+\frac{b}{\sqrt{a}}\right)^2}\right\} . \tag{A-4}$$

$$\int x\,\mathrm{erf}(x)\,dx = \frac{1}{2}\left[x^2\mathrm{erf}(x) + \frac{x}{\sqrt{\pi}}\,e^{-x^2} - \frac{1}{2}\,\mathrm{erf}(x)\right] . \tag{A-5}$$

$$\int x^2\mathrm{erf}(x)\,dx = \frac{1}{3}\left[x^3\mathrm{erf}(x) + \left(\frac{x^2}{\sqrt{\pi}}+\frac{1}{\sqrt{\pi}}\right)e^{-x^2}\right] . \tag{A-6}$$

$$\int x^3 e^{-ax^2-2bx-c} dx = e^{\frac{b^2-ac}{a}} \{ \frac{x^3}{2} \frac{\sqrt{\pi}}{\sqrt{a}} \text{erf}(\sqrt{a}x + \frac{b}{\sqrt{a}}) - \frac{\sqrt{\pi}}{\sqrt{a}} (\frac{x^3}{2} + \frac{b^3}{2a^3} + \frac{3b}{4a^2})$$

$$\cdot \text{erf}(\sqrt{a}\, x + \frac{b}{\sqrt{a}}) - (\frac{\frac{2}{x}}{2a} - \frac{bx}{2a^2} + \frac{b^2}{2a^3} + \frac{1}{2a^2}) e^{-(\sqrt{a}\, x + \frac{b}{\sqrt{a}})^2} \} \quad \text{(A-7)}$$

Equation (3.15) may be expressed as

$$_{L}R_{11}(t_*) = \int_{\theta=0}^{\pi} \int_{\phi=0}^{2\pi} \{ \frac{F(t_*)}{2^{\frac{5}{2}} \pi \alpha^{\frac{3}{2}} \alpha_3 I A^{\frac{1}{2}}} \int_{\xi=0}^{\infty} \xi^2 e^{-B\xi^2-\xi} (1-\frac{\xi}{2} \sin\theta) d\xi \}$$

$$\sin\theta \, d\phi d\theta \quad \text{(A-8)}$$

From Equation (A-4), the first integral in the bracket becomes

$$\int_{\xi=0}^{\infty} \xi^2 e^{-B\xi^2-\xi} d\xi = e^{\frac{1}{4B}} \sqrt{\pi} (\frac{1}{4B^{\frac{3}{2}}} + \frac{1}{8B^{\frac{5}{2}}})(1 - \text{erf}(\frac{1}{2B^{\frac{1}{2}}})) - \frac{1}{4B^2} \quad \text{(A-9)}$$

The second term in the bracket can be integrated by using Equation (A-7) such that

$$\int_{\xi=0}^{\infty} \xi^3 e^{-B\xi^2-\xi} d\xi = \frac{1}{8B^3} + \frac{1}{2B^2} - e^{\frac{1}{4B}} \sqrt{\pi} (\frac{1}{16B^{\frac{7}{2}}} + \frac{3}{8B^{\frac{5}{2}}})(1-\text{erf}(\frac{1}{2B^{\frac{1}{2}}}))$$

Two asymptotic properties of the error function are applied during the calculations,

(i) $\lim_{\xi \to \infty} \text{erf}(\xi) = 1$

(ii) $\lim_{\xi \to \infty} \xi^2 e^{-(\sqrt{B}\, \xi + \frac{1}{2\sqrt{B}})^2} = 0.$

Equation (3.16) is produced by substituting Equations (A-9) and (A-10) into Equation (A-8).

APPENDIX B

LIMITATIONS OF THE APPROACH

In addition to the simplified assumption employed in the model, there are some restrictions on the numerical approach for the Lagrangian autocorrelation function.

The present approach separated the Eulerian space-time correlation into two parts--the temporal and spatial correlations--which introduced the double integration in Equation 3.16. Unfortunately, the integration does not converge as time increases. If one examines the isotropic case, $\alpha_1 = \alpha_2 = \alpha_3$ and $\Gamma_s T_{11} = 0$, Equation 3.16 returns to Equation 3.12 so that

$$L^R_{11}(t_*) = F_1(t_*) \{e^{\alpha^2 I}(1 - \mathrm{erf}(\alpha^2 I))(1+4\alpha^2 I + 4/3\ \alpha^4 I^2) - \frac{2}{3}\frac{\sqrt{\alpha^2 I}}{\sqrt{\Pi}}(5+2\alpha^2 I)\} \quad . \tag{B-1}$$

From Equation 7.1.13 in Abramowitz and Stegun (1975), $e^{\alpha^2 I}(1 - \mathrm{erf}(\alpha^2 I))$ satisfies the inequalities

$$\frac{2}{\sqrt{\Pi}\ (\alpha^2 I + \sqrt{\alpha^4 I^2+2})} < e^{\alpha^2 I}\ (1-\mathrm{erf}(\alpha^2 I)) \leqq \frac{2}{\sqrt{\Pi}\ (\alpha^2 I + \sqrt{\alpha^4 I^2 + 4/\Pi})} \tag{B-2}$$

when $\alpha^2 I \geqq 0$.

Equation B-1 thus reduces to

$$L^R_{11}(t_*) = F_1(t_*) \{\frac{1}{\sqrt{\Pi}}\ (\frac{1}{\sqrt{\alpha^2 I}} + \frac{2}{3}\sqrt{\alpha^2 I})\} \tag{B-3}$$

when $\alpha^2 I$ is large enough (for instance, $\alpha^2 I \leqq 10.0$) such that

$$e^{\alpha^2 I}\ (1 - \mathrm{erf}(\alpha^2 I)) \cong \frac{1}{\sqrt{\Pi}\ \alpha^2 I}.$$

One notices that the bracket term in Equation B-3 increases as $\alpha^2 I$ increases and that it diverges to infinity, asymptotically. Fortunately, $F(t_*)$ converges to zero after t_* is greater than 15.0; $L^R_{11}(t_*)$ then converges to zero before $\alpha^2 I$ outgrows $F(t_*)$.

In a non-isotropic turbulence, $\alpha_2^2 I$ and $\alpha_3^2 I$ are the same order of magnitude as $\alpha_1^2 I$. Therefore, the equations still converge smoothly. But when the uniform shear is introduced in the turbulence field, the elongation of turbulent eddies replaces the longitudinal plume spread from $2\alpha_1^2 I$ to $\Gamma^2_s T^2_{11} \alpha_3^2 II + 2\alpha_1^2 I$ where $\Gamma^2_s T^2_{11} \alpha_3^2 II$ is much greater than $2\alpha_1^2 I$. Hence, in the vicinity of the streamwise axis, $\theta \to 0$ in the transformed coordinates, B approaches to $\frac{1}{2(\Gamma^2_s T^2_{11} \alpha_3^2 II + 2\alpha_1^2 I)}$ in Equation 3.16. With the aid of Equation B-2, the integrand in Equation 3.16 behaves as $(1/2B + \sin^2\theta/8B^2)\sin\theta$. It diverges to a very large value near $\theta = 0$, but converges to zero at $\theta = 0$. When the shear effect is strong, this implies that the double integration term outgrows $F(t_*)$ so that a secondary peak will appear in ${}_L R_{11}(t_*)$ before it converges to zero.

Even in an isotropic homogeneous turbulence field with uniform velocity, the secondary peak is still observed in ${}_L R_{11}(t_*)$ for a very dispersive cloud. An example to visualize such effect is to increase α to a larger value. A test has shown that when $\alpha = 10$, then at $t_* = 3.52$ the secondary peak is observed. Physically, this is due to the rather flattened probability density function for a very dispersive cloud. The flattened probability density function enhances the bracket term in Equation B-1 outgrow $F_1(t_*)$.

However, the secondary peak of ${}_L R_{11}(t_*)$ is practically unrealistic. It is avoided by extrapolating ${}_L R_{11}(t_*)$ from the declining curve to yield the estimated Lagrangian autocorrelation function for strong sheared flow.

NRC FORM 335 (11.81)

U.S. NUCLEAR REGULATORY COMMISSION

BIBLIOGRAPHIC DATA SHEET

1. REPORT NUMBER (Assigned by DDC)
NUREG/CR-4072

4. TITLE AND SUBTITLE (Add Volume No., if appropriate)
The Estimation of Atmospheric Dispersion at Nuclear Power Plants Utilizing Real Time Anemometer Statistics

2. (Leave blank)

3. RECIPIENT'S ACCESSION NO.

7. AUTHOR(S)
W. W. Li and R. N. Meroney

5. DATE REPORT COMPLETED
MONTH: October YEAR: 1984

9. PERFORMING ORGANIZATION NAME AND MAILING ADDRESS (Include Zip Code)
Department of Civil Engineering
Colorado State University
Fort Collins, Colorado 80523

DATE REPORT ISSUED
MONTH: January YEAR: 1985

6. (Leave blank)

8. (Leave blank)

12. SPONSORING ORGANIZATION NAME AND MAILING ADDRESS (Include Zip Code)
Division of Radiation Programs and Earth Sciences
Office of Nuclear Regulatory Research
U. S. Nuclear Regulatory Commission
Washington, D.C. 20555

10. PROJECT/TASK/WORK UNIT NO.

11. FIN NO.
B7585

13. TYPE OF REPORT

PERIOD COVERED (Inclusive dates)

15. SUPPLEMENTARY NOTES

14. (Leave blank)

16. ABSTRACT (200 words or less)

Dispersion and turbulence measurements were conducted in a simulated atmospheric boundary layer. Field experiments and wind tunnel results for the behavior of lateral plume dispersion are compared to three semi-emperical expressions based on Taylor's diffusion theory. Agreement between the field data and laboratory measurements supports using wind tunnel results to simulate atmospheric transport phenomena. Eulerian space-time correlations with streamwise separations were measured for all three velocity components in the simulated boundary layer. Results were compared to previous measurements which were performed under different flow configurations. A universal shape of the Eulerian space-time correlation seems to exist when presented in a normalized time coordinate. Turbulence measurements of fixed-point Eulerian velocity statistics were employed to estimate the Lagrangian velocity statistics through the Baldwin and Johnson approach. The approach was modified to account for the uniform shear stress effect in a homogenous turbulent flow field. The estimated Lagrangian integral time scale agrees with estimates inferred from dispersion measurements within only a 20% error. Such agreement supports the methodology of using real time anemometer statistics to predict the atmospheric turbulent dispersion near a nuclear reactor site.

17. KEY WORDS AND DOCUMENT ANALYSIS

17a. DESCRIPTORS

Wind Tunnel
Turbulence
Diffusion
Lagrangian statistics
Space-time correlation

17b. IDENTIFIERS/OPEN-ENDED TERMS

18. AVAILABILITY STATEMENT
Unlimited

19. SECURITY CLASS (This report)
Unclassified

21. NO. OF PAGES

20. SECURITY CLASS (This page)
Unclassified

22. PRICE
$

NRC FORM 335 (11.81)

UNITED STATES
NUCLEAR REGULATORY COMMISSION
WASHINGTON, D.C. 20555